Advanced Control and Optimization Paradigms for Energy System Operation and Management

Editors:

Kirti Pal

Saurabh Mani Tripathi

Shruti Pandey

River Publishers

Advanced Control and Optimization Paradigms for Energy System Operation and Management

RIVER PUBLISHERS SERIES IN ENERGY MANAGEMENT

The "River Publishers Series in Energy Management" is a series of comprehensive academic and professional books focussing on management theory and applications for energy related industries and facilities. Books published in the series serve to provide discussion and exchange information on management strategies, techniques, methodologies and applications, with a focus on the energy industry.

Topics include management systems, handbooks for facility management, safety, security, industrial strategies, maintenance and financing, impacting organizational communications, processes and work practices. Content is also featured for energy resilient and high-performance buildings.

The main aim of this series is to serve as a useful reference for academics, researchers, managers, engineers, and other professionals in related matters with energy management practices.

Books published in the series include research monographs, edited volumes, handbooks and textbooks. The books provide professionals, researchers, educators, and advanced students in the field with an invaluable insight into the latest research and developments.

Topics covered in the series include, but are not limited to:

- Facility management;
- Safety and security;
- Management systems and solutions;
- Industrial energy strategies;
- Financing and costs;
- Energy resilient buildings;
- Green buildings management.

For a list of other books in this series, visit www.riverpublishers.com

Advanced Control and Optimization Paradigms for Energy System Operation and Management

Editors

Kirti Pal

School of Engineering, Gautam Budhha University, Greater Noida, India

Saurabh Mani Tripathi

Kamla Nehru Institute of Technology, Sultanpur, India

Shruti Pandey

Krishna Institute of Engineering & Technology, Ghaziabad, India

Contents

2   Hybrid Harmony Search and Modified Harmony Search Optimizations Performance in Economical Load Dispatch   41

Tanmoy Mulo, Amalendu Bikash Choudhury, and Prasid Syam

3   Techno-Economic Assessment and Choice of Battery for Hybrid Energy using HOMER Software   61

Vidhi Tiwari and Kirti Pal

Preface

The distributed energy technologies are gaining popularity nowadays. Owing to the extensive penetration of distributed generation (DG) units, electrical energy systems are facing the challenges of fast transition which has increased their complexity much more than ever. Due to the highly intermittent characteristics of the distributed energy resources, a larger penetration of these resources into the distribution grid network becomes of major concern. The main concern is to cope with the highly intermittent nature of renewable sources with the requirements for quality power and system stability. With eight original chapters, this edited volume is an extensive collection of state-of-the-art studies intended to integrate current research and innovations for the control, optimization, and management of electric energy systems. This edited book serves as a resource for the engineers, scientists, and professionals working on the energy systems.

Chapter 1 of this book proposes an iterative distributed algorithm to achieve the real-time available transfer capability (ATC) assessment that can overcome the inaccuracies in the existing distributed algorithms based on network equivalent techniques. Different IEEE test systems have been used to conduct numerical simulations to examine the convergence and accuracy of the proposed iterative distributed ATC assessment.

To solve economic load dispatch (ELD) problems, *Chapter 2* proposes a Modified Harmony Search (MHS) optimization technique that has better features in terms of the best solution, convergence time, fitness value convergence, and computational efficiency.

In *Chapter 3*, using HOMER Pro software, the performance of different types of batteries such as lead acid (LA), lithium-ion (LI), Li-ion Nickel-Manganese-Cobalt Oxide battery (LiNiMnCoO$_2$), Zinc Bromine flow battery and Nickel Iron battery has been evaluated for hybrid energy system (HRES).

The authors of *Chapter 4* propose an efficient and convergent hybrid crisscross optimization (HCSO) technique to solve the thermal power dispatch problem with a single fuel type generation system. The authors stressed that the solution to the economic load dispatch problem using the proposed HCSO is competitive and best compared to previous results reported in the literature.

The optimal allocation problem of various reactive compensation devices (RCDs) in distribution systems is dealt within *Chapter 5*, in which Bald Eagle Search (BES) optimization algorithms are used together to achieve simultaneous objectives such as minimizing power loss, low cost reactive compensator, better voltage profile, and better system stability.

A novel nature-inspired optimizer based on the pedal scent marking and sniffing behavior of brown-bears has been introduced by the authors of *Chapter 6* to solve the economic dispatch problem (EDP). The authors confirmed that the proposed algorithm outperforms many existing optimization algorithms in obtaining optimal solutions for the benchmark test functions.

The author of *Chapter 7* presents an average pq-SRF reference current extraction technique for active filtering to mitigate the current harmonics generated in any power system network due to the tremendous increase of load that exhibits non-linear behavior.

In addition, an effective approach based on the Harris' Hawks Optimization Algorithm (HHOA) is used in *Chapter 8* to select the appropriate capacity and position of decentralized renewable energy resources (DRERs) to reduce the real power loss and voltage variance in electric power networks. The authors of *Chapter 8* found that adding more DRER improves the overall performance of the system.

The editors hope that readers will find this book inspiring and very useful when conducting their own research in the domain area of energy systems.

Kirti Pal, *Ph.D*
Department of Electrical Engineering,
School of Engineering, Gautam Buddha University, Greater Noida, India.

Saurabh Mani Tripathi, *Ph.D*
Department of Electrical Engineering,
Kamla Nehru Institute of Technology, Sultanpur, India.

Shruti Pandey, *Ph.D*
Electrical and Electronics Engineering,
Krishna Institute of Engineering and Technology, Ghaziabad, India.

Acknowledgments

List of Figures

List of Tables

List of Contributors

Ahmad, Eid, *College of Engineering, Qassim University, Unaizah, Saudi Arabia; E-mail: ahmadeid@aswu.edu.eg*

Amalendu, Bikash Choudhury, *Indian Institute of Engineering Science and Technology, Shibpur, India; E-mail: ab_choudhury@yahoo.com*

Aprajita, Salgotra, *Indian Institute of Technology, Kanpur, India; E-mail: aprajita.salgotra3@gmail.com*

Chia-Chi, Chu, *National Tsing Hua University, Taiwan; E-mail: ccchu@ee.nthu.edu.tw*

Hussein, Abdel-mawgoud, *Faculty of Engineering, Aswan University, Aswan, Egypt; E-mail: hussein.abdelmawgoud@yahoo.com*

Jian-Hong, Liu, *National Taiwan Ocean University, Keelung City 202301, Taiwan; E-mail: jhliu727@mail.ntou.edu.tw*

Kanchan, Pawani, *Sant Longowal Institute of Engineering and Technology, Longowal, India; E-mail: kanchanpawani24@gmail.com*

Kirti, Pal, *Gautam Buddha University, Greater Noida, India; E-mail: kirti.pal@gbu.ac.in*

Kumar, Reddy Cheepati, *KSRM College of Engineering (Autonomous), Kadapa, India; E-mail: kumareeephd@gmail.com*

Manmohan, Singh, *Sant Longowal Institute of Engineering and Technology, Longowal, India; E-mail: singh_manmohan@msn.com*

Prasid, Syam, *Indian Institute of Engineering Science and Technology, Shibpur, India; E-mail: prasidsyam@gmail.com*

Praveen, Prakash Singh, *Tallinn University of Technology (TalTech), Estonia; E-mail: prsing@taltech.ee*

Salah, Kamel, *Faculty of Engineering, Aswan University, Aswan, Egypt; E-mail: skamel@aswu.edu.eg*

Sri Niwas, Singh, *Indian Institute of Technology, Kanpur, India;*
E-mail: snsingh@iitk.ac.in

Sumit, Verma, *Indian Institute of Technology, Kanpur, India;*
E-mail: drsumitverma007@gmail.com

Suprava, Chakraborty, *Vellore Institute of Technology, Vellore, India;*
E-mail: suprava1008@gmail.com

Tanmoy, Mulo, *Indian Institute of Engineering Science and Technology,*
Shibpur, India; E-mail: tmulo.nit.dgp@gmail.com

Tapan, Prakash, *VIT University, Vellore, India;*
E-mail: tapan.prakash@vit.ac.in

Vidhi, Tiwari, *Gautam Buddha University, Greater Noida, India;*
E-mail: tiwarividhi412@gmail.com

Vinay, Pratap Singh, *MNIT Jaipur, Jaipur, India;*
E-mail: vinay.ee@mnit.ac.in

List of Reviewers

Ahmad, Eid, *College of Engineering, Qassim University, Unaizah, Saudi Arabia*

Amitesh, Kumar, *National Institute of Technology, Patna, India*

Amit, Vilas Sant, *Pandit Deendayal Energy University, Gandhinagar, India*

Arvind, Jain, *National Institute of Technology, Agartala, India*

Ashwini, Patil, *KBT College of Engineering, Nashik, India*

Deshdeepak, Sharma, *MJP Rohilkhand University, Bareilly, India*

Devesh, Shukla, *Institute of Engineering and Technology, Lucknow, India*

Farhad, Ilahi Bakhsh, *National Institute of Technology, Srinagar, India*

Hemant, Ahuja, *Ajay Kumar Garg Engineering College, Ghaziabad, India*

Jeykishan, Kumar, *Central Power Research Institute, Bengaluru, India*

Jian-Hong, Liu, *National Taiwan Ocean University, Keelung City 202301, Taiwan*

Mandhir, Verma, *GL Bajaj Group of Institution, Mathura, India*

Manmohan, Singh, *Sant Longowal Institute of Engineering and Technology, Longowal, India*

Natwar, Singh Rathore, *KIET Group of Institutions, Ghaziabad, India*

Pallavi, Verma, *Gautam Buddha University, Greater Noida, India*

Shubham, Tiwari, *KIET Group of Institutions, Ghaziabad, India*

Sudhakar, Babu Thanikanti, *Universiti Tenaga National Institute of Power Engineering Kajang, Selangor, Malaysia*

Suprava, Chakraborty, *Vellore Institute of Technology, Vellore, India*

Tanmoy, Mulo, *Indian Institute of Engineering Science and Technology, Shibpur, India*

Tulika, Bhattacharjee, *Central Power Research Institute, Bengaluru, India*

Tushar, Kanti Bera, *National Institute of Technology, Durgapur, India*

Urvashi, Chauhan, *Gautam Buddha University, Greater Noida, India*

Vikas, Singh Bhadoria, *ABES Engineering College, Ghaziabad, India*

Vinaya, Rana, *Gautam Buddha University, Greater Noida, India*

List of Abbreviations

ADMM	Alternative direction multiplier method
ABC	Artificial bee colony
ACO	Ant colony optimization
AI	Artificial intelligence
ALO	Ant-lion optimization
ANN	Artificial neural network
AOA	Archimedes optimization algorithm
APP	Auxiliary problem principle
APPM	Auxiliary problem principle method
Apq-SRF	Averaging pq- synchronous reference frame
ASO	Atom search algorithm
ATC	Available transfer capability
BA	Bat algorithm
BES	Bald eagle search
BESS	Battery energy storage system
BFO	Bacterial foraging optimization
BOA	Brown-bear optimization algorithm
CEP	Classical evolutionary programming
CLPSO	Comprehensive learning particle swarm optimizer
CPFLOW	Continuation power flow
CPSO	Classical particle swarm optimization
CSA	Cuckoo search algorithm
CSO	Criss-cross optimization
CTLBO	Comprehensive teaching learning-based optimization
DE	Differential evolutionary
DER	Distributed energy resource
DG	Diesel generator
DG	Distributed generations
DRER	Decentralized renewable energy resources
DSP	Digital signal processing

DSTATCOM	Distribution-static synchronous compensators
EcSS	Electrochemical energy storage system
ED	Economic dispatch
EDP	Economic dispatch problem
ELD	Economic load dispatch
ELM	Electromagnetism-like mechanism
EP	Evolutionary programming
ESO	Efficient evolutionary strategies optimization
FA	Firefly algorithm
FACTS	Flexible AC transmission system
FBSM	Forward/backward sweep method
FC	Fixed capacitor
FEP	Fast evolutionary programming
FERC	Federal energy regulatory commission
FF	Fitness function
FPA	Flower pollination algorithm
FV	Fitness value
GA	Genetic algorithm
GHI	Global horizontal irradiation
GSA	Gravitational search algorithm
GWO	Grey-wolf optimizer
HC	Horizontal crossover
HCC	Hystersis current controller
HCSO	Hybrid crisscross optimization
HES	Hybrid energy system
HHOA	Harris' Hawks optimization algorithm
HHS	Hybrid harmony search
HMM	Harmony memory matrix
HMRC	Rate of harmony memory consideration
HES	Hybrid renewable energy system
HOMER	Hybrid optimization model for electric renewables
HS	Harmony search
HS-OBL	Harmony search-opposition based learning technique
ICA	Imperialist colony algorithm
I-DBEA	Improved decomposition based evolutionary algorithm
IEEE	Institute of electrical and electronics engineers

IFEP	Improved fast evolutionary programming
IGA-MU	Improved genetic algorithm with multiplier updating
IMOEHO	Improved multi-objective elephant herding optimization
IMPA	Improved marine predator algorithm
ISSO	Improved social-spider optimization
JADE	Adaptive differential evolution
KHO	Krill herd optimization
LHS	Latin hypercube sampling
MFEP	Mutation in fast evolutionary programming
MHS	Modified harmony search
MOEA	Multiobjective evolutionary algorithm
MOO	Multiobjective optimization
MPI	Message-passing interface
MPSO	Modified particle swarm optimization
MRI	Midwest research institute
MRPSO	Moderate random search particle swarm optimization
MSSO	Modified social-spider optimization
NERC	North American electric reliability council
NFL	No free lunch
NISSO	Novel improved social-spider optimization
NMC	Nickel-manganese-cobalt
NN-EPSO	Neural network evolutionary particle swarm optimization
NPC	Net present cost
NREL	National renewable energy laboratory
OBSSO	Opposition-based social-spider optimization
OCD	Optimality condition decomposition
OPF	Optimal power flow
PAR	Pitch adjusting rate
PCC	Point of common coupling
PCPM	Predictor-corrector proximal multiplier
PI	Proportional-integral
PID	Proportional-integral-derivative
PLL	Phase locked loop
PSO	Particle swarm optimization

QOTLBO	Quasi-oppositional teaching learning based optimization
QPSO	Quantum-behaved particle swarm optimization
RCD	Reactive compensating device
RE	Renewable energy
REI	Radial equivalent independent
RPO	Renewable purchase obligations
SA	Simulated annealing
SoC	State of charge
SPO	Solar purchase obligation
SRF	Synchronous reference frame
SSO	Social-Spider Optimization
SVC	Static Var compensator
TLBO	Teaching learning-based optimization
TS	Taboo search
TVD	Total voltage deviation
UC	Unit commitment
VPL	Valve point loading
VSA	Voltage security assessment
VSC	Voltage-source converter
WGO	Wild goats optimization
WIPSO	Weight improved particle swarm optimization
WOA	Whale optimization algorithm

1

A Distributed Framework of Real-Time Available Transfer Capability Assessment in Modern Multi-Area Power Grids

Jian-Hong Liu[1] and Chia-Chi Chu[2]

[1]Dept. of Electrical Eng. National Taiwan Ocean University, Keelung City 202301, Taiwan
[2]Dept. of Electrical Eng. National Tsing Hua University, HsinChu 30013, Taiwan
E-mail: jhliu727@mail.ntou.edu.tw; ccchu@ee.nthu.edu.tw

Abstract

An iterative distributed algorithm to achieve the real-time Available Transfer Capability (ATC) assessment is proposed in this chapter. Mathematically, ATC assessment can be formulated as an optimization problem formed as a particular Optimal Power Flow (OPF) problem. This task can be performed in the decomposition-based iterative methods linked to constrained augmented Lagrangian approaches. The proposed work is designed on the three distributed frameworks, including (i) Alternative Direction Multiplier Method (ADMM), (ii) Auxiliary Problem Principle Method (APPM), and (iii) Predictor-Corrector Proximal Multiplier (PCPM) approach for the real-time ATC estimation. The proposed distributed algorithm is designated under the partitioned system's efficient distributed computation architecture, coordinating between boundary and associated non-overlapping subsystems. The numerical simulations of ATC assessment are conducted in the proposed iterative distributed algorithm under the three IEEE test systems, and the accuracies and the effectiveness of the proposed distributed algorithm are validated.

Keywords: Available transfer capability, distributed algorithm, distributed framework, system partition.

1.1 Introduction

As legal, economic, and environmental concerns are stressed in modern power systems, power transfers between areas have been increasing considerably faster than the transfer capability. Due to these changes, there might be some technical difficulties in the power system operation, such as degraded system security and reliability. Thus, to precisely provide power transfer information under an interconnected power network, real-time Available Transfer Capability (ATC) assessment has become a critical issue and widely studied recently [1–3].

According to the definition of ATC raised by the North American Electric Reliability Council (NERC), ATC is recognized as the estimation of transfer capability persisting in the power grid and further utilized for power transmission [1]. In order to meet the requirement of real-time applications, continuous ATC information is designed and monitored on an hourly and daily basis for system operators, which is suggested by the Federal Energy Regulatory Commission (FERC). Since ATC computation is computationally demanding, the real-time ATC estimation is computationally demanding, mainly when some preventive or corrective control actions are conducted against the outage and uncertainties in power grids [2]. Moreover, in the case of a multi-area system, ATC computation becomes more challenging, owing to the reluctance of individual areas to share their operating information [4].

In early advances, ATC estimation was sensitivity-based under a power flow model, appearing efficient in the computational speed. Nevertheless, since typical large-scale power grids are physically formulated in non-linear power flow equations, including practical physical constraints, most linearized models cannot be adopted for accurate ATC estimation. Along with this idea, several non-linear approaches, such as continuation methods [5–7], direct methods [8], and non-linear optimization approaches [9, 10], have been exploited independently to provide precise ATC estimation. However, these model-based approaches are computationally demanding, such that their real-time applications are obstructed. In recent advances, distributed multi-processors have been significantly developed and utilized to promote the computation capacity in the multi-agent-based distributed framework. In the multi-agent-based distributed framework, the compensation mechanism between agents can be achieved when the agent fails. Under this situation, the

robustness of this class of multi-agent-based algorithms can be guaranteed. In recent years, numerous power system problems have been studied in this direction. For instance, (i) Optimal Power Flow (OPF) problems [11–17], (ii) distributed state estimations [18, 19], (iii) distributed control for distributed networks [20, 21], (iv) distributed contingency analysis [22], and (v) voltage stability monitoring problems [23, 24]. Moreover, the approximate measurement-dependent injection distribution factors were applied to evaluate real-time ATC with less computation burden [25].

Recently, a probabilistic assessment of Available Transfer Capability (ATC) was investigated by Optimality Condition Decomposition (OCD) techniques and Latin Hypercube Sampling (LHS) method in power systems with penetration of wind energy resources [26]. Meanwhile, advanced artificial intelligence and machine learning methods have drawn much attention in real-time ATC calculations. For example, the multi-time-series classification model was utilized to perform the short-term ATC [27]. By incorporating PMU data, the Artificial Neural Network (ANN) was adopted for training as a real-time prediction model for ATC estimation [28]. Furthermore, the comprehensive operation scenarios, including N-1 contingencies, were considered in training regression machine learning models [29]. Even though several works have been studied in this direction, these approximate methods and machine-learning-based approaches are still highly dependent on the accuracy of data acquisition, and the accuracy of the ATC is restricted.

From the above literature review, it can be concluded that developing the real-time ATC calculation in a distributed manner is the current trend for technological developments in smart grid operation. However, this distributed ATC assessment still suffers technical difficulties to obtain an equivalent model of the external system for diminishing the computation complexities. Traditionally, the network decomposition approach is widely considered. The decomposition of the power grid can obtain a multi-area power network, and the equivalent model of external areas can be utilized by using an appropriate distributed and coordinated mechanism. By following this direction, few works have been proposed. For instance, external areas are modeled by the Radial Equivalent Independent (REI) equivalence technique for each decomposed area [4]. However, during the iteration process, parameters updating of external areas is not considered in REI equivalents. Some inaccuracies can be expected in these REI-based methods.

In order to overcome the predicament, the iterative distributed algorithm is proposed to obtain accurate real-time multi-area ATC estimations. By extending our previous work [30], this chapter will provide a comprehensive

survey of existing works and provide an iterative distributed framework for real-time ATC assessment of multi-area power systems from aspects of theoretical analysis, distributed algorithms, and practical implementations. The proposed framework will be proceeded by the following steps. First, the ATC assessment will be formulated as a distributed multi-area optimal power flow problem. Equality constraints from power flow equations and physic inequality constraints, such as reactive generator power and thermal limits, can be included in this problem formulation. By assuming the load variation direction at specified buses, the available power transfer can be defined in the objective function of the proposed optimization problem. Subsequently, several distributed computation algorithms are explored. The dual ascent method and constrained augmented Lagrange are reviewed and represented first. Three distributed algorithms, including (i) Predict-Corrector Proximal Multiplier Method (PCPM), (ii) Auxiliary Problem Principle Method (APPM), and (iii) Alternative Direction Multiplier Method (ADMM), are investigated and utilized to formulate the first-order approximation of constrained augmented Lagrange. Thirdly, the real-time Voltage Security Assessment (VSA) is studied in a distributed computation framework. In the proposed system partition, the entire power grid can be modeled as several interconnected subsystems whose computation works can be proceeded in distributed processors. Those distributed processors can be coordinated concurrently to complete the significant computation task efficiently. For the system partition, non-overlapping and boundary subsystems are also studied in detail. Thus, in the proposed distributed ATC assessment, the preliminary computation work can be distributed to those subsystems and computed in multiple distributed processors. These multiple distributed processors can be operated concurrently and cooperatively. Finally, the boundary subsystem is responsible for the coordination between all the distributed subsystems.

The significant contribution and novelty of the proposed work can be addressed. The proposed distributed algorithm can overcome the inaccuracy in the existing distributed algorithm based on network equivalent techniques and ultimately solve ATC estimation numerically. Numerical simulations on IEEE 14-bus, IEEE 57-bus, and IEEE 118-bus test systems are performed to verify the accuracy of the proposed approach.

1.2 Problem Formulation

Given a configured power system under physical constraints of inequality or equality equations regarding to the physical operation limits, such as

transmission line thermal limits and generator reactive power limits, the ATC is defined as the maximal loading factor or the maximum power transfer capability in the interconnect power grid [3]. Hence, ATC estimation can be performed by using non-linear programming methods. Considering a power grid with n buses and a load direction $b \in \mathbf{R}^{2n}$, ATC estimation can be typically formulated as a non-linear optimization problem, as expressed by

$$st.\ g(u) = \begin{bmatrix} \min_{\lambda \in \mathbf{R}} \lambda \\ F(x, \lambda) = f(x) + \lambda^2 b \\ h(x) - z = 0 \\ h_{lower} \leq z \leq h_{upper} \end{bmatrix} \quad (1.1)$$

In (1.1), a scaled parameter λ is utilized to represent the *maximal loading factor* along the load direction b with its squared-form λ^2 for the ATC estimation. $x^T = [\theta^T, V^T] \in \mathbf{R}^{2n}$ denotes phase angles and magnitudes of bus voltage. Power flow equations parametrized by continuation active and reactive power variations along the load direction b can be expressed by $F^T(x, \lambda) = [P^T(x, \lambda), Q^T(x, \lambda)]$ [7]. The real power formula $P_i = (x, \lambda)$ and the reactive power formula $Q_i(x, \lambda)$ of the power flow equations at the ith bus can be depicted by

$$P_i(x, \lambda) = \sum_{j=1}^{n} |V_i\,||V_j||\,Y_{ij}| \cos(\delta_{ij} - \theta_i + \theta_j) + \lambda^2 b_{Pi}$$

$$Q_i(x, \lambda) = -\sum_{j=1}^{n} |V_i\,||V_j||\,Y_{ij}| \sin(\delta_{ij} - \theta_i + \theta_j) + \lambda^2 b_{Qi} \quad (1.2)$$

where the phase angle of the entry Y_{ij} in the system admittance is denoted by δ_{ij}. Entries of power variation vector b include real and reactive power variations b_{Pi} and b_{Qi}. It is worthy mentioning that the formulation in (1.1) is slightly different from the conventional notion used in [7]. However, this new formulation facilitates the later development of the distributed algorithm.

All inequality constraints, addressed in $h_{lower} \leq z \leq h_{upper}$, are transferred into the equality constraints, described by $h(x) - z = 0$, through the surplus variables $z \in \mathbf{R}^m$. Thus, the compact form, defined by $g(x, y, \lambda) = 0 \in \mathbf{R}^{l=2n+m}$, can be utilized to represent all involved constraints. To simplify the expression, a composite vector is defined by $u = [x^T, z^T, \lambda]^T$ to include all state variables.

1.3 Distributed Algorithms for ATC Estimation

The optimization problem mentioned above can be solved efficiently in a distributed computation framework. Such distributed framework can be implemented in a guaranteed decomposition-coordination method. Along this direction, distributed computational approaches can be categorized into two methods, including one-level and two-level methods. In the one-level method, subsystems are not designed to be solved coordinately. The two-level methods utilize the multipliers to coordinate the solutions between sub-systems.

1.3.1 Overview

The Lagrange Multiplier formula is the typical method to solve the special OPF problem in (1.1), and accordingly, the *dual ascent* method can be performed iteratively. Specifically, (1.1) can be utilized to formulate the *Lagrange*, as defined by

$$\underset{h_{lower} \leq z \leq h_{upper}}{\mathcal{L}(u, \beta)} = \lambda + \beta^T g(u) \tag{1.3}$$

where the primal and dual variables can be denoted by u and β. (1.3) can further define the dual problem in which the dual function is given by

$$h(\beta) = \inf_u \mathcal{L}(u, \beta) \tag{1.4}$$

If the strong duality assumption meets, the duality gap between the primal and the dual problems can be eliminated such that the corresponding optimal values become identical. Therefore, the optimizer u^* in the primal problem can be recovered from the optimizers β^* of the dual problem, as mentioned by [34]

$$u^* = \arg\min_u \mathcal{L}(u, \beta^*) \tag{1.5}$$

The dual ascent approach utilizes the gradient ascent to solve the dual problem, and it can be specified as follows:

- By adopting the constant β^k at the previous iteration, the first step is to find the minimizer u of the following optimization problem shown by

$$u^{k+1} = \arg\min_u \mathcal{L}\left(u, \beta^k\right) \tag{1.6}$$

- Then, multiplier variables are accordingly updated in the second step, as expressed by

$$\beta^{k+1} = \beta^k + \alpha^k g\left(u^{k+1}\right) \tag{1.7}$$

where the step-size is denoted by $\alpha^k > 0$.

Practically, the dual ascent method may suffer convergence problems in the conventional Lagrangian techniques due to the insufficient strict convexity of the objective function.

In order to deal with such a predicament, the *constrained augmented Lagrangian* of (1.1) is considered by:

$$\mathcal{L}_A(u, \beta) \atop h_{lower} \leq z \leq h_{upper}} = \lambda + \beta^T g(u) + \frac{\gamma}{2} \|g(u)\|^2 \qquad (1.8)$$

where the Lagrangian multipliers are represented by β and an associated constant is given by γ. Referring to solving (1.1) iteratively by the dual ascent approach, at the k-th iteration, by using the *first order approximation*, the constrained augmented Lagrangian of (1.8) can be approximated as

$$\mathcal{L}_A^k \atop \Delta z \in \Omega} = \lambda^k + \Delta\lambda + \beta^{k^T} \left[g\left(u^k\right) + \nabla_u g^k \Delta u \right] + \frac{\gamma}{2} \left\| g\left(u^k\right) + \nabla_u g^k \Delta u \right\|^2 \qquad (1.9)$$

where $\Delta u = [\Delta u^T, \Delta z^T, \Delta\lambda]^T$ is presented. The inequality constraints of surplus variables can be defined in the set of $\Omega = \Delta z | h_{lower} \leq z^k + \Delta z \leq h_{upper}$. The Jacobian matrix $\nabla_u g^k$ is defined by the derivatives of $g(u^k)$ with respect to u. In the iterative method, the main step is to find the minimizers Δu of the *approximate constrained augmented Lagrangian* of (1.9). However, some difficulties may be made in the minimization step of (1.9) due to considering the set Ω. In order to relax such circumstances, a *two-phase projection method* is utilized [35]:

- In the first phase, by discarding the subset Ω, the approximate constrained augmented Lagrangian (1.9) can be reformulated as an unconstrained augmented Lagrangian and solved to find the minimizer Δu.
- In the second phase, the inaccurate $\Delta\tilde{z}$ of Δu obtained in the first phase is projected onto the defined subset Ω and corrected as the accurate surplus variables Δz according to the projection principle:

$$\Delta z = \begin{cases} h_{upper} - z^k & if \ z^k + \Delta\tilde{z} > h_{upper} \\ h_{lower} - z^k & if \ z^k + \Delta\tilde{z} < h_{lower} \\ \Delta z & otherwise \end{cases} \qquad (1.10)$$

Afterward, state variables can be updated iteratively, as expressed by:

$$u^{k+1} = u^k + \alpha_u \Delta u \qquad (1.11)$$

with the step-size $\alpha_u^T = [\alpha_x^T, \alpha_z^T, \alpha_\lambda]$. Since state variables u^k may be much distant from the equality constraints, in order to avoid such circumstances, Armijo's rule is designed to be applied along with the penalty of violating constraints [35].

When the augmented technique is applied, there exists the problem of the separability destroy among all optimization variables, Δx, Δz, and $\Delta \lambda$, in the augmented term $\frac{\gamma}{2}||g(u^k)+\nabla_u g^k \Delta u||^2$. Due to the coupling augmented term, it is recognized as the main difficulties and shortcomings of the augmented Lagrangian, which has long been found [14].

In order to diminish this obstacle, three distinct strategies have been proposed to relax such difficulty: (i) Predictor-Corrector Proximal Multiplier Method (PCPM), (ii) Auxiliary Problem Principle Method (APPM), and (iii) Alternative Direction Multiplier Method (ADMM).

1.3.2 Predictor-Corrector Proximal Multiplier Method (PCPM)

Predictor-Corrector Proximal Multiplier method (PCPM) is based on its primal-dual method, which associates an augmented Lagrangian with an additional quadratic proximal term related to variables u [14, 30]. By applying PCPM in (1.1), the corresponding constrained augmented Lagrangian can be formulated as

$$\mathcal{L}_{PCPM}(u, \beta) = \lambda + \beta^T g(u) + \frac{1}{2\gamma}||g(u)||^2 + \frac{\gamma}{2}||u - \hat{u}||^2 \qquad (1.12)$$
$$\scriptstyle h_{lower} \leq z \leq h_{upper}$$

where γ is a constant. $\hat{u}$ represents state variables at the previous iteration. The first-order approximation of the formula (1.12) for the k-th iteration can be formulated as

$$\mathcal{L}_{PCPM}^k = \lambda^k + \Delta\lambda + \beta^{k^T} \left[g\left(u^k\right) + \nabla_u g^k \Delta u \right]$$
$$\scriptstyle \Delta_z \in \Omega$$

$$+ \frac{1}{2\gamma} \left\| g\left(u^k\right) + \nabla_u g^k \Delta u \right\|^2 + \frac{\gamma}{2} \left\| u^k + \Delta u - u^k \right\|^2 \qquad (1.13)$$

Two-phase projection theory can also be adopted to relax the difficulty in minimizing (1.13). By regarding the constrained augmented Lagrangian (1.13) as an unconstrained augmented Lagrangian, differentiating (1.13) with respect to Δu leads to obtain Δu^k as expressed below:

$$\Delta u^k = - \left[\nabla_u g^{k^T} \left(\beta^k + D^k/\gamma \right) - M \right] /\gamma \qquad (1.14)$$

where $M = [\mathbf{0}_{1 \times l} 1]^T$ and $D^k \equiv g(u^k) + \nabla_u g^k \Delta u^k$. Difficulties with the above scheme are that the iterates Δu^k are coupled by the implicit computation of the constraint D^k, therefore, they cannot be computed separately. To remove difficulties, explicit computation of the constraint expression in (1.14) is suggested by defining the predicted multiplier variables $\tilde{\beta}^{k+1}$ in the following iterative scheme

$$\Delta u^k = \left(-\nabla_u g^{k^T} \tilde{\beta}^{k+1} - M \right) / \gamma \tag{1.15}$$

The predicted multiplier variable $\tilde{\beta}^{k+1}$, using the estimated u^{k-1} in the previous iteration, can be defined by

$$\tilde{\beta}^{k+1} = \beta^k + \left[g\left(u^{k-1} \right) + \nabla_u g^{k-1} \Delta u^{k-1} \right] / \gamma = \beta^k + \Delta \beta^{k-1} / \gamma \tag{1.16}$$

The above scheme can be interpreted as a partial implicit-explicit method: implicit for objectives and explicit for constraints. Subsequently, the second phase of the two-phase project theory is conducted to correct the predicted $\Delta \tilde{z}^k$ as Δz^k according to the principle stated in (1.10). Also, the predicted multiplier variables $\tilde{\beta}^{k+1}$ can be corrected as β^{k+1}, denoted by

$$\beta^{k+1} = \beta^k + \frac{1}{\gamma} \left[g\left(u^k \right) + \nabla_u g^k \Delta u^k \right] = \beta^k + \frac{1}{\gamma} \Delta \beta^k \tag{1.17}$$

Furthermore, the deviation Δu^k can be used to update variables u^{k+1}, as expressed by (1.11). In summary, the pseudo-code of the PCPM can be outlined in Table 1.1.

1.3.3 Auxiliary Problem Principle Method (APPM)

The optimization problem of (1.3) can be solved to find the minimizers by using the Auxiliary Problem Principle (APP) in which a sequence of auxiliary problems is considered [14, 31, 33]. Let a master problem defined by

$$\min_u T_1(u) + T_2(u) \quad \text{st. } \Theta\Theta(u) = 0 \tag{1.18}$$

where $T_2(u)$ and $\Theta(u)$ are both additives, and $T_1(u)$ is differentiable. Along with the similar ideas of (1.8), the optimizer of the optimization problem (1.18) can be found by solving the following equivalent master augmented Lagrangian:

$$\min_{u,\beta} \mathcal{L}(u, \beta) = T_1(u) + T_2(u) + \langle \beta + \eta\Theta(u), \Theta(u) \rangle \tag{1.19}$$

where a constant is defined by η. The operation of the inner product is denoted by the notation $<,>$. In APPM, an auxiliary augmented Lagrangian is defined through substituting $T_1(u)$ by $G(u)$ and solving to obtain the minimizer of (1.19) [34, 35]. The following lemma addresses the issue of choosing $G(u)$ appropriately.

Theorem (APP) [34]: Given a convex and differential function, $G(u)$, and assume a minimizer u^* in the following auxiliary augmented Lagrangian

$$\min_{u,\beta} G(u) + T_2(u) + \langle \beta + \eta\Theta(u), \Theta(u) \rangle \qquad (1.20)$$

In the master augmented Lagrangian of (1.19), the necessary and sufficient condition for the existence of the minimizer u^* is addressed by [34]

$$\langle \nabla_u T_1(u^*), u - u^* \rangle + T_2(u) - T_2(u^*) \geq 0 \qquad (1.21)$$

If assuming

$$\nabla_u G(u^*) = \nabla_u T_1(u^*) \qquad (1.22)$$

the same condition of (1.21) can be found through the defined auxiliary augmented Lagrangian of (1.20) along with the master augmented Lagrangian of (1.19). Thus, this condition reveals that solving (1.20) is equivalent to solve (1.19). In order to satisfy (1.22), $G(u)$ can be defined by [34]

$$G^v(u) = \gamma K(u) + \langle \nabla_u T_1(v) - \gamma \nabla_u K(v), u \rangle \qquad (1.23)$$

where a constant and a dummy variable are represented by γ and v. $K(u)$ is the auxiliary function and can be chosen abstractly. Once $G(u)$ is well-defined, (1.22) can be verified as follows:

$$\nabla_u G^v(v) = \nabla_u T_1(v) \qquad (1.24)$$

Here, the auxiliary augmented Lagrangian of (1.20) is designed to be solved in an iterative algorithm such that the variable v can be approximated to v^* iteratively. In this aspect, the auxiliary augmented Lagrangian of (1.20) is designed to be solved in a two-level algorithm [34]:

- The auxiliary problem is solved by assessing u^{k+1}

$$\min_{u} \gamma K(u) + \langle \nabla_u T_1(u^k) - \gamma \nabla_u K(u^k), u \rangle + \langle \beta^k + \eta\Theta(u^k), \Theta(u) \rangle \qquad (1.25)$$

- Update $\beta^{k+1} = \beta^k + \eta\Theta(u^{k+1})$

- If $|u^k - u^{k+1}|$ is lower than the designed convergency tolerance, the algorithm stops. Otherwise, continues the algorithm, go to step 1, and set $k = k + 1$.

In this position, APPM can be successfully applied to the proposed ATC estimation problem of (1.1) by setting $T_1(u) = 0$, $T_2(u) = \lambda$, and $\Theta(u) = g(u)$.

Accordingly, the overall distributed ATC estimation is re-phrased as follows:

$$u^{k+1} = \arg\min_u \{\gamma K(u) + \lambda - \gamma \nabla K(u^k)^T u + \langle \beta^k + \eta g(u^k), g(u) \rangle\}$$
$$\beta^{k+1} = \beta^k + \eta g(u^{k+1}) \qquad (1.26)$$

In order to provide the flexibility of the algorithm convergence, the auxiliary function $K(u)$ is adopted and conventionally set by $K(u) = ||u||^2/2$ [13, 14]. Thus, (1.26) can be expanded as

$$u^{k+1} = \arg\min_u \{\lambda + \frac{\gamma}{2}||u - u^k||^2 + (\beta^k)^T g(u) + \eta g(u^k)^T g(u)\} \quad (1.27)$$

By examining (1.27), the proposed augmented Lagrangian associated with the APP algorithm can be simply defined by

$$\mathcal{L}_{APPM}_{h_{lower} \leq z \leq h_{upper}} (u, \beta) = \lambda + \beta^T g(u) + \frac{\gamma}{2}||u - \hat{u}||^2 + \eta g(\hat{u})^T g(u) \quad (1.28)$$

where the state calculated at the previous iteration is denoted by $\hat{u}$. Furthermore, by using the first-order approximation, the constrained augmented Lagrangian can be calculated at the *k*th iteration, as represented by

$$\mathcal{L}^k_{APPM}_{\Delta_z \in \Omega} = \lambda^k + \Delta\lambda + (\beta^k)^T [g(u)^k + \nabla_u g^k \Delta u] + \frac{\gamma}{2}||\Delta u||^2$$
$$+ \eta[g(u^{k-1}) + \nabla_u g^{k-1} \Delta u^{k-1}]^T \times [g(u^k) + \nabla_u g^k \Delta u] \quad (1.29)$$

Subsequently, through applying the two-phase projection method in the minimization step, the unconstrained augmented Lagrangian of (1.29) is proceeded by the derivatives with respect to Δu, and the state Δu^k at the *k*th iteration can be determined by

$$\Delta u^k = (-\nabla_u g^{k^T} \tilde{\beta}^{K+1} - M)/\gamma \qquad (1.30)$$

where $M = [0_{1 \times l} 1]^T$. These predicted multiplier variables $\tilde{\beta}^{k+1}$ can be defined by

$$\tilde{\beta}^{k+1} = \beta^k + \eta[g(u^{k-1}) + \nabla_u g^{k-1} \Delta u^{k-1}] = \beta^k + \eta \Delta \beta^{k-1} \qquad (1.31)$$

Table 1.1   Summary of the three distributed algorithms in ATC estimation

Algorithms	Algorithm Procedure
PCPM	$\tilde{\beta}^{k+1} = \beta^k + \frac{1}{\gamma}\Delta\beta^{k-1}$ $$\Delta u^k = \arg\min_{\Delta u}\left\{\left(\tilde{\beta}^{k+1}\right)^T \nabla_u g^k \Delta u + \frac{\gamma}{2}\|\Delta u\|^2 + \Delta\lambda M\right\}$$ $\Delta z^k \leftarrow \Delta\tilde{z}^k \text{in} \Delta u^k$ $\beta^{k+1} = \beta^k + \frac{1}{\gamma}\Delta\beta^k$ $u^{k+1} = u^k + \alpha_u\Delta u^k$
APPM	$\tilde{\beta}^{k+1} = \beta^k + \eta\Delta\beta^{k-1}$ $$\Delta u^k = \arg\min_{\Delta u}\left\{\left(\tilde{\beta}^{k+1}\right)^T \nabla_u g^k \Delta u + \frac{\gamma}{2}\|\Delta u\|^2 + \Delta\lambda M\right\}$$ $\Delta z^k \leftarrow \Delta\tilde{z}^k \text{ in } \Delta u^k$ $\beta^{k+1} = \beta^k + \eta\Delta\beta^k$ $u^{k+1} = u^k + \alpha_u\Delta u^k$
ADMM	$\tilde{\beta}^{k+1} = \beta^k + \frac{1}{\gamma}\Delta\beta^{k-1}$ $$\Delta u^k = \arg\min_{\Delta u}\left\{\left(\tilde{\beta}^{k+1}\right)^T \nabla_u g^k \Delta u + \frac{\mu}{2}\|\Delta u\|^2 + \Delta\lambda M\right\}$$ $\Delta z^k \leftarrow \Delta\tilde{z}^k \text{ in } \Delta u^k$ $\beta^{k+1} = \beta^k + \frac{1}{\gamma}\Delta\beta^k$ $u^{k+1} = u^k + \alpha_u\Delta u^k$

The prediction $\Delta\tilde{z}^k$ of Δu^k can be further corrected and modified as Δz^k in the second phase. Then, β^{k+1} and u^{k+1} can be accordingly updated by

$$\beta^{k+1} = \beta^k + \eta\Delta\beta^k \quad u^{k+1} = u^k + \alpha_u\Delta u^k \tag{1.32}$$

The outline of APPM is summarized in Table 1.1. Note that (1.31) and (1.32) are similar to (1.16) and (1.17). Thus, PCPM can be treated as a special case of APPM if the parameter $\eta = 1/\gamma$ in APPM is selected.

1.3.4 Alternative Direction Multiplier Method (ADMM)

Consider a basic augmented Lagrangian formulated from the problem of ATC of (1.1), as expressed by

$$\mathcal{L}_{ADMM}_{h_{lower}\leq z\leq h_{upper}}(u,\beta) = \lambda + \beta^T g(u) + \frac{1}{2\gamma}\|g(u)\|^2 \tag{1.33}$$

At the k-th iterate, the first-order approximation in (1.33) is

$$\mathcal{L}^k_{ADMM}_{\Delta z\in\Omega} = \lambda^k + \Delta\lambda + \beta^{k^T}[g(u^k) + \nabla_u g^k \Delta u] + \frac{1}{2\gamma}\|g(u^k) + \nabla_u g^k \Delta u\|^2$$

$$\tag{1.34}$$

Similar to the previous two methods, the unconstrained formula of (1.34) is designed to be minimized with respect to Δu through applying the two-phase projection theory. The relative formula with respect to Δu can be expressed by

$$\nabla_u g^{k^T}[\beta^k + \frac{1}{\gamma}D^k] + M = 0 \qquad (1.35)$$

In formula (1.35), each Δu_i^k is coupled with others Δu^k such that extracting each Δu_i^k separately meets some difficulties. In order to relax the difficulty, Alternative Direction Multiplier Method (ADMM) is adopted. The principle of ADMM is based on the relaxation approach in order to minimize the augmented Lagrangian. The strategy of relaxing the augmented Lagrangian is to minimize each state variable by fixing other state variables and the multiplier at their last iterates.

Once all state variables have proceeded, the multiplier can be updated subsequently [14, 25]. Thus, in minimizing each state variable, fixing other state variables can eliminate the coupling effect from other state variables such that the difficulty in the minimization step can be relaxed. With the benefit of ADMM, extracting each Δu_i^k can now be facilitated by fixing other variables $\Delta u_{j,j\neq i}^{k-1}$ at their last iterates. Thus, formula (1.35) can be modified as

$$\nabla_u g^{k^T}[\beta^k + D^{k-1}/\gamma] + M + \mu \Delta u^k = 0 \qquad (1.36)$$

where $D^{k-1} \equiv g(u^{k-1}) + \nabla_u g^{k-1}\Delta u^{k-1}$. By defining the predicted multiplier variable as $\tilde{\beta}^{k+1} = \beta^k = \beta^k + \frac{1}{\gamma}D^{k-1}$, (1.36) can be rearranged as

$$\Delta u^k = (-\nabla_u g^{k^T}\tilde{\beta}^{k+1} - M)/\mu \qquad (1.37)$$

Subsequently, two-phase projection theory is used to correct the predict $\Delta \tilde{z}^k$ as Δz^k. Finally, updating variables β^{k+1} and u^{k+1} can be expressed by

$$\beta^{k+1} = \beta^k + \Delta\beta^k/\gamma \quad u^{k+1} = u^k + \alpha_u \Delta u^k \qquad (1.38)$$

Table 1.1 denotes the ADMM algorithm. Note that PCPM is also a special case of ADMM if $\mu = \gamma$ is selected. In addition, ADMM is equivalent to APPM by properly setting the free parameters. It can be concluded that PCPM and ADMM are the special cases in APPM, and APPM will be adopted to develop the proposed iterative distributed framework for the real-time ATC assessment.

1.4 Distributed Framework of Real-Time ATC Estimation

Next, the real-time ATC estimation will be implemented in a distributed computation framework based on APPM. The distributed calculation is designed to separate all state variables in the developed distributed computation framework, including power system state variables x, loading parameter λ^2, surplus variables z, and Lagrangian multipliers β. In this case, using system partition, the overall computation is separated into several sub-tasks and proceeded separately and concurrently.

1.4.1 The Framework of the Distribution System

A distributed system represents the physical arrangement for distributed processing, which is organized by a computer network. A common problem of a bulk power grid can be solved by using distributed computers concurrently. Based on the system partition, several sub-tasks can be constructed by dividing the main task and further distributed to multiple distributed processors to be dealt with simultaneously. Since these distributed processors can be coordinated, concurrent computation on the main task can be conducted efficiently. Generally, the design of a distributed system is based on three steps: (1) Task Allocation, (2) Synchronization, and (3) Data Communication [36]. Detailed descriptions of these three steps are illustrated below.

(1) Task Allocation:

Based on the system partition, the partitioning of the main task is the first mission of developing a distributed system, and these sub-tasks from the partition are further allocated to distributed processors. It is worthy to notice that the number of sub-tasks cannot exceed the number of available processors. Another essential concern is the issue of balancing loads of subtasks among processors. In order to achieve more efficient execution performance between processors, the load of each processor is designed to be commensurate according to its performance.

(2) Synchronization:

Synchronization is an important mechanism when several distributed processors work jointly on the main task. It allows processors to wait at some time for the completion of other distributed processors' computations.

In other words, processors complete computations and communication tasks in synchronous rounds. Particularly, synchronization can ensure the convergence of computations in a distributed system.
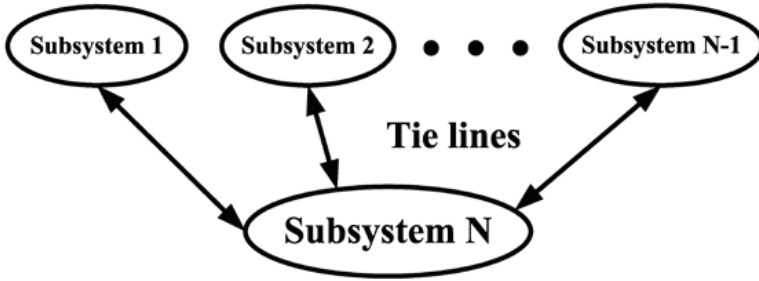
Figure 1.1 Representations of System Partition. © [2015] IEEE. Reprinted, with permission, from IEEE Transactions on Smart Grid [30]

(3) Data Communication:

One efficient data communication mechanism is Message-Passing Interface (MPI). MPI is a communication protocol for facilitating data transmission among distributed processors. With MPI, each processor can store its computation data in its local memory and then exchange its data with other processors. Computation data is transferred as packets of information over communication links. MPI organizes the cooperation of data transmission between processors.

1.4.2 System Partition

In the system partition, the primary system will be partitioned into several subsystems. The associated sub-tasks in these subsystems are further distributed into distributed processors and proceeded concurrently [35]. In order to optimize the efficiency of data communication, the partition of the primary system is based on the physical interconnection of subsystems, and data exchanging among processors has occurred in variables of boundary buses. In the network topology, the concerned N subsystems are constructed from $N - 1$ interconnected sub-areas. Furthermore, the reconstructed N subsystems consist of non-overlapping $N - 1$ subsystems, and the N-th subsystem is named the boundary subsystem and organized by all boundary buses of the subsystem. Figure 1.1 depicts the diagram of the system partition. Under this framework, the computation tasks on these subsystems can be proceeded concurrently. In this case, these distributed processors can be coordinated to complete the main task's computation efficiently. Specifically, the computation algorithm in the proposed distributed framework can be depicted in the following two steps:

(1) Gathering Step:

In the gathering step, the state variable Δu^k is computed for the k-th iteration. According to the system partition, the calculations on Δu^k are organized in the matrix form, as shown by [36]

$$
\begin{bmatrix} \Delta u_1^k \\ \Delta u_2^k \\ \vdots \\ \Delta u_N^k \end{bmatrix} = \begin{bmatrix} \nabla_u g_{1,1}^k & \mathbf{0} & \cdots & \nabla_u g_{1,N}^k \\ \mathbf{0} & \nabla_u g_{2,2}^k & \mathbf{0} & \nabla_u g_{2,N}^k \\ & \mathbf{0} & \cdots & \ddots & \vdots \\ \nabla_u g_{N,1}^k & \nabla_u g_{N,2}^k & \cdots & \nabla_u g_{N,N}^k \end{bmatrix}^T \begin{bmatrix} -\tilde{\beta}_1^{k+1}/\gamma \\ -\tilde{\beta}_2^{k+1}/\gamma \\ \vdots \\ -\tilde{\beta}_N^{k+1}/\gamma \end{bmatrix} - \frac{1}{\gamma} M
$$

(1.39)

Apparently, from (1.39), it can be observed that Δu^k can be computed in N processors individually and simultaneously. In more specific explanations,

- Under $i = 1, \ldots, N-1$, the computation of Δu_i^k is conducted in the i-th processor by the following expression

$$
\Delta u_i^k = \frac{-1}{\gamma} \left[(\nabla_u g_{i,i}^k)^T \tilde{\beta}_i^{k+1} + (\nabla_u g_{N,i}^k)^T \tilde{\beta}_N^{k+1} \right]
$$

(1.40)

where in subsystem i, the Jacobian matrix $\nabla_u g_{i,i}^k$ is defined with respect to u_i. Also, the Jacobian matrix $\nabla_u g_{N,i}^k$ is designed for subsystem N. The prediction multipliers for the ith and the Nth subsystems are denoted by $\tilde{\beta}_i^{k+1}$ and $\tilde{\beta}_N^{k+1}$. At the Nth subsystem, the boundary variables, including u_N^k and predicted multipliers $\tilde{\beta}_N^{k+1}$, can be collected to generate the Jacobian matrix $\nabla_u g_{N,i}^k$ and perform the calculation on Δu_i^k for the processor i.

- By referring to (1.32), the calculation on Δu_N^k can be proceeded in the Processor N by the following formula

$$
\Delta u_N^k = \frac{-1}{\gamma} \left[\Sigma_{i=1}^{N-1} (\nabla_u g^k_{i,N})^T \tilde{\beta}_i^{k+1} + (\nabla_u g^k_{N,N})^T \tilde{\beta}_N^{k+1} \right] - \frac{1}{\gamma} M' \quad (1.41)
$$

where $M' = [0_{1 \times n'} 1]^T$ with $u_N^k \in \mathbf{R}^{n'}$. In sub-system i, the Jacobian matrix with respect to u_N represents $\nabla_u g_{i,N}^k$. The Jacobian matrix $\nabla_u g_{N,N}^k$ in subsystem N is defined with respect to u_N. Furthermore, the Jacobian matrix $\nabla_u g_{i,N}^k$ can be assessed by accumulating $\tilde{\beta}_N^{k+1}$ and u_i^k to calculate Δu_N^k. In addition, $\Delta \tilde{z}_i^k$ and $\Delta \tilde{z}_N^k$ are modified as $\Delta \tilde{z}_i^k$ and $\Delta \tilde{z}_N^k$ in the two-phase projection theory, as shown in (1.10).

(2) Broadcasting Step:

In the broadcasting step, $\Delta\beta^k$ is produced in order to perform the update of u^{k+1}, β^{k+1}, and $\tilde{\beta}^{k+2}$. The computation efforts on $\Delta\beta_i^k$ and $\Delta\beta_N^k$, addressed in processors i and N, are linked to the following formula

$$\Delta\beta_i^k = g_i(u_i^k, u_N^k) + \nabla_u g_{i,i}^k \Delta u_i^k + \nabla_u g_{i,N}^k \Delta u_N^k$$

$$\Delta\beta_N^k = g_N(u^k) + \nabla_u g_{N,N}^k \Delta u_N^k + \sum_{i=1}^{N-1} \nabla_u g_{N,i}^k \Delta u_i^k \qquad (1.42)$$

Specifically,

- By accumulating Δu_N^k broadcasted from the subsystem N, the computation on $\Delta\beta_i^k$ can be accomplished at Processor i, where $i = 1,\ldots,N-1$.

- Referring to formulas $u_i^{k+1} = u_i^k + \alpha_u \Delta u_i^k$, $\beta_i^{k+1} = \beta_i^k + \eta\Delta\beta_i^k$, and $\tilde{\beta}_i^{k+2} = \beta_i^{k+1} + \eta\Delta\beta_i^k$, the variable updates, u_i^{k+1}, β_i^{k+1}, and $\tilde{\beta}_i^{k+2}$, can be accomplished in the processes i.

- Next, the state Δu_i^k at the first $N - 1$ subsystem can be accumulated to perform the calculation of $\Delta\beta_N^k$ in Processor N, and associated variable updates, $u_N^{k+1} = u_N^k + \alpha_u \Delta u_N^k$, $\beta_N^{k+1} = \beta_N^k + \eta\Delta\beta_N^k$, and $\tilde{\beta}_N^{k+2} = \beta_N^{k+1} + \eta\Delta\beta_N^k$, can be reached.

1.4.3 Computational Algorithm

In this position, the distributed computational algorithm developed in Figure 1.2 can be addressed in the following steps:

Step 1: The main power network is partitioned into the N subsystems, consisting of the boundary subsystem, accommodating all boundary buses, and the $N - 1$ non-overlapping subsystems. These subsystems are distributed to the N processors.

Step 2: For $i = 1, \ldots, N-1$, state variables, x_i^k and x_N^k, are initiated under the flat start at the initial iteration $k = 0$. The convergence tolerance ϵ is assigned.

Variables, $z_i^k, z_N^k, \beta_i^k, \tilde{\beta}_i^{k+1}, \beta_N^k, \tilde{\beta}_N^{k+1}$ and λ^k, are started from zero to iterate in processors.
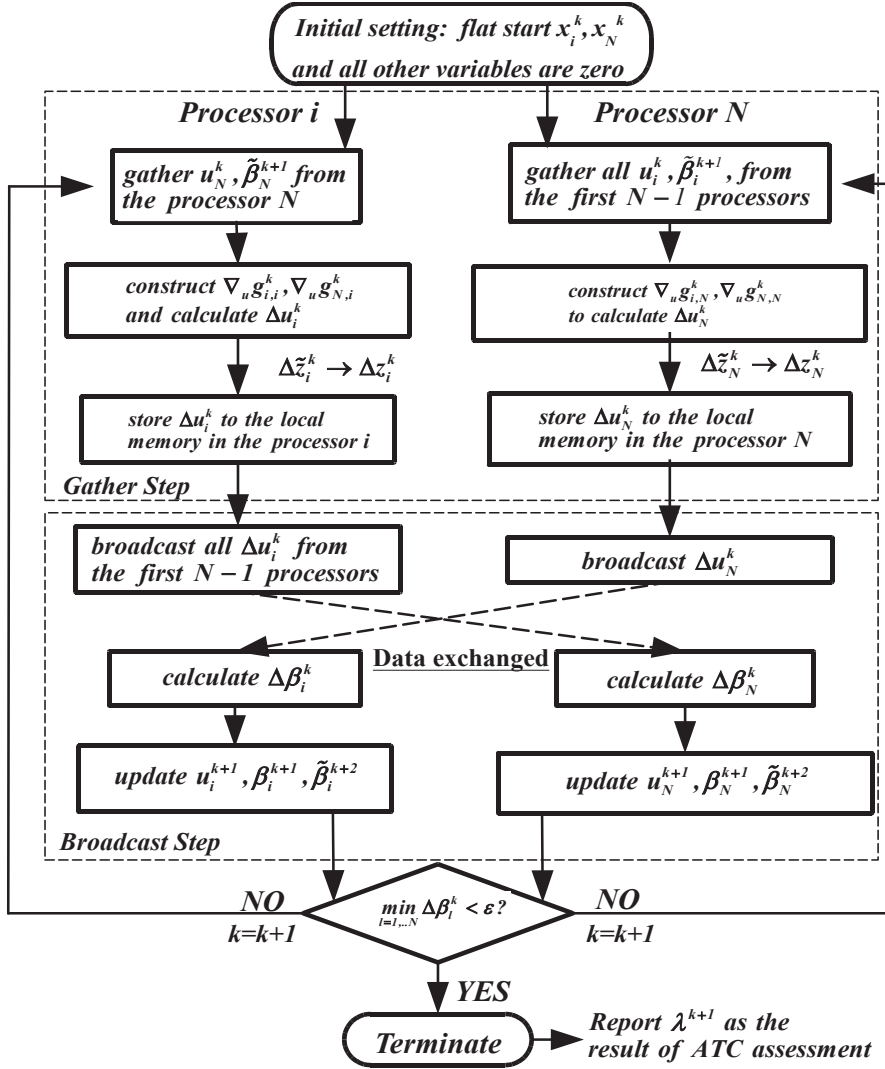
Figure 1.2   The flowchart of the iterative distributed algorithm. © [2015] IEEE. Reprinted, with permission, from IEEE Transactions on Smart Grid [30]

Step 3: In order to calculate the Jacobian matrices $\nabla_u g_{i,i}^k$ and $\nabla_u g_{N,i}^k$, the gathering step is to collect $\tilde{\beta}_N^{k+1}$ and u_N^k. By referring to (1.40), Δu_i^k can be determined. In addition, by assessing $\tilde{\beta}_i^{k+1}$ and u_i^k in the first $N-1$ distributed processors, the Jacobian matrix, $\nabla_u g_{i,N}^k$

Figure 1.3 System partition of IEEE 14-bus system © [2015] IEEE. Reprinted, with permission, from IEEE Transactions on Smart Grid [30]

and $\nabla_u g_{N,N}^k$, can be calculated. Equation (1.41) can be referred to generate Δu_i^k. Finally, the principle of (3.8) is utilized to correct Δz_N^k and Δz_i^k.

Step 4: Equation (1.42) can be referred for the broadcasting step. The state Δu_N^k, broadcasted from the processor N, is received in processor i and utilized to calculate $\Delta \beta_i^k$. Simultaneously, through accumulating Δu_i^k broadcasts from these $N-1$ processor, the calculation of $\Delta \beta_N^k$ can proceed concurrently. Subsequently, the update of variables in distributed processors can be accomplished.

Step 5: If the termination criterion $\min_{l=1,\ldots,N} \Delta \beta_l^k < \epsilon$ is checked, the iteration in all distributed processors stops. The final maximum loading parameter λ^{k+1} is reported as the ATC estimation. Otherwise, setting $k = k + 1$, the algorithm goes back to Step 3.

Figure 1.3 represents the system partition of the IEEE 14-bus system

1.5 Simulation Results

In this section, several IEEE test systems are utilized to conduct the numerical simulation to validate the proposed distributed ATC estimation accuracy. In the proposed ATC estimation, generator reactive power limits are included in the simulation analysis. The proposed algorithm can achieve the coordination between processors and perform data exchanging between boundary and non-overlapping subsystems. Thus, the validation of numerical stability in the proposed algorithm can be examined in the variables of the boundary

subsystem. Through examining the convergences for the boundary variables, the feasibility of the proposed method can be verified. Moreover, the self-healing mechanism in the proposed distributed framework is also verified. The robustness can be verified in the proposed distributed framework by considering line contingencies where the disconnection between subsystems occurs.
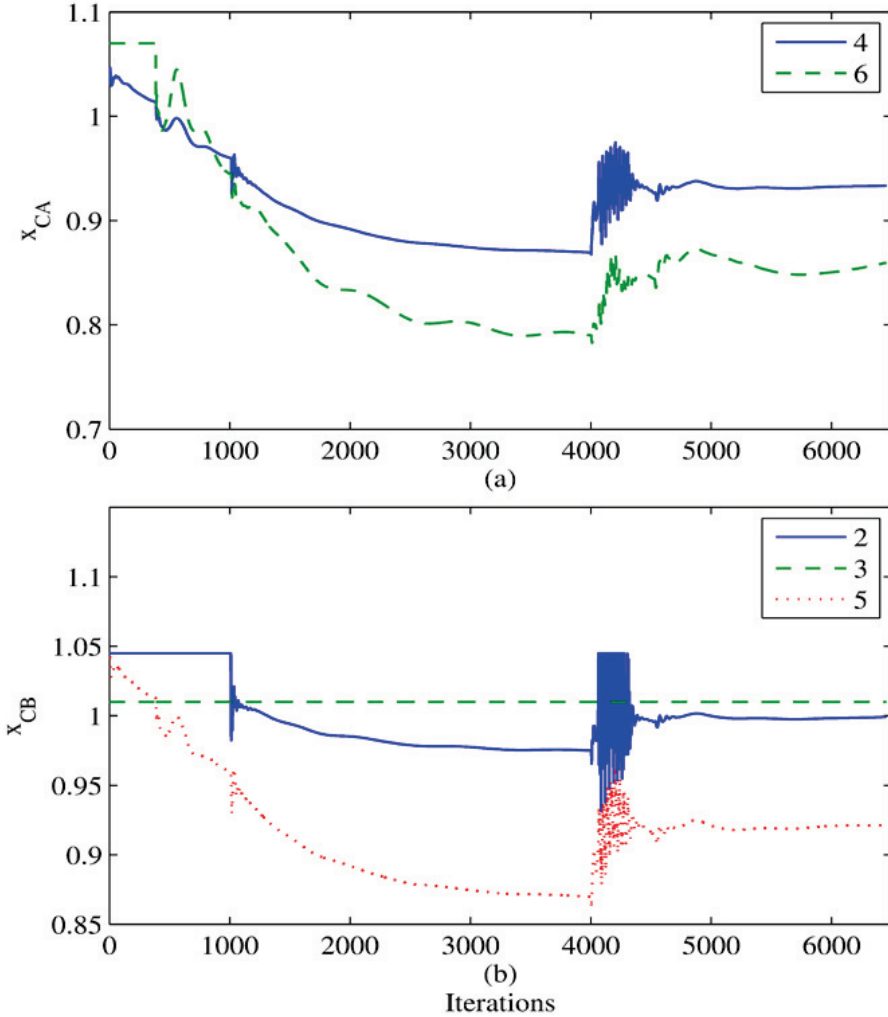
Figure 1.4   Boundary variables (a) x_{CA} and (b) x_{CB} in IEEE 14-bus system. © [2015] IEEE. Reprinted, with permission, from IEEE Transactions on Smart Grid [30]

1.5.1 IEEE 14-Bus Test System

In this section, the numerical simulations are conducted in the IEEE 14-bus test system. In the system, the variations on generator and load buses are utilized to form the power variations. The power direction, $\Delta P_i = \Delta Q_i = 0.1$, is given at the load bus i. The scheduled variation of the generator real power is designed by $\Delta P_j = 0.1$ at the generator bus j. The four generators, installed in buses 2, 3, 6, and 8, consider the reactive power limits and link to the inequality constraints formulated by the surplus variables z_1 to z_4. The reactive power limit is set by $-1 \leq z_{1,...4} \leq 1$. The system partition is designed in the IEEE 14-bus test system and depicted in Figure 1.3. For the area 1, the buses 4 and 6 are recognized as the boundary buses while the buses 2, 3, and 5 are collected as the boundary buses for the area 2.

By gathering all boundary buses to form the boundary subsystem C, two non-overlapping subsystems, A and B, can be constructed accordingly as depicted in Figure 1.3. Here, the boundary variable variation in the processor C is used to validate the convergent robustness of the proposed method. Besides, the case study considers the tripping of the two lines, addressed between bus 4-bus 7 and bus 4-bus 9, and is utilized to examine the self-healing mechanism in the proposed algorithm. In the proposed algorithm, the simulation specification, convergence tolerance $\epsilon = 10^{-3}$ under the settings $\alpha_u = 0.82$ and $\eta = 0.05$, is assumed. Also, it is assumed that this disconnection occurs at the iteration number of 4000.

With respect to processors A and B, the variations of the boundary variables x_{CA} and x_{CB} in processor C on the IEEE-14 bus system during the iterations of the proposed algorithm are depicted in Figure 1.4. Moreover, to the processors A and B, the boundary multipliers β_{CA} and β_{CB} in processor C are illustrated in Figure 1.5. Obviously, significant transient variations after the assumed disconnection between subsystems can be found in Figures 1.4 and Figure 1.5. It can be clearly observed that the proposed distributed algorithm has the adaption to the topology change of the distributed system since the numerical convergence of the boundary variables can attain.

Thus, the self-healing function can work and be guaranteed in the proposed algorithm. Furthermore, the comparison between the ATC estimation of the proposed algorithm and the one based on the Continuation Power Flow (CPFLOW) in PSAT [37] is conducted in Figure 1.6. Apparently, referring to the CPFLOW results, the maximal loading factor λ^2 of the proposed algorithm can be successfully changed from the pre-contingency state ($\lambda^2_{CPFLOW} = 2.6407$) to the post-contingency state ($\lambda^2_{CPFLOW} = 2.1376$) during this disconnection.
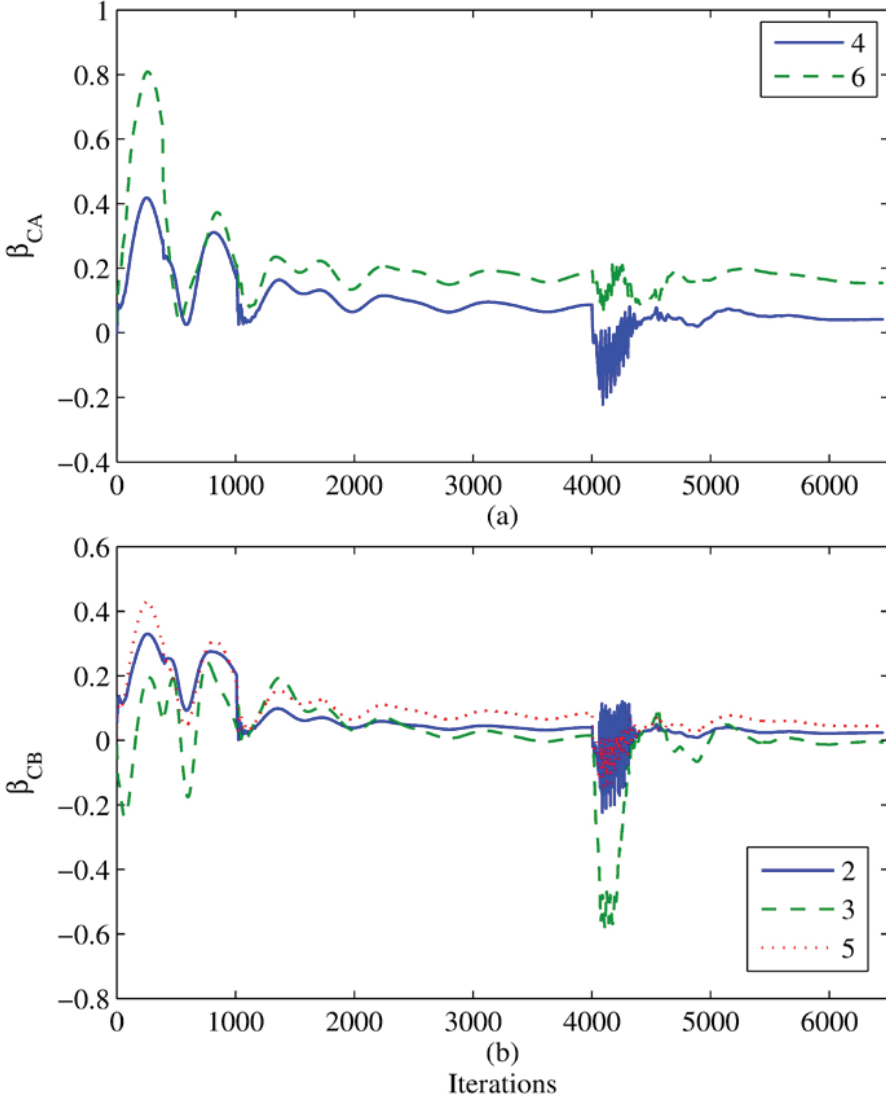
Figure 1.5   Multipliers (a) β_{CA} and (b) β_{CB} in IEEE 14-bus system. © [2015] IEEE. Reprinted, with permission, from IEEE Transactions on Smart Grid [30]

In addition, the convergence criterion, $\Delta\beta^* = min\Delta\beta_A, \Delta\beta_B, \Delta\beta_C \approx 0$, can also be examined in Figure 1.7 for the proposed algorithm, and the self-healing mechanism can be ensured evidently. Next, the generator reactive power limits are also examined in the proposed algorithm. In Figure 1.8, the
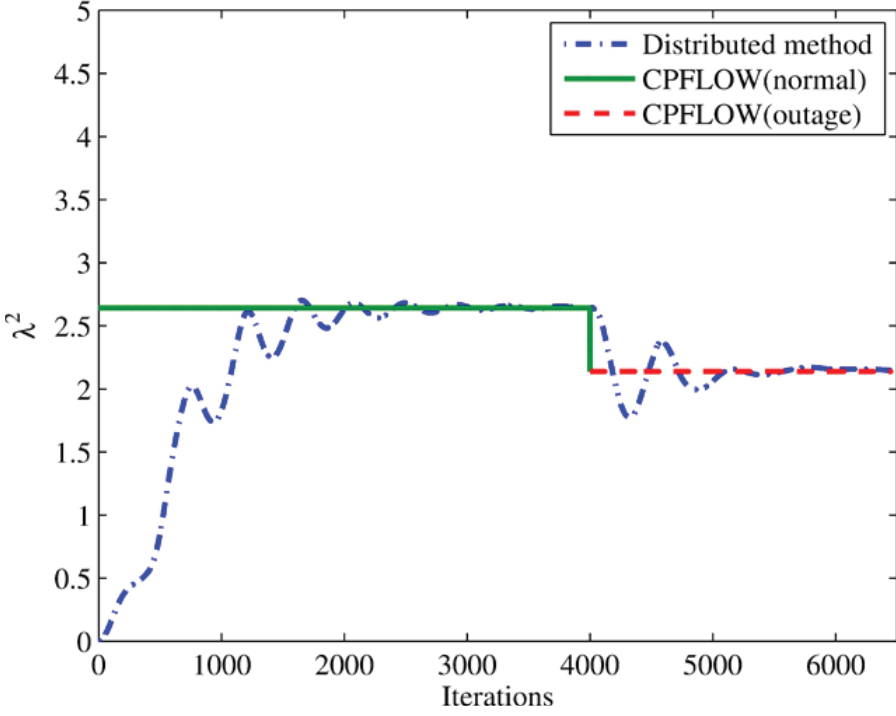
Figure 1.6 Maximal loading parameter λ^2 of Processor C in IEEE 14-bus system. © [2015] IEEE. Reprinted, with permission, from IEEE Transactions on Smart Grid [30]

surplus variables, z_1, z_3 and z_4, depict that the reactive power limits of the three generators reach under the limits, $-1 \le z_{1,\dots,4} \le 1$, during numerical iterations.

By further analyzing Figure 1.8, the three termination points, $\zeta 1$, $\zeta 2$, and $\zeta 3$ corresponding to the surplus variables z_1, z_3, and z_4, can be found and utilized to represent the case of hitting generator reactive power limits. Thus, the corresponding number of the numerical iterations at these three termination points can be addressed in Table 1.2. Certainly, the generator

Table 1.2 Iteration numbers at the points hitting the reactive power limits

Test systems	Location: Iteration Numbers
IEEE 14 bus	$\zeta 1$: 1000, $\zeta 2$: 400, $\zeta 3$: 1200
IEEE 57 bus	$\kappa 1$: 2000, $\kappa 2$: 3000, $\kappa 3$: 2500
IEEE 118 bus	$\xi 1$: 3.8×10^4, $\xi 2$: 1.9×10^4, $\xi 3$: 4×10^4, $\xi 4$: 3.1×10^4, $\xi 5$: 10^4, $\xi 6$: 1.9×10^4
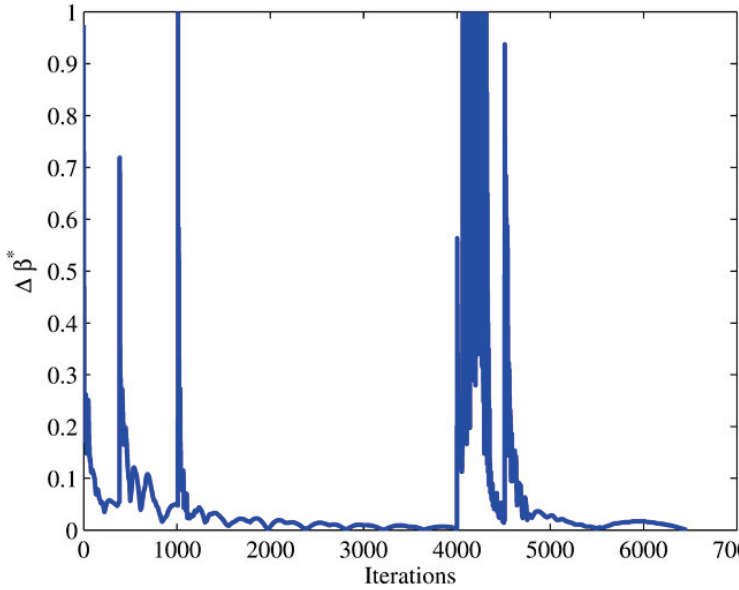
Figure 1.7   Minimal multiplier deviation $\Delta\beta^*$ of all processors in IEEE 14-bus system. ©
[2015] IEEE. Reprinted, with permission, from IEEE Transactions on Smart Grid [30]
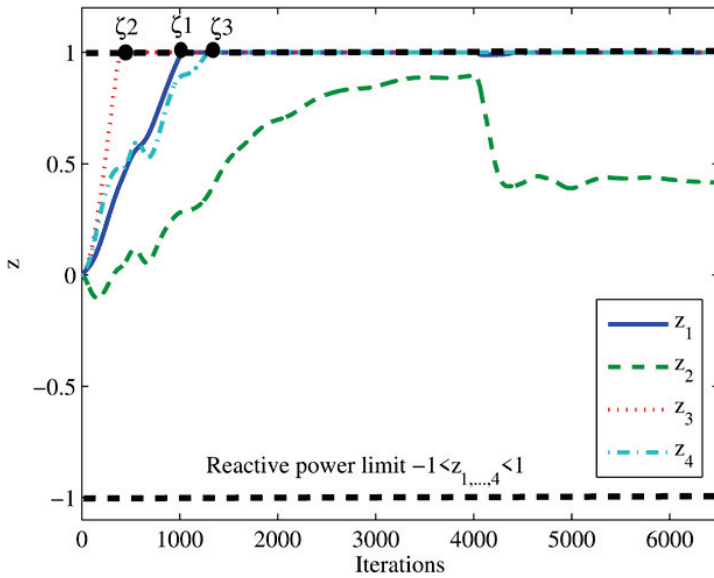
Figure 1.8   Surplus variables z_1 to z_4 under the reactive power limit $-1 \le z_{1,\ldots 4} \le 1$ in the
IEEE 14-bus system. © [2015] IEEE. Reprinted, with permission, from IEEE Transactions
on Smart Grid [30]

reactive power limits can also be reflected in the proposed algorithm, even for the circumstance of line outage, as shown in Figure 1.8. In this case, the surplus variables z_1, z_3, and z_4 finally settle down at a constant as their limits act. After the line outage, the surplus variable z_2 can react to the change. Therefore, the simulation results indeed reveal that the proposed algorithm can provide the self-healing mechanism against the system disturbance.

1.5.2 IEEE 57-Bus Test System

In this subsection, IEEE 57-bus is used to perform the numerical simulation of the proposed algorithm. In this case, the load direction is set by $\Delta P_i = 0.1$ and $\Delta Q_i = 0.2$ for the ith load bus while the generator real power variation is set by $\Delta P_j = 0.1$ for the jth generator bus. In the studied test system, seven generators are considered at buses 3, 6, 8, 9, 12, 28, and 29 under its reactive power limits. In the proposed algorithm, the seven generators correspond to the surplus variables, z_1 to z_7. In particular, the reactive power limits are assigned by $-1.5 \leq z_{1,...,4} \leq 1.5$ for the surplus variables z_1 to z_4 while the surplus variables, z_5 to z_7, are constrained by the reactive power limits $-0.5 \leq z_{5,...,7} \leq 0.5$. The studied test system can be partitioned into two subsystems, as depicted in Figure 1.9. In the partitioned system, by
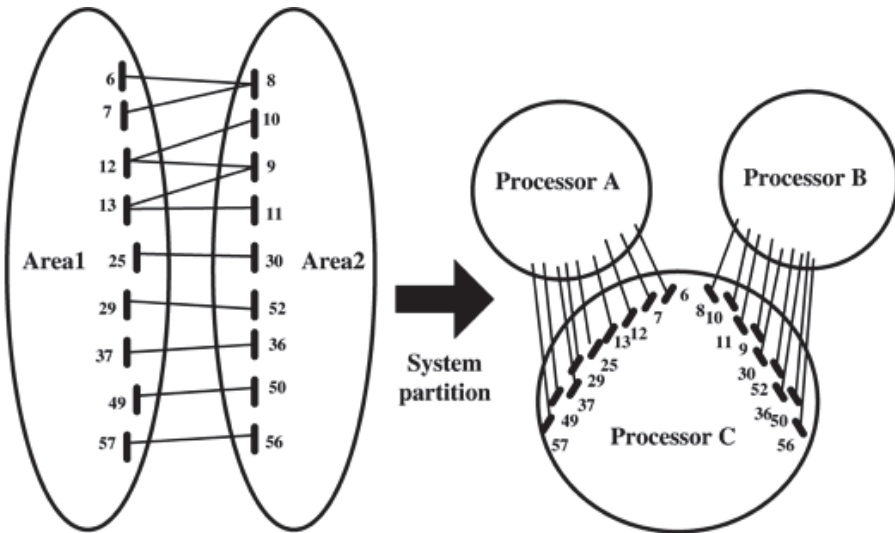
Figure 1.9 System partition of IEEE 57-bus system. © [2015] IEEE. Reprinted, with permission, from IEEE Transactions on Smart Grid [30]

gathering buses 8, 9, 10, 11, 30, 36, 50, 52, 56 from the second area and buses 7, 6, 13, 12, 25, 29, 49, 37, and 57 in the first area, the boundary buses
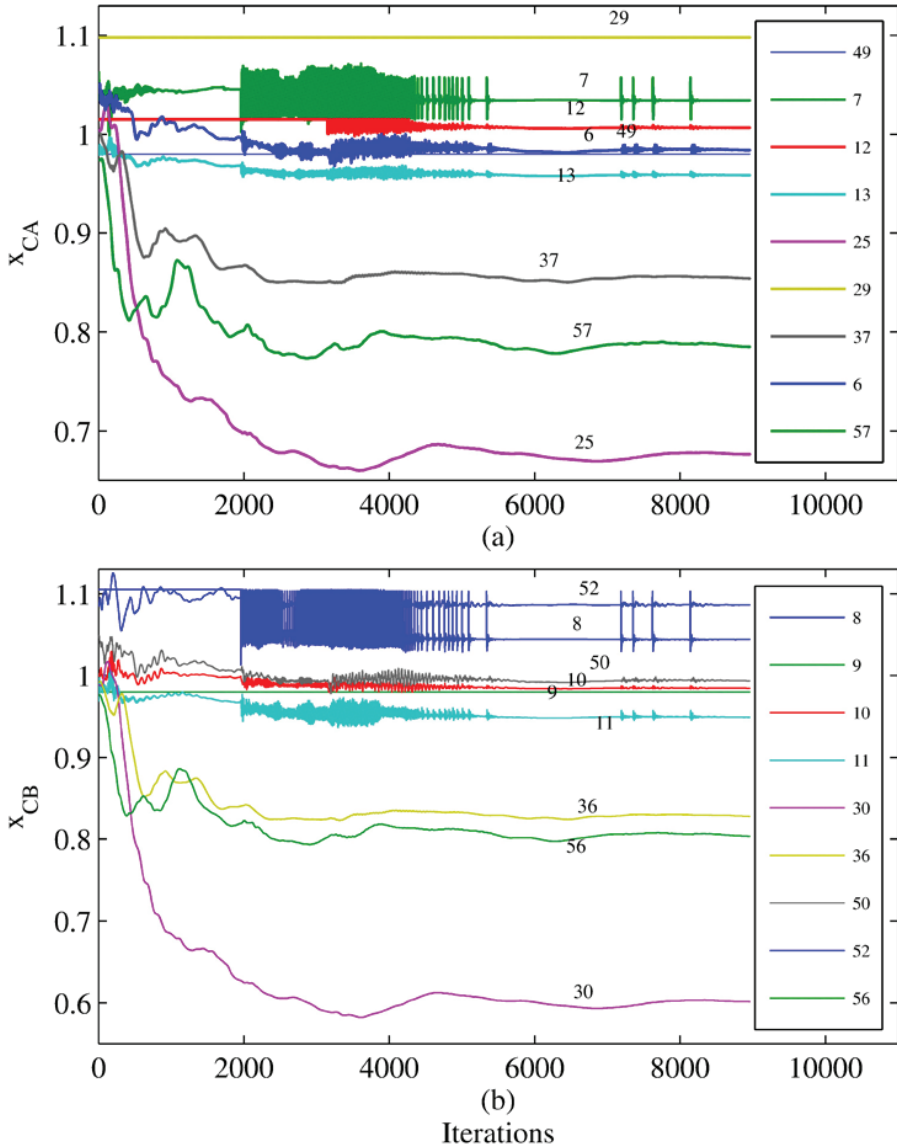
Figure 1.10   Boundary variables (a) x_{CA} and (b) x_{CB} in IEEE 57-bus system. © [2015] IEEE. Reprinted, with permission, from IEEE Transactions on Smart Grid [30]

can be formed. Furthermore, all boundary buses can be used to create the boundary subsystem C, and accordingly, the two associated non-overlapping subsystems, A and B, can be obtained, as illustrated in Figure 1.9. By examining the numerical convergence in boundary variables in the processor C, the practicality of the proposed distributed approach can be validated. In the simulation, the convergence tolerance is specified by $\epsilon = 10^{-3}$ under the parameter settings, $\eta = 0.03$ and $\alpha_u = 0.82$. With the coordination of processor C with processor's A and B, the numerical simulation results of the boundary variables, x_{CA} and x_{CB}, and boundary multipliers, β_{CA}, and β_{CB}, can be depicted in Figure 1.10 and Figure 1.11. It is noted that the number in the two figures indicates the numbers of the boundary buses. Figure 1.10 and Figure 1.11 clearly show the numerical convergence in the proposed distributed algorithm. Moreover, by examining the maximum loading parameter λ^2 in Figure 1.12, it clearly indicates that the proposed algorithm is feasible since the simulated maximum loading parameter finally reaches the actual one ($\lambda^2_{CPFLOW} = 2.1376$), as shown in Figure 1.12. On the other hand, through further examining the numerical convergence of the multiplier deviation, as shown in Figure 1.13, the numerical convergence of the proposed distributed algorithm can be guaranteed firmly.

During the numerical iterations, the surplus variables, z_3, z_5, and z_6, attain the upper reactive power limits, as shown in Figure 1.14. Specifically, according to the reactive power limit $-1.5 \leq z_{1,...,4} \leq 1.5$, the surplus variable z_3 reaches its limit, as shown in Figure 1.14(a) while the surplus variables, z_5 and z_6, arrive at their limits under the reactive power limit $-0.5 \leq z_{5,...,7} \leq 0.5$, as addressed in Figure 1.14(b). Also, the three termination points, κ_1, κ_2, and κ_3 corresponding to the surplus variables, z_3, z_5, and z_6, are illustrated in Figure 1.14 to indicate the encountering of the generator reactive power limits. Table 1.2 addresses the explicit number of the numerical iterations corresponding to the three termination points. In the proposed distributed algorithm, the two-phase projection principle is adopted to constrain the surplus variables under its operation limits when the surplus variables, z_3, z_5 and z_6, attain their operation limits.

1.5.3 IEEE 118-Bus Test System

In the IEEE 118-bus test system, the load direction b is defined by $\Delta P_i = \Delta Q_i = 0.1$ for load buses and $\Delta P_i = 0.1$ for generator buses. In the simulation, 38 generators are considered under the reactive power limits and corresponded to the surplus variables z_1 to z_{38}. The reactive power limits
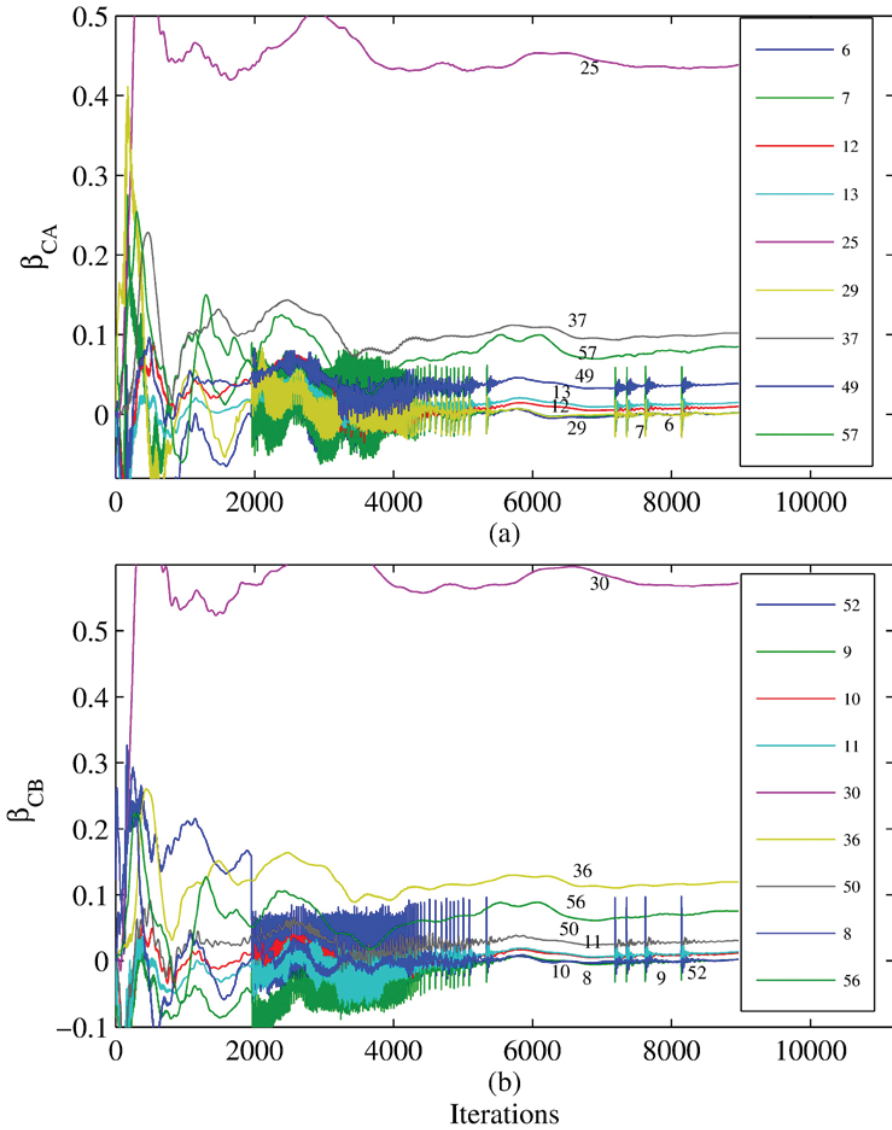
Figure 1.11   Multipliers (a) β_{CA} and (b) β_{CB} in IEEE 57-bus system. © [2015] IEEE. Reprinted, with permission, from IEEE Transactions on Smart Grid [30]

$-1.5 \leq z_{1,...,38} \leq 1.5$ are assigned to the surplus variables, z_1 to z_{38}. The partitioned system in the IEEE 118-bus test system can be illustrated in Figure 1.15. In the first area, the buses 19, 15, 30, and 23 are selected as the boundary
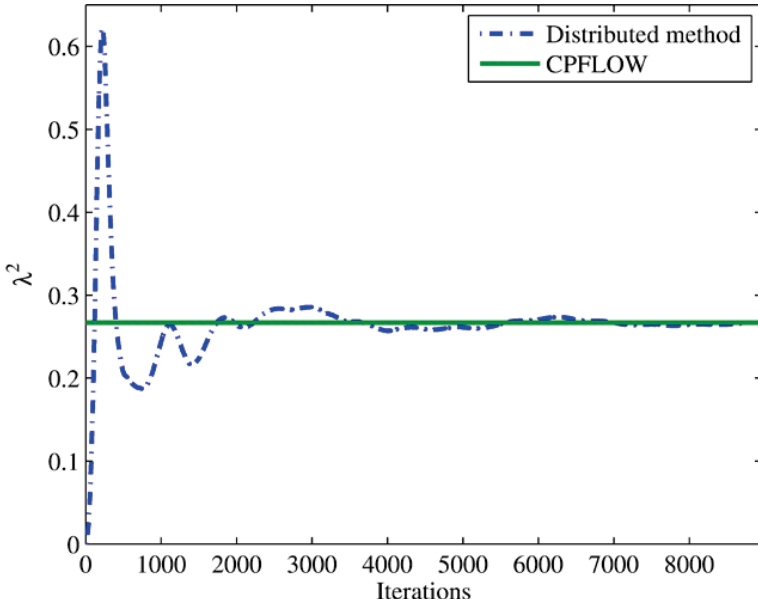
Figure 1.12 Maximal loading parameter λ^2 of Processor *C* in IEEE 57-bus system. ©
[2015] IEEE. Reprinted, with permission, from IEEE Transactions on Smart Grid [30]
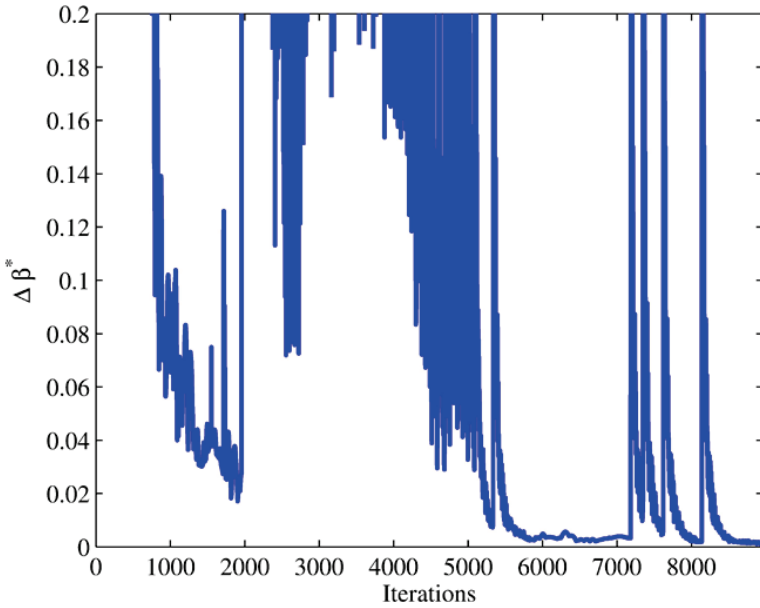
Figure 1.13 Minimal multiplier deviation $\Delta\beta^*$ of all processors in IEEE 57-bus system. ©
[2015] IEEE. Reprinted, with permission, from IEEE Transactions on Smart Grid [30]
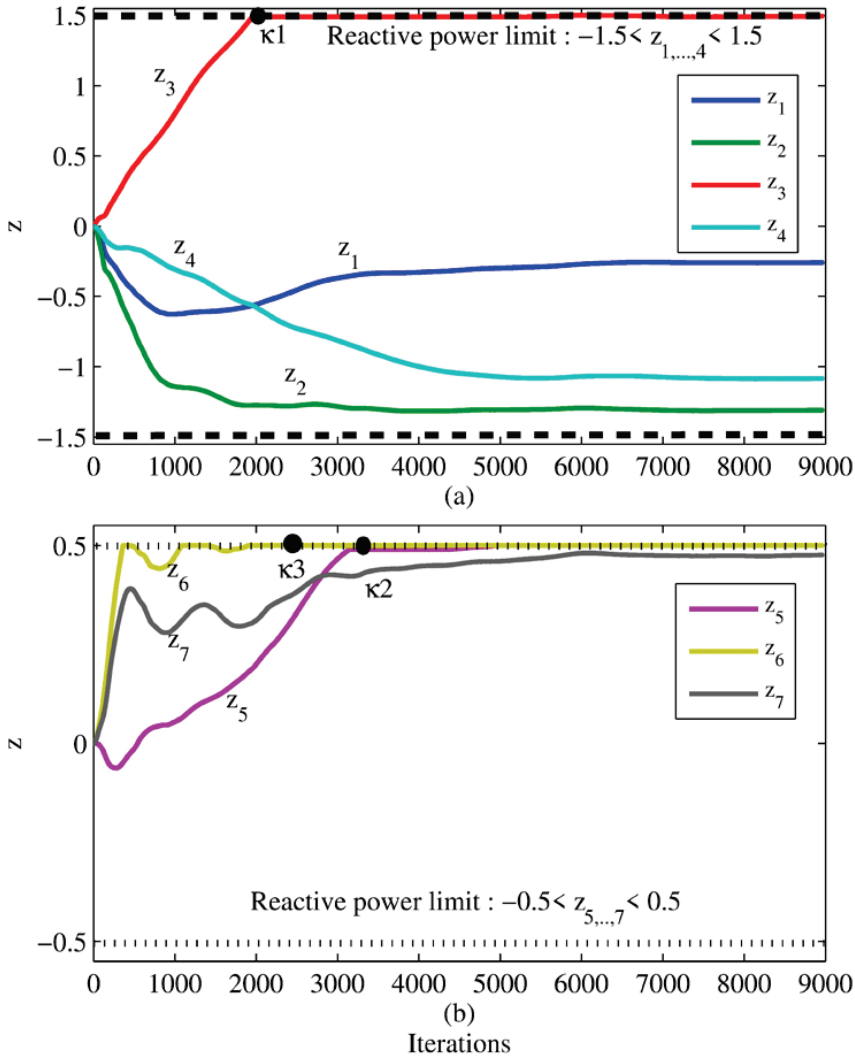
Figure 1.14 (a) Surplus variables z_1 to z_4 under the reactive power limit $-1.5 \leq z_{1,...,4} \leq 1.5$ and (b) z_5 to z_7 under the reactive power limit $-0.5 \leq z_{5,...,7} \leq 0.5$ in the IEEE 57-bus system. © [2015] IEEE. Reprinted, with permission, from IEEE Transactions on Smart Grid [30]

buses while the buses 34, 33, 68, 38, and 69 are designed as the boundary buses for the second area. In the third area, the boundary buses are identified as the buses 70, 24, 77, 75, and 81. All boundary buses are gathered as the boundary subsystem and assigned to the Processor D. Accordingly, the three
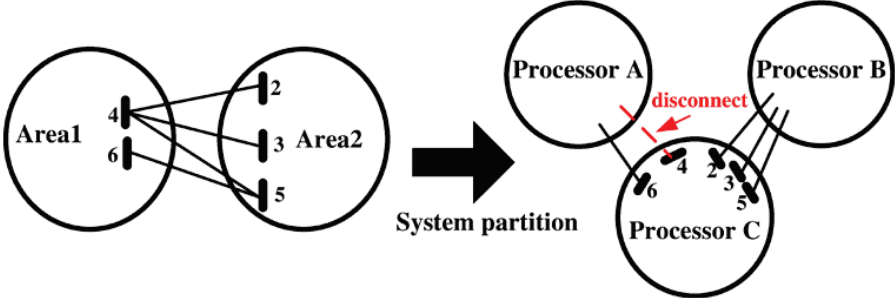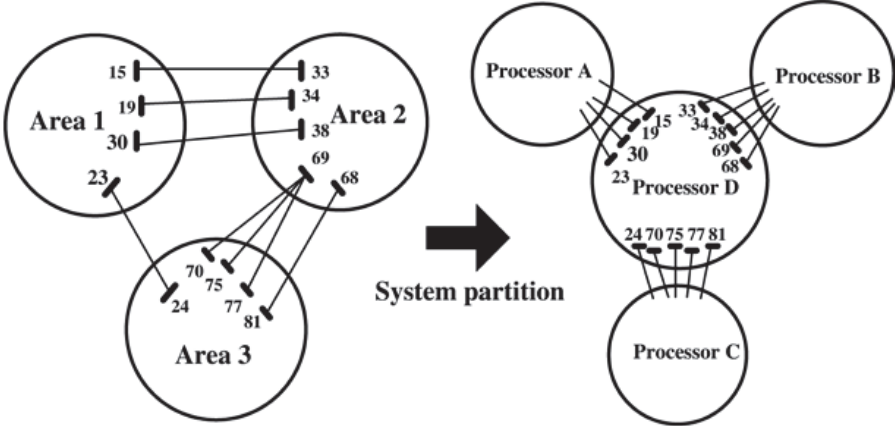
Figure 1.15 System partition of IEEE 118-bus system. © [2015] IEEE. Reprinted, with permission, from IEEE Transactions on Smart Grid [30]

non-overlapping subsystems are created and distributed to the Processors A, B, and C. Regarding the Processors A, B, and C, the boundary variables, x_{DA}, x_{DB}, and x_{DC}, and the boundary multipliers, β_{DA}, β_{DB}, and β_{DC}, in the Processor D can be depicted in Figure 1.16 and Figure 1.17. The boundary buses can be numbered in these two figures. In the simulation, the specification of the convergence tolerance is set by $\epsilon = 10^{-3}$ under the parameter settings $\eta = 0.008$ and $\alpha_u = 0.7$. Obviously, the numerical convergence can be found in the proposed algorithm by examining the boundary variables. Besides, the accurate maximum loading parameter λ^2 is also reported in the proposed algorithm by examining the CPFLOW result (λ^2_{CPFLOW}), as shown in Figure 1.18. The multiplier deviations, illustrated in Figure 1.19, are also examined and provide the guarantee of the numerical convergence in the proposed algorithm.

Next, the generator reactive power limits are also examined. In the simulation, six generators, corresponding to the surplus variables, z_6, z_{21}, z_{28}, z_{35}, z_{36}, and z_{37}, are located at the buses 49, 12, 77, 65, 85, and 80 and encounter the generator reactive power limits, as shown in Figure 1.20(a). Accordingly, it can be observed that the six surplus variables reach the upper operation limits while other surplus variables are depicted in Figure 1.20(b). In Figure 1.20(a), there exist six termination points, $\xi 1$ to $\xi 6$, indicating that the six surplus variables attain their upper operation limits. The number of the numerical iterations at the six termination points can be detailed in Table 1.2.
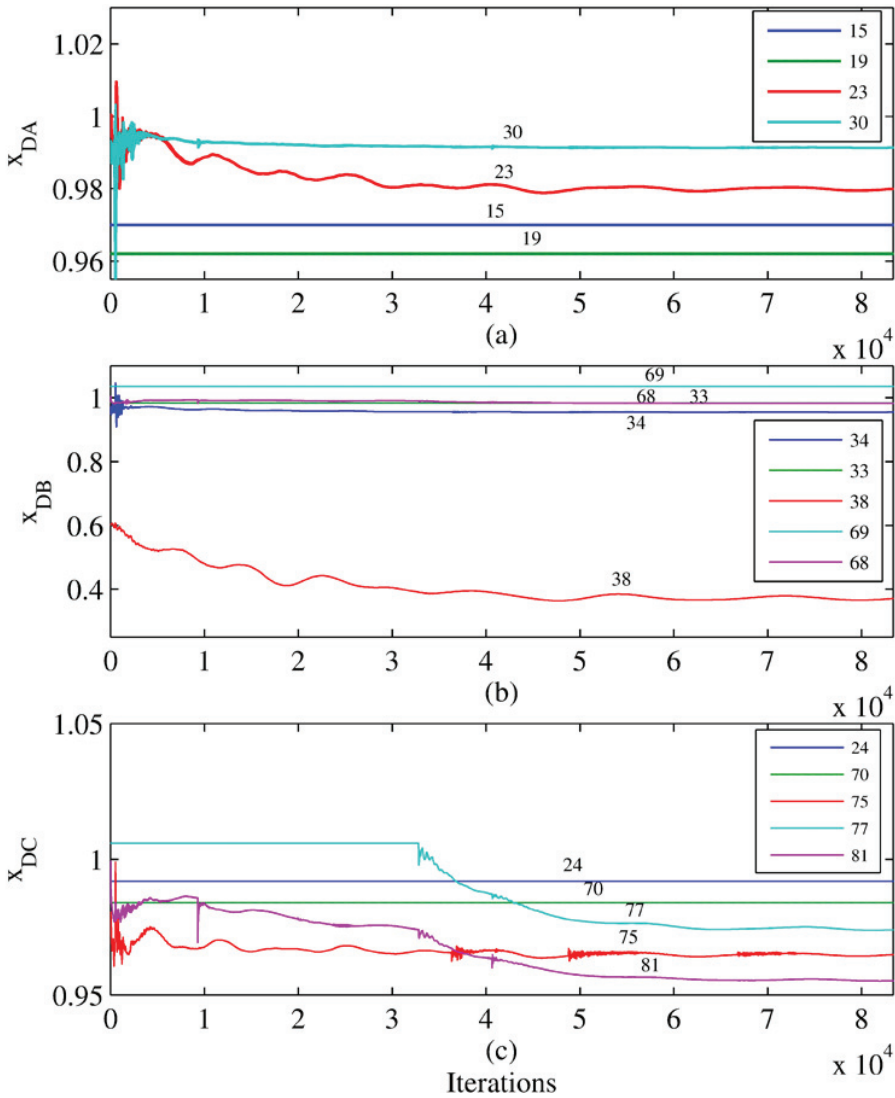
Figure 1.16   Boundary variables (a) x_{DA}, (b) x_{DB} and (c) x_{DC} in IEEE 118-bus system. ©
[2015] IEEE. Reprinted, with permission, from IEEE Transactions on Smart Grid [30]
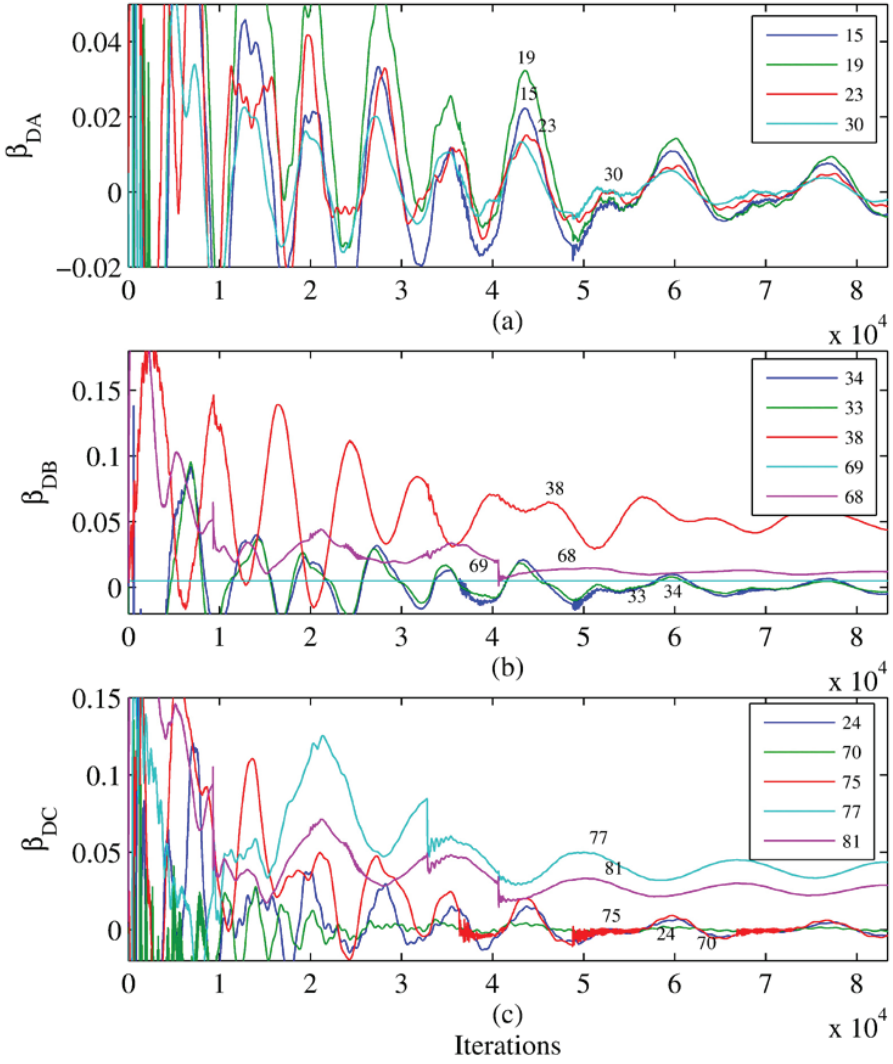
Figure 1.17 Multipliers (a) β_{DA}, (b) β_{DB} and (c) β_{DC} in IEEE 118-bus system. © [2015] IEEE. Reprinted, with permission, from IEEE Transactions on Smart Grid [30]
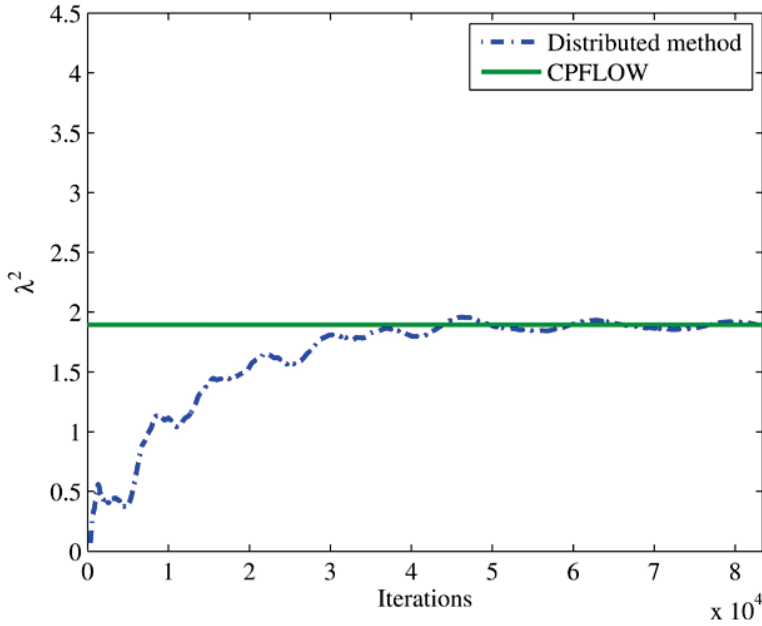
Figure 1.18 Maximal loading parameter λ^2 of Processor D in IEEE 118-bus system. ©
[2015] IEEE. Reprinted, with permission, from IEEE Transactions on Smart Grid [30]
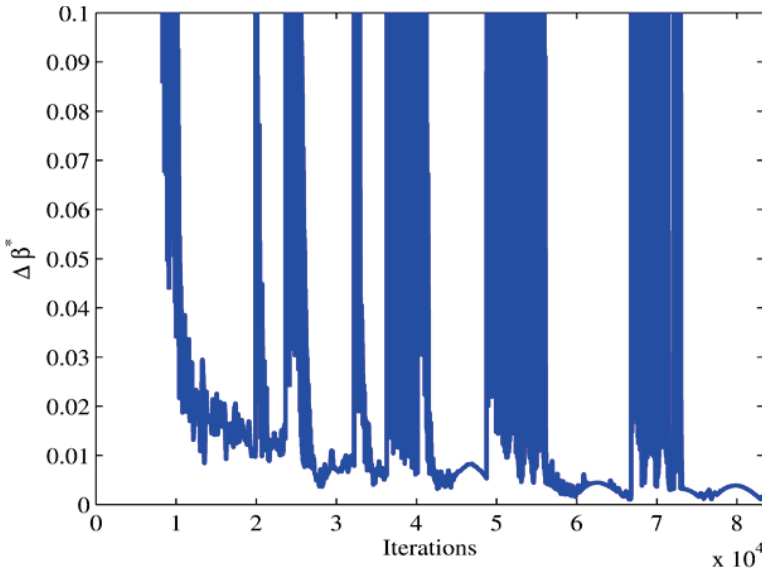
Figure 1.19 Minimal multiplier deviation $\Delta\beta^*$ of all processors in IEEE 118-bus system.
© [2015] IEEE. Reprinted, with permission, from IEEE Transactions on Smart Grid [30]
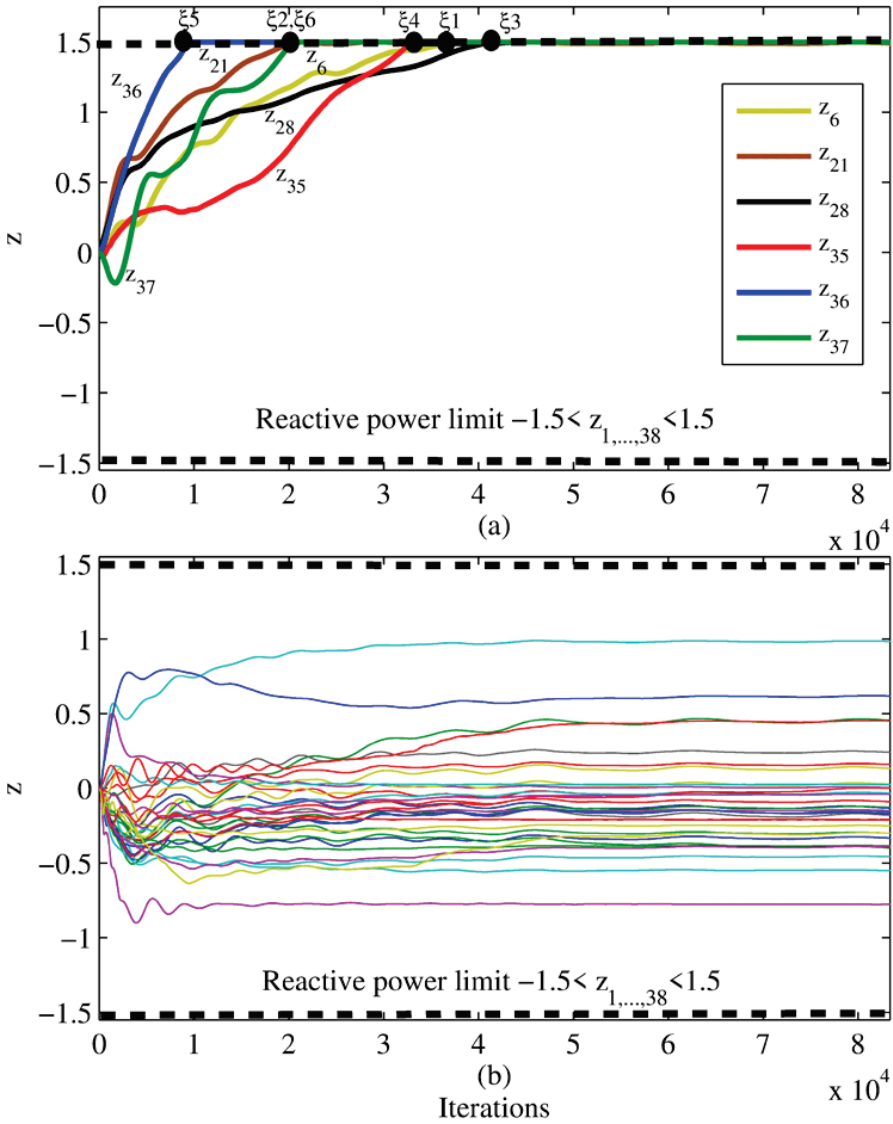
Figure 1.20 (a) Six surplus variables z_6, z_{21}, z_{28}, z_{35}, z_{36}, and z_{37}, and (b) other surplus variables under the reactive power limit $-1.5 \leq z_{1,...,38} \leq 1.5$ in the IEEE 118-bus system. © [2015] IEEE. Reprinted, with permission, from IEEE Transactions on Smart Grid [30]

1.6 Conclusion

In the proposed algorithm, the ATC estimation is formulated as a particular non-linear OPF optimization problem. Thus, a distributed iterative algorithm based on constrained augmented Lagrangian is proposed for the real-time ATC estimation. Specifically, three technical advances are addressed as follows:

- Three distributed schemes, including (i) Predictor-Corrector Proximal Multiplier (PCPM) method, (ii) Auxiliary Problem Principle Method (APPM), and (iii) Alternative Direction Multiplier Method (ADMM), have been investigated for distributed ATC estimation.
- By analyzing the three distributed algorithms, it can be concluded that PCPM or ADMM is a special case of APPM in the iterative distributed ATC estimation problem. Therefore, APPM is selected to develop the proposed iterative distributed algorithm for the real-time ATC estimation.
- The partition of the main system is investigated and leads to a boundary subsystem and several non-overlapping subsystems.

Three IEEE test systems are utilized to conduct numerical simulations to verify the efficiency of the proposed iterative distributed ATC assessment. In the proposed distributed algorithm, the generator reactive power limit can be included in the real-time ATC estimation.

References

[1] A. R. Bergen and V. Vittal, *Power System Analysis*, 2nd ed., New Jersey, Prentice Hall, 2000.

[2] G. C. Ejebe, J. Tong, J. G. Waight, J. G. Frame, X. Wang, and W. F. Tinney, "Available transfer capability calculations," *IEEE Trans. on Power Systems*, vol. 13, no. 4, pp. 1521–1527, November 1995.

[3] H. D. Chiang and H. Li, "On-Line ATC Evaluation for Large-Scale Power Systems: Framework and Tool," Ch. 5 of *Applied Mathematics for Restructured Electric Power Systems*, Spring-Verlag, 2005.

[4] L. Min and A. Abur, "Total transfer capability computation for multi-area power systems," *IEEE Trans. on Power Systems*, vol. 21, no. 3, pp. 1141–1147, August 2006.

[5] C. A. Canizares, F. L. Alvarado, C. L. DeMarco, I. Dobson, and W. F. Long, "Point of collapse methods applied to AC/DC power

systems," *IEEE Trans. on Power Systems*, vol. 7, no. 2, pp. 673–683, May 1992.

[6] V. Ajjarapu and C. Christy, "The continuation power flow: a tool for steady state voltage stability analysis," *IEEE Trans. on Power Systems*, vol. 7, no. 1, pp. 416–422, February 1992.

[7] H. D. Chiang, A. J. Flueck, K. S. Shah, and N. Balu, "CPFLOW: a practical tool for tracing power system steady-state stationary behavior due to load and generation variation," *IEEE Trans. on Power Systems*, vol. 10, no. 2, pp. 623–633, May 1995.

[8] I. Dobson, "Computing a closest bifurcation instability in multidimensional parameter space," *Journal of Nonlinear Science*, vol. 3, no. 1, pp. 307–327, 1993.

[9] C. A. Canizares, "Calculating optimal system parameters to maximize the distance to saddle-node bifurcations," *IEEE Trans. on Circuit and Systems-I Fundamental Theory and Applications*, vol. 45, no. 3, pp. 225–237, March 1998.

[10] G. D. Irisarri, X. Wang, J. Tong, and S. Mokhtari, "Maximum loadability of power systems using interior point nonlinear optimization method," *IEEE Trans. on Power Systems*, vol. 12, no. 1, pp. 6162–172, February 1997.

[11] A. G. Bakirzis and P. N. Biskas, "A decentralized solution to the DC-OPF of interconnected power systems," *IEEE Trans. on Power Systems*, vol. 18, no. 3, pp. 1007–1013, August 2003.

[12] C. H. Lin and S. Y. Lin, "Distributed optimal power flow with discrete control variables of large distributed power systems," *IEEE Trans. on Power Systems*, vol. 23, no. 3, pp. 1383–1392, August 2008.

[13] B. H. Kim and R. Baldick, "Coarse-grained distributed optimal power flow," *IEEE Trans. on Power Systems*, vol. 12, no. 2, pp. 932–939, May 1997.

[14] B. H. Kim and R. Baldick, "A comparison of distributed optimal power flow algorithms," *IEEE Trans. on Power Systems*, vol. 15, no. 2, pp. 599–604, May 2000.

[15] S. Talukdar and V. C. Rameh, "A multi-agent technique for contingency constrained optimal power flows," *IEEE Trans. on Power Systems*, vol. 9, no. 2, pp. 855–861, May 1994.

[16] W. Yan, L. Wen, W. Li, C. Y. Chung, and K. P. Wong, "Decomposition–coordination interior point method and its application to multi-area optimal reactive power flow," *Int. J. Electric Power and Energy Systems*, vol. 33, no. 1, pp. 55–60, January 2011.

[17] J. Contreras, A. Losi, M. Russo, and F. F. Wu, "Simulation and evaluation of optimization problem solutions in distributed energy management systems," *IEEE Trans. on Power Systems*, vol. 17, no. 1, pp. 57–62, February 2002.

[18] R. Ebrahimian and R. Baldick, "State estimation distributed processing," *IEEE Trans. on Power Systems*, vol. 15, no. 14, pp. 1240–1246, November 2000.

[19] D. M. Falcao, F. F. Wu, and L. Murphy, "Parallel and distributed state estimation," *IEEE Trans. on Power Systems*, vol. 10, no. 2, pp. 724–730, May 1995.

[20] P. Sulc, S. Backhaus, and M. Chertkov, "Optimal distributed control of reactive power via the alternating direction method of multipliers," *arXiv preprint arXiv:1310.5748*, 2013.

[21] Q. Yang, J. A. Barria, and T. C. Green, "Communication infrastructures for distributed control of power distribution networks," *IEEE Trans. on Industrial Informatics*, vol. 7, no. 2, pp. 316–327, May 2011.

[22] Q. Morante, N. Ranaldo, A. Vaccaro, and E. Zimeo, "Pervasive grid for large-scale power systems contingency analysis," *IEEE Trans. on Industrial Informatics*, vol. 2, no. 3, pp. 165–175, August 2006.

[23] J. Zhao, P. Xu, and F. S. Chen, "A distributed computation method for voltage stability assessment of a sub-grid within the large interconnected power system," *17th power system computation conference*, Stockholm, Sweden, August 22-26, 2011.

[24] L. Xie, Y. Chen, and H. Liao, "Distributed online monitoring of quasi-static voltage collapse in multi-area power systems," *IEEE Trans. on Power Systems*, vol. 27, no. 4, pp. 2271–2279, November 2012.

[25] N. Fabian Avila and C. C. Chu, "Distributed probabilistic ATC assessment by optimality conditions decomposition and LHS considering intermittent wind power generation," *IEEE Trans. on Sustainable Energy*, vol. 10, no. 1, pp. 375-385, Jan. 2019.

[26] S. Kesherwani, S. C. Srivastava, and A. Mohapatra, "Synchrophasor measurement-based approach for online available transfer capability evaluation," *IET Gener. Trans. Distrib.*, vol. 13, no. 17, pp. 3941–3950, Sept. 2019.

[27] J. D. Pinzon and D. G. Colome, "Real-time multi-state classification of short-term voltage stability based on multivariate time series machine learning," *International Journal of Electrical Power & Energy System.*, vol. 108, pp. 402–414, June 2019.

[28] D. Shukla, and S. P. Singh, "Real-time estimation of ATC using PMU data and ANN," *IET Gener. Trans. Distrib.*, vol. 14, no. 17, pp. 3604–3616, Sept. 2020.

[29] K. D. Dharmapala, A. Rajapakse, K. Narendra, and Y. Zhang, "Machine learning based real-time monitoring of long-term voltage stability using voltage stability indices," *IEEE Access*, vol. 8, pp. 222544 - 222555, Dec. 2020.

[30] J. H. Liu and C. C. Chu, "Iterative distributed algorithms for real-time available transfer capability assessment of multiarea power systems," *IEEE Trans. on Smart Grid*, vol. 6, no. 5, pp. 2569-2578, September 2015.

[31] S. Boyd, N. Parikh, E. Chu, B. Peleato, and J. Eckstein, "Distributed optimization and statistical learning via the alternating direction method of multipliers," Stanford University, Stanford, CA, Technical Report, January 2011.

[32] C. H. Lin and S. Y. Lin, "A new dual-type method used in solving optimal power flow problems," *IEEE Trans. on Power Systems*, vol. 12, no. 4, pp. 1667–1675, November 1997.

[33] G. Chen and M. Teboulle, "A proximal-based decomposition method for convex minimization problems," *Math. Programming*, vol. 64, pp. 81–101, 1994.

[34] G. Cohen, "Auxiliary problem principle and decomposition of optimization problems," *Journal of Optimization Theory and Application*, vol. 32, no. 3, pp. 277–305, November 1980.

[35] G. Cohen, "Optimization by decomposition and coordination: a unified approach," *IEEE Trans. on Automatic Control*, vol. AC-32, no. 2, pp. 222–232, April 1978.

[36] M. Shahidehpour and Y. Wang, *Communication and Control in Electric Power Systems, Application of Parallel and Distributed Processing*. Piscataway, NJ: IEEE Press, pp. 47–192, 2003.

[37] Federico Milano, "Power System Analysis Toolbox (PSAT)," version 2.0.0, February 2008.

2

Hybrid Harmony Search and Modified Harmony Search Optimizations Performance in Economical Load Dispatch

Tanmoy Mulo, Amalendu Bikash Choudhury, and Prasid Syam

Dept. of Electrical Eng., Indian Institute of Engineering Science and Technology, Shibpur, India
E-mail: tmulo.nit.dgp@gmail.com; ab_choudhury@yahoo.com; prasidsyam@gmail.com

Abstract

New optimization methods are an essential tools to analyze the performance of modern hybrid grids appropriately. Multiple hybridizations are performed in the basic conventional optimization methods available such as Genetic Algorithm (GA), Particle Swarm Optimization (PSO), Differential Evolutionary (DE), and Harmony Search (HS). Limitations noticed in existing methods, (i) high complexity and large convergence time in GA, (ii) large convergence time in case of PSO, (iii) initial population size for DE, and (iv) frequent use of memory in HS. The Modified Harmony Search (MHS) algorithm reaches a global optimum solution on harmony memory, and Hybrid Harmony Search (HHS) is of PSO, DE, and HS. Both methods are applied in the Economical Load Dispatch requirement (ELD). Initially, proposed methods, PSO, and GA have been applied for a six-unit system, which includes six thermal units, forty-six transmission paths, and twenty-six buses. It is observed that the proposed MHS provides a better loss minimization. Further study has been performed on fifteen, twenty, and forty-unit systems using the MHS method. It is observed that in the fifteen-unit system, the proposed MHS method provides improved performance in terms of both loss and cost minimization

as compared to PSO [1] and GA (RANKSUM method). In twenty and forty-unit systems, MHS gives a better solution.

Keywords: Differential evolutionary (DE), economic load dispatch (ELD), genetic algorithm (GA), harmony search (HS), hybrid harmony search (HHS), modified harmony search (MHS), particle swarm optimization (PSO).

2.1 Introduction

Electricity is an essential requirement in every aspect of our daily life. The electric supply and interconnected grid are increasing regularly to provide reliable load demand from the electric supply or grid. As the load demand is increasing, the reliability, quality, and quantity should be maintained properly. As a result, the grid voltage and connection become hybrid and complex. In order to minimize the total generation cost, Economical Load Dispatch (ELD) of the power system requires an optimization technique and all units should run within the highest and lowest limits of generation capacities. Earlier this problem of ELD was solved by numerous techniques such as the participation factor technique, gradient technique, and Lambda-iteration technique [2, 3]. These methods essentially require the incremental cost curve which is dependent on cost coefficient values, so the cost value is not constant and non-linear throughout the operation. Hence the Genetic Algorithm (GA) technique is used in optimizing these sets of problems of ELD. Deficiencies still persist in GA such as complexity and larger execution time. Even though the problem of larger execution time is solved by interconnected personal computers using TCP/IP socket [4], still complexity persists. The Particle Swarm Optimization (PSO) [5] was introduced in 1995 which is faster than GA. But it also has a drawback in that it takes more time to reach a global solution. In 2011, the researchers Rocca, P. Olivery, and G. Massa invented the Differential evolutionary algorithm which is the fastest algorithm till now [6]. However, it has been seen that for a small number of initial populations, the Differential Evolutionary optimization [7] technique does not converge exactly to the best or optimal solution [8] among all feasible solutions. In the year 2001, harmony search [9] was invented by Zong Woo Geem et al. in 2001 [10]. Nevertheless, this method is more dependent on harmony memory. The Harmony Search-Opposition Based Learning technique (HS-OBL) [9] is used effectively so as to protect the solutions not to getting trapped into local optimum.

Here a modified Harmony Search technique [11] has been proposed which is faster than DE in certain aspects (details in section 2.6). This is a study of two proposed methods, one MHS [12] and Hybrid Harmony Search technique (HHS). The primary objective is to utilize exact operations using both methods [6, 13–15] to solve ELD problems.

2.2 Equality and Inequality Constraints

The ELD is a major requirement to estimate the generators' output (MW) [16] of a given operating region which will be satisfied to obtain the consumer demand (nearly). Unit Commitment (UC) is defined as a polynomial or quadratic equation-based optimization-related issue. A set of different combination units, i.e., kVA loading of the generators is written down periodically throughout the operation. Different optimization techniques have been applied to the recorded data; the optimal and best generation will be uploaded [17] in the output among all operating unit ranges. Those units are calculated eventually to satisfy the system load or consumer demand without disturbing the operating constraints of generating units [1].

2.2.1 Actual Operation Constraints of Generator

The operating cost of input in a power station may be expressed in $/h. The system may also be a microgrid system [18]. The fuel-price vs. generator output characteristics can be obtained by fitting a polynomial curve which is a function of active power and is represented as:

$$f\left(P_{gi}\right) = \mu_i P_{gi}{}^2 + \theta_i + \delta_i \tag{2.1}$$

where
$f(P_{gi})$ = fuel cost of ith thermal unit.

P_{gi} = Real power supplied by of ith generator
$\mu_i \theta_i \delta_i$ are generating units' constants

$$\sum_{i=1}^{m} P_{gi} = P_L + P_D \tag{2.2}$$

where
P_L = Total line losses (in MW)

P_D = Total consumer demand (in MW)

2.2.2 Inequality Constraints

Generator constraints

The thermal limit must not exceed under certain kVA loading of the generators. The highest and lowest, real and reactive powers respectively, are restricted by the thermal constraint so that the rise in temperature should be constant within limits.

$$P_{\min} \leq P \leq P_{\max}$$
$$Q_{\min} \leq Q \leq Q_{\max} \tag{2.3}$$

where P_{min}, and P_{max} are real output powers at the lowest and highest limit operating region of the generation units respectively (in MW).

Q_{min}, and Q_{max} are reactive output powers at the lowest and highest level operating range of the generation units (in MVAR).

Loss constraints

$$P_L = \sum_{i=1}^{m} \sum_{j=1}^{m} P_i B_{ij} P_j + \sum_{i=1}^{m} B_{0i} P_i + B_{00} \tag{2.4}$$

Cost of Operation Equations

$$FV = \sum_{i=1}^{m} f_i \left(P_{gi} \right) \tag{2.5}$$

2.3 Generalized Harmony Search Algorithms

In 2001, Zong Woo Geem, Joong Hoon Kim, and G.V. Loganathan originally introduced the Harmony Search method inspired by the phenomenon of– mimicking metaheuristic optimization search. MHS as an optimization [19] tool provides a search process where, after each functional evaluation, the new set of values is updated in the harmony memory. The values that are generated depend on the constant value of the rate of Harmony Memory Consideration (HMRC) and Pitch Adjusting Rate (PAR). Let X indicates the initial set of values. HMRC and PAR are two constant values. The ith values of X are given below:

$$X_i = [X_{i1}, X_{i2}, ...,X_{id}] \tag{2.6}$$

where d is dimension space which also represents total variables, i=1 to 10 (as the population is ten). Now this X_{10xd} passes through the objective function

and evaluates the fitness values. The fitness values along with the X variable create a harmonious memory matrix which contains elements as below:

$$HMM_i = [X_{i1}, X_{i2}, \ldots\ldots\ldots, X_{id}, f_i([X_{i1}, X_{i2}, .., X_{id}])] \qquad (2.7)$$

Based on their fitness values, the values in the harmony memory matrix are arranged in ascending order $f_1 < f_2 < f_3 < f_4 \ldots\ldots\ldots < f_{10}$.

The dimension of the Harmony Memory Matrix (HMM) is 10*(d+1). HMRC and PAR parameters are control loops for generating new $(k+1)^{th}$ value of X variable as shown below.

$$X_{k+1} = \begin{cases} HMM_1\,(X_{11}, X_{12}, \ldots\ldots\ldots X_{1d}) \\ HMM_1\,(X_{11} + \Delta X, X_{12} + \Delta X, \ldots\ldots X_{1d} + \Delta X) \\ Random\ value\ \left(X_{11\,Min}^{\,Max}, X_{12\,Min}^{\,Max}, \ldots\ldots X_{1d\,Min}^{\,Max}\right) \end{cases} \qquad (2.8)$$

In (2.8) first value is taken from the harmony matrix which is the first row without fitness value. The second data can be selected from the first values with some delta amount of shift and in the third case, values are generated randomly within the maximum and minimum range as given for all the d dimension variables. The HMM matrix is updated with new values of X_{k+1} and corresponding fitness values are as per the condition mentioned:

$$f(X_{k+1}) < f_1$$

$$HMM_1 = X_{k+1}, f(X_{k+1})) \qquad (2.9)$$

Eq. (2.9) is applicable only in the case of first value updation and the rest nine values can be updated by the following condition:

$$f_j < f(X_{k+1}) \le f_{j+1}$$
$$HMM_{j+1} = (X_{k+1}, f(X_{k+1})) \qquad (2.10)$$

where j=1 to 9 and k=1 to the number of functional evaluations or similar term to the number of iterations (e.g. 10000, Table-2.4).

2.4 Details of Modified Harmony Search Optimization with Flowchart

FIRST STEP: MHS method also consists of four parameters such as HMM, HMRC, PAR, and X (variables) as in the normal HS method. In between them HMRC and PAR are two fixed value parameters having values are 0.9 and

0.1 respectively. Here the X variable is taken as six values (six units' system) and according to that HMM can be created which is denoted as a matrix known as Harmony Memory Matrix (HMM) similar to the HS technique. This can be changed as per the generalized d dimension space as explained previously. X and HMM are the two Matrices; where X represents as an initial set of solution for the objective function, HMRC relates as a ratio denoting whether the new child value or harmony is generated from the HMM Matrix or randomly in between lower and upper boundary. Pitch Adjusting Rate (PAR), is defined as the improvement of the solution by finding a nearby area or global solution such as it never get captured in local optimum region or solution.

SECOND STEP: For six unit's system objective function consists of six variables. So, the initial solution is stored in X (matrix) variables, whose dimension is X_{10x6} (to form one to ten ranking data) which is formed initially by taking random values in between each variable's lower and upper boundary. Then the Fitness Values (FV) are evaluated for the corresponding initial solutions. Now inside the HMM matrix these values are inserted according to the FV in ascending order.

HMM will become HMM_{10X7} as shown below:

$$HMM = \begin{bmatrix} X_1^1, X_2^1, X_3^1, X_4^1, X_5^1, X_6^1, f\left(X^1\right) \\ X_1^2, X_2^2, X_3^2, X_4^2, X_5^2, X_6^2, f\left(X^2\right) \\ \dots\dots\dots\dots\dots\dots\dots\dots\dots\dots\dots\dots\dots \\ \dots\dots\dots\dots\dots\dots\dots\dots\dots\dots\dots\dots\dots \\ X_1^{10}, X_2^{10}, X_3^{10}, X_4^{10}, X_5^{10}, X_6^{10}, f\left(X^{10}\right) \end{bmatrix} \qquad (2.11)$$

Where $f\left(X^1\right) < f\left(X^2\right) < f\left(X^3\right) \dots\dots\dots < f\left(X^{10}\right)$.

THIRD STEP: Now having the HMM Matrix, the iteration begins with the help of the next data generation or **New Harmony** creation as below condition for MHS;

$X_{K+1} = \{$

    1. New data generation from HMM 1st row value with proportional 10% as (1-HMRC)

    2. New data may be generated from HMM matrix 1st row value with a small increment with sharing of 9% as HMRC*PAR

    3. Otherwise New harmony data is generated randomly, each variable's lower and upper boundary region consisting of 81%data as HMRC*(1-PAR)

       $\}$

Now find the fitness value for this new harmony data selected as discussed above and replace HMM by new harmony data and fitness value in the desired position maintaining ascending order or ranking.

If in new $f(X_{K+1}) < f(X^1)$, or the first fitness value of HMM, then

HMM_1st row=$[x_1^1 \ x_2^1 \ x_3^1 \ x_4^1 \ x_5^1 \ x_6^1 \ f(x^1)]$

will be replaced by=$[x_1^{T_i} \ x_2^{T_i} \ x_3^{T_i} \ x_4^{T_i} \ x_5^{T_i} \ x_6^{T_i} \ f(x^{T_i})]$

Similarly, if $f(X_{K+1}) < f(X^2)$, then second row of the HMM will be updated.
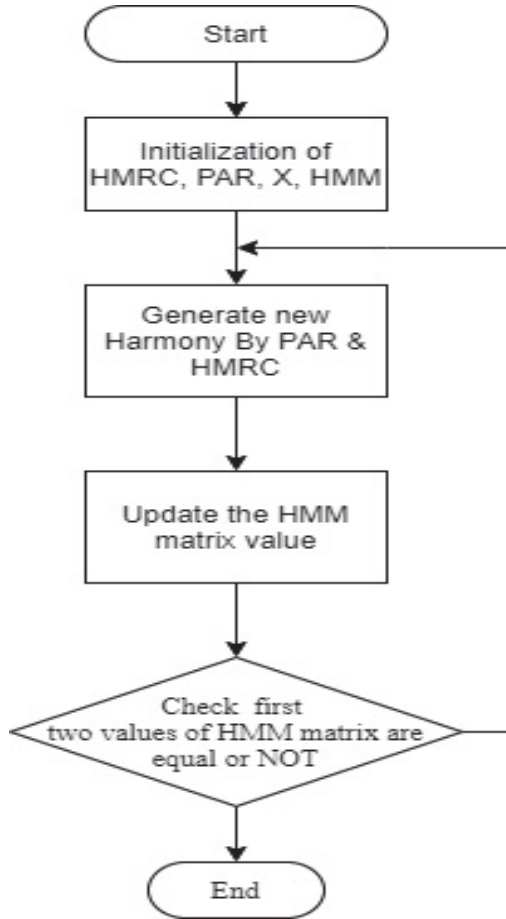
Figure 2.1 Flowchart of modified harmony searching optimization

This iteration process will be continuing until 1st and 2nd row's fitness value of HMM are the same. When these two are equal, the iteration process is stopped. The first row of HMM matrix indicates the best solution for the objective function.

After 10000th iterations HMM matrix is given below:

$$\text{HMM} = \begin{bmatrix} X_1^{T_1}, X_2^{T_1}, X_3^{T_1}, X_4^{T_1}, X_5^{T_1}, X_6^{T_1}, f\left(X^{T_1}\right) \\ X_1^{T_2}, X_2^{T_2}, X_3^{T_2}, X_4^{T_2}, X_5^{T_2}, X_6^{T_2}, f\left(X^{T_2}\right) \\ \dots\dots\dots\dots\dots\dots\dots\dots\dots\dots\dots\dots\dots\dots \\ \dots\dots\dots\dots\dots\dots\dots\dots\dots\dots\dots\dots\dots\dots \\ X_1^{T_3}, X_2^{T_3}, X_3^{T_3}, X_4^{T_3}, X_5^{T_3}, X_6^{T_3}, f\left(X^{T_3}\right) \end{bmatrix} \quad (2.12)$$

From this HMM matrix, it is clear that the data of the first row has been updated on the T_1^{th} iteration, the second row at T_2^{th} iteration, and so on, where

$$1 \leq T_1, T_2, T_3 \leq 10000$$

FOURTH STEP: The main difference between HS and MHS methods is the data selection procedure. In the normal HS method, the random data
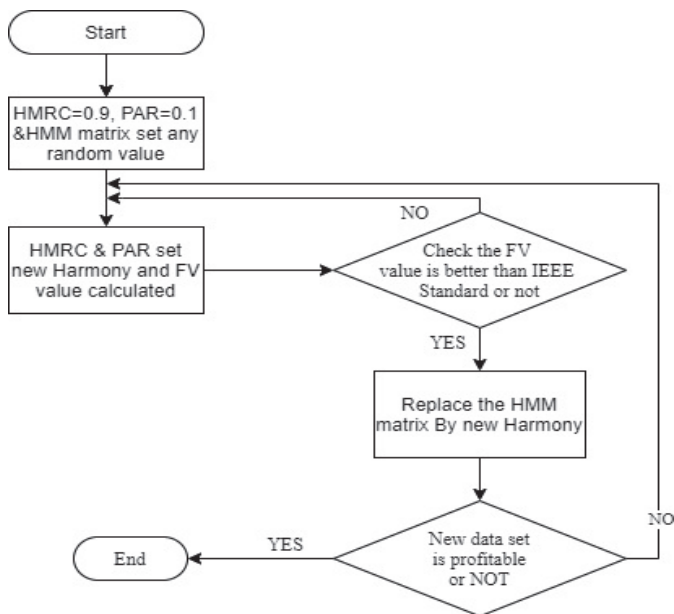
Figure 2.2 Flowchart of MHS optimization in ELD requirement

Table 2.1 (a) Six unit generating constants [1] and capacities

UNIT	P_{imin} (MW)	P_{imax} (MW)	μ_i ($)	θ_i ($/MW)	δ_i ($/MW^2)
1	100	500	240	7	0.0070
2	50	200	200	10	0.0095
3	80	300	220	8.5	0.0090
4	50	150	200	11	0.0090
5	50	200	220	10.5	0.0080
6	50	120	190	12	0.0075

(b) Loss coefficient matrices [1]

$$B_{ij} = \begin{bmatrix} 0.0017 & 0.0012 & 0.0007 & -0.0001 & -0.0005 & -0.0002 \\ 0.0012 & 0.0014 & 0.0009 & 0.0001 & -0.0006 & -0.0001 \\ 0.0007 & 0.0009 & 0.0031 & 0.0000 & -0.0010 & -0.0006 \\ -0.0001 & 0.0001 & 0.0000 & 0.0024 & -0.0006 & -0.0008 \\ -0.0005 & -0.0006 & -0.0010 & -0.0006 & 0.0129 & -0.0002 \\ -0.0002 & -0.0001 & -0.0006 & -0.0008 & -0.0002 & 0.0150 \end{bmatrix}$$

$$B_{0i} = 1e^{-03} * \begin{bmatrix} -0.3908 & -0.1297 & 0.7047 & 0.0591 & 0.2161 & 0.6635 \end{bmatrix}$$

$$B_{00} = 0.056$$

generation i.e. each variable's lower and upper boundary is only 10%, and most of the data is selected from the memory matrix i.e. 81% and the rest of the data is chosen from the incremented or delta-shifted value of HMM matrix 1st row. In the proposed MHS method, this new harmony generation is being made as mentioned in the **third step** such that less memory dependence occurs.

Profit calculation using MHS is mentioned below:

$$\begin{aligned} \text{Profit/hr} = 1000 \ & \times \ \text{Tarif} \times (P_{stdloss} - P_{mhsloss}) + \\ & 65 \times (T_{gstd\,cost} - T_{gmhs\,cost}) \end{aligned} \tag{2.13}$$

Here, the electricity tariff is taken as Rs. 7/kWh. $P_{stdloss}$, $P_{mhsloss}$ are standard loss and proposed method loss data in MW respectively and $T_{gstd\,cost}$, $T_{gmhs\,cost}$ are standard cost and proposed method cost data in USD respectively (1 USD = Rs. 65). We have set a profit value in stopping criteria as more than 5 USD. Execution time may change in MHS according to the condition below:

If sum (kk)>=1276 && loss1<12.293 && f11<=15470.88

If prof<=0

Display ('losses are going on so continue to run once');

Otherwise

Stop iteration & Result displayed

{ for six-unit system }

Economic load dispatch requirement using MHS techniques has been studied initially for a sixunit system that includes six thermal units, forty-six transmission path, and twenty-six buses. The load or consumer demand P_D is 1263 MW. The generating constants and capacities of all thermal or coal units [1] are mentioned in Table 2.1(a). The loss coefficient matrices B_{ij}, B_{0i}, and B_{00} with 100-MVA base value capacity are given in Table 2.1(b).

2.5 Hybrid Harmony Search Technique (HHS)

This method is mainly a combination of three methods, namely DE, PSO, and HS methods. It is similar to the harmony search method, with only a few changes in the new value updating inside or in the data generating loop. This method can be implemented by following three loops as mentioned below: In Loop1, the child generation is selected as per the harmony memory matrix 1st- row values or the rank one data which means the data generation is

$X_{k+1} = \{$

1. New data generation from HMM 1st row value with proportional 10 percentage such as $100 \times (1\text{-HMRC})$
2. child harmony=$\{$

    2.a $hms(1,1) + F \times (hms(2,1) - hms(3,1))$ *if* $rand(1,1) \leq 0.1$ ⟸ DE way

    2.b *else* $vl_{new} = rand(1,1) \times vl_0 + C1(max(hms(:,1)) - hms(2,1))$

    $\qquad + C2(hms(1,1) - hms(2,1))$ ⟸ PSO way

    $\qquad \}$ data generated with consisting of $(10+71)=81$ percentage such as $100 \times HMRC*(1\text{-PAR})$
3. Otherwise New data or child may be generated randomly, each variable's lower and upper boundary region of 9 percentage such as $(100\text{-}81\text{-}10)$ percentage

    $\}$

Figure 2.3   New child generation in HHS optimization

Table 2.2 Summary of HHS algorithm

Algorithm name		Hybrid Harmony Search (HHS) Technique
1.		Set Initial value of HMRC, PAR, X, hms
	2.	**Loop start** New data generation from HMM 1st row value with proportional 10 percentage such as 100_(1-HMRC)
	3.	2. child harmony={ **a. DE [20] way** => 2: hms(1;1) + F _ (hms(2; 1)-hms(3; 1)) if rand(1; 1) <=0.1 **b. PSO [21] way**=> 2: else V_1^{new}=rand (1,1) *v_1^{0}+C1*(max(hms(:1))-hms(2; 1))+C2(hms(1,1)- hms(2; 1)) data generated with consisting of (10+71)=81percentage such as 100_HMRC*(1-PAR)
Child generation	**4.**	Otherwise, New data or child may be generated randomly, with each variable's lower and upper boundary region of 9 percentage such as (100-81-10) percentage
5.		Stopping criteria **End**

performed at 10 percent (1-HMRC) *100 of total loops data in the first loop as in MHS method.

In Loop2, (1-PAR) *HMRC means 81 percentage data of the total loop, which again consists of two subloops. In subloop1 where 10 percentage data are generated as per the DE rule which is also known as loop2.a and another (81-10) =71 percentage data of subloop2 are generated by using PSO concept which is also known as loop2.b as mentioned in Table 2.2 and rest of the data (100-81-10) = 9% of the total loop is being generated in between the search space randomly. Here the search space means each variable's upper and lower boundary value.

2.6 Hybrid Harmony Search and Modified Harmony Search Optimization Results

Case I: (Example with the six-unit system)

For a six-unit system, the total load demand is 1263 MW; losses are less than 12.98 MW by using the loss coefficient matrices. The Fitness Value or cost of generation is taken in an iteration as FV≤15470 $/h [1]. The simulation codes are written in MATLAB R2014a and executed in a core i5 6500T, 8-GB RAM for both the proposed methods. The simulated results are given in Table 2.3.

Table 2.3   Best possible solution of six-unit system

ITEM (MW)	HHS	MHS	HS	PSO
$P1$	446.8189	443.1489	425.22	447.497
$P2$	173.234	171.6703	167.6	173.3221
$P3$	253.9324	241.6113	231.45	263.4745
$P4$	146.0897	163.0114	155.09	139.0594
$P5$	167.1325	168.643	173.74	165.4761
$P6$	88.0622	87.3535	122.56	87.128
P_L+P_D	1275.3	1275.4	1275.7	1276.01
P_L	12.34	12.086	12.42	12.9584
FV ($/h)	15444	15458	15476	15450

Proposed HHS provides multi-objective performance in both losses as well as cost. Though proposed MHS optimization provides more generating cost value ($) but losses are minimized in a six-unit system. The Profit has been calculated as mentioned in (2.13). This phenomenon occurs due to the reduction of line losses. It will save approximately 882.951 (Rs/h). Table 2.3 represents the comparison of simulation data for six-unit system between the proposed MHS, GA, and PSO. It is observed that total losses in the transmission lines are minimum as compared to other conventional methods [1] but generating cost ($/hr) is marginally higher. It also provides a good loss minimization task though the cost is marginally higher given in Table 2.3, Table 2.5, and Table 2.6. Figure 2.4 indicates convergence characteristics of MHS considering 200 trials with same number of functional evaluations. Average generation cost changes with a number of functional evaluations.

Case II: (Example to compare the execution time)

An example [22] has been considered for a three-unit system for a lossless line, representing one unit (P_3) in terms of fixed load demand and the other two generating units. The aim is to optimize two units, P_1 and P_2. The primary aim of this case study is to compare the execution time of the proposed MHS method with the existing optimization methods like DE and PSO so that further study on multi-objective optimization can be carried out considering line losses. The objective function of (P_1, P_2) is given in (2.14), and the boundary region is defined in (2.15). Three optimization techniques have been applied to the objective function and the results are tabulated in Table 2.4. It is observed from Table 2.4 that the increase in time of convergence with an increase in functional evaluation is minimum in the case of MHS. After getting the optimized values of P_1 and P_2 one can find $P_3 = (L_D - P_1 - P_2)$.

Table 2.4   Time comparison of three methods

MHS	P_1	179.08	186.44	184.74	183.85
	P_2	46.74	45.51	44.82	45.67
	FV	3483.1	3482.9	3482.9	3482.9
DE	P_1	183.96	183.96	183.96	183.96
	P_2	45.47	45.53	45.53	45.53
	FV	3482.9	3482.9	3482.9	3482.9
PSO	P_1	183.96	183.96	183.96	183.96
	P_2	45.53	45.53	45.53	45.53
	FV	3482.9	3482.9	3482.9	3482.9
No of Iterations /Functional Evaluations		100	1000	10000	100000
MHS Time (seconds)		**0.2112**	**0.2453**	**0.542**	**3.5669**
DE Time (seconds)		0.3382	0.5911	3.133	28.579
PSO Time (seconds)		0.2694	1.2660	11.18	111.23

i.e. the fixed unit's value of $P_3 = 70$ MW ($L_D = 300$ MW). Equation (2.10) indicates that the proposed method is less dependent on Harmony Memory than random data. Table 2.7 shows the improved performance in both loss and cost minimization with a normal memory updating algorithm. MHS has the ability to deal with both discrete as well as continuous types of problems [23].

$$\text{Objective function} \, (Rs/hr)$$
$$= P_1{}^2 + P_2{}^2 + (300 - P_1 - P_2)^2 + 8.663 \, P_1 + 10.04 \, P_2$$
$$+ 9.760 \, (300 - P_1 - P_2) + 524.2 \tag{2.14}$$

$$50 \text{ MW} \leq P_1 \leq 250 \text{ MW}$$
$$5 \text{ MW} \leq P_2 \leq 150 \text{ MW} \tag{2.15}$$

Case III:

From Table 2.7, it is clear that the proposed MHS optimization gives better results to PSO and GA in cost and time as mentioned in [1]. The blue-colored data indicates that both loss and cost are minimized at the same time by using the RANKSUM method though the ZDT test has not been performed for the proposed method. Normal HS method data are mentioned in parentheses. The CPU time required to reach a global solution with respect to a number of

Table 2.5   Fifteen unit generating constants and capacities [1] (reference data)

UNIT	P_{i_min} (MW)	P_{i_max} (MW)	μ_i ($)	θ_i ($/MW)	δ_i ($/MW^2)
1	150.0	455.0	671.0	10.10	0.0002990
2	150.0	455.0	574.0	10.20	0.0001830
3	20.0	130.0	374.0	8.80	0.0011260
4	20.0	130.0	374.0	8.80	0.0011260
5	150.0	470.0	461.0	10.40	0.0002050
6	135.0	460.0	630.0	10.10	0.0003010
7	135.0	465.0	548.0	9.80	0.0003640
8	60.0	300.0	227.0	11.20	0.0003380
9	25.0	162.0	173.0	11.20	0.0008070
10	25.0	160.0	175.0	10.70	0.0012030
11	20.0	80.0	186.0	10.20	0.0035860
12	20.0	80.0	230.0	9.90	0.0055130
13	25.0	85.0	225.0	13.10	0.0003710
14	15.0	55.0	309.0	12.10	0.0019290
15	15.0	55.0	323.0	12.40	0.0044470

Table 2.6   Optimal solution of 15 unit system

ITEM(MW)	MHS	PSO	GA
P1	411.0747	439.1162	415.3108
P2	424.2158	407.9727	359.7206
P3	125.0798	119.6324	104.4250
P4	86.4588	129.9925	74.9853
P5	347.7906	151.0681	380.2844
P6	450.6439	459.9978	426.7902
P7	438.4679	425.5601	341.3164
P8	92.6657	98.5699	124.7867
P9	44.0810	113.4936	133.1445
P10	65.9600	101.1142	89.2567
P11	20.2027	33.9116	60.0567
P12	63.7005	79.9583	49.9998
P13	38.2062	25.0042	38.7713
P14	19.3462	41.4140	41.9425
P15	35.1166	35.6140	22.6445
P_L+P_D	2663.01	2662.4	2668.4
P_L	32.2758	32.4306	38.2633
FV ($/h)	32836	32858	33113

Table 2.7 Cost, losses and execution time changes with functional evaluation for different units

Unit	k/iteration ($\times 10^3$)	40	70	90
	ITEM			
6 Unit	FV ($/h) P_L(MW) Execution Time (s) CPU Time/iteration (s)	15455 (15507) 11.9812 (12.3) 7.53 (0.578) 0.0056 (0.0004)	15458 (15486) 12.518 (11.54) 5.21 (1.01) 0.0045 (0.0008)	**15450** (15465) **11.804** (12.22) **21.168** (0.708) **0.01** (0.0003)
15 Unit	FV ($/h) P_L(MW) Execution Time(s) CPU Time/iteration (s)	32874 (33082) 31.07 (31.99) 22.8 (18.19) 0.0106 (0.008)	**32844** (33048) **31.37** (31.54) **6.77** (3.25) **0.0072** (0.0028)	32860 (33018) 32.08 (32.107) 8.006 (2.746) 0.0033 (0.001)
20 Unit	FV ($/h) P_L(MW) Execution Time (s) CPU Time/iteration (s)	**71028** (73991) **68.2023** (69.5) **24.05** (3.83) **0.0103** (0.0015)	73869 (73020) 69.8906(68.744) 8.41 (1.12) 0.0144 (0.0048)	73697 (73551) 70.648 (68.45) 10.65 (8.28) 0.0142 (0.011)
40 Unit	FV ($/h Execution Time (s) CPU Time/iteration (s)	**123640** (127890) **17.71** (0.558) **0.059** (0.0001)	125100(139110) 19.13 (4.64) 0.0547 (0.013)	125720 (132080) 13.37 (3.79) 0.0594 (0.0002)

functional evaluation (k) in the case of six-unit, fifteen-unit, twenty-unit, and forty-unit systems are given in Figure 2.5. Figure 2.6 shows the midpoint or average CPU time needed to reach the global solution with respect to various unit systems.

Novelty: Proposed MHS is faster than DE and PSO and even less dependent on Harmony Memory as mentioned in Table 2.3 [24]. The Hybrid Harmony Search technique (HHS) provides a multi-objective performance in the six-unit system studied.
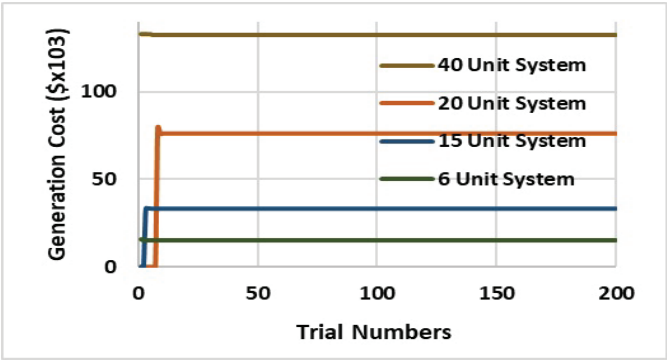
Figure 2.4 Convergence properties using the MHS method for all units (lower to higher as 6 to 40 units)
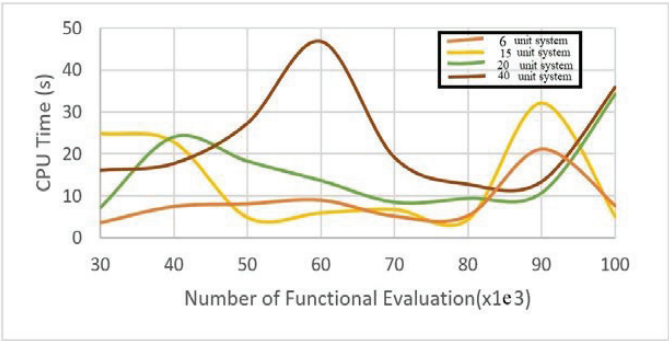
Figure 2.5 CPU time to reach solutions with a number of functional evaluations in all units
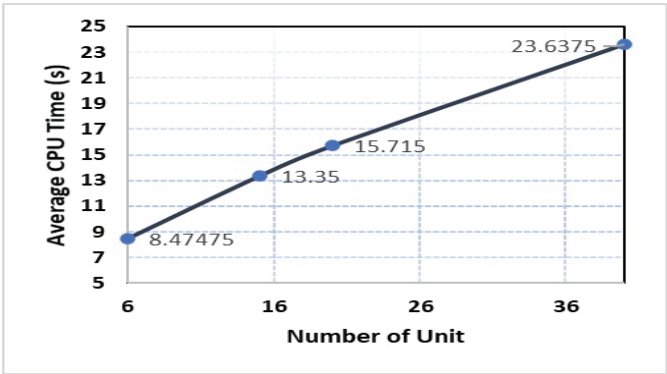
Figure 2.6 CPU time to reach solutions with number of functional evaluations for all units in ascending order (6,15,20,40 units)

2.7 Conclusion

In this chapter, MHS optimization technique for getting the global solution of ELD requirement in a power system analysis along with generator parameters (both inequality and equality constraints) has been incorporated. The MHS algorithm has better features in terms of extreme aspect solution, time to convergence, fitness value convergence, and computational efficiency. Many functions like thermal unit parameter and loss function are taken into account for practical generation operation in the proposed MHS method. The proposed method gives a better solution in respect of high computational efficiency, convergence property, and best solution. It is observed that in the fifteen-unit system, the proposed method provides multi-objective performance (both loss minimization and cost minimization) in comparison to PSO and GA algorithms (using the RANKSUM approach). In twenty-unit & forty-unit systems the proposed method has a better result as compared to PSO and GA. Hybrid Harmony Search provides a good result in multi-objective. The HHS method is left open to work in the case of fifteen, twenty- and forty-unit systems in the future.

References

[1] Zwe-Lee Gaing, "Particle Swarm Optimization to Solving the Economic Dispatch Considering the Generator Constraints," in *IEEE Transactions on Power Systems*, vol. 18, no. 3, pp. 1187-1195, Aug. 2003.

[2] F. N. Lee and A. M. Breipohl, "Reserve constrained economic dispatch with prohibited operating zones," in *IEEE Transactions on Power Systems*, vol. 8, no. 1, pp. 246-254, Feb. 1993.

[3] Ching-TzongSu and Gwo-Jen Chiou, "A fast-computation Hopfield method to economic dispatch of power systems," in *IEEE Transactions on Power Systems*, vol. 12, no. 4, pp. 1759-1764, Nov. 1997.

[4] C. C. Fung, S. Y. Chow, and K. P. Wong, "Solving the economic dispatch problem with an integrated parallel genetic algorithm," *PowerCon 2000. 2000 International Conference on Power System Technology. Proceedings (Cat. No.00EX409), Perth, WA, Australia*, 2000, pp. 1257-1262 vol. 3.

[5] H. Yoshida, K. Kawata, Y. Fukuyama, S. Takayama, and Y. Nakanishi, "A particle swarm optimization for reactive power and voltage control considering voltage security assessment," in *IEEE Transactions on Power Systems*, vol. 15, no. 4, pp. 1232-1239, Nov. 2000.

[6] B. Y. Qu and P. N. Suganthan, "Multi-objective evolutionary programming without non-domination sorting is up to twenty times faster," 2009 *IEEE Congress on Evolutionary Computation, Trondheim*, 2009, pp. 2934-2939.

[7] M. Paramasivam, A. Salloum, V. Ajjarapu, V. Vittal, N. Bhatt, and S. Liu, "Dynamic optimization based reactive power planning to mitigate slow voltage recovery and short-term voltage instability," 2014 *IEEE PES General Meeting | Conference & Exposition, National Harbor*, MD, 2014, pp. 1-1. doi: 10.1109/PESGM.2014.693907.

[8] K. P. Wong and Y. W. Wong, "Genetic and genetic/simulated-annealing approaches to economic dispatch," in *IEE Proceedings - Generation, Transmission and Distribution*, vol. 141, no. 5, pp. 507-513, Sep. 1994.

[9] Y. Zhang, "Improved harmony search algorithm applied in power system economic load dispatch," 2018 *Chinese Control And Decision Conference (CCDC), Shenyang*, 2018, pp. 5333-5336.

[10] Z. Woo, J. Hoon, & G. V. Loganathan, (2001). A New Heuristic Optimization Algorithm: Harmony Search. SIMULATION, 76(2)

[11] T. Mulo, P. Syam, and A. B. Choudhury, "Economical Load Dispatch Using Modified Harmony Memory Search Optimization Technique," 2018 *5th IEEE Uttar Pradesh Section International Conference on Electrical, Electronics and Computer Engineering (UPCON), Gorakhpur*, 2018, pp. 1-6.

[12] M. S. P. Subathra, S. E. Selvan, T. A. A. Victoire, A. H. Christinal, and U. Amato, "A Hybrid with Cross-Entropy Method and Sequential Quadratic Programming to Solve Economic Load Dispatch Problem," in *IEEE Systems Journal*, vol. 9, no. 3, pp. 1031-1044, Sep. 2015.

[13] G. T. Heydt, "Multiobjective Optimization: An Educational Opportunity in Power Engineering," in *IEEE Transactions on Power Systems*, vol. 24, no. 3, pp. 1631-1632, Aug. 2009. doi: 10.1109/TPWRS.2009.2021196.

[14] P. Kankanala, S. C. Srivastava, A. K. Srivastava, and N. N. Schulz, "Optimal Control of Voltage and Power in a Multi-Zonal MVDC Shipboard Power System," in *IEEE Transactions on Power Systems*, vol. 27, no. 2, pp. 642-650, May 2012. doi: 10.1109/TPWRS.2011.2178274.

[15] G. T. Heydt, "Multiobjective Optimization: An Educational Opportunity in Power Engineering," in *IEEE Transactions on Power Systems*, vol. 24, no. 3, pp. 1631-1632, Aug. 2009. doi: 10.1109/TPWRS.2009.2021196.

[16] B. Zhao et al., "Energy Management of Multiple Microgrids Based on a System of Systems Architecture," in *IEEE Transactions on*

Power Systems, vol. 33, no. 6, pp. 6410-6421, Nov. 2018. doi: 10.1109/TPWRS.2018.2840055.

[17] N. Kumar, T. Mulo, and V. P. Verma, "Application of computer and modern automation system for protection and optimum use of High voltage power transformer," 2013 *International Conference on Computer Communication and Informatics, Coimbatore*, 2013, pp. 1-5. doi: 10.1109/ICCCI.2013.6466257.

[18] H. Ding, F. Gao, K. Liu, and X. Guan, "An economic dispatch model based on scenario tree in industrial micro-grid with wind power," *The 27th Chinese Control and Decision Conference (2015 CCDC), Qingdao*, 2015, pp. 5028-5033, doi: 10.1109/CCDC.2015.7162824.

[19] L. Thurner et al., "Pandapower—An Open-Source Python Tool for Convenient Modeling, Analysis, and Optimization of Electric Power Systems," in *IEEE Transactions on Power Systems*, vol. 33, no. 6, pp. 6510-6521, Nov. 2018. doi: 10.1109/TPWRS.2018.2829021.

[20] T. Mulo, P.Syam, A. B. Choudhury (2020) Application of Modified Harmony Search and Differential Evolution Optimization Techniques in Economic Load Dispatch. In: Basu T., Goswami S., Sanyal N. (eds) Advances in Control, Signal Processing and Energy Systems. Lecture Notes in Electrical Engineering, vol 591. Springer, Singapore.

[21] X. Sui, Y. Tang, H. He, and J. Wen, "Energy-Storage-Based Low-Frequency Oscillation Damping Control Using Particle Swarm Optimization and Heuristic Dynamic Programming," in *IEEE Transactions on Power Systems*, vol. 29, no. 5, pp. 2539-2548, Sept. 2014. doi: 10.1109/TPWRS.2014.2305977.

[22] D.P.Kothari & J.S.Dhillon, "Power System Optimization".

[23] E. Babaei and S. Shahmohammadi, "Voltage stability and economical optimization of reactive power in power systems with wind generators by harmony search method," *20th Iranian Conference on Electrical Engineering (ICEE2012), Tehran*, 2012, pp. 392-397.

[24] N. Kumar, B. Singh and B. K. Panigrahi, "Harmony Search with Wavelet Mutation evolutionary approach for ramp rate constrained unit commitment," 2015 *Annual IEEE India Conference (INDICON), New Delhi*, 2015, pp. 1-6. doi: 10.1109/INDICON.2015.7443695.

3

Techno-Economic Assessment and Choice of Battery for Hybrid Energy using HOMER Software

Vidhi Tiwari and Kirti Pal

Dept. of Electrical Eng., Gautam Buddha University, Greater Noida, India
E-mail: tiwarividhi412@gmail.com; kirti.pal@gbu.ac.in

Abstract

The usage of renewable energy to generate electricity is growing day by day and solar and wind energy is seen as the most viable electrification options. In comparison to a single renewable source, hybrid electric systems have recently gained a lot of attention due to their various advantages. Different types of energy generating systems such as generators, electrical energy storage systems, and renewable energy sources are combined in hybrid systems. This technology appears to be the most viable option for off-grid power generation. Battery energy storage is required for this hybrid system in order to store excess energy generated by renewable resources and provide it during times of scarcity. Many battery technologies are developing these days with superior features to traditional batteries, which may be compared in terms of reaction time, deep cycle discharge, efficiency, lifetime, and so on. The goal of this study is to use HOMER Pro software to build and model a Hybrid Energy System (HES) that includes Photovoltaic (PV), wind energy, and a diesel generator. Secondly, several battery types such as Lead Acid (LA) battery, Lithium Ion (LI) battery, Li-ion Nickel-Manganese-Cobalt Oxide battery ($LiNiMnCoO_2$), Zinc Bromine Flow Battery, and Nickel Iron Battery are used to design HES. Finally, the Hybrid Renewable Energy System (HRES) is compared in terms of system size, economy, technical performance, and environmental stability utilizing various battery technologies.

Keywords: HOMER software, Hybrid Renewable Energy System (HRES), lead acid (LA) battery lithium ion (LI) battery, Li-ion Nickel-Manganese-Cobalt Oxide battery (LiNiMnCoO$_2$), Nickel Iron battery, State of charge, Zinc Bromine flow battery.

3.1 Introduction

With a total installed capacity of 374.2 GW as of 31 November 2020, India is the world's third-biggest producer and user of electricity [1]. In India, the use of conventional energy sources for power generation is widespread, but this has resulted in a slew of environmental concerns, necessitating a shift to renewable energy sources [2, 3]. Renewable energy, which includes major hydropower facilities, accounts for about 36.17% of India's total installed capacity. Solar and wind energy provide the most among all renewable energy sources. In 2019, wind energy will contribute approximately 37,505 MW, while solar energy will contribute around 33,712 MW. Madhya Pradesh is the state with the highest developed renewable energy sources, with a total installed power generating capacity of 24950.60 MW as of 31 July 2020, with an installed solar capacity of about 2237.48 MW and an installed wind capacity of around 2519.890 MW in 2019. As a result, solar energy is mostly employed to generate power for hybrid system design. However, owing to the unpredictability of solar energy and the fluctuation of cloud cover, sole reliance on solar energy is not a viable option. As a result, wind energy is employed to generate power in addition to solar energy. When both wind and solar systems are not producing energy, hybrid systems use batteries and/or a diesel-powered engine generator to generate power [4]. If the batteries aren't large enough, the engine generator is utilized to generate power and recharge the batteries so they may be used again. The usage of a diesel generator can help to minimize the size of the system's other components. Lead Acid (LA), Lithium Ion (LI), Li-ion Nickel-Manganese-Cobalt Oxide battery (LiNiMnCoO$_2$), nickel-iron, and Zinc Bromine flow battery (FB) are the most common battery types used in renewable energy systems.

3.2 Battery Energy Storage Systems (BESS)

Battery Energy Storage Systems (BESS) are very essential component of HRES since they allow storing extra power and using it when needed [5]. BESS consists of a large number of electrochemical cells connected in series or parallel to produce electricity at a particular capacity and voltage.

Because the energy held in batteries is in the form of electrochemical energy, batteries are prone to chemical reactions and necessitating frequent maintenance. However, with the advent of rechargeable batteries and technological advancements, the amount of battery care has decreased. This chapter presents a study of integrating battery storage to a Wind-PV-Diesel off-grid HRES. Batteries that are used for the analysis are Lithium Ion (LI) batteries, Flow Batteries (FB), Li-ion Nickel-Manganese-Cobalt Oxide battery (LiNiMnCoO$_2$), Zinc Bromine flow battery, and Nickel Iron Battery. The most popular energy- storing technique is the Electrochemical Energy Storage System (EcSS), which uses an electrolyte as the active material for generating and storing DC power [6]. EcSS is available in energy densities ranging from 10 kW/ kilograms to 13 kW/ kg, with an efficiency of 70-80% [7, 8].

One of the earliest rechargeable batteries with a quick reaction time is the lead-acid battery. From 1 Ah to 1000 Ah, it provides energy storage with an excellent cost-performance ratio and a low daily self-discharge rate (0.3 percent) [9]. Because of their safe operation, temperature tolerance, high cycle efficiency of 60-90 percent, minimal maintenance, and low capital costs, they are utilized in a variety of applications. But the disadvantage of lead acid battery is that it has a low energy density of 50-90Wh/L and it is heavy in weight. In addition to this, it has a low cycle life of around 2000 cycles. It requires periodic water maintenance and it is toxic in nature due to the presence of lead.

In Lithium-ion Battery, each cell in a Li-ion battery has a voltage of 4 V and is cylindrical in shape [10]. Because of its high energy density (about 6 to 8 times that of flooded (vented) lead-acid batteries in terms of per unit volume (75-200 Wh/kg), Li-ion batteries are widely employed in a variety of commercial applications. It has a lightweight, a long life cycle, a steady cycle, quick charge/discharge, a low self-discharge rate (less than 8% per month), and a long life cycle. It also features a fast response time, measured in milliseconds, as well as a high efficiency.

Li-ion Nickel-Manganese-Cobalt Oxide battery (LiNiMnCoO$_2$), lithium cobalt oxide (LiCoO$_2$), lithium titanate (Li$_4$Ti$_5$O1$_2$), lithium manganese oxide (LiMn$_2$O$_2$), and lithium iron phosphate are the different types of Li-ion batteries (LiFePO$_4$). Li-ion Nickel-Manganese-Cobalt Oxide battery (LiNiMnCoO$_2$) is a successful lithium-ion system with a Nickel-Manganese-Cobalt (NMC) cathode combination. The Li-ion Nickel-Manganese-Cobalt Oxide battery (LiNiMnCoO$_2$) of TeslaPW2 is considered in this chapter. It has a capacity of about 2,800mAh and is capable of delivering 4 to 5 amps. Li-ion Nickel-Manganese-Cobalt Oxide battery (LiNiMnCoO$_2$) NMC

has good performance, the lowest self-heating rate, and good specific energy (90–120 Wh/Kg) that's why it is nowadays preferred for the electric vehicles, medical applications, E-bikes, etc [11].

RedFlow Limited in Australia created the ZCell battery, a zinc-bromine flow battery that is a form of a hybrid flow battery. It has a 15.7–39 Wh/L energy density, a charge/discharge efficiency of 75.9%, cycle durability of over 2,000 cycles, and a nominal cell voltage of 1.8 V. Two tanks are filled with zinc bromide solution and kept in this battery. The solutions are pumped through a reactor stack and back into the tanks when the battery is charged or discharged. The electrolyte for positive electrode reactions is kept in one tank, while the electrolyte for negative electrode reactions is kept in the other. On a daily basis, the zinc–bromine battery has a high energy density and a 100 percent depth of discharge capability. But every few days, it is needed to be fully discharged [12].

In nickel–iron battery, potassium hydroxide is used as an electrolyte. It has iron on its negative plate and nickel (III) oxide-hydroxide positive plates. Here for the study Nickel iron battery of Edison of 200Ah is considered. It is very tolerant to over-discharge, overcharge, and short-circuiting and has a longer life span as it can last for more than 20 years that's why it is used in backup situations. But this battery is replaced by other more advanced rechargeable battery for various applications due to its poor charge retention, high cost of manufacture, and low specific energy.

3.3 Introduction to HOMER Pro Software

HOMER is an acronym for Hybrid Optimization Model for Electric Renewables (HOMER). The Midwest Research Institute (MRI) owns the rights to it, which was produced by the US National Renewable Energy Laboratory (NREL). HOMER primarily carries out three data functions: simulation, optimization, and sensitivity analysis.

HOMER can readily simulate a broad range of power system designs, including solar PV, wind turbines, Diesel Generators (DG), and battery energy storage systems. It may be used in on-grid and off-grid power systems. HOMER simulates the computations for the system configuration in question. In the simulation process, HOMER serves primarily two functions. It first determines the viability of the proposed system, and then it calculates the entire cost of installation, maintenance, fuel, and operation during the system's lifespan [13]. Many other applications of HOMER software to analyze various hybrid systems are described in [14–17].

The original grid search method and the proprietary derivative-free technique are utilized in HOMER for optimization. If each sensitivity variable is defined as an input, the optimization procedure in HOMER is repeated. To begin, first, choose a specific geographical place by entering its latitude and longitude. Following the specification of the site, the addition of load is required (residential, industrial, etc.). Then, after adding various components that are necessary for system design, run the simulation to obtain the best results. Figure 3.1 shows the flow chart for optimization in Homer Pro software.
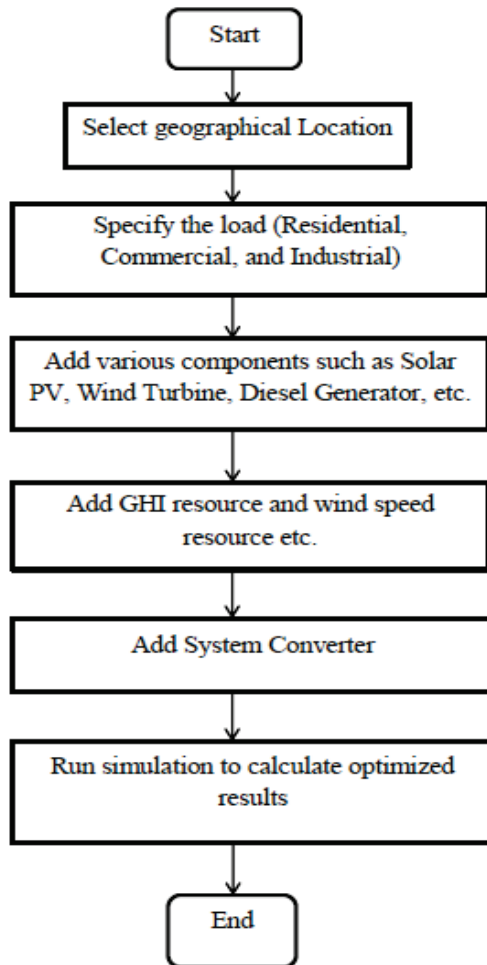
Figure 3.1 Flow chart for optimization in Homer Pro software

Figure 3.2   Setting the geographical location

3.4 Procedure

The procedure for the designing the system includes the following steps:

Step 1: Select the geographical location by entering the latitude and longitude of that area or simply entering the location name in HOMER software [18, 19]. So considering both solar and wind energy resources a location specified in HOMER is Hukumchand Marg, Itawaria Bazaar, Maharaja Tukoji Rao Holker Cloth Market, Indore, Madhya Pradesh 452002, India **(22°43.0'N, 75°50.8'E).** Figure 3.2 shows the selected location in the HOMER software.

Step 2: Add specific load: For the design of the system the average energy is 165.59 kWh/day, the average load is 6.9 kW and the peak load is 23.31 kW. Figure 3.3 shows the daily and annual load profile of the selected location.

Step 3: Add various components for the system such as solar PV, wind turbine, diesel generator, system convertor, and batteries [19, 20].

3.4.1 Solar Photovoltaic System

A generic flat plate solar PV system is assumed to be 1 kW with a lifespan of 25 years and an 80 percent derating factor. It has a 17 percent efficiency
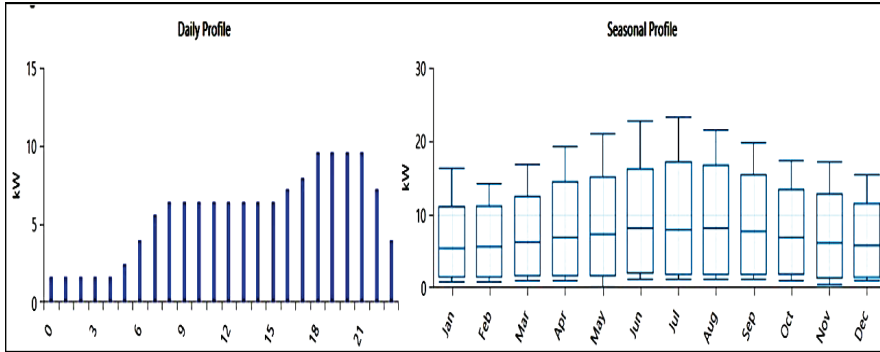
Figure 3.3 Specific load of the selected site
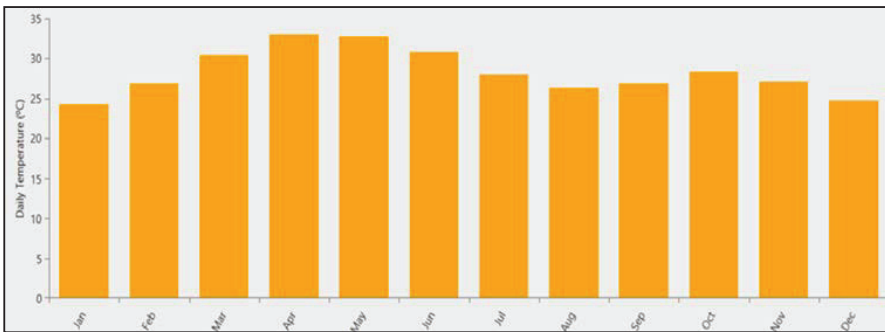
Figure 3.4 Average daily temperature (in degrees Celsius)

rating. Solar PV has a capital cost of ₹ 30,000 and an operating cost of ₹ 30,000. On 10 December 2020, data are taken from NASA Satellite Surface Meteorology and Solar Energy department provided average solar energy potential in the Indore Madhya Pradesh region, which reveals that the annual average solar radiation is 5.18 kWh/m^2/Day. Figure 3.4 shows the average daily temperature annually at the selected location.

3.4.2 Wind Turbine

A generic 10 kW wind turbine with a 20-year lifespan and a hub height of 24 m is considered with the capital cost of ₹ 50,000, the operational cost of ₹ 50,000, and a replacement cost of ₹ 500. On 10 December 2020 data taken from NASA Satellite Surface Meteorology and Solar Energy department provided average data on wind energy potential in the Indore Madhya Pradesh
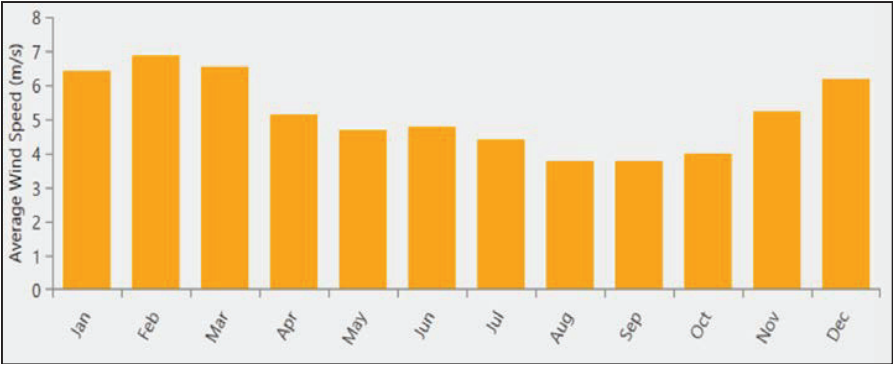
Figure 3.5   Average wind speed (m/s)

area, which indicates an annual average wind speed of 3.07 m/sec. Figure 3.5 shows the average wind speed annually at the selected location.

3.4.3 Battery Energy Storage System

A battery energy storage system is needed to store excess energy generated by renewable resources and supply it when electricity is needed. Table 3.1 shows the specifications of different batteries used for the designing of HRES in HOMER Pro software.

3.4.4 Diesel Generator

For the diesel generator, an Autosize Genset is chosen. The Autosize Genset will automatically set its size to supply the load requirement when needed.

Table 3.1   Specifications of various batteries

Type of battery and their various Parameters	Li ion battery	Lead acid battery	Zinc Bromine Flow battery	LiNiMnCoO$_2$ Battery	Nickel Iron Battery
Nominal voltage (V)	6	12	48	220	1.2
Nominal capacity (Ah)	167	83.4	207	60	200
Round Trip efficiency (%)	90	80	75	89	85
Maximum charge current (A)	167	16.7	50	31.8	100
Maximum Discharge current (A)	500	24.3	100	31.8	100

Table 3.2 Specific diesel properties

Lower Heating Value (MJ/kg)	43.20
Carbon Content (%)	88.00
Density (kg/m3)	820
Sulphur Content (%)	0.4
Fuel price rupees/L	73.56

Table 3.3 Emissions

CO (g/L fuel)	16.5
Unburned HC(g/L fuel)	0.72
Particulates (g/L fuel)	0.1
Nox(g/L fuel)	15.5
Unburned HC (g/L fuel)	0.72

The various specific diesel properties and associated emissions are given in Table 3.2 and Table 3.3 respectively.

Step 4: Insert the specified site's average wind speed (m/s) and Global Horizontal Irradiation (GHI) resource. GHI is used to determine solar PV output, which is primarily a total of the beam, ground reflected, and diffuses irradiance.

Step 5: Calculate the optimized results. For the overall analysis, six system configurations are designed with the same components but with different batteries (lead-acid battery, Lithium Ion (LI) battery, Li-ion Nickel-Manganese-Cobalt Oxide battery (LiNiMnCoO$_2$), Zinc Bromine flow battery, Nickel Iron Battery, and then all systems are compared.

Here, the cost summary of the system consisting of different batteries are considered in which there is the calculation for net present cost, capital cost, replacement cost, operating cost, cash flow and cost of energy. In order to know the technical performances of the different batteries, their State of Charge (SoC), a number of batteries required, string size, autonomy, losses, energy in, energy out, annual throughput, usable nominal capacity, and lifetime throughput are calculated. Finally, the emission of the overall system is also considered to compare different kinds of batteries used for the system design.

3.5 Modelling of the HRES with Different kinds of Batteries

Figure 3.6 to 3.10 shows the various models designed in HOMER PRO software using different kinds of batteries such as lead acid battery, Lithium
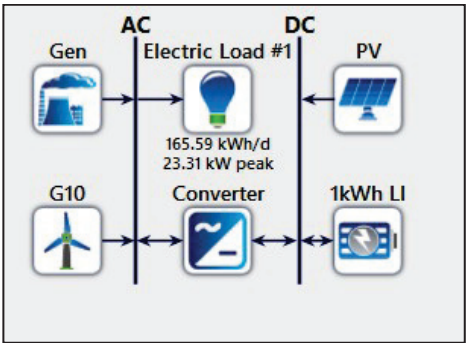
Figure 3.6   HRES with Lithium Ion battery
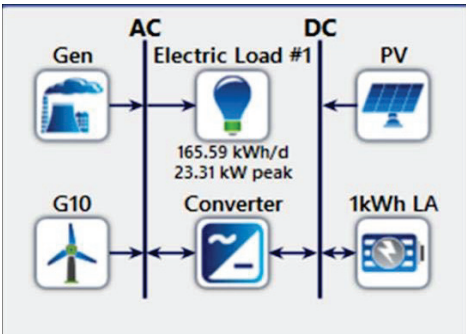
Figure 3.7   HRES with Lead acid battery
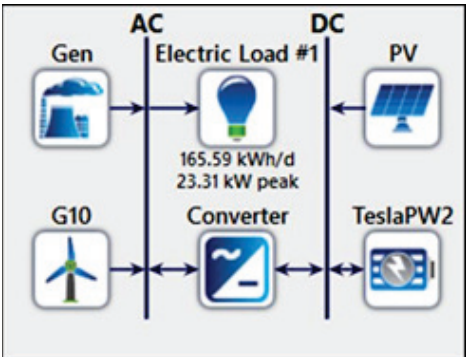
Figure 3.8   HRES with $LiNiMnCoO_2$ battery

Ion (LI) battery,Li ion Li-ion Nickel-Manganese-Cobalt Oxide battery ($LiNiMnCoO_2$), Zinc Bromine flow battery, Nickel Iron Battery.
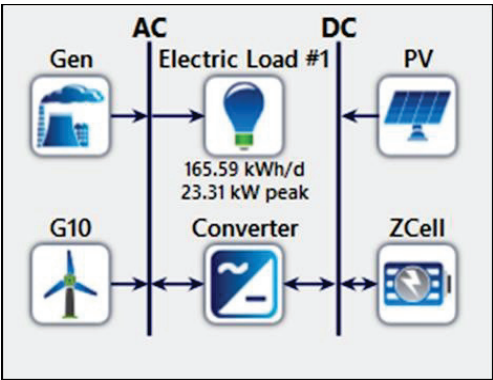
Figure 3.9   HRES with Zinc Bromine battery
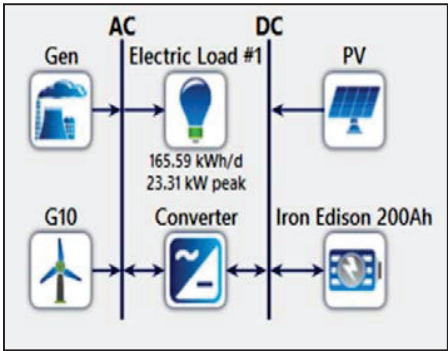
Figure 3.10   HRES with Nickel Iron battery

3.6 System Metrics

Different sizes of solar PV, wind turbine, diesel generator, system converter, and batteries are used in each HRES, using the lead acid battery, Lithium Ion (LI) battery, Zinc Bromine Flow Battery (FB), Li-ion Nickel-Manganese-Cobalt Oxide battery and Nickel Iron battery. According to the economic metrics and technical performance metrics, the most suitable configuration is chosen and proposed for installation.

3.6.1 Economic Metrics

The total cost of a system with different batteries is indicated in Table 3.4 below. This comprises the system's capital cost, replacement cost, operations and maintenance cost, fuel cost, salvage value, and overall Net Present Cost

(NPC). Total NPC, which ranks primarily the planned system configuration and estimates the total yearly cost of energy also [21, 22], is the most important economic output in HOMER. Total NPC is the sum of all expenses associated with the installation and operation of all components during the project's lifetime, minus the present value of any revenues earned during that period. A formula may be used to determine the total NPC, as illustrated below:

$$Total\ NPC = \sum_t T\ C_{cap,t} + C_{o\&M,t} + C_{replace,t} + C_{fuel,t} + P_{salvage,t}$$
(3.1)

The capital cost is incurred in the first year of the project, or year zero. The yearly Operating and Maintenance (O&M) and fuel expenses occur at the end of each year, whereas replacement costs occur every 3.52 years.

Salvage value in HOMER refers to the value left in a component of the power system at the conclusion of the project's lifespan. In HOMER, components depreciation is considered to be linear, which implies that a component's salvage value is precisely proportionate to its remaining life. The salvage value is calculated by the replacement cost rather than the initial capital cost. HOMER uses the following calculation to compute the salvage value:

$$S = C_{rep}.\ R_{rem}/R_{comp}$$
(3.2)

$$R_{rem} = R_{com} - (R_{proj} - R_{rep})$$
(3.3)

where

C_{rep} is the cost of replacement ()
R_{comp} stands for component lifespan (yr)
R_{rem} is the component's remaining life at the end of the project once in a lifetime (yr)
R_{rep} denotes the period of the replacement cost.
R_{proj} denotes the duration of a project (yr)

The total NPC of the HRES with Nickel Iron Battery and Lead Acid Battery is about ₹ 6, 05,546.5 and ₹ 4, 38,525.0 correspondingly, as shown in Table 3.4. The HRES with Lithium Ion Battery has the lowest overall cost of about ₹ 3, 37,081.8, followed by the HRES with LiNiMnCoO$_2$ and Z Cell, which have total NPCs of around ₹ 3,65,816.1 and ₹ 3,81,816.1 respectively. In terms of overall NPC, the Lithium Ion battery is the most cost-effective option for HRES. As a result, in terms of the total cost, the Lithium Ion battery is favored above the other batteries.

Table 3.4   Total net present cost (NPC) of HRES with different kinds of the batteries

System with different types of batteries	Capital cost(₹)	Replacement cost (₹)	O&M cost (₹)	Fuel cost(₹)	Salvage Value (₹)	Total NPC(₹)
Li ion battery	2,30,589.9	54,770.7	34,657.0	69,998.7	−16,934	3,37,081.8
Lead acid battery	1,69,462.5	1,03,9750	41,766.2	1,34,583.2	−11,262	4,38,525.0
Zinc Bromine Flow battery	2,48,749.2	63,158.9	25,318.1	65,766.9	−21,294	3,81,698.7
LiNiMnCoO$_2$ battery	1,54,886.1	53,356.9	24,479.6	1,47,097.9	−14,004	3,65,816.1
Nickel Iron Battery	67,272.80	1,09,991.5	94,410.2	3,44,813.1	−10,941	6,05,546.5

3.6.2 Technical Performance of the Overall System

In order to compare the HRES in terms of technical performance, monthly average electricity, contributions of solar PV, wind turbine, and diesel generator are considered shown in further sections. The monthly average electricity production is given in Table 3.5. The entire electricity produced annually by solar PV, wind turbines, and diesel generators is taken into account. The quantity of power generated in excess during the year, given as a proportion of total electrical output, is referred to as excess electricity. The capacity and contribution of the diesel generator for the HRES with LiNiMnCoO$_2$ battery and Nickel Iron Battery is quite high, more than 50%, with very little contribution of renewable energy, owing to the total cost of the system fuel expense increasing. Furthermore, it will also lead to environmental degradation with the release of harmful emissions [23, 24].

The renewable fraction is mainly the electricity generated by renewable resources, which is 0 for the HRES with Nickel Iron Battery, whereas renewable fraction is highest for the HRES with Zinc Bromine Flow battery around 76.6% followed by HRES with Li-Ion battery with a renewable fraction of 70.2%.

3.6.3 Contribution of Solar PV

Table 3.6 shows the overall capacity and production by solar PV for HRES with different batteries. In HOMER, the output of the solar PV is calculated

Table 3.5 Monthly average electricity production

System with different types of batteries	Li ion battery	Lead acid battery	Zinc Bromine Flow battery	LiNiMnCoO$_2$ battery	Nickel Iron Battery
Solar PV (kWh/yr)	53,624 (70.5%)	41,202 (55%)	63,964 (79.9%)	31,491 (43.4%)	1,393 (1.89%)
Diesel Generator (kWh/yr)	18,018 (23.7%)	32,446 (43.3%)	14,151 (17.7%)	38,569 (53.2%)	68,031 (92.2)
Wind Turbine (kWh/yr)	4,398 (5.78%)	1,264 (1.69%)	1,963 (2.45%)	2,470 (3.41%)	4,398 (5.96%)
Excess electricity (kWh/yr)	9,668 (12.7%)	7,872 (10.5%)	10,233 (12.8%)	4,258 (5.87%)	13,016 (17.6)
Maximum renewable Penetration	1,403	1,137	1,681	898	351

Table 3.6 Solar PV output

System with different types of batteries	Li ion battery	Lead acid battery	Zinc Bromine Flow battery	LiNiMnCoO$_2$ battery	Nickel Iron Battery
Rated Capacity(kW)	29.2	25.2	37.4	19.8	0.774
Mean Output(kW)	6.12	4.7	7.3	3.59	0.159
Capacity factor (%)	20.9	18.7	19.5	18.2	20.6
Total Production (kWh/yr)	53,624	41,202	63,964	31,491	1,393
PV penetration (%)	88.7	68.2	106	52.1	2.31
Hours of operation (hrs. /yr)	4,370	4,404	4,365	4,358	4,403

by the following equation:

$$P_{PV} = Y_{PV} f_{PV}(G_t/G_{t,\ STC})[1 + \alpha_p(T_c - T_{c,\ STC})] \qquad (3.4)$$

where
- PV's rated capacity is denoted by Y_{PV} (kW)
- The PV derating factor is F_{PV} (%)
- The incident solar radiation on the PV array (kW/m^2) is denoted by G_t

- The incident solar radiation at standard test conditions (1 kW/m^2) is denoted by $G_{t,STC}$
- The temperature coefficient of power (% /°C) is denoted by α_p
- Tc is the current temperature of the PV cell (in °C).
- The temperature of the PV cell under normal test circumstances (25 °C) is $T_{c,STC}$

Total solar PV production is highest for the HRES with Zinc Bromine flow battery and Li-Ion battery at approximately 63,964 kWh/yr and lowest for the HRES with Nickel Iron Battery at around 53,624 kWh/yr PV penetration is expressed as a proportion of total peak power generated by PV to peak load apparent power, given as a percentage.

3.6.4 Contribution of Wind Turbine and Diesel Generator

The capacity and total production of the wind turbine and diesel generator utilized for HRES with different batteries are presented in Table 3.7 and Table 3.8. Generators used in system design may be dispatched in HOMER, which means the system can switch them on and off as needed. When there is insufficient energy to provide the load, a dispatch strategy is utilized to control the operation of a generator as well as the storage tank. The wind turbine has a rated capacity of 10 kW HRES. The wind turbine's capacity factor is the ratio of average power production to maximum power capacity. The output of a wind turbine is determined by air density, which is computed in HOMER using the following equation:

$$P_{WTG} = (\rho/\rho o)\, P_{WTG,\, STP} \tag{3.5}$$

Table 3.7   Wind turbine output

System with different types of batteries	Li ion battery	Lead acid battery	Zinc Bromine Flow battery	LiNiMnCoO$_2$ battery	Nickel Iron Battery
Rated capacity(kW)	10	10	10	10	10
Mean output(kW)	0.502	0.144	0.224	0.282	0.502
Capacity factor (%)	5.02	1.44	2.24	2.82	5.02
Total production (kWh/yr)	4,398	1,264	1,963	2,470	4,398
Wind penetration (%)	7.28	2.09	3.25	4.09	7.28
Hours of operation (hrs/yr)	5,433	3,403	4,156	4,659	5,433

Table 3.8   Contribution of diesel generator

System with different types of batteries	Li ion battery	Lead acid battery	Zinc Bromine Flow battery	LiNiMnCoO$_2$ Battery	Nickel Iron Battery
Electrical Production (kWh/yr)	18,018	32,446	14,151	38,569	68,031
Mean Electrical output (kW)	22.4	15.8	10.2	25.2	7.83
Fuel consumption (L)	5,415	10,411	5,087	11,379	26,673
Mean electrical Efficiency (%)	33.8	31.7	28.3	34.4	25.9
Hours of operation (hrs/yr)	806	2,050	1,390	1,533	8,692
Operational life (yr)	18.6	7.32	10.8	9.78	1.73
Capacity factor (%)	7.91	14.2	6.21	16.9	29.9

where

- The power output of a wind turbine is measured in kW and is referred to as P_{WTG}.
- Wind turbine power output in kW at standard temperature and pressure is given as $P_{WTG, STP}$
- ρ is the actual air density in kilograms per cubic meter.
- ρo is the density of air at standard temperature and pressure, i.e. 1.225 kg/m^3.

3.6.5 Technical Specification of Different Batteries Used in HRES

To evaluate different batteries, a variety of parameters must be examined such as State of Charge (SoC), autonomy, capacity, and so on. Table 3.9 compares the number of batteries, string size, autonomy, nominal capacity, and useable nominal capacity, energy in, energy out, losses, yearly throughput, and lifetime throughput. The number of batteries linked in series determines the string size. The capacity of the storage bank divided by the average electrical demand yields autonomy (which is measured in hours) [25]. HOMER calculates the storage bank autonomy using the following equation:

$$A_{batt} = N_{batt}V_{nom}Q_{nom}(1 - q_{min}/100)(24h/d)/(L_{prim}(1000Wh/kWh))$$
$$(3.6)$$

Table 3.9   Technical performances of batteries used in HRES

System with different types of batteries	Li ion battery	Lead acid Battery	Zinc Bromine Flow battery	LiNiMnCoO$_2$ battery	Nickel Iron Battery
Quantity required	126	88	10	4	10
String size	1	1	1	1	1
Autonomy(hr.)	14.6	7.66	14.4	7.65	0.313
Nominal capacity(kWh)	126	88.1	99.3	52.8	2.4
Usable nominal capacity(kWh)	101	52.8	99.3	52.8	2.16
Expected life(yr)	14.8	4.18	16.3	10	8.61
Energy In	26,911	18,833	28,211	28,422	1,385
Energy out	24,284	15,072	21,239	25,304	1,178
Losses (kWh/yr)	2,695	3,767	7,065	3,127	208
Annual throughput (kWh/yr)	25,598	16,851	24,525	26,823	1,278
Lifetime throughput(kWh)	3,78,000	70,400	4,00,000	2,68,226	1,10,000

where

- The number of batteries in the storage bank is denoted by N_{batt}.
- V_{nom} is a single storage's nominal voltage [V]
- Q_{nom} is single storage's nominal capacity [Ah]
- q_{min} is the storage bank's minimum state of charge [%]
- L_{prime} is the primary load average [kWh/d]

The number of batteries required for HRES with Li-ion battery is around 126, followed by HRES with lead acid battery, as indicated in Table 3.9. A Nickel Iron battery has a minimum autonomy of 0.313 hours. The autonomy of the Lithium Ion and Zinc Bromine Flow batteries is nearly identical, at 14.6 hours and 14.4 hours, respectively. The autonomy of the lead acid battery and the LiNiMnCoO$_2$ battery is similar, at roughly 7.66 hours and 7.65 hours, respectively.

3.7 State of Charge of Battery

The battery's minimum state of charge is the lowest level of charge at which the storage bank cannot be drained. Many rechargeable batteries cannot be fully drained since this might cause irreversible harm to the battery.
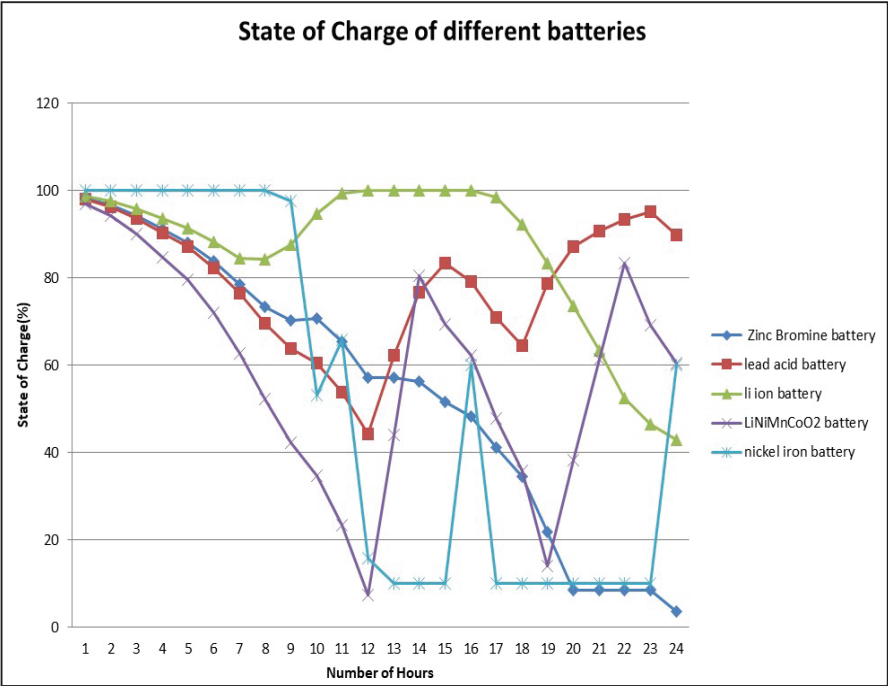
Figure 3.11   State of Charge of different batteries

To minimize any damage to the storage bank owing to excessive discharge, the minimum state of charge is generally maintained at 30–50 percent [26, 27].

The graph in Figure 3.11 shows the State of Charge of different batteries such as Lead acid (LA) battery, lithium ion (LI) battery, Li-ion Nickel-Manganese-Cobalt Oxide battery (LiNiMnCoO$_2$), Zinc Bromine flow battery, Nickel Iron Battery used in HRES for 24 hours.

3.8 Emissions through a Different System with Different Batteries

The environmental hazards associated with the HRES are emissions from the diesel generator due to the use of diesel as a fuel and, through the use and disposal of batteries. Carbon dioxide, carbon monoxide, unburned hydrocarbons particulate matter, sulphur dioxide, and nitrogen oxides are some of the contaminants that HOMER calculates emissions for. Table 3.10

Table 3.10 Emissions through the HRES with different batteries

System with different types of batteries	Li ion battery	Lead acid battery	Zinc Bromine Flow battery	LiNiMnCoO$_2$ battery	Nickel Iron Battery
Carbon Dioxide (kg/yr)	14,174	27,251	13,317	29,785	69,819
Carbon Monoxide (kg/yr)	89.3	172	83.9	188	440
Unburned Hydrocarbons (kg/yr)	3.90	7.50	3.66	8.19	19.2
Particulate Matter (kg/yr)	0.541	1.04	0.509	1.14	2.67
Sulfur Dioxide (kg/yr)	34.7	66.7	32.6	72.9	171
Nitrogen Oxides (kg/yr)	83.9	161	78.9	176	413

presents the emission detail through the HRES with different batteries. Diesel generators are responsible for a huge spike in pollution due to the increased amount of PM2.5 and PM10 by 30% and they are also constant emitters of CO_2. Similarly, batteries are also harmful to the environment because of their disposal. Lead acid batteries used for various applications pose a threat due to the presence of lead, which is dangerous for health. Now about 99% of lead acid batteries are recyclable. For Li-ion batteries, lithium extraction leads to air and soil contamination. In the Zinc Bromine Flow battery, very little free bromine is present but, bromine is dissolved in the aqueous electrolyte, and liquid or gaseous bromine is hazardous.

HRES with Nickel Iron Battery, and LiNiMnCoO$_2$ requires a large capacity of diesel generator, thus releasing a large amount of emissions as compared to other systems. For example, carbon dioxide from the system consisting of LiNiMnCoO$_2$ is 29,785 Kg/yr and from that consisting Nickel Iron Battery is 69,819 Kg/yr. The system with a Zinc Bromine Flow battery releases fewer amounts of emissions as compared to other systems. Emissions released by the Li-ion battery are also comparable with a Zinc Bromine battery.

3.9 Conclusions

The aim of this chapter is to accomplish three major goals, firstly to design an off-grid HRES using a PV-wind diesel generator with different types of batteries which are used to supply electricity whenever it is needed and the system is modeled and simulated with the help of HOMER Pro software. Secondly, several battery types such as lead acid (LA) battery, lithium ion (Li-ion) battery, Li-ion Nickel-Manganese-Cobalt Oxide battery (LiNiMnCoO$_2$), Zinc Bromine flow battery, and Nickel Iron Battery are used to test the developed model. Finally, the HRES is compared in terms of system size, economy, technical performance, and environmental stability utilizing different battery technologies. Amongst all the battery types used in HRES, the Li-ion battery is highly recommended. Considering the overall cost of the system, the HRES with this battery offers significantly lesser costs as compared to other batteries. The total NPC of HRES with a Li-ion battery is ₹ 3,37,081.85. The HRES with Li-ion battery configuration offers very compact design as solar PV of 29.2 kW, wind turbine of 10 kW is used.

On Comparing the State of charge of the different batteries, it is can be seen that Li-ion battery has SoC of 80-100% of the maximum capacity, for Lead acid battery it is between 40-90% of the maximum capacity and SoC of other batteries decreases to 5-10% of the maximum capacity which is not desirable. It is desirable for any battery to set SoC of 30-50% in order to avoid damage to the battery. Now, considering the environmental impacts, HRES with Li-ion battery emits less amount of pollutants mainly carbon dioxide of 14,174 kg/yr. Although emissions through the Zinc Bromine flow battery is almost equal to the HRES with Li-ion battery, but it cannot be considered because of its technical performance such as SoC which in the case of Zinc Bromine flow battery reduces to 0% for a specific period of time which is not desirable.

References

[1] V. Khare, S. Nema, and P. Baredar, 'Status of solar-wind renewable energy in India', *Renewable and Sustainable Energy Reviews*, vol. 27, 2013.

[2] S. K. Sahoo, 'Renewable and sustainable energy reviews solar photo-voltaic energy progress in India: A review', *Renewable and Sustainable Energy Reviews, Elsevier*, vol. 59, June, pp. 927- 939, 2016.

[3] T. Adefarati, and R. C. Bansal, 'Integration of Renewable Distributed Generators into the Distribution System: A Review', *IET Renewable Power Generation*, vol. 10, Issue 7, pp. 873-884, 2016.

[4] J. D. Navamani, A. Lavanya, C. M. Prahadheeshwar, and S. M. Riyazudeen, 'Hybrid Power System Design using Homer Pro', *International Journal of Recent Technology and Engineering (IJRTE)* ISSN: 2277-3878, vol. 8, Issue-1S4, 2019.

[5] M. A. Elhadidy, 'Performance evaluation of hybrid (wind/solar/diesel) power systems, Renewable Energy, 26:401e13, 2002.

[6] F. Nadeem, S. M. S. Hussain, P. K. Tiwari, A.K. Goswami, and T. S. Ustun, 'Comparative Review of Energy Storage Systems, Their Roles, and Impacts on Future Power Systems, *IEEE Acess*, pp. 9-12, vol. 7, 2019.

[7] K. Divya, and J. Østergaard, 'Battery energy storage technology for power systems An overview', *Elect. Power Syst. Res.*, vol. 79, no. 4, pp. 511-520, 2009.

[8] J. Cho, S. Jeong, and Y. Kim, 'Commercial and research battery technologies for electrical energy storage applications, *Prog. Energy Combust. Sci.*, vol. 48, pp. 84-101, 2015.

[9] S. M. Lukic, J. Cao, R. C. Bansal, F. Rodriguez, and A. Emadi, 'Energy storage systems for automotive applications,' *IEEE Trans. Ind. Electron.*, vol. 55, no. 6, pp. 2258-2267, 2008.

[10] K. T. Chau, Y.S. Wong, and C. C. Chan, 'An overview of energy sources for electric vehicles, Energy Convers. Manage, vol. 40, no. 10, pp. 1021-1039, 1999.

[11] K. L. Tharani, and R. Dahiya, 'Choice of battery energy storage for a hybrid renewable energy system', *Turkish Journal of Electrical Engineering & Computer Sciences ,Turk J Elec Eng & Comp Sci*, vol. 26, pp. 666 -676, 2018.

[12] P. Kumar,P., R. Pukale, N. Kumabhar, and U. Patil, 'Optimal Design Configuration Using HOMER', *International Conference on Emerging Trends in Engineering, Science and Technology (ICETEST)*, 2015.

[13] N. A. A. Razak, M. M. B. Othman, and I. Musirin, 'Optimal sizing and operational strategy of hybrid renewable energy system using homer', *Power Engineering and Optimization Conference (PEOCO)*, 2010.

[14] Kumar C Sanjay, M Karthikeyan, K K M Prasannakumaran, and V. Kirubakaran, 'Techno Commercial Study of Hybrid Systems for the Agriculture Farm Using Homer Software', *chapter5, Hybrid Renewable Energy Systems*, pp. 115-133, Mar. 2021.

[15] N. Majdi Nasab, J. Kilby, and L. Bakhtiaryfard, 'Case Study of a Hybrid Wind and Tidal Turbines System with a Microgrid for Power Supply to a Remote Off-Grid Community in New Zealand', *Energies 2021*, 14, 3636. https://doi.org/ 10.3390/en14123636

[16] Kamal Kant Sharma et al., 'Economic evaluation of a hybrid renewable energy system (HRES) using hybrid optimization model for electric renewable (HOMER) software—a case study of rural India', *International Journal of Low-Carbon Technologies*, 16, 814–821, 2021.

[17] Sunaina, Harpreet Kaur Channi, and Surbhi Gupta, 'Optimization and Simulation of Solar PV Based Hybrid System Using Homer Software', *International Journal of Advanced Science and Technology*, 29(12s), 715 – 728, 2020.

[18] U. S. Magarappanavar, and S. Koti, 'Optimization of Wind-Solar-Diesel Generator Hybrid Power System using HOMER', *International Journal of Recent Technology and Engineering (IRJET)* E- ISSN: 2395 -0056 vol. 03, 2016.

[19] W. Zhou W., C. Lou, Z. Li , L. Lu, and H. Yang, 'Current status of research on optimum sizing of stand- alone hybrid solar-wind power generation system', *Applied Energy*; 87(2):380-389, 2010.

[20] R. Raval, and S. Choubey, 'Calculation and Modelling of Hybrid Power Generation System Using Solar Energy', *International Conference on Intelligent Sustainable Systems (ICISS)*, 2017.

[21] U. Sureshkumar, P. S. Manoharan, and A. P. S. Ramalakshmi, 'Economic cost analysis of hybrid renewable energy system using HOMER,' *IEEE-International Conference on Advances in Engineering, Science and Management (ICAESM)*, 2012.

[22] V. Prema V, K. Uma Rao, 'Sizing of Microgrids for Indian Systems using HOMER', *1st IEEE International Conference on Power Electronics, Intelligent Control and Energy Systems (ICPEICES)*, 2016.

[23] G. Sandeep, and V. S. Vakula,, 'Optimal combination and sizing of a standalone hybrid power system using HOMER', *International Conference on Electrical, Electronics, and Optimization Techniques (ICEEOT)* , 2016.

[24] S. Ghose, A. Shahat, and E. R. J. Haddad, 'Wind-solar hybrid power system cost analysis using HOMER for Statesboro, Georgia,' *SoutheastCon 2017, Charlotte, NC*, 2017.

[25] K. E. Okedu, and R.Uhunmwangho, 'Optimization of Renewable Energy Efficiency using HOMER', *Int. J. Renew. Energy Res.*, vol. 4, no. 2, 2014.

[26] Wen-Yeau Chang, 'The State of Charge Estimating Methods for Battery: A Review.Hindawi', *Publishing Corporation ISRN Applied Mathematics, Article ID 953792*, 2013.

[27] N. Watrin, B. Blunier, and A. Miraoui, 'Review of adaptive systems for lithium batteries state-of- charge and state-of-health estimation', *Proceedings of IEEE Transportation Electrification Conference and Expo*, pp. 1–6, Dearborn, Mich, USA, 2012.

4

Economic Load Dispatch Using Hybrid Crisscross Optimization

Kanchan Pawani, and Manmohan Singh

Department of Electrical and Instrumentation Eng., Sant Longowal Institute of Engineering and Technology, Longowal, Punjab, India
E-mail: kanchanpawani24@gmail.com; singh_manmohan@msn.com

Abstract

This chapter proposes a hybrid crisscross optimization technique to solve the thermal power dispatch problem with a single fuel type as a nonlinearly constrained optimization problem considering the operating cost problem as participating objective. The Crisscross optimization consists of horizontal cross-over and vertical cross-over operations to find a solution. These crossover operations aids the algorithm in view of diversity of solutions and hence enhance the chance of hitting the global optimum. The horizontal cross-over splits search space into hypercubes and reduces the unreachable region in search space. The vertical cross-over prevents the population from stucking into local minima due to one of the stagnant dimensions. In the proposed method, a local search is embedded in crisscross optimization to help the algorithm in the improvement of the solution obtained by the basic crisscross algorithm further and find a better solution in the nearby vicinity of the stagnated solution. The proposed method is validated on 8 benchmark test functions and small (3,6,13) and medium (40) generator problems. The suggested modified algorithm is able to obtain the lowest fuel cost of thermal generators than other methods, as evident from the results tabulated. As compared to other mentioned optimization approaches in the literature, the obtained results are feasible and better.

4.1 Introduction

The electric power grids are massively interconnected systems and have a major impact on the country's economy. It requires thorough analysis to ensure an efficient and determined operation. The analysis of the Economic Load Dispatch (ELD) problem to operate the thermal system in a coordinated and cost-effective manner. The ELD is an online mechanism for allocating generation to reduce total generation cost among available generating units while also meeting equality and inequality constraints [1–3]. The primary objective is to schedule the generating units that have been committed and improvement in generation scheduling leads to cost-saving. Due to the inclusion of multiple valves in the system, the ELD problem is nonlinear [4].

There are many optimization techniques used for solving the ELD problem. Researchers have used a variety of traditional and non-conventional optimization approaches to solve ELD problems. Several traditional approaches are dynamic programming, mixed-integer linear programming [5], quadratic programming [6], Lagrange relaxation method, and network flow method used to solve the problem. Traditional approaches are sensitive toward initial estimates, stuck to the local optimal solution, and failed to solve a non-linear optimization problem. Researchers proposed modern heuristic optimization techniques to provide better solution are Evolutionary Programming (EP) [7], Genetic Algorithm (GA) [8–13], Simulated Annealing (SA) [14, 15], Particle Swarm Optimization (PSO) [16–21], Grey Wolf Optimization (GWO) [22], Artificial Intelligence (AI) [23] for better solution. Gaing [16] described a PSO which is used to deal with Economic Dispatch (ED) issues related to many non-linear characteristics of generation and prohibits the drawbacks of premature convergence of GA and provides a better solution quality with more computational power. Park et al. described a modified PSO [24] which elaborates a method for fine-tuning the resultant region that combines the PSO algorithm and the key optimizer with sequential quadratic programming, such as a local optimizer. Chen Yeh [25] describes the four modified versions of PSO applied to find the solution to the ELD problem. Vlachogiannis Lee [26] proposed three new PSO algorithms, compared to the current state of PSO, such as reactive power and voltage control, for optimal PSO steady-state efficiency. Selvakumar, Thanushkodi [27] proposes a new PSO to resolve ED problems. Wang, Singh [28] proposed a new method of fuzzified

multi-objective PSO to resolve issues that arising from emission pollutant produced by fossil fuels as well as minimize the total cost of fuel. There are several available approaches to solve the ELD problem but none of them assured to global solution proven by the No Free Lunch (NFL) theorem [29].

This chapter proposed a Hybrid Crisscross Search Algorithm (HCSO) having two interfacing activities particularly horizontal and vertical operation embedded with the local search method. A local search is implemented in basic Crisscross Optimization (CSO) in the proposed strategy to facilitate the algorithm in further improving the solution produced by the basic criss cross approach and finding a better solution in the surrounding region of the stagnated solution.

4.2 Problem Formulation

Talaq et al. [31], suggested a judicious formulation of the economic dispatch problem as a nonlinear and nonconvex in behavior.

4.2.1 Economic Load Dispatch

ELD is a constrained nonlinear optimization problem in the area of power system operation and planning. The main purpose of ELD is just to schedule the produced output of determined generating units to satisfy fundamental demand at the least conceivable cost while meeting all unit and system operating constraints [32]. Mathematically, the ELD problem of the jth unit is calculated as

$$F_j(P_j) = a_j P_j^2 + b_j P_j + c_j \$/h \tag{4.1}$$

Due to the impact of multiple valves in the system, nonlinearities and discontinuities are introduced the system. Then, the ELD problem is calculated as

$$F_j(P_j) = a_j P^2 + b_j P + c_j + \left| e_j Sin(f_j(P_j^{\min} - P_j)) \right| \$/h \tag{4.2}$$

where a_j, b_j, c_j, e_j, f_j are the cost coefficient of jth generator unit. P_j and $P_j^{\min}$ are generating power and minimum power of jth generator.

The objective problem of ELD is to minimize the sum of all individual costs F_T subjected to

$$F_T = F_1 + F_2 + F_3 + F_4 + \ldots\ldots\ldots + F_N = \sum_{j=1}^{N} F_j(P_j) \tag{4.3}$$

where N is the total number of thermal units.

4.2.2 System Constraints

4.2.2.1 Power balance constraints

The sum of power produced by the system is equal to the sum of load demand P_D and total loss P_L of the system [33]

$$\sum_{j=1}^{N} P_j = P_D + P_L \tag{4.4}$$

where P_L is the transmission loss determined by using Kron's formula

$$P_L = \sum_{j=1}^{N} \sum_{k=1}^{N} P_j B_{jk} P_k + \sum_{j=1}^{N} B_{0j} P_j + B_{00} \tag{4.5}$$

where j,k denotes thermal unit indexes, B_{jk}, B_{0j}, and B_{00} are the power loss coefficients that can be assumed to be constant under standard operating circumstances.

4.2.2.2 Generator capacity constraints

The operating performance of each jth unit can be bounded by the maximum and minimum limits of the generator and expressed as follows

$$P_j^{\min} \leq P_j \leq P_j^{\max} \tag{4.6}$$

where, $P_j^{\max}$, $P_j^{\min}$ are maximum and minimum power production limits of the jth thermal unit respectively.

4.3 Constraint Handling

The constraint handling method is used to bring back the solutions from an infeasible range to a feasible range and solve constraint violating problems. There are various types of methods to handle constraints. In this chapter, the mutated form of the constraint handling method proposed by Singh and Dhillon [34] is used to check the feasibility of each search agent. The power generation is fixed within the minimum and maximum boundary of generation using Equation (4.6) and the power balance constraint is calculated using Equations (4.4) and (4.5). The difference between power demand and the sum of generation is calculated as follows

$$DP_D(i) = P_D - \sum_{j=1}^{N_g} P_j + P_L \tag{4.7}$$

The DP_D is distributed among all generating units, by choosing the jth generating unit. The control of the ith member of the total population expressed as

$$P_{ij} = \begin{cases} P_{ij} + DP_1(i) & DP_D(i) > 0 \\ P_{ij} - DP_2(i) & DP_D(i) < 0 \end{cases} \qquad (4.8)$$

where,

$$DP_1(i) = k.r.(P_j^{max} - P_{ij}). \left| \frac{DP_D(i)}{P_j^{max} - P_j^{min}} \right| \qquad (4.9)$$

$$DP_2(i) = k.r.(P_{ij} - P_j^{min}). \left| \frac{DP_D(i)}{P_j^{max} - P_j^{min}} \right| \qquad (4.10)$$

and r is the uniform random number in the range [0,1].

Algorithm 1: Constraint handling

- compute DP_D (i) using eq. (4.7)
- while max $|DP_D(i)| >$ epsilon
  - if $DP_D(i) > 0$
    - calculate $DP_1(i)$ using eq. (4.9)
    - compute $P(i, j)$ using eq. (4.8)
  - end if
  - if $DP_D(i) < 0$
    - calculate $DP_2(i)$ using eq. (4.10)
    - compute $P(i, j)$ using eq. (4.8)
  - end if
    - check limits $P(i, j)$ using eq. (4.4) & (4.6)
- end while

4.4 Proposed Method

4.4.1 Crisscross Optimization

Crisscross Optimization (CSO) is a stochastic search technique based on the population that involves iterative Horizontal Cross-over (HC) and Vertical Cross-over (VC) [30]. CSO generates offspring by conducting both crossover operations at each generation, those parents who can reproduce their moderate solution can survive otherwise eliminated from the competition.

The HC splits the multidimensional search space into half population hypercube succeeded by a competitive operator. This provides exploration searchability. The drawback of HC is to converge in local minima. The VC prevents the dimension from loophole of stagnant dimension. In VC, the arithmetic operation is performed between the different dimensions of all populations. The VC is also followed by a competitive operator to reproduce their offspring termed the moderate solution.

The procedure of CSO is explained as follows:

In CSO, the population is randomly created between maximum and minimum values with NP population and D dimension. Mathematically, it is given by

$$P_{ij} = P_j^{\min} + r_{ij}(P_j^{\max} - P_j^{\min});$$
$$(i = 1, 2, 3, 4, ...NP; \ j = 1, 2, 3, ..., D) \qquad (4.11)$$

The HC is an arithmetic cross-over that is performed between the different populations of every dimension. The $P(i_1)$, $P(i_2)$ are two randomly selected individuals to generate MSHC of dth dimension using Equations (4.12) and (4.13).

$$MSHC(i_1, d) = r_1.P(i_1, d) + (1 - r_1).P(i_2, d)$$
$$+ C_1.(P(i_1, d) - P(i_2, d)) \qquad (4.12)$$
$$MSHC(i_2, d) = r_2.P(i_2, d) + (1 - r_2).P(i_1, d)$$
$$+ C_2.(P(i_2, d) - P(i_1, d)) \qquad (4.13)$$

Here, r_1, r_2 are random numbers between [0,1]. C_1 and C_2 are uniformly scattered numbers [-1,1]. From the above equation, it is clear that a moderate solution consisting two terms. Firstly, the offspring describes the random location of offspring within scope. Secondly, it diminishes blind spots and enhances global searchability. The HC probability (P_{HC}) is taken as 1 to search better solution.

The arithmetic cross-over is performed for all populations of two different selected dimensions called VC. Consider the dimension d_1 and d_2 are used to perform VC. Normalize the parent individuals situated in a different dimension and the generated offspring of VC is formulated as

$$MSVC(i, d_1) = r.P(i, d_1) + (1 - r_1).P(j, d_2), d_1 \ \text{and}$$
$$d_2 \in (1, D) \qquad (4.14)$$

Algorithm 2 : Horizontal crossover

- input : DSVC, NP, D
- let P = DSVC
- B = permutate (M)
- normalize the matrix P
- for i =1 : NP/2

  - generate random number $p \in (0, 1)$.
  - if p < P_1, THEN Let $no1 = B(2 * i - 1)$ and $no2 = B(2 * i)$.

    - for j=1:D
    - create a uniformly random number
      $r_1, r_2 \in (0, 1); c_1, c_2 \in (-1, 1).$
    - $MSHC(no1, j) = r_1.P(no1, j) + (1 - r_1).P(no2, j)$
      $+C_1.(P(no1, j) - P(no2, j))$
    - $MSHC(no2, j) = r_2.P(no2, j) + (1 - r_2).P(no1, j)$
      $+C_2.(P(no2, j) - P(no1, j))$
    - end for

  - end if

- end for
- reverse normalize the matrix P.
- update DSHC with a competitive operator.

After performing VC, reverse normalization is executed. DSHC and DSVC are parent-dominated solutions and MSHC and MSVC are moderate offspring of HC and VC. The VC probability (P_{VC}) is taken as 1 to search better solution.

A competitive operator gives a chance to the rivalry between the posterity populace and its parent populace. The competition is executed between moderate solution and parent solution, then stored in DSHC and DSVC.

Algorithm 3 : Vertical crossover

- input: DS$_{hc}$, M, D
- X← DS$_{hc}$
- normalize the matrix.
- let B = permutate (D).
  - for i = 1 to D/2
    - generate a uniformly random number $p \in (0, 1)$.
    - if $p < P_2$, THEN Let $no\,1 = B(2 * i - 1)$ and $no\,2 = B(2 * i)$.

- for $j = 1$ to M
  - generate a uniformly random number $r \in (0, 1)$.
  - $MSvc(j, no1) = X(j, no1) + (1 - r).X(j, no2)$.
- end for j
- end if
- end for i
- reverse normalization.
- update DS_{vc} with the competitive operator.

Algorithm 4 : Competitive operator

- for i = 1:NP
- evaluate MS(i)

  - if MS(i) is preffered than its parent X(i), Then

    - DS(i) ← MS(i)
    - else DS(i) ← X(i)

  - end if

- end for

4.4.2 Hybridization of CSO with Local Search Method

In the proposed modified HCSO algorithm, a local search (LS) adds up with the basic CSO algorithm. When the basic CSO algorithm stops improving the position of the members further, the LS helps the members to search for a better solution near the vicinity of the stagnated position.

Local search is a sequential technique of exploration in the vicinity of the already achieved solution and exploitation of the direction of position updating in the exploration step. The first kind of move includes exploring the local objective function and the second kind includes the advantage of direction. In the process of finding a feasible result nearby search space, the step function is taken as

$$stepP_j = \frac{P_j^{\max}}{a} \tag{4.15}$$

The new explored position of a member is found as

$$P_{ij}^{new1} = P_{ij} + stepP_j \tag{4.16}$$

$$P_{ij}^{new2} = P_{ij} - stepP_j \tag{4.17}$$

The comparison between the fuel costs at position values P_{ij}^{new1}, P_{ij}^{new2} and P_{ij} is made and the new explored position is updated with the lowest fuel cost. Next, the exploitation step consists of updating the new better position by exploiting the direction of the position updating in the exploration step.

Algorithm 5: ELD Algorithm

- initialize population.
- if any constraints are violated, fix constraints by adopting constraint handling using Algorithm 1.
- evaluate fuel cost F_i using eq. (4.1) & eq. (4.2).
- calculate P_{ij}.
- update the best position.
- for iteration=1, max iteration
- evaluate horizontal crossover from eq. (4.12) and (4.13) using Algorithm 2 .
- compute the solution using the competitive operator discussed in Algorithm 4.
- evaluate objective function fuel cost F_i, P_{ij} using eqs. (4.1) , (4.2).
- update the best position.
- evaluate vertical crossover from eq. (4.14) using Algorithm 3.
- compute the solution using the competitive operator discussed in Algorithm 4.
- calculate P_{ij}
- evaluate objective function F_i using eq. (4.1) , (4.2).
- update the best position.
- end for iteration.
- update the best solution by using a local search routine

4.5 Result and Discussion

The performed HCSO algorithm is employed to evaluate standard test functions, ELD problems having 3, 6, 13, 40 unit systems, and comparison with other methods in the literature. The results are obtained by selecting a population size of 100. MATLAB 2015a is used to employ the HCSO technique.

Table 4.1 Function details

S.No.	Function	Function description	D	Range	Min value
I	Sphere	$f_1(x) = \sum\limits_{j=1}^{D} x_j^2$	30.0	$[-100, 100]$	0.0
II	Schwefel 2.22	$f_2(x) = \sum\limits_{j=1}^{D} |x_j| + \prod\limits_{j=1}^{D} |x_j|$	30.0	$[-100, 100]$	0.0
III	Schwefel 2.23	$f_3(x) = \sum\limits_{j=1}^{D} x_j^{10}$	30.0	$[-10,10]$	0.0
IV	Step	$f_4(x) = \sum\limits_{j=1}^{D} (\lfloor x_j + 0.5 \rfloor)^2$	30.0	$[-100,100]$	0.0
V	Rastrigin	$f_5(x) = $ $\sum\limits_{j=1}^{D} [x_j^2 - 10\cos(2*pi*x_j) + 10]$	30.0	$[-5.12,5.12]$	0.0
VI	Powell	$f_6(x) = \sum\limits_{j=1}^{D/4} (x_{4j-3} + 10x_{4j-2})^2 +$ $5(x_{4j-1} - x_{4j})^2 + (x_{4j-2} - x_{4j-1})^4 +$ $10(x_{4j-3} - x_{4j})^4$	30.0	$[-4,5]$	0.0
VII	Griewank	$f_7 = \frac{\sum\limits_{j=1}^{D} x_j^2}{4000} - \prod\limits_{j=1}^{D} \cos(x_j/\sqrt{j}) + 1$	30.0	$[-600,600]$	0.0
VIII	Alpino	$f_8(x) = \sum\limits_{j=1}^{D} |x_j \sin x_j + 0.1x_j|$	30.0	$[-10,10]$	0.0

4.5.1 Benchmark Function

To estimate the performance of the proposed HCSO technique, standard test functions [35] are used. The result obtained by selecting swarm size 100, dimension (D) for each of the standard benchmark functions are taken as 30 at a fixed number of iteration 500. Details of benchmark functions utilized in the experiment are summarized in Table 4.1. The results obtained from different benchmark functions using the projected HCSO algorithm are listed below in Table 4.2.

To eliminate any uncertainty, the results obtained by all experiments depended on 30 free runs. The least error of the proposed HCSO technique is provided in Table 4.2 and the maximum number of function evaluations (NFE) is set as 3×10^5. The Sphere function, uni-model in nature, has a minimum error value of 5.50×10^{-134}. The minimum error obtained by uni-modal Schwefel 2.22 is 2.67×10^{-65}. The Schwefel 2.23, Step and Rastrigin, and Griewank functions are obtained all minimum error, average error,

Table 4.2 Result of benchmark functions

x^*	Sphere	Schwefel 2.22	Schwefel 2.23	Step	Rastrigin	Powell	Griewank	Alpino
1	-1.37×10^{-132}	5.8176×10^{-67}	2.880×10^{-33}	-0.2336	-2.1703	0.297833	1.44×10^{-09}	0.2888
2	-195×10^{-132}	1.793×10^{-66}	-1.642×10^{-33}	-0.0977	-4.51715	-0.02967	-2.73×10^{-8}	-1.0968
3	-7.93×10^{-133}	5.2672×10^{-69}	-3.0127×10^{-34}	0.1004	4.000962	0.286781	-7.41×10^{-8}	0.4947
4	-6.66×10^{-133}	-3.6429×10^{-66}	-1.1297×10^{-33}	-0.1657	0.001495114	0.299343	2.04×10^{-8}	-1.9538
5	2.24×10^{-132}	-9.8941×10^{-67}	-2.070×10^{-33}	0.3245	1.103749	0.232779	5.55×10^{-8}	-0.0542
6	-3.08×10^{-132}	9.6485×10^{-67}	8.5244×10^{-35}	0.3333	-1.32755	-0.02278	1.68×10^{-8}	-0.1635
7	1.66×10^{-132}	2.5256×10^{-66}	3.4645×10^{-33}	-0.2645	0.392666	0.294081	-8.01×10^{-8}	-0.4449
8	-2.05×10^{-132}	6.6933×10^{-67}	-9.756×10^{-34}	-0.4905	-0.06696	0.293094	-5.89×10^{-8}	-1.1638
9	-5.53×10^{-133}	-2.0368×10^{-66}	-6.007×10^{-34}	0.0562	0.785685	0.165379	-9.15×10^{-8}	1.8883
10	2.25×10^{-132}	3.0069×10^{-66}	-2.447×10^{-34}	0.161	1.404343	-0.01659	4.82×10^{-8}	0.2512
11	9.36×10^{-133}	-1.0608×10^{-66}	-5.259×10^{-34}	-0.0761	4.078729	0.111713	5.49×10^{-8}	-0.8166
12	-2.42×10^{-132}	2.5198×10^{-67}	3.2070×10^{-33}	-0.309	-0.71439	0.112401	8.02×10^{-8}	-0.6918
13	2.16×10^{-132}	-1.7323×10^{-66}	-2.197×10^{-34}	-0.2582	-1.28383	0.185939	1.52×10^{-8}	0.8041
14	-2.17×10^{-132}	-5.2338×10^{-67}	4.0423×10^{-33}	-0.1557	0.750031	-0.01856	-8.99×10^{-8}	5.0007
15	-4.18×10^{-133}	-2.4258×10^{-66}	-7.8237×10^{-34}	-0.2128	1.157964	0.140341	8.63×10^{-8}	-0.9594
16	5.24×10^{-133}	-3.2920×10^{-67}	-1.9572×10^{-33}	-0.1007	0.527305	0.141099	-2.56×10^{-9}	-0.3719
17	-1.89×10^{-132}	5.6117×10^{-68}	1.6019×10^{-33}	-0.0728	-1.22592	0.102985	1.30×10^{-8}	-3.4610
18	8.19×10^{-133}	1.4455×10^{-67}	3.46552×10^{-33}	0.4103	1.478656	-0.01024	1.05×10^{-7}	0.7640
19	-8.90×10^{-133}	7.5695×10^{-67}	-3.0266×10^{-33}	0.0498	-0.28738	0.147541	-6.80×10^{-8}	-1.4710
20	-1.14×10^{-132}	1.8887×10^{-67}	2.835×10^{-33}	-0.1352	1.707117	0.148726	-1.54×10^{-7}	-1.8009
21	1.70×10^{-132}	8.6298×10^{-67}	3.6702×10^{-33}	-0.0525	-1.63897	0.268424	-3.99×10^{-8}	0.6815
22	4.02×10^{-132}	-1.5493×10^{-67}	4.1558×10^{-33}	0.0042	-1.0882	-0.02664	3.00×10^{-8}	-0.3777
23	-2.25×10^{-132}	1.9090×10^{-67}	-6.874×10^{-34}	-0.2356	-1.50979	0.177696	-8.87×10^{-8}	-0.6913
24	5.08×10^{-133}	-2.1428×10^{-67}	-4.0929×10^{-33}	0.2318	0.012937	0.180664	-4.73×10^{-8}	-1.5320
25	1.14×10^{-133}	-6.9845×10^{-68}	-2.083×10^{-33}	-0.0504	1.031841	-0.12881	2.25×10^{-8}	0.6191

(Continued)

Table 4.2   *(Continued)*

x^*	Sphere	Schwefel 2.22	Schwefel 2.23	Step	Rastrigin	Powell	Griewank	Alpino
26	2.46×10^{-133}	7.4988×10^{-68}	2.1361×10^{-33}	0.0039	-4.62835	0.012707	-4.84×10^{-9}	-2.3411
27	-2.46×10^{-133}	-2.6911×10^{-67}	-1.4262×10^{-33}	0.2809	2.176958	-0.15914	8.82×10^{-8}	1.0008
28	-2.36×10^{-132}	1.6827×10^{-66}	2.261×10^{-33}	-0.3916	-1.19279	-0.15911	1.42×10^{-7}	0.6134
29	-1.72×10^{-132}	2.9343×10^{-67}	-7.4530×10^{-34}	-0.1267	3.753716	0.014622	-8.99×10^{-8}	-0.3399
30	3.29×10^{-133}	-3.4056×10^{-68}	-6.9703×10^{-34}	0.2882	4.54×10^{-10}	1.143649	1.57×10^{-7}	-7.867×10^{-67}
$f(x^*)$	5.50×10^{-134}	2.6757×10^{-65}	0	0	0	0.026034	0	6.1862×10^{-133}

and the standard deviation is zero which results in faster convergence. The minimum error, average error, and deviation error of the Powell function are 0.026034, 0.060982, and 0.012801. The minimum error of the Alpino function is 6.1862×10^{-133} and its average error and standard deviation are 2.85×10^{-15} and 4.51071×10^{-15}.

4.5.2 Economic Load Dispatch Problem

The proposed HCSO algorithm is analyzed on a single objective ELD problem of small (3,6,13 units) and medium (40 unit) power system problems. The population length for all the considered cases is taken as 100 and, the maximum iteration is 1000. The maximum function evaluation number of the proposed HCSO is taken as 6×10^5. The strength of the proposed technique is guaranteed by 30 commonly autonomous runs of the proposed technique for every one of the cases.

4.5.2.1 Problem 1: Three generator problem

Three generator thermal power systems are taken [12] with a power demand (P_D) of 850 MW along with generator constraints. The generation scheduling data for the problem is taken from reference [12]. The minimum cost of 3 generator problem and their generations are listed in Table 4.3 without losses after performing 30 independent runs of the ELD problem. The obtained solution of the proposed HCSO algorithm is 8233.3986. After performing 30 independent runs, the average cost, peak cost, and Standard Deviation (std) of the proposed algorithm are 8244.9, 8272.30 and 47.8422. Table 4.4 shows that obtained minimum fuel cost by HCSO is improved than the cost obtained by previously listed methods Social-Spider Optimization (SSO) [36], novel improved social-spider optimization (NISSO) [37], Modified Social-Spider Optimization (MSSO) [38], Opposition-Based Social-Spider Optimization (OBSSO) [39], Comprehensive Learning Particle Swarm Optimizer (CLPSO) [40], adaptive differential evolution (JADE) [12], Classical Evolutionary Programming (CEP) [12], Mutation in Fast Evolutionary Programming (MFEP) [12], Fast Evolutionary Programming (FEP) [12], Improved Fast Evolutionary Programming (IFEP) [12] and Improved Social-Spider Optimization (ISSO) [41]. Figure 4.1 shows the convergence nature of the 3 generator problem.

4.5.2.2 Problem 2: Six generator problem

A six generator thermal power system is taken under [42] 1263 MW P_D along with transmission losses and generator constraints. The generation scheduling

Table 4.3   Generation output of 3 generator problem

HCSO Output	P_1	P_2	P_3	$\sum P_i$	Fuel cost
	149.7361	399.7135	300.451	849.9	8233.3985

Table 4.4   Comparison of 3 generator solutions with other methods

Methods	Minimum	Mean	Maximum	Std
SSO[36]	8234.070	8240.890	8244.150	–
NISSO[37]	8234.070	8238.440	8242.040	–
MSSO[38]	8234.070	8236.080	8240.570	–
OBSSO[39]	8234.070	8235.960	8241.70	–
CLPSO[40]	8234.070	8234.070	8234.070	–
JADE[12]	8234.070	8234.070	8234.070	–
CEP[12]	8234.070	8235.970	8241.830	–
FEP[12]	8234.070	8234.240	8241.780	–
MFEP[12]	8234.080	8234.710	8241.80	–
IFEP[12]	8234.070	8234.160	8234.540	–
ISSO[41]	8234.070	8234.070	8234.070	–
HCSO	8233.3985	8244.9	8272.30	47.8422
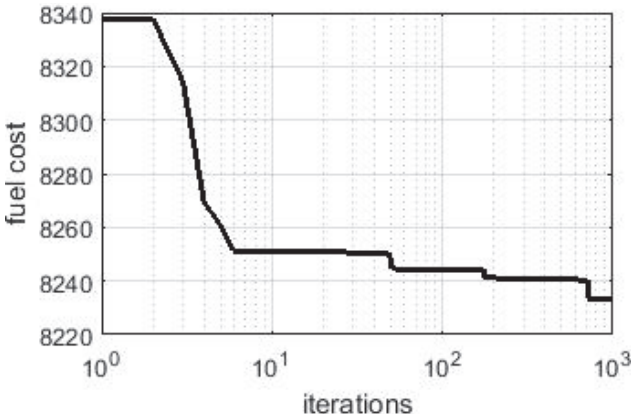
Figure 4.1   Convergence diagram of 3 Generator Problem

data for the problem is taken from [42]. The minimum cost and generated output of generating units are listed in Table 4.5 of the ELD problem by the proposed HCSO. Table 4.6 also displays the comparison of the solutions obtained by the HCSO algorithm with other existing methods PSO [42], classical PSO (CPSO) [42], Weight Improved PSO (WIPSO) [42], Moderate Random Search PSO (MRPSO) [42] for solving six generator problem and found that HCSO provides a better solution than the other available methods.

Table 4.5 Generation output of 6 generator problem

P(MW)	1	2	3	4	5	6	$\sum P_i$	Fuel cost
HCSOOutput	403.98	199.28	229.70	127.85	199.52	115.75	1276.07	15573.37

Table 4.6 Comparison of 6 generator results with other methods

Unit P (MW)	PSO [42]	CPSO [42]	WIPSO [42]	MRPSO [42]	Proposed HCSO
1	443.034	467.550	437.82	442.07	403.98
2	169.03	163.05	173.28	167.23	199.28
3	262.02	253.415	271.97	267.09	229.70
4	134.78	115.07	138.7	132.81	127.85
5	147.47	169.45	146.98	155.02	199.52
6	125.35	113.24	103.632	107.023	115.75
Fuel cost	16372.9	16329.2	16327.0	16310.76	15573.37
Losses	18.68	18.70	18.08	18.03	13.07
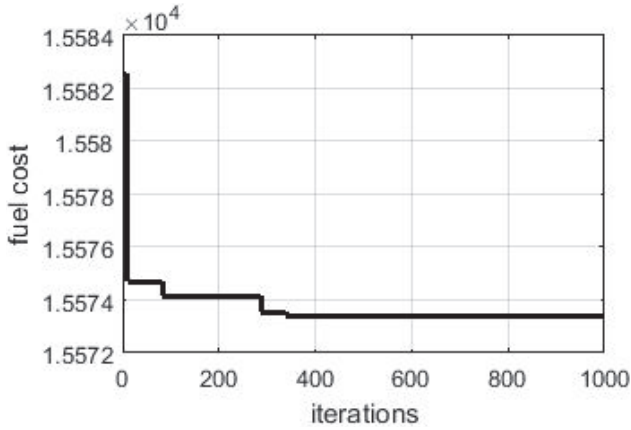
Figure 4.2 Convergence diagram of 6 Generator Problem

The obtained minimum fuel cost of six generators with valve point loading (VPL) by using the proposed method is 15573.37. The least cost, mean cost, maximum cost, standard deviation, and losses of six generators with VPL are 15573.37, 15628.68, 15669.64, 23.88258, and 13.07 after 30 consecutive trials. Figure 4.2 displays the convergence of 6 generator problems.

4.5.2.3 Problem 3: Thirteen generator problem

Thirteen generator problems considering VPL with P_D of 1800 MW. The scheduling data is taken from the reference [12]. The least cost, mean cost, maximum cost, and deviation of the proposed HCSO are 18008.94,
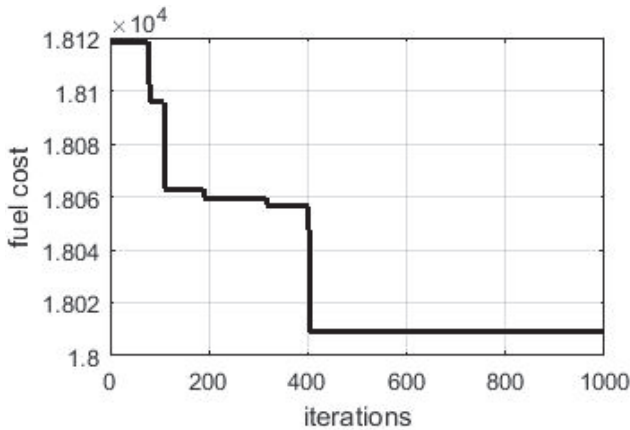
Figure 4.3   Convergence diagram of 13 Generator Problem

18037.64, 18070.3, and 30.424, respectively as described in Table 4.7 after completing 30 successive runs. The generation scheduling of 13 generators is also described in Table 4.7. The execution of the proposed HCSO method is compared with Neural Network Evolutionary PSO (NN-EPSO) [43] and Grey Wolf Optimizer (GWO) [43] as shown in Table 4.7 and it is concluded that convergence of HCSO is better than NN-EPSO [43] and GWO [43]. Figure 4.3 displays the converged nature of HCSO in 13 generator problems.

4.5.2.4 Problem 4: Forty generator problem

A forty generator thermal power system is taken under 10500 MW power demand along with generator constraints. The data for the generation schedule of the ELD problem is extracted from [30]. The minimum cost of ELD listed in Table 4.8 is 121438.471 after performing thirty independent runs with 1000 iterations. The attained cost of the HCSO is preferred over the methods PSO [30], Quantum-Behaved PSO (QPSO) [30], Improved Genetic Algorithm with Multiplier Updating (IGA-MU) [30], efficient Evolutionary Strategies Optimization (ESO) [30], Modified PSO (MPSO) [30], the Electromagnetism-Like Mechanism (ELM) [30], CSO [30] and ISSO [41] as depicted in Table 4.9. Figure 4.4 depicts the converged nature of forty generator. The proposed method improves the results and provides a better solution.

Table 4.7 Generated output and comparison of 13 generator results with other methods

P(MW)	1	2	3	4	5	6	7	8	9	10	11	12	13	Fuel cost
Methods														
NN-EPSO	490.0	189.0	214.0	160.0	90.0	120.0	103.0	88.0	104.0	13.0	58.0	66.0	55.0	18442.59
GWO	807.125	144.869	297.943	60.0	60.0	60.0	60.0	60.0	60.036	40.0	40.027	55.0	55.0	18051.11
HCSO	629.6379	147.9132	223.767	110.404	109.0087	109.6217	110.3344	60.0081	109.2031	40	40.00234	55	55	18008.94

Table 4.8 Generation output of 40 generator problem

P(MW)	1	2	3	4	5	6	7	8	9	10
	110.66806	110.71068	96.955739	179.16522	87.774561	139.88615	259.58284	284.30633	284.14966	273.67359
11	12	13	14	15	16	17	18	19	20	21
169.26022	243.67294	394.31047	393.52545	304.55589	304.52329	489.10829	399.46185	421.52977	511.02889	523.27289
22	23	24	25	26	27	28	29	30	31	32
523.60145	523.21116	523.29753	520.69273	523.2189	10.112243	10.093604	10.024621	88.584315	159.75533	160.09385
33	34	35	36	37	38	39	40	Fuel cost		
159.88378	166.78019	164.63772	164.68505	80.922345	109.84381	108.27282	511.07417	121438.47		

Table 4.9 Comparison of 40 generator results with other methods

P(MW)	CSO [30]	PSO [30]	QPSO [30]	ELM [30]	MPSO [30]	ESO [30]	IGA-MU [30]	ISSO [41]	Proposed HCSO
1	111.0136	114	113.9947	74.4681	114	114	111.9206	113.81	110.6680571
2	111.5514	114	113.9345	74.4740	114	114	110.8223	110.94	110.7106846
3	97.3929	120	97.4006	94.6381	120	120	97.4081	119.93	96.95573917
4	129.8951	80	179.7331	81.0080	182.222	190	179.7336	179.71	179.1652206
5	96.8922	97	96.9971	72.6285	97	97	88.2042	96.91	87.77456066
6	105.4232	140	139.9985	99.3476	140	140	139.9976	140	139.8861513
7	260.0494	300	300	298.6358	300	300	259.7454	300	259.5828445
8	284.7791	284.3341	286.4702	298.3461	299.021	288.88	286.1419	300	284.306331
9	284.6225	285.2316	285.4186	298.0049	300	285.91	285.6566	284.64	284.1496563
10	130.1038	203.6777	130.0315	132.4660	130	203.02	130	130	273.6735914
11	168.7252	169.2903	94.0016	94.2445	94	94.36	168.7987	94	169.2602249
12	168.7715	168.5973	94.0015	98.3919	94	96.45	94.0006	94	243.6729409
13	214.7692	483.9889	214.7606	125.0009	125	211.51	304.4441	125	394.3104732
14	394.3310	394.3104	304.5218	498.6214	304.485	301.46	394.2794	214.77	393.525446
15	394.1768	394.1969	394.2796	484.3611	394.607	394.80	394.2788	304.39	304.5558919
16	394.1995	483.7718	394.2800	483.4443	305.323	300.15	394.2808	483.77	304.5232898
17	489.3000	399.4243	489.2847	494.0316	490.272	490.90	489.2802	498.09	489.1082854
18	489.3798	500	489.4841	497.5470	500	489.13	489.2832	489.49	399.4618457
19	511.3281	511.2445	511.4715	549.3579	511.404	512.03	511.2821	511.5	421.5297701
20	511.3635	511.2965	511.2812	547.2354	512.174	512.08	511.2809	511.22	511.028892
21	523.3249	433.7442	523.2897	520.1491	550	521.92	523.3001	523.27	523.27289
22	523.3247	523.9082	523.2933	543.2105	523.655	532.09	523.2806	546.12	523.6014486
23	523.4176	344.0649	523.4033	548.2634	534.661	527.14	523.2821	549.56	523.2111577

Table 4.9 *Continued*

24	523.6748	433.7470	523.3060	547.4293	550	524.54	523.2796	549.47	523.2975299
25	523.3194	522.6389	523.2924	528.8353	525.057	522.88	523.2822	549.97	520.6927292
26	523.3496	523.7630	523.2909	548.3278	549.155	522.42	523.2791	549.76	523.2188998
27	10.1067	10.000	10.0102	11.6232	10	10.42	10.0001	10.21	10.11224335
28	10.0432	10.000	10.0005	11.7375	10	10.71	10.0002	10	10.09360447
29	10.0455	10.000	10.0110	11.3373	10	13.96	10.0001	10.03	10.02462118
30	88.0888	97.000	96.9991	73.8150	97	85.35	87.9676	88.18	88.58431464
31	189.9297	190.00	189.9987	188.4214	190	189.92	160.2761	190	159.7553335
32	189.9582	190.000	189.9999	188.7283	190	190	162.2347	190	160.0938468
33	189.9093	190.00	190.000	178.6045	190	189.16	165.9863	190	159.8837806
34	165.8554	200	199.9986	91.5903	200	197.28	165.8653	200	166.7801866
35	165.0159	200	180.5082	168.7271	200	166.31	199.9996	200	164.637715
36	165.8350	200	199.9998	174.5438	200	199.36	164.8574	200	164.685051
37	109.9105	110	109.9715	86.0329	110	109.69	89.8252	110	80.92234518
38	109.9144	25	109.9996	70.0475	110	108.57	91.4569	110	109.8438113
39	95.5888	110	109.9998	62.1027	110	108.90	89.7082	109.98	108.2728207
40	511.3198	421.6701	511.2822	548.4804	512.964	514.02	511.2792	511.29	511.0741723
Total output	10500	10499.9005	10500	10498.2602	10500	10500.61	10500	10500.01	10499.9084
Fuel Cost	121772.59010	125322.5881	121811.5911	125923.6577	122252.265	122122.16	121819.2521	122519.24	121438.471
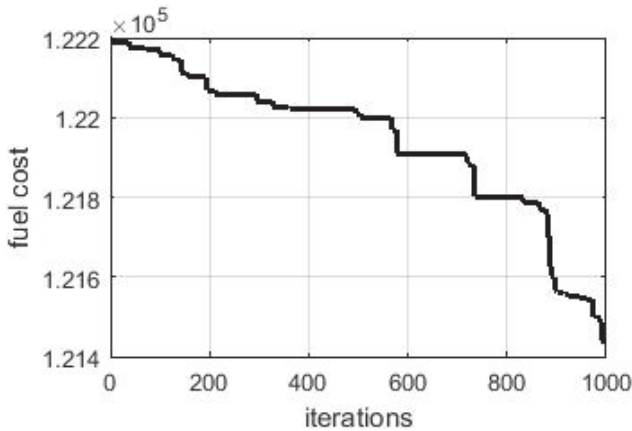
Figure 4.4   Convergence diagram of 40 Generator Problem

4.6 Conclusion

This chapter presents the local search embedded Crisscross optimization technique to solve single fuel type thermal power dispatch non-convex optimization problems subject to constraints owing to the physical limitations of the equipment involved. The ELD problem formulation is presented with valve point loading effect, transmission losses, and generator constraints. The main parts of the basic criss-cross algorithm are horizontal and vertical crossover operations. The horizontal cross-over divides the search space into hypercubes, hence reducing the inaccessible zones of the search space. The vertical cross-over keeps the population from being trapped in local minima owing to a static dimension. In the proposed HCSO basic CSO is embedded with a local search method that upgrades the quality of results. A local search is incorporated in CSO to aid the algorithm for further improving the solutions as produced by the basic CSO and finding a better solution in the near neighborhood area of the stalled solution.

Applicability of HCSO is validated by applying it to solve Benchmark optimization functions; and real-world small (3,6,13 unit systems) and medium (40 unit system) generation scheduling problems. The numerical solutions of the test functions conclude that this method is efficient in searching for nearly global results. The attained solutions from the proposed hybrid CSO are competitive and the best compared to previous outcomes recorded in the literature. The result shows that the proposed HCSO is efficient and convergent.

Future plan

The HCSO algorithm can be applied to solve multi-disciplinary thermal dispatch issues with renewable availability.

References

[1] L. V. N. Rao, "PSO Technique for Solving the Economic Dispatch Problem Considering the Generator Constraints," *Int. J. Adv. Res. Electr. Electron. Instrum. Eng.*, vol. 3, no. 7, pp. 10439–10454, 2014.

[2] S. Tiwari, B. Dwivedi, M. P. Dave, A. Shrivastava, A. Agrawal, and B. V. Singh, "Unit commitment problem in a renewable integrated environment with storage: A review," *Int. Trans. Electr. Energy Syst.*, no. October 2020, p. e12775, 2021.

[3] S. Tiwari, B. Dwivedi, and M. P. Dave, "A Two Stage Solution Methodology for Deterministic Unit Commitment Problem," in *2016 IEEE Uttar Pradesh Section International Conference on Electrical, Computer and Electronics Engineering (UPCON)*, 2016, pp. 317–322.

[4] D. N. Jayakumar and P. Venkatesh, "Glowworm swarm optimization algorithm with topsis for solving multiple objective environmental economic dispatch problem," *Appl. Soft Comput. J.*, vol. 23, pp. 375–386, 2014.

[5] S. Pan, J. Jian, H. Chen, and L. Yang, "A full mixed-integer linear programming formulation for economic dispatch with valve-point effects, transmission loss and prohibited operating zones," *Electr. Power Syst. Res.*, vol. 180, p. 106061, 2020.

[6] G. P. Granelli and M. Montagna, "Security-constrained economic dispatch using dual quadratic programming," *Electr. Power Syst. Res.*, vol. 56, no. 1, pp. 71–80, 2000.

[7] H. Yang, P. Yang, and C.-L. Huang, "EVOLUTIONARY PROGRAMMING BASED ECONOMIC DISPATCH FOR UNITS WITH NON-SMOOTH FUEL COST FUNCTIONS," *IEEE Trans. Power Syst.*, vol. 11, no. 1, pp. 112–118, 1996.

[8] F. N. Lee and A. M. Breipohl, "Reserve constrained economic dispatch with prohibited operating zones," *IEEE Trans. Power Syst.*, vol. 8, no. 1, pp. 246–254, 1993.

[9] A. Bakirtzis, V. Petridis, and S. Kazarlis, "Genetic algorithm solution to the economic dispatch problem," *IEE Proceeding Gener. Transm. Distrib.*, vol. 141, no. 4, pp. 377–382, 1994.

[10] G. B. Sheble and K. Britting, "Refined Genetic Algorithm - Economic Dispatch Example," *IEEE Trans. Power Syst.*, vol. 10, no. 1, pp. 117–124, 1995.

[11] P. Chen and H. Chang, "Large-scale economic dispatch by genetic algorithm," vol. 10, no. 4, pp. 1919–1926, 1995.

[12] N. Sinha, R. Chakrabarti, and P. K. Chattopadhyay, "EVOLUTION-ARY PROGRAMMING TECHNIQUE FOR ECONOMIC LOAD DIS-PATCH," *IEEE Trans. Evol. Comput.*, vol. 7, no. 1, pp. 83–94, 2003.

[13] Y. H. Song and C. S. V Chou, "Large-Scale Economic Dispatch by Artificial Ant Colony Search Algorithms," *Electr. Mach. Power Syst.*, vol. 27, no. 7, pp. 679–690, 1999.

[14] K. P. Wong and Y. W. Wong, "Genetic and genetic / simulated-annealing approaches to economic dispatch," *IEE Proc. Gener. Transm. Distrib.*, vol. 141, no. 5, pp. 507–513, 1994.

[15] K. P. Wong and Y. W. Wong, "Short-term hydrothermal scheduling Part I: simulated annealing approach," *IEE Proc. Gener. Transm. Distrib.*, vol. 141, no. 5, pp. 497–501, 1994.

[16] Z. Gaing, "Particle Swarm Optimization to Solving the Economic Dispatch Considering the Generator Constraints," vol. 18, no. 3, pp. 1187–1195, 2003.

[17] L. dos S. Coelho and V. C. Mariani, "Economic Dispatch Optimization Using Hybrid Chaotic Particle Swarm Optimizer," in *IEEE International Conference on Systems*, 2007, pp. 1963–1968.

[18] J. Kennedy and R. Eberhart, "Particle Swarm Optimization," in *ICNN'95-international conference on neural networks, IEEE*, 1995, pp. 1942–1948.

[19] A. I. S. Kumar, K. Dhanushkodi, J. J. Kumar, and C. K. C. Paul, "Particle Swarm Optimization Solution to Emission and Economic Dispatch Problem," in *Conference on Convergent Technologies for Asia-Pacific Region, IEEE.*, 2003, pp. 435–439.

[20] Z. Gaing, "Constrained dynamic economic dispatch solution using particle swarm optimization," in *IEEE Power Engineering Society General Meeting*, 2004, pp. 153–158.

[21] P. Sriyanyong, "Solving Economic Dispatch Using Particle Swarm Optimization Combined with Gaussian Mutation," in *5th International Conference on Electrical Engineering/Electronics, Computer, Telecommunications and Information Technology*, 2008, pp. 885–888.

[22] S. Tiwari, V. Bhadoria, and B. Dwivedi, *Application of Artificial Intelligence-Based Solution Methodology in Generation Scheduling Problem*. 2021.

[23] S. Tiwari, B. Dwivedi, and M. Dave, "A multi-stage hybrid artificial intelligence-based optimal solution for energy storage integrated mixed generation unit commitment problem," *J. Intell. Fuzzy Syst.*, vol. 35, pp. 4909–4919, 2018.

[24] J. Park, K. Lee, J. Shin, and K. Y. Lee, "A Particle Swarm Optimization for Economic Dispatch With Nonsmooth Cost Functions," *IEEE Trans. Power Syst.*, vol. 20, no. 1, pp. 34–42, 2005.

[25] C. H. Chen and S. N. Yeh, "Particle Swarm Optimization for Economic Power Dispatch with Valve-Point Effects," in *IEEE/PES Transmission & Distribution Conference and Exposition: Latin America*, 2006, vol. 00, pp. 1–5.

[26] J. G. Vlachogiannis and K. Y. Lee, "A Comparative Study on Particle Swarm Optimization for Optimal Steady-State Performance of Power Systems," *IEEE Trans. Power Syst.*, vol. 21, no. 4, pp. 1718–1728, 2006.

[27] A. I. Selvakumar and K. Thanushkodi, "A New Particle Swarm Optimization Solution to Nonconvex Economic Dispatch Problems," *IEEE Trans. Power Syst.*, vol. 22, no. 1, pp. 42–51, 2007.

[28] L. Wang and C. Singh, "Environmental/economic power dispatch using a fuzzified multi-objective particle swarm optimization algorithm," *Electr. Power Syst. Res.*, vol. 77, no. 12, pp. 1654–1664, 2007.

[29] D. H. Wolpert and W. G. Macready, "No Free Lunch Theorems for Optimization," *IEEE Trans. Evol. Comput.*, vol. 1, no. 1, pp. 67–82, 1997.

[30] A. Meng, Y. Chen, H. Yin, and S. Chen, "Crisscross optimization algorithm and its application," *Knowledge-Based Syst.*, vol. 67, pp. 218–229, 2014.

[31] J. H. Talaq, F. El-Harwary, and M. E. El-Harwary, "A SUMMARY OF ENVIRONMENTAL/ECONOMIC DISPATCH ALGORITHMS," *IEEE Trans. Power Syst.*, vol. 9, no. 3, pp. 1508–1516, 1994.

[32] J. S. Dhillon, J. S. Dhillon, and D. P. Kothari, "Economic-emission load dispatch using binary successive approximation-based evolutionary search," *IET Gener. Transm. Distrib.*, vol. 3, no. 1, pp. 1–16, 2009.

[33] D. Singh and J. S. Dhillon, "Ameliorated grey wolf optimization for economic load dispatch problem," *Energy*, vol. 169, pp. 398–419, 2019.

[34] M. Singh and J. S. Dhillon, "Multiobjective thermal power dispatch using opposition-based greedy heuristic search," *Electr. power energy Syst.*, vol. 82, pp. 339–353, 2016.

[35] G. Xiong, D. Shi, and X. Duan, "Enhancing the performance of biogeography-based optimization using polyphyletic migration operator and orthogonal learning," *Comput. Oper. Res.*, vol. 41, pp. 125–139, 2014.

[36] E. Cuevas, M. Cienfuegos, D. Zaldívar, and M. Pérez-cisneros, "A swarm optimization algorithm inspired in the behavior of the social-spider," *Expert Syst. Appl.*, vol. 40, no. 16, pp. 6374–6384, 2013.

[37] T. T. Nguyen, "A high performance social spider optimization algorithm for optimal power flow solution with single-objective optimization," *Energy*, vol. 171, pp. 218–240, 2019.

[38] C. E. Klein, E. H. V Segundo, V. C. Mariani, and L. dos S. Coelho, "Modified Social-Spider Optimization Algorithm Applied to Electro-magnetic Optimization," *IEEE Trans. Magn.*, vol. 52, no. 3, pp. 1–4, 2016.

[39] R. A. Ibrahim, M. A. Elaziz, D. Oliva, E. Cuevas, and S. Lu, "An opposition-based social spider optimization for feature selection," *Soft Comput.*, vol. 23, no. 24, pp. 13547–13567, 2019.

[40] J. J. Liang, A. K. Qin, P. N. Suganthan, and S. Baskar, "Comprehensive Learning Particle Swarm Optimizer for Global Optimization of Multimodal Functions," *IEEE Trans. Evol. Comput.*, vol. 10, no. 3, pp. 281–295, 2006.

[41] W. Yang, T. Cheng, Y. Guo, Z. Yang, and W. Feng, "A Modified Social Spider Optimization for Economic Dispatch with Valve-Point Effects," *Complexity*, vol. 2020, 2020.

[42] N. Singh and Y. Kumar, "Economic Load Dispatch with Valve Point Loading Effect and Generator Ramp Rate Limits Constraint using MRPSO," *Int. J. Adv. Res. Comput. Eng. Technol.*, vol. 2, no. 4, pp. 1472–1477, 2013.

[43] V. K. Kamboj, S. K. Bath, and J. S. Dhillon, "Solution of non-convex economic load dispatch problem using Grey Wolf Optimizer," *Neural Comput. Appl.*, vol. 27, no. 5, pp. 1301–1316, 2016.

5

Shunt Reactive Compensations
for Distribution Network Optimization

Ahmad Eid[1], Salah Kamel[2], and Hussein Abdel-mawgoud[3]

[1,2,3]Department of Electrical Engineering, Faculty of Engineering, Aswan University, 81542 Aswan, Egypt
[1]Department of Electrical Engineering, College of Engineering, Qassim University, 56452 Unaizah, Saudi Arabia
E-mail: ahmadeid@aswu.edu.eg; skamel@aswu.edu.eg; hussein.abdelmawgoud@yahoo.com

Abstract

The distribution system's voltage profile and power losses are affected by actual and imaginary power loading conditions. This problem may be efficiently handled by optimizing the sizes and locations of Reactive Compensating Devices (RCDs) and controlling the active and reactive power flow. This methodology provides an efficient scheme to include different RCD types of Fixed Capacitors (FC), Static Var Compensators (SVC), and Distribution-Static Synchronous Compensators (DSTATCOM) according to their size in the analysis and optimization. The Bald Eagle Search (BES) optimization algorithm efficiently tackles the allocation problem of different RCDs into distribution systems to achieve simultaneous objectives. These objectives include lessening the power loss and cost of reactive compensators and enhancing the voltage profile and system stability. The study optimizes these objectives in single-and Multiobjective Optimization (MOO) problems. Four different MOO case studies are investigated to validate the BES algorithm capability and study all possible scenarios in distribution systems. The proposed method is applied to the IEEE 69-bus radial distribution system. The obtained results show the effectiveness and superiority of the BES algorithm compared to Archimedes Optimization Algorithm (AOA), Atom Search

Algorithm (ASO), and Particle Swarm Optimization (PSO) in convergence speed and fitness values. Moreover, the voltage profile and stability index enhance, and the power loss and costs decrease with the optimal allocation of the RCDs.

Keywords: DSTATCOM, fixed capacitors, optimization of distribution systems, power loss, reactive compensation, SVC.

5.1 Introduction

The integration of renewable energy sources into the electricity network is becoming a pressing challenge to overcome fossil fuel shortages, with rising load demand. FACTS products contribute to optimum system operations by decreasing power losses and enhancing voltage profiles. The power flow of essential lines can be increased due to the rapid controllability of the operating margins. Moreover, the capacity for transmission lines may generally be raised to their thermal values. Hence, FACTS increases the transient stability level, enhances the dynamic system operation, and reduces cascading blackouts [1, 2]. FACTS concept is based on power-electronic controllers, which increase the value of transmission networks by boosting their capacity utilization [3, 4]. It is being implemented in several countries.

The primary purposes of shunt Reactive Compensating Devices (RCDs) are to minimize the feeder loading due to excessive current, especially during peak demand times, and to compensate for the enormous reactive power needed by the demand, which is mainly inductive. Once the distribution networks are compensated by these RCDs such as Fixed Capacitors (FC), Static Var Compensators (SVC), and Distribution-Static Compensators (DSTAT-COM), the required reactive power from the far slack bus is tremendously reduced. Hence, the quadrature current component is minimized as well as the total feeder currents. Consequently, the total power generation capacity and fuel cost are minimized as well.

SVC and DSTATCOM are more efficient than a single FC, although they are more expensive [5]. The advantages of reactive power compensation rely heavily on the positioning and size of the fitted compensators. It is unneeded and economically unfeasible to install shunt controllers in all buses. The SVC and DSTATCOM are commonly employed on power networks for their benefits in system improvement performance. They are considered generators or absorbers with adjustable output to offer voltage support for exchanging

capacitive and inductive currents. The FC works only as a fixed reactive power generator.

The allocation of these devices in power systems is optimized with several approaches. The challenge of placing the RCD is typically handled using evolutionary programming approaches. The misallocation of these devices may result in opposite and unwanted objectives. Thus, the RCDs must be located and sized carefully to achieve the purposes of their installation of reducing power loss, enhancing voltage stability, or any other objectives. A Genetic Algorithm (GA) [6] is applied to allocate Distributed Generations (DGs) and FC into distribution systems to achieve the minimum total cost of the planning period. A multiobjective evolutionary algorithm based on decomposition (MOEA/D) [7] is adopted to optimize DG and FC working with distribution systems to reduce the active and reactive power losses. The GSA [8] has been applied to optimally allocate FC into distribution systems to reduce the losses and maximize the net savings. Other authors [9] used a hybrid local search-GA in a similar study. Considering the uncertainty, the PSO is adopted in [10] to simultaneously allocate DG units and FC banks to reduce power loss, improve voltage stability, and balance feeder currents. The Whale Optimization Algorithm (WOA) [11] is adopted to allocate FC banks in distribution systems to reduce losses and enhance the stability and reliability of the system. Ant Colony Optimization (ACO) [12] has been applied to optimal allocate FC banks to improve the voltage profile and reduce the losses of distribution systems. The Flower Pollination Algorithm (FPA) [13] has been applied to place FC banks into distribution systems in order to reduce losses and costs. The authors in [14] used the Archimedes Optimization Algorithm (AOA) in a multiobjective optimization to optimally allocate different renewable energy sources with distribution systems.

The SVC is very famous for reactive power compensation in transmission and distribution systems for many years. The authors of [15] proposed the SVC to mitigate the voltage flicker of an arc furnace using closed-loop control, while those in [16] used the SVC to enhance the power quality of the systems. The adaptive differential search algorithm [17] has been adopted to optimally allocate Distributed Generations (DGs) and SVC devices to reduce power losses. The adaptive and exponential versions of Particle Swarm Optimization (PSO) have been used [17] in active distribution systems to optimally allocate different renewable sources. In a recent study, an Improved Marine Predator Algorithm (IMPA) [18] has been applied to allocate active and reactive power sources into the distribution systems to minimize the system losses, total voltage deviations and increase system stability. An SVC

planning methodology is applied in [19] to increase the photovoltaic hosting capacity in distribution networks using a stochastic approach. The study included minimizing the SVC planning cost and maximizing the PV hosting capacity in a multiobjective problem. The GA optimization [20] is used to optimally allocate different DGs and SVC devices in distribution networks in order to minimize the total MVA taken from the mains and the power losses of the system. The adaptive PSO and modified Gravitational Search Algorithm (GSA) algorithms are used [21] to integrate DGs into distribution systems with optimal sizes and locations to achieve different objectives such as reducing the power loss and TVD and maximizing the stability index of the system. The study included both single and multiobjective optimization analysis.

On the other hand, many researchers considered the optimal allocation of the DSTATCOM in many applications and optimization problems. Using the voltage Stability Index (SI) and the Bat Algorithm (BA) [22], the DSTATCOM is optimally located, and sized to minimize the power losses of distribution systems when considering the load variations. Cuckoo Searching Algorithm (CSA) [23] is used in multiobjective analysis to optimally allocate DG units and DSTATCOM into distribution systems to achieve minimum losses, and maximize the voltage profile. Golden Ratio Optimization (GRO) [24] optimally allocates FC banks and DSTATCOM devices into distribution systems with fuzzy logic decision-making to enhance voltage profile and reduce losses. Other researchers used optimization algorithms in different environmental applications and water desalination systems [25–27].

Researchers in this paper suggest the "Bald Eagle Search" algorithm [28], which is a unique, nature-inspired meta-heuristic optimization algorithm that replicates the bald eagles' hunting technique or social intelligence as they search for fish. In comparison to other sophisticated meta-heuristic algorithms and traditional techniques, the BES algorithm takes the crown. In this chapter, the BES metaheuristic optimization algorithm is adopted to control the reactive power flow inside the distribution networks in order to enhance their performance and optimize the sizes and locations of RCDs. Different RCDs, including SC, SVC, and DSTATCOM, are explained, optimized, and compared concerning the performance of the distribution networks. Both single and multiple objective functions are optimized to enhance and control the reactive power flow inside the distribution networks. Different case studies are conducted to illustrate the BES algorithm's capacity to solve multiple objective problems. As a consequence of the findings and debates, it may be

concluded that the BES algorithm is the best alternative to AOA [27], ASO [28], and PSO [29] algorithms.

The main scope of this chapter can be summarized as follows:

- Solving the nonlinear optimization problem of allocating Reactive Compensating Devices (RCD) into distribution networks.
- The mathematical formulations of the RCD effects on the performance of the distribution network are derived and demonstrated.
- Different optimization functions in single- and multiobjective optimizations are proposed and solved, such as reducing network losses, enhancing voltage profile, improving network stability, and reducing RCD costs.
- The effectiveness and capability ofthe BES algorithm are justified by comparing the obtained results with other published algorithms.

5.2 Reactive Compensating Devices (RCDs)

The use of shunt compensation can achieve reactive power compensation. This may be accomplished through the use of traditional shunt capacitors or the recently released FACTS controllers.

5.2.1 Fixed Capacitor

Fixed Capacitors (FCs) are very simple to install and maintain and have a long service life. The installation of shunt capacitors in the load region or at the point where they are required will improve the voltage stability of the system. On the other hand, FCs have difficulty with voltage control, and after a certain degree of compensation has been reached, it is impossible to achieve a stable working point. The reactive power provided by the FC is proportional to the square of its terminal voltage; as a result, when the terminal voltage is low, the voltage support of the shunt capacitor lowers, aggravating the situation, as follows:

$$Q_C = \omega C |V|^2 \qquad (5.1)$$

where, Q_C is the reactive power of the FC with a capacitance of C; ω is the radian frequency of the system; V is the bus voltage at which the FC is connected.

The V-I and V-Q characteristics of an FC are shown in Figure 5.1. The relationship between the voltage across and current through the FC is linear. The current is negative, referring to the capacitor injecting currents with a
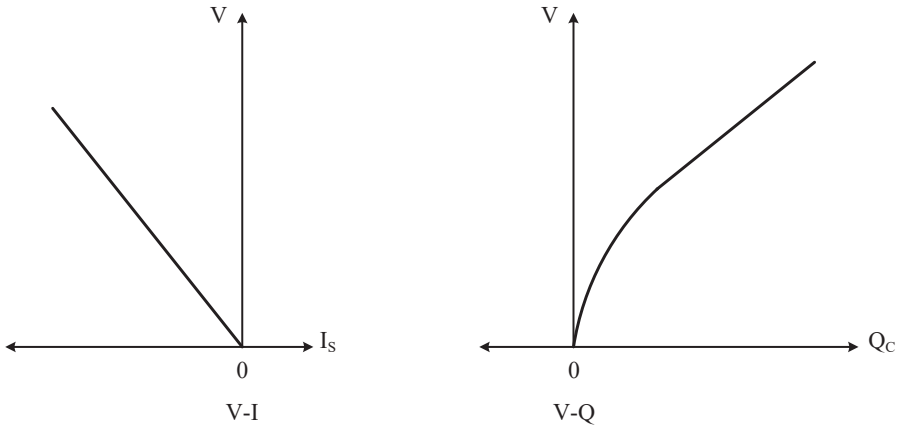
Figure 5.1 V-I and V-Q characteristics of FC

leading power factor (capacitive Vars) into the system. Moreover, the V-Q characteristic is nonlinear, and at low voltages, the reactive power decreases quickly.

5.2.2 Static Var Compensator

The Static Var Compensator (SVC) is a shunt-connected absorber that exchanges inductive/capacitive power to regulate specific power system characteristics [5]. It is claimed in [29] that there are more than 800 SVCs installed in the world with a rating reactive power of 60-600 MVar. The precision, availability, and quick reaction of SVCs allow such instruments to achieve outstanding performance regarding the system voltage in steady-state and transient conditions. SVCs are also utilized to enhance transient stability, and moist swings and decrease system losses via reactive power monitoring [30]. The V-I characteristic of the SVC is shown in Figure 5.2. The designed reactive power of the SVC limits its maximum capacitive susceptance (B_{Cmax}) and inductive susceptance (B_{Lmax}) while the voltage is regulated to the reference value (V_O) through a voltage droop control. The system voltage in terms of the current (I_S) and the slope reactances (X_S) operates in reactive power control mode [29]:

$$V = -\frac{I_S}{B_{Cmax}}, \quad B = B_{Cmax} \tag{5.2}$$

$$V = \frac{I_S}{B_{Lmax}}, \quad B = B_{Lmax} \tag{5.3}$$
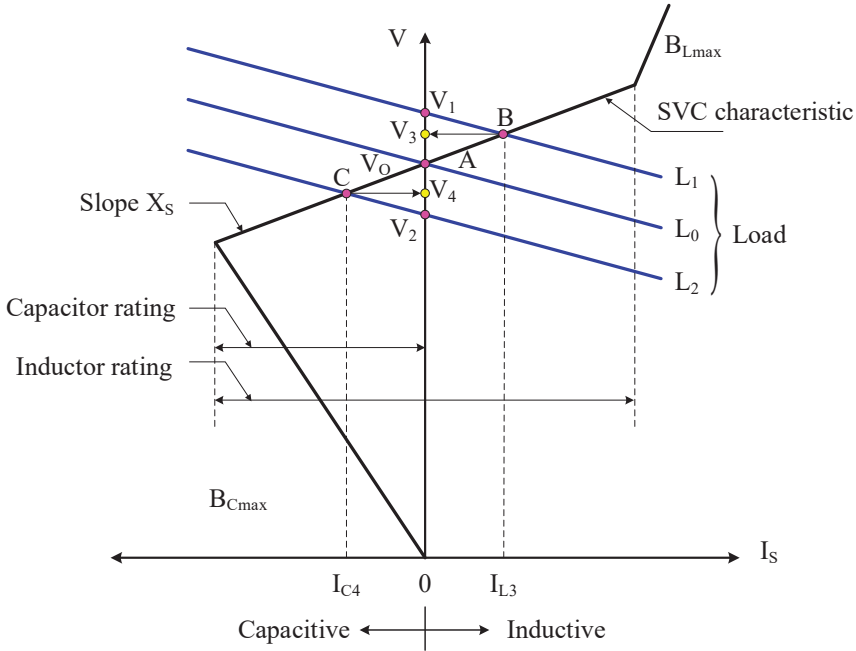
Figure 5.2 V-I characteristic of SVC

The second mode of operation is the voltage control, where the suscep-
tance lies between the extreme values:

$$V = V_O + I_S \times X_S, \quad -B_{Cmax} < B < B_{Lmax} \tag{5.4}$$

The SVC is considered the most straightforward FACTS device already
in use in different areas of the world. An SVC can control the voltage range of
a certain bus to improve the voltage profile of the system. The primary job of
an SVC is to maintain a specific bus voltage by a reactive power adjustment
(obtained by varying the firing angle of the thyristors). It can also improve the
damping of power oscillations and the power flow over the line. The required
voltage control determines the characteristic (droop) slope value, the desired
reactive power production sharing across different sources, and other system
requirements. The droop usually amounts to 1% to 5% [20]. When the SVC
operates in reactive power control mode, the system sees it as a capacitor
when $B = B_{Cmax}$, or as an inductor when $B = B_{Lmax}$. In the active control
range ($B_{Cmax} < B < B_{Lmax}$), the SVC regulates the voltage according to the
load characteristic or power factor.

The middle load characteristic (L_0) represents the nominal operation of the system where the voltage is equal to the reference voltage (V_O) at point A where no current is drawn/injected by the SVC. When the load characteristic moves to L_1, the system voltage increases to V_1 either by increasing the source voltage or decreasing the system load. In this case, the SVC controller senses the voltage increase and guides the SVC to operate in the inductive mode to absorb some amount of reactive power from the system with an absorbing current magnitude of I_{L3}. Thus the SVC becomes like an inductive load which makes the voltage decrease. Consequently, the operating point moves to point B, where the system voltage decreases to V_3. In different circumstances, the load characteristic becomes L_2 due to an increase in load level, the system voltage decreases to V_2. To restore the voltage to a better value, the SVC injects a capacitive current magnitude I_{C4} with a suitable amount of capacitive reactive power. Hence the voltage increases from V_2 to V_4 by moving the operating point to C on the characteristic. The SVC regulates the voltage and maintains it in an acceptable range according to the operating conditions.

5.2.3 DSTATCOM

DSTATCOM is a Voltage-Source Converter (VSC)-based Flexible Ac Transmission System (FACTS) device connected in shunt with the power system. Most significantly, it can exchange dynamic reactive power with the ac system. DSTATCOM is used in voltage regulation and voltage stabilization, power factor management, voltage flicker correction, and power-quality enhancement in distribution systems [1]. It is possible to achieve both capacitive and inductive compensation using the DSTATCOM, which separately controls the output current range while maintaining ac system voltage. Even when the system voltage is low, the DSTATCOM can supply full capacitive-reactive power, as shown in Figure 5.3. For DSTATCOM, one of its defining characteristics is that it can provide a nearly complete output of capacitive production regardless of the system voltage (constant-current output at lower voltages). In such instances, the DSTATCOM is vital because it stabilizes the system voltage during and after failures that would otherwise restrict voltage collapse. The STATCOM rating shows a rise in both the capacitive- and the inductive-operating areas in transient conditions. When the DSTATCOM is equipped with a storage device, it can regulate active and reactive powers in the four-quadrant operations. Since DSTATCOM can keep reactive current output at its nominal value across a broad range of bus voltages, it is better
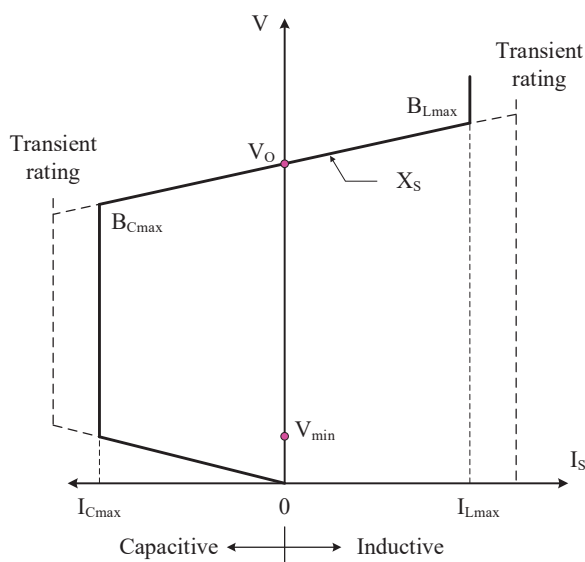
Figure 5.3 V-I characteristic of STATCOM

than SVC [31] for delivering dynamic VARs. While the SVC utilizes bulky inductors and banks of capacitors to absorb and produce reactive power, the STATCOM uses small inductors and capacitors to absorb and provide reactive power [2]. The controller modifies the voltage and current waveforms and controls the reactive power generation, either leading or lagging. In contrast to the SVC, which represents a changeable susceptance, the DSTATCOM behaves as a variable voltage source connected to the system. Although the STATCOM technology delivers better technical performance, it nevertheless has a larger price than the SVC technology [1].

The prices of FACTS devices may vary depending on the initial installation cost, operation, and maintenance costs. Other important factors also affect the prices, such as device type, power rating, operating system voltage, and other operational constraints. An estimation of the FACTS prices is listed in Table 5.1 [32–35]. Moreover, according to the optimal size of the reactive

Table 5.1 Size and cost of different RCDs

Shunt compensator	Q_{max} (kVar)	Cost (US \$/kVar)
FC	$Q \leq 250$	8
SVC	$250 < Q \leq 750$	40
DSTATCOM	$Q > 750$	50

power compensation, the type of the RCD can be determined accordingly. It is worth mentioning that the listed costs of the RCDs are for the controller part only and do not include the price of the device itself.

5.3 Mathematical Problem Formulations

This study includes single- and multiobjective optimization problems to optimally choose the size and site of the RCD in order to achieve optimal operations for the distribution systems. The BES algorithm optimally determines the size of RCD units, and hence, the type is determined with the help of Table 5.1.

5.3.1 Objective Functions

The objective functions and the optimization constraints are discussed as follows:

A. *Power Loss*

The power loss inside a distribution system is calculated from the branch current and the resistance of the branch as follows:

$$P_{Loss} = \sum_{k=1}^{N_b} R_k \times |I_k|^2 \tag{5.5}$$

where, P_{Loss} is the total power loss, R_k is the branch resistance, I_k is the branch current, and N_b is the total branches of the system. The first objective function is:

$$f_1 = \min (P_{Loss}) \tag{5.6}$$

B. *Total Voltage Deviation*

The Total Voltage Deviation (TVD) is calculated as the sum of voltage deviations of the system as:

$$TVD = \sum_{k=1}^{N_s} |1 - |V_k|| \tag{5.7}$$

where, N_s is the number of system buses, and V_k is the voltage at any bus k. The second objective function becomes:

$$f_2 = \min (TVD) \tag{5.8}$$

C. *Stability Index*

The voltage stability index of any branch k, and connected between two buses m, n is calculated from:

$$SI_k = 1 - \left[2\left(P_n R_k + Q_n X_k\right) - |V_m|^2\right]^2 - 4\left(P_n^2 + Q_n^2\right)\left(R_k^2 + X_k^2\right) \quad (5.9)$$

where, P_n, Q_n are the active and reactive powers at the receiving end of the branch, R_k, X_k are the branch resistance and reactance, respectively, V_m is the voltage magnitude at the sending end of the branch.

According to the SI definition, the most strong branch is when SI approaches zero. The SI is calculated for all branches as:

$$SI = SI_{N_b},\ SI_{N_b-1},\ SI_{N_b-2},\ \ldots\ ,\ SI_2,\ SI_1 \quad (5.10)$$

The objective function is to minimize the maximum value of SI as:

$$f_3 = \min\left(SI\right) \quad (5.11)$$

D. *Cost Minimization*

The cost of each RCDs is listed in Table 5.1. The total cost of RCD controllers is estimated as:

$$Cost_{RCD} = \sum_{k=1}^{N_{RCD}} Cost\left(Q_k\right) \quad (5.12)$$

where, $Cost_{RCD}$ is the total cost of the installed RCD devices, $Cost\left(Q_k\right)$ is the kth cost of an individual RCD device, and N_{RCD} is the number of installed devices.

The objective is to minimize the total cost as possible, and hence the fourth objective is:

$$f_4 = \min\left(Cost_{RCD}\right) \quad (5.13)$$

5.3.2 Multi-Objective Optimization

Multiobjective Optimization (MOO) is adopted when two or more objectives are optimized simultaneously. In this case, compromise solutions are provided, and the system operator has to choose the optimal solution from them according to the operating conditions. The MOO problem can be described for minimization objectives as follows [36]:

$$\text{Minimize}: f_{Tot}^{obj} = f_1^{obj}\left(x\right),\ f_2^{obj}\left(x\right), \ldots, f_n^{obj}\left(x\right)$$

$$subject\ to: g_i\left(x\right) = 0,\ i = 1:m$$
$$h_i\left(x\right) = 0,\ i = 1:k$$
$$X_{min,i} \leq x_i \leq X_{max,i} \qquad\qquad (5.14)$$

where, f_{Tot}^{obj} is the total objective function; n represents the number of the considered objective functions; $g_i\left(x\right)$ is the inequality constraints and m is their number; $h_i\left(x\right)$ is the equality constraints and k is their number; $X_{min,i}$, $X_{max,i}$ represent the boundaries of the element i in the vector x.

There is an approach to deal with the MOO called the aggregated sum. In the aggregate sum method, the objective functions are normalized and summed according to certain weighting factors as:

$$f_{Tot}^{obj} = \omega_1 f_1^{obj} + \omega_2 f_2^{obj} + \cdots + \omega_n f_n^{obj} \qquad\qquad (5.15)$$

where, the sum of the weighting factors is unity:

$$1 = \omega_1 + \omega_2 + \cdots + \omega_n \qquad\qquad (5.16)$$

The value of each weighting factor can be determined according to many factors, such as the importance of individual objective function, system constraints, and other technical or economic operating conditions.

5.3.3 System Constraints

The proposed optimization of the distribution system does not violate any of the system or operational constraints. To implement these constraints in the load flow, the best fitness is equated to infinity whenever a constraint is violated.

A. *Voltage limits*: the bus voltage at any iteration of the load flow solution must lie between the standard limits of the per-unit voltage to maintain power quality and stability of the system, as:

$$V_{min} \leq V_k \leq V_{max} \qquad\qquad (5.17)$$

where, V_{min}, V_{max} are the acceptable voltage minimum and maximum limits of 0.95, and 1.05 pu, respectively, V_k is the voltage of the kth bus.

B. *RCD size*: the optimized size of any RCD is limited to the values listed in Table 5.1. While the FC size is up to 250 kVar, the SVC is limited between 250 and 750 kVar. On the other hand, the DSTATCOM size lies between 750 and 1250 kVar.

C. RCD capacities: the total injected reactive power of the RCD units is limited to a total load of a distribution system such as:

$$Q_{RCD} \leq Q_L \tag{5.18}$$

where, Q_{RCD} is the RCD reactive power, and Q_L is the load reactive power.

D. Power flow balance: The power flow balance equations are satisfied at every iteration of the load flow. The active and reactive power flow balance equations are:

$$P_S - P_{Loss} - P_L = 0 \tag{5.19}$$

$$Q_S \pm Q_{RCD} - Q_{Loss} - Q_L = 0 \tag{5.20}$$

where, P_S, Q_S are the substation active and reactive power, respectively (at slack-bus), P_L, Q_L are the load total active and reactive power, respectively. It should be noted that both SVC and DSTATCOM inject or absorb reactive power according to their control outputs and system performance. In this study, to reduce the objective functions while working in a steady-state, the RCD units are assumed to work as a reactive power generator. Hence, the RCD always injects reactive power into the distribution system.

5.3.4 Optimization Algorithm

In this study, the Bald Eagle Search (BES) algorithm [28] is adopted and used to optimally size and locate the RCD units into distribution systems to minimize the different objective functions. The BES algorithm is a new metaheuristic optimization algorithm that mimics the bald eagle during the hunting process of its prey.

5.3.5 Load Flow Solution

In order to solve the distribution system efficiently, the well-known Forward/Backward Sweep Method (FBSM) load flow [37] is adopted for its simplicity and efficacy.

5.4 Single-Objective Optimization of RCD Units

In this section, the IEEE 69-bus Radial Distribution System (RDS) is solved using the FBSM load flow and optimized using the BES optimization algorithm. The 69-bus RDS is 12.66 kV with a total load of 3801.89 kW, and 2694.10 kVar with balanced load and branches have no mutual coupling,
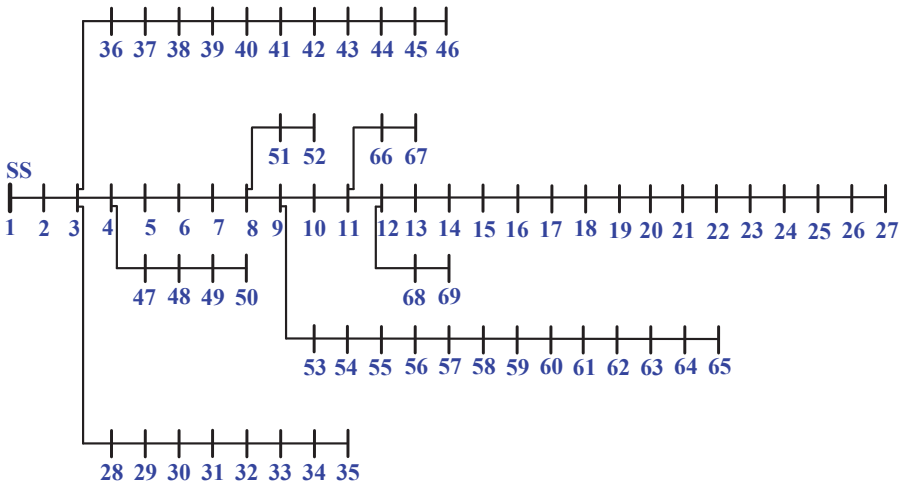
Figure 5.4   The 69-bus radial distribution system

as shown in Figure 5.4. The RCD units are optimally allocated using the BES algorithm to reduce the previous objective functions.

Three units of RCD are optimally located at the 69-bus RDS, where the first three objectives are minimized; power loss, TVD, and the SI. The optimal sizes and sites of the three RCDs are listed in Table 5.2. To minimize the power loss, three different devices of FC, SVC, and DSTATCOM are located on buses 21, 11, and 61, respectively, with different sizes. For minimizing the TVD and SI objectives, the sizes of the RCDs are equal to the maximum size per phase of 900 kVar. All of the devices are of the DSTATCOM type. For the TVD objective, the three RCDs are located at buses 21, 25, 64, while for the SI objective, they are located at buses 61, 62, and 64.

The power losses (P_{Loss}, Q_{Loss}), and the total cost of the optimized RCDs are charted in Figure 5.5, for the three objective functions and compared to the base case. The corresponding performance parameters of V_{min}, V_{max}, TVD, and SI are shown in Figure 5.6. According to the specific objective function, the different performance parameters are enhanced compared to the base case. When the power loss is the objective function, the P_{Loss}, and Q_{Loss} are reduced to 145.08 kW and 67.64 kVar compared to 224.94 kW and 102.14 kVar of the base case. The voltage profile is enhanced where the minim voltage (V_{min}) becomes 0.9314pu compared to 0.9092 pu at the base case. The corresponding cost of the RCDs is about $80 thousand.

Table 5.2 Type and size of three RCD units for different objective functions

$f_{obj} = P_{Loss}$			$f_{obj} = TVD$			$f_{obj} = SI$		
type	size	site	type	Size	site	type	size	site
DSC*	1232.4	61	DSC	900	25	DSC	900	62
SVC	412.84	11	DSC	900	21	DSC	900	61
FC	230.45	21	DSC	900	64	DSC	900	64

*DSC=DSTATCOM
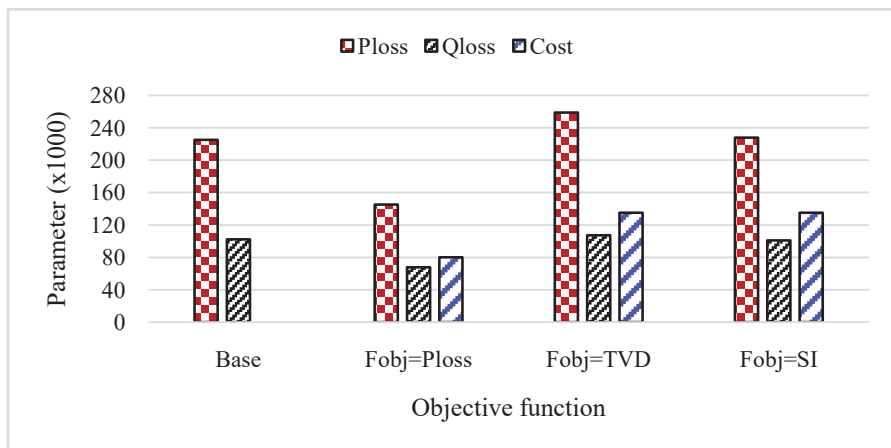
Figure 5.5 The power losses and cost of the RCDs with objective functions
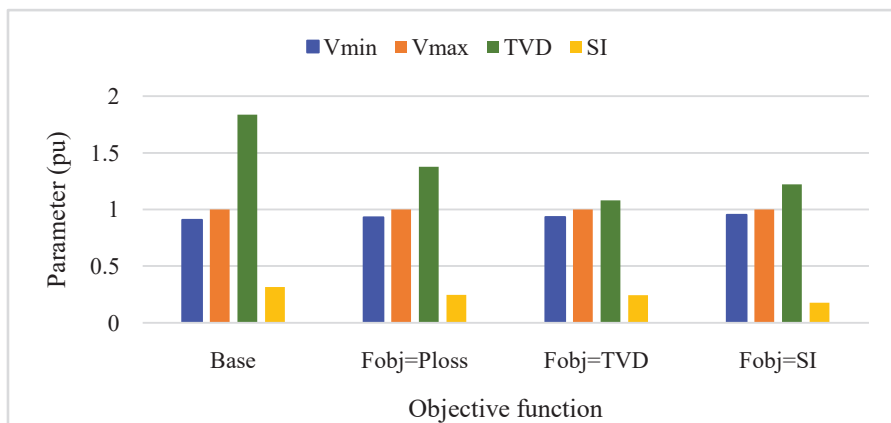
Figure 5.6 The performance parameters with objective functions

The BES algorithm optimizes three equal-size DSTATCOM devices to reduce the TVD to the optimum value as an objective function, as listed in Table 5.2. We must, of course, pump as much reactive power into the distribution system as feasible to raise the voltages on various buses close to unity. The optimal sites are 21, 25, and 64, with an equal size of 900 kVar, and all of them are of the DSTATCOM type. The TVD is minimized to 1.0799 pu while the corresponding power losses are 258.64 kW, 107.18 kVar, and the total cost is optimized to $135 thousand. Moreover, the minimum voltage raises to 0.9322 pu, and the SI reduces to 0.245 pu. Reduction of the SI means the system becomes more robust or more stable.

The last objective function, the BES algorithm, minimizes the SI of the system by optimally allocating three DSTATCOM with a size of 900 kVar at buses 61, 62, and 64. The SI has been reduced to 0.1775 pu, which is the lowest value among the previous cases. The total cost stills the same as the previous case of $135 thousand. While the active loss is slightly increased, the reactive loss is slightly decreased. The TVD is reduced to 1.22 pu, and the minimum voltage has reached the most significant value of 0.9522 pu.

The maximum voltage for all four case studies is always one pu at the slack bus (main supply). The voltage profile at each bus of the system is typically enhanced compared to the original case without RCDs, as shown in Figure 5.7. The obtained results show the effectiveness of the BES algorithm in optimizing the RCDs into the 69-bus RDS at different objective functions. Moreover, the more RCDs are assigned, the more system performance metrics are improved.
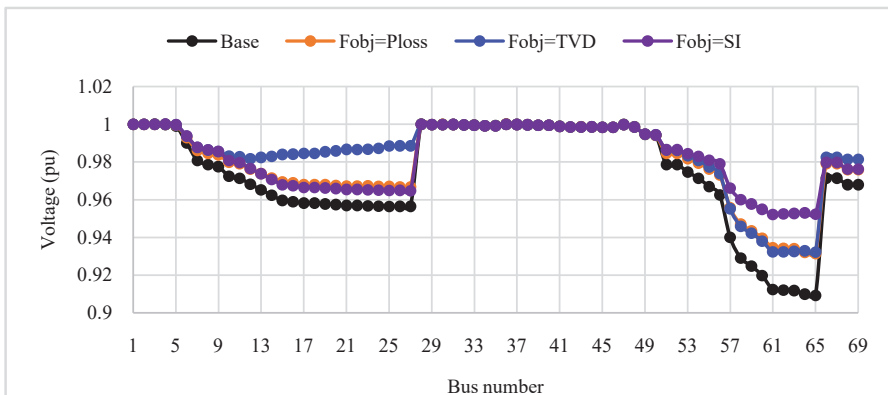
Figure 5.7   The voltage profile for different objective functions with three RCDs

Table 5.3   Case studies of MOO

Case study	ω_1	ω_2	ω_3	ω_4
A	0.4	0.3	0.2	0.1
B	0.3	0.2	0.1	0.4
C	0.2	0.1	0.4	0.3
D	0.1	0.4	0.3	0.2

5.5 Multiobjective Optimization of RCDs

In this section, six RCDs are optimized by the BES algorithm to minimize the objective functions working together or with different combinations. As there are four objective functions, it is challenging to use POF. Using the aggregated sum technique is much simpler, and it is adopted here. The system performance will be recorded for each number of the RCDs and each case study listed in Table 5.3. The obtained results will be investigated and compared. As these four objectives are different and have different values, they are normalized in the total objective function to their values of the base case without adding any RCDs:

$$f_{obj} = \omega_1 P_{Loss}^n + \omega_2 TVD^n + \omega_3 SI^n + \omega_4 Cost^n \tag{5.21}$$

where, the superscript n refers to the normalized values for the objectives. The normalized components are calculated as follows:

$$P_{Loss}^n = \frac{P_{Loss}}{P_{Loss}^{Bc}}, \; TVD^n = \frac{TVD}{TVD^{Bc}}, \; SI^n = \frac{SI}{SI^{Bc}}, \; Cost^n = \frac{Cost}{Cost^{Mx}} \tag{5.22}$$

where, the superscript Bc refers to the base case value for each function, and $Cost^{Mx}$ is the maximum cost of the installed RCDs. It is calculated as all the installed devices are assumed DSTATCOM.

$$Cost^{Mx} = 1250 \; kVar \times \; 50 \times N_{RCD} \tag{5.23}$$

The 69-bus RDS is simulated under aggregated sum MOO in different case studies with different RCDs, as listed in Table 5.4. The BES algorithm effectively determines the optimal sizes and sites of different RCDs. The corresponding RCD types are also illustrated according to the maximum size of each type. For case study A with a single RCD, the optimal size is 1585.8 kVar for a DSTATCOM at bus 61. In general, when the number of RCDs is small, the types are either SVC and/orDSTATCOM. On the contrary, when the number of RCDs increases, the FC appears with the SVC. The

Table 5.4　Optimal size, site, and type with different numbers of RCDs

Case study	1Q Size (site)	Type*	3Q Size (site)	Type	5Q Size (site)	Type	7Q Size (site)	Type
A	1585.82 (61)	3	530.22 (18)	2	249.25 (66)	1	249.94 (21)	1
			830.52 (53)	3	249.65 (56)	1	249.96 (65)	1
			1333.4 (61)	3	249.88 (65)	1	249.97 (54)	1
					498.58 (18)	2	249.99 (56)	1
					1246.5 (61)	3	249.99 (15)	1
							435.70 (67)	2
							1225.0 (61)	3
B	1558.03(61)	3	490.6 (18)	2	250.0 (65)	1	13.68 (21)	1
			876.5 (9)	3	250.0 (16)	1	250.00 (61)	1
			1327.0 (61)	3	250.0 (11)	1	250.00 (9)	1
					250.0 (21)	1	250.00 (18)	1
					751.0 (61)	3	250.00 (65)	1
							250.00 (11)	1
							701.63 (62)	2
C	1502 (61)	3	444.85 (18)	2	249.97 (65)	1	58.82 (65)	1
			919.70 (9)	3	249.99 (62)	1	250.00 (21)	1
			1298.5 (61)	3	250.00 (21)	1	250.00 (12)	1
					482.33 (64)	2	250.00 (59)	1
					749.95 (61)	2	250.00 (64)	1
							575.55 (63)	2
							597.22 (61)	2
D	2553.3 (61)	3	500.95 (16)	2	250.00 (22)	1	249.98 (65)	1
			579.29 (23)	2	250.00 (18)	1	249.99 (15)	1
			1613.9 (61)	3	250.00 (25)	1	250.00 (12)	1
					588.14 (65)	2	604.06 (64)	2
					1356.0 (62)	3	685.17 (57)	2
							750.00 (21)	2
							1340.1 (61)	3

* Type; 1: FC, 2: SVC, 3: DSTATCOM

Table 5.5　Performance parameters with different numbers of RCDs

Parameter	1Q	3Q	5Q	7Q
P_{Loss} (kW)	154.55	151.38	152.38	153.9
Q_{Loss} (kVar)	71.27	70.522	70.755	71.69
V_{min} (pu)	0.9345	0.9357	0.9386	0.9394
V_{max} (pu)	1	1	1	1
TVD (pu)	1.4484	1.2285	1.2268	1.1954
SI (pu)	0.2375	0.2334	0.2235	0.2208
$Cost$ ($1000)	79.29	129.40	88.271	73.248

performance parameters of case study A are listed in Table 5.5 for the variable number of RCDs. The voltage profile of the system with a different number of RCD units is shown in Figure 5.8. It can be seen that adding RCD enhances the voltage profile and increases the minimum voltage of the system.
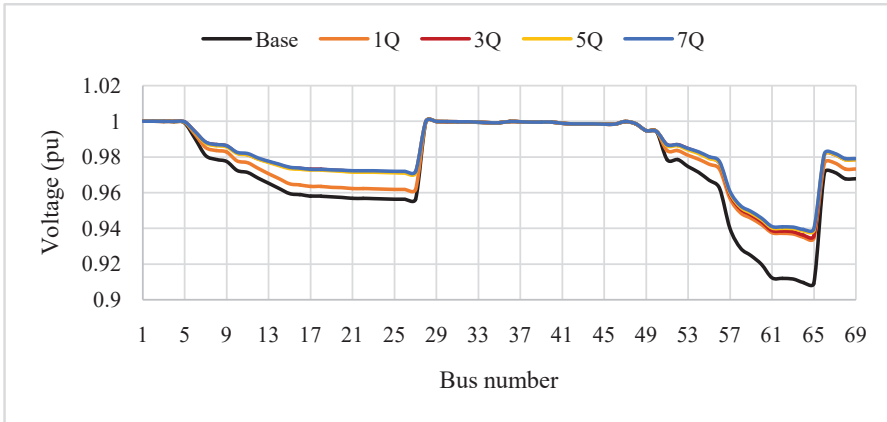
Figure 5.8   The voltage profile for different RCDs in case study A

The comparisons between A-D case studies are shown in Figure 5.9 to Figure 5.12 for power loss, TVD, SI, and cost objectives. There are minor variations of the power loss in cases A-C with the RCD units. The sharing of the power loss in the objective function is relatively large except for case study D, where it is the lowest value at 10% only. The power loss values are more significant in the case of study D relative to other cases A-C due to the deficient sharing of 10%, and the main sharing is for the TVD with 40% and SI with 30%. At the same time, the sizes and locations of the RCD units affect the overall value of the objective function.

The TVD is relatively large for all case studies with one RCD (1Q); otherwise, its value is varied according to the number of RCD units (see Figure 5.10). The value of the TVD is almost the same for cases A-C and smaller for case D with one RCD. The same behavior with three RCDs. With five RCDs, the maximum value happens with case B and the minimum with case D, where the TVD sharing is 40% of the objective function. The same happens with seven RCDs where the minimum value is at case D (highest sharing of 40%).

Regarding the third objective function of SI, there are slight variations in its values especially, with a small number of RCDs, see Figure 5.11, for the first three case studies. In the third and fourth case studies, the SI value is always less than the other cases where sharing represents 40% and 30% of the total objective function.

The fourth objective function is the total cost of the RCD components. The cost depends mainly on the type of RCDs, as listed in Table 5.1. In this
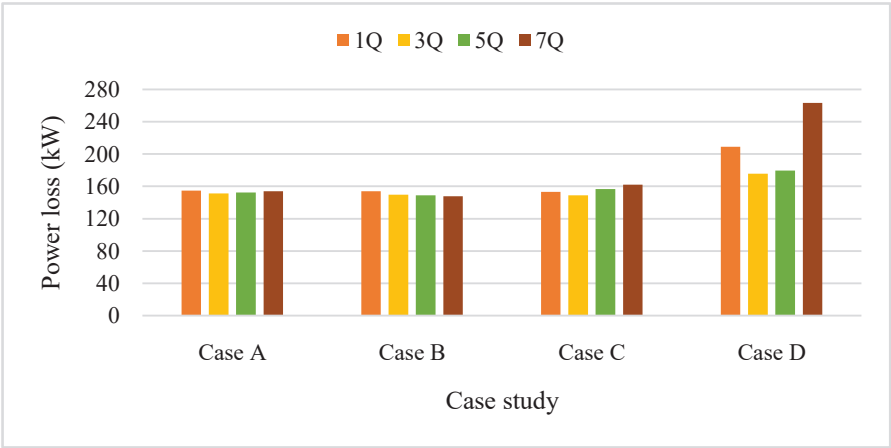
Figure 5.9 The power loss for different cases and RCD units
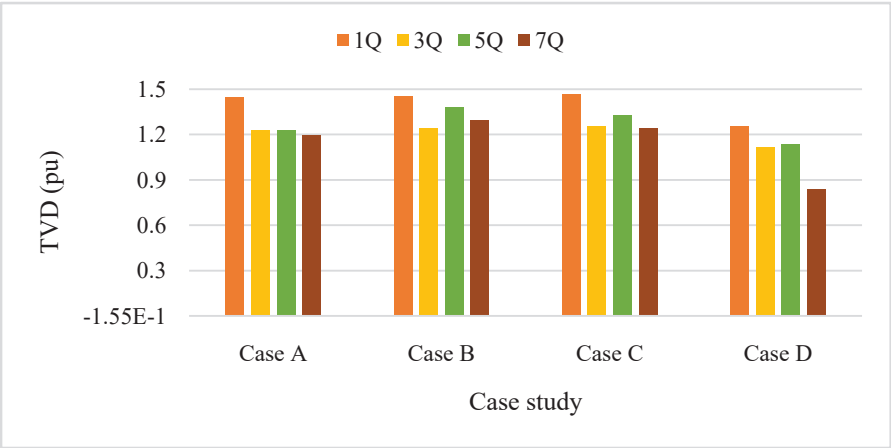
Figure 5.10 The TVD for different cases and RCD units

case, variations of this objective with the number of RCDs are expected, as shown in Figure 5.12. In case study A, where the cost represents 10% of the total fitness function, the lowest price is when the BES algorithm optimally allocates seven RCDs (7Q). The lowest price comes from the selection of the FC as much as possible by the BES algorithm. Contrary, when the optimal device is DSTATCOM or SVC, the expected price is large as they are costly compared to the price of the FC. With optimizing three RCDs (3Q) the cost is almost constant for all case studies. The cost is generally small for large
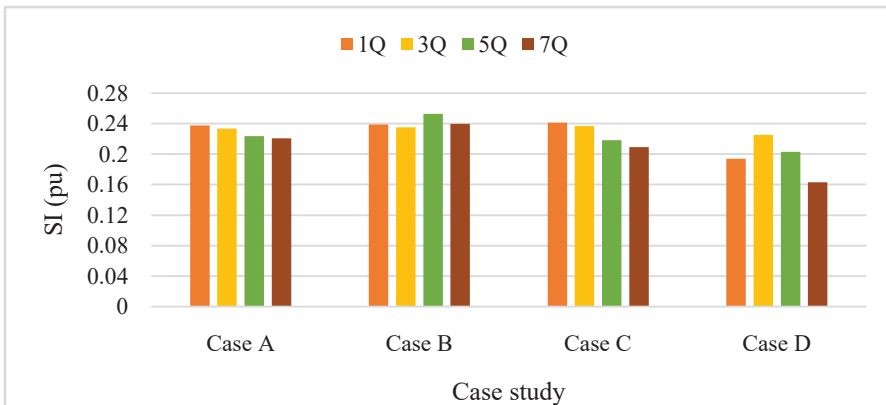
Figure 5.11 The SI for different cases and RCD units
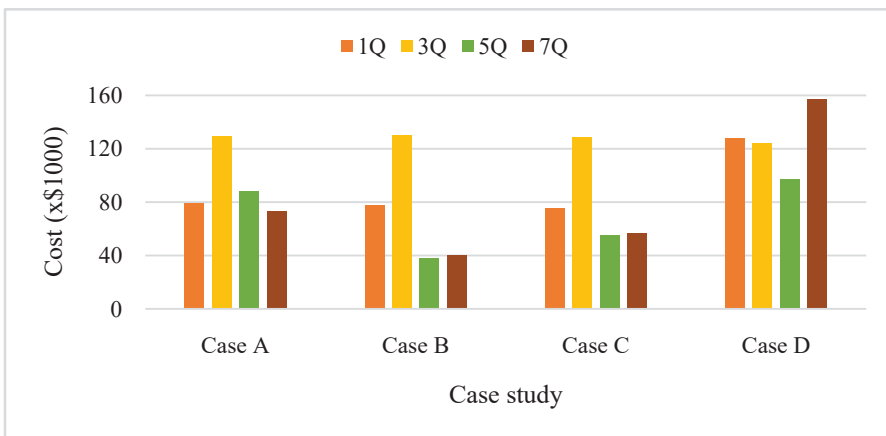
Figure 5.12 The cost for different cases and RCD units

RCD numbers for case studies B and C as the cost represents the maximum values of 40% and 30% of the total fitness function.

There is a strong relationship between the TVD and SI values and the bus voltages. The smaller is the TVD or SI values, the larger are the bus voltages and hence better minimum voltages. This relationship can be justified from Figure 5.13. When the sharing percentage of the TVD is a minimum of 10% in case study C or the SI represents 10% in case study B, the minimum voltage values for different numbers of RCDs are smaller compared to other case studies. When the TVD represents the maximum sharing of 40% in case study
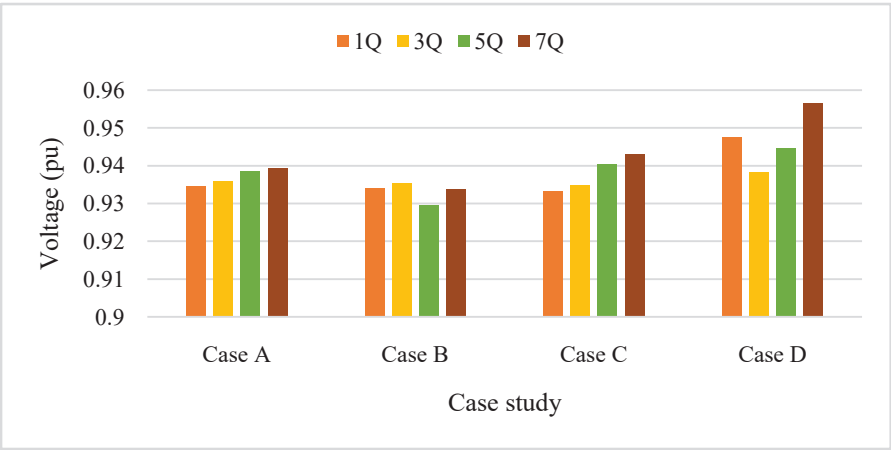
Figure 5.13   The minimum voltage for different cases and RCD units

D, the voltage profile improves, and the minimum voltages at different RCDs are higher than in other case studies.

5.6 Comparisons Using Different Algorithms

In this study, the BES algorithm is adopted to solve the optimization problem of allocating different RCDs into distribution systems. However, many optimization algorithms can perform this task with different accuracies. A proficient algorithm should provide adequate solutions quickly and accurately. A four metaheuristic optimization algorithm of Archemedis Optimization Algorithm (AOA), Atomic Search Optimization (ASO), Particle Swarm Optimization (PSO), and BES algorithms solve the same MOO problem of allocating seven RCDs into the 69-bus RDS with equal percentage sharing (25%) for all objectives. The convergence of the MOO objective function is drawn for all algorithms for comparison purposes, as shown in Figure 5.14. It is clear from the figure that the BES algorithm is the fastest and the most accurate of all algorithms.

For a fair comparison, all the optimization algorithms solve the same problem ten times where the average ($\bar{x}$), standard deviation (σ), and standard error (S_E) are calculated and listed in Table 5.6. From this comparison, the BES algorithm achieves the lowest average and consequently the lowest standard deviation and standard error. The BES algorithm comes in the first rank, followed by the AOA, PSO, and ASO algorithms in the second, third, and
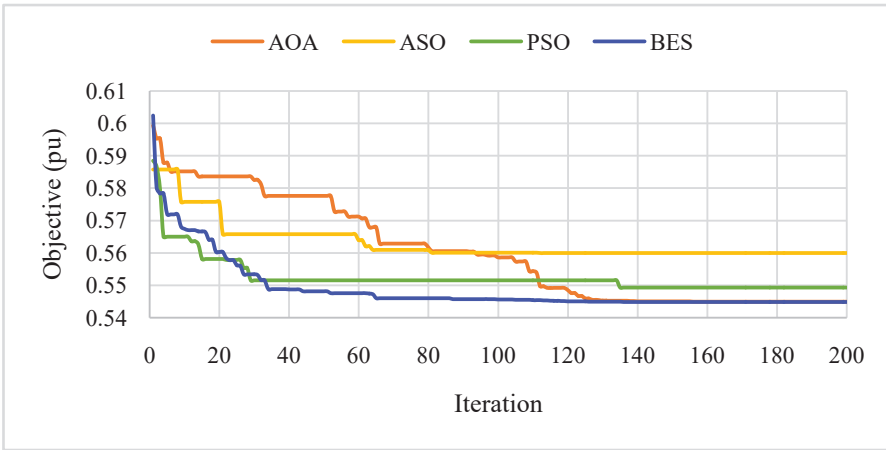
Figure 5.14 Objective function convergence using different algorithms

Table 5.6 Statistical comparisons of different algorithms

Algorithm	$\bar{x}$	σ	S_E	Rank ($\bar{x}$)
AOA	0.54758	4.103E-3	1.298E-3	2
ASO	0.55841	3.720E-3	1.176E-3	4
PSO	0.55295	3.795E-3	1.200E-3	3
BES	0.54492	8.333E-06	2.635E-06	1

fourth ranks. These results emphasize the efficient capability and suitability of the BES algorithm in solving such nonlinear optimization problems.

5.7 Conclusions

Different reactive compensating devices (RCDs), including fixed capacitor (FC), SVC, and DSTATCOM, are allocated into the 69-bus distribution system in order to reduce different objectives using the Bald Eagle Search (BES) optimization algorithm. The power loss, TVD, SI, and cost of the RCDs are optimized separately. The BES algorithm optimizes one, three, five, and seven RCD units for each objective. The four objectives in different case studies in multiobjective optimization are optimized according to their percentage sharing in the total fitness function. The effectiveness of the BES algorithm is outlined and pointed out when compared to other famous algorithms such as AOA, ASO, and PSO. The BES algorithm achieves the most accurate results with the fastest convergence. The obtained results show that increasing the RCD units results in more enhancing in the voltage profile

and the performance parameters of the system. In contrast, the minimum voltage of the system enhances with the increase of the percentage sharing of the TVD or SI objectives, and the power loss increases. The cost of the RCDs depends mainly on their types. Moreover, the methodology provides an efficient method to include different RCD types of FC, SVC, and DSTATCOM according to their size in the analysis and optimization. In the future, the methodology can be applied to different balanced and unbalanced distribution systems with uncertainties in demand or renewable sources. Moreover, the suggested algorithm could be applied to solve other optimization problems, including water treatment and reverse osmosis desalination systems.

References

[1] N. G. Hingorani and L. Gyugyi, Understanding *FACTS: concepts and technology of flexible AC transmission systems*. Wiley-IEEE Press, 2000.

[2] K. R. Padiyar, *FACTS controllers in power transmission and distribution*. New Delhi: New Age International Ltd. Publisher, 2016.

[3] R. M. Mathur and R. K. Varma, *Thyristor-based FACTS controllers for electrical transmission systems*. New York: Wiley-IEEE Press, 2002.

[4] K. K. Sen and M. L. Sen, *Introduction to FACTS controllers theory, modeling, and applications*. New Jersey: Wiley-IEEE Press, 2009.

[5] R. Sirjani, A. Mohamed, and H. Shareef, "Optimal allocation of shunt Var compensators in power systems using a novel global harmony search algorithm," *Int. J. Electr. Power Energy Syst.*, vol. 43, no. 1, pp. 562–572, 2012.

[6] M. Rahmani-Andebili, "Simultaneous placement of DG and capacitor in distribution network," *Electr. Power Syst. Res.*, vol. 131, 2016.

[7] P. P. Biswas, R. Mallipeddi, P. N. Suganthan, and G. A. J. Amaratunga, "A multiobjective approach for optimal placement and sizing of distributed generators and capacitors in distribution network," *Appl. Soft Comput. J.*, vol. 60, pp. 268–280, Nov. 2017.

[8] Y. Mohamed Shuaib, M. Surya Kalavathi, and C. Christober Asir Rajan, "Optimal capacitor placement in radial distribution system using Gravitational Search Algorithm," *Int. J. Electr. Power Energy Syst.*, vol. 64, pp. 384–397, 2015.

[9] E. A. Almabsout, R. A. El-Sehiemy, O. N. U. An, and O. Bayat, "A Hybrid Local Search-Genetic Algorithm for Simultaneous Placement of

DG Units and Shunt Capacitors in Radial Distribution Systems," *IEEE Access*, vol. 8, pp. 54465–54481, 2020.

[10] A. Zeinalzadeh, Y. Mohammadi, and M. H. Moradi, "Optimal multi objective placement and sizing of multiple DGs and shunt capacitor banks simultaneously considering load uncertainty via MOPSO approach," *Int. J. Electr. Power Energy Syst.*, vol. 67, pp. 336–349, 2015.

[11] D. B. B. Prakash and C. Lakshminarayana, "Optimal siting of capacitors in radial distribution network using Whale Optimization Algorithm," *Alexandria Eng. J.*, vol. 56, no. 4, pp. 499–509, Dec. 2017.

[12] A. A. Abou El-Ela, R. A. El-Sehiemy, A. M. Kinawy, and M. T. Mouwafi, "Optimal capacitor placement in distribution systems for power loss reduction and voltage profile improvement," *IET Gener. Transm. Distrib.*, vol. 10, no. 5, pp. 1209–1221, 2016.

[13] V. Tamilselvan, T. Jayabarathi, T. Raghunathan, and X. S. Yang, "Optimal capacitor placement in radial distribution systems using flower pollination algorithm," *Alexandria Eng. J.*, vol. 57, no. 4, pp. 2775–2786, 2018.

[14] A. Eid and H. El-kishky, "Multi-objective Archimedes optimization algorithm for optimal allocation of renewable energy sources in distribution networks," *Lect. Notes Networks Syst.*, vol. 211, pp. 65–75, 2021.

[15] M. Èeròan, Z. Müller, J. Tlustz, and V. Valouch, "An improved SVC control for electric arc furnace voltage flicker mitigation," *Int. J. Electr. Power Energy Syst.*, vol. 129, no. August 2020, 2021.

[16] Y. W. Liu, S. H. Rau, C. J. Wu, and W. J. Lee, "Improvement of Power Quality by Using Advanced Reactive Power Compensation," *IEEE Trans. Ind. Appl.*, vol. 54, no. 1, pp. 18–24, 2018.

[17] A. Eid, "Performance improvement of active distribution systems using adaptive and exponential PSO algorithms," *Int. Rev. Electr. Eng.*, vol. 16, no. 2, pp. 147–157, 2021.

[18] A. Eid, S. Kamel, and L. Abualigah, "Marine predators algorithm for optimal allocation of active and reactive power resources in distribution networks," *Neural Comput. Appl.*, vol. 4, 2021.

[19] X. Xu, J. Li, Z. Xu, J. Zhao, and C. S. Lai, "Enhancing photovoltaic hosting capacity—A stochastic approach to optimal planning of static var compensator devices in distribution networks," *Appl. Energy*, vol. 238, no. October 2018, pp. 952–962, 2019.

[20] B. Singh, V. Mukherjee, and P. Tiwari, "GA-based optimization for optimally placed and properly coordinated control of distributed generations

and Static Var Compensator in distribution networks," *Energy Reports*, vol. 5, pp. 926–959, 2019.

[21] A. Eid, "Allocation of distributed generations in radial distribution systems using adaptive PSO and modified GSA multi-objective optimizations," *Alexandria Eng. J.*, vol. 59, no. 6, pp. 4771–4786, 2020.

[22] T. Yuvaraj, K. Ravi, and K. R. Devabalaji, "DSTATCOM allocation in distribution networks considering load variations using bat algorithm," *Ain Shams Eng. J.*, vol. 8, no. 3, pp. 391–403, 2017.

[23] T. Yuvaraj and K. Ravi, "Multi-objective simultaneous DG and DSTAT-COM allocation in radial distribution networks using cuckoo searching algorithm," *Alexandria Eng. J.*, vol. 57, no. 4, pp. 2729–2742, 2018.

[24] A. Noori, Y. Zhang, N. Nouri, and M. Hajivand, "Hybrid Allocation of Capacitor and Distributed Static Compensator in Radial Distribution Networks Using Multi-Objective Improved Golden Ratio Optimization based on Fuzzy Decision Making," *IEEE Access*, no. May, pp. 1–1, 2020.

[25] N. S. Rathore, V. P. Singh, and B. D. H. Phuc, "A modified controller design based on symbiotic organisms search optimization for desalination system," *J. Water Supply Res. Technol. - AQUA*, vol. 68, no. 5, pp. 337–345, 2019.

[26] N. S. Rathore and V. P. Singh, "Whale optimization algorithm-based controller design for reverse osmosis desalination plants," *Int. J. Intell. Eng. Informatics*, vol. 7, no. 1, pp. 77–88, 2019.

[27] N. S. Rathore, "Design of optimal PID controller for the reverse osmosis using teacher-learner-based-optimization," *Singh, V. P.*, vol. 9, no. 2, pp. 129–136, 2018.

[28] H. A. Alsattar, A. A. Zaidan, and B. B. Zaidan, "Novel meta-heuristic bald eagle search optimization algorithm," *Artif. Intell. Rev.*, vol. 53, no. 3, pp. 2237–2264, 2020.

[29] F. H. Gandoman et al., "Review of FACTS technologies and applications for power quality in smart grids with renewable energy systems," *Renew. Sustain. Energy Rev.*, vol. 82, no. August 2017, pp. 502–514, 2018.

[30] C. F. Lu, C. H. Hsu, and C. F. Juang, "Coordinated control of flexible AC transmission system devices using an evolutionary fuzzy lead-lag controller with advanced continuous ant colony optimization," *IEEE Trans. Power Syst.*, vol. 28, no. 1, pp. 385–392, 2013.

[31] T. Aziz, M. J. Hossain, T. K. Saha, and N. Mithulananthan, "VAR planning with tuning of STATCOM in a DG integrated industrial system," *IEEE Trans. Power Deliv.*, vol. 28, no. 2, pp. 875–885, 2013.

[32] A. Sode-Yome and N. Mithulananthan, "Comparison of shunt capacitor, SVC and STATCOM in static voltage stability margin enhancement," *Int. J. Electr. Eng. Educ.*, vol. 41, no. 2, pp. 158–171, 2004.

[33] R. Sirjani, A. Mohamed, and H. Shareef, "Comparative study of the effectiveness of different var compensation devices in large-scale power networks," *J. Cent. South Univ.*, vol. 20, no. 3, pp. 715–723, 2013.

[34] A. Eid and S. Kamel, "Optimal allocation of shunt compensators in distribution systems using the turbulent flow of waterbased optimization Algorithm," *2020 IEEE Electr. Power Energy Conf. EPEC 2020*, vol. 3, 2020.

[35] S. Rezaeian Marjani, V. Talavat, and S. Galvani, "Optimal allocation of D-STATCOM and reconfiguration in radial distribution network using MOPSO algorithm in TOPSIS framework," *Int. Trans. Electr. Energy Syst.*, vol. 29, no. 2, pp. 1–25, 2019.

[36] A. Eid, S. Kamel, A. Korashy, and T. Khurshaid, "An Enhanced Artificial Ecosystem-Based Optimization for Optimal Allocation of Multiple Distributed Generations," *IEEE Access*, vol. 8, pp. 178493–178513, 2020.

[37] U. Ghatak and V. Mukherjee, "An improved load flow technique based on load current injection for the modern distribution system," *Int. J. Electr. Power Energy Syst.*, vol. 84, pp. 168–181, 2017.

6

A Novel Brown-bear Optimization Algorithm for Solving Economic Dispatch Problem

Tapan Prakash[1], Praveen Prakash Singh[2], Vinay Pratap Singh[3], and Sri Niwas Singh[4]

[1]School of Electrical Engineering, VIT University, Vellore, TN, India
[2]Department of Electrical Power Engineering and Mechatronics, TalTech, Estonia
[3]Department of Electrical Engineering, MNIT Jaipur, Jaipur, RJ, India
[4]Department of Electrical Engineering, IIT Kanpur, Kanpur, UP, India
E-mail: tapan.prakash@vit.ac.in; prsing@taltech.ee; vinay.ee@mnit.ac.in; snsingh@iitk.ac.in

Abstract

For optimal operation of a modern power system, an efficient optimizer is needed. There are many conventional and intelligent system-based optimization tools available. Conventional approaches suffer from many drawbacks such as the requirement of derivatives of objective function and constraints, close initial guess, etc. Getting optimal solutions using intelligent system-based methods is challenging too. Stable and reliable operation of the power system depends a lot on the efficient solutions to such problems. In this chapter, a novel optimizer named as Brown-Bear Optimization Algorithm (BOA) based on the mode of communication between brown-bears featuring pedal scent marking and sniffing behaviors is introduced to solve the Economic Dispatch Problem (EDP) which is an important problem of optimal operation of power system. Pedal scent marking behavior of bears, which is a fundamental mode of communication between them, is characterized by different features such as maintaining a characteristic gait while walking, careful stepping on the pedal marks and twisting of feet on depressions made

on ground. Sniffing behavior found in them further strengthens their communication. The mathematical model featuring the aforementioned behaviors of bears is developed to form BOA. The algorithm maintains a balance between exploration and exploitation and is free from algorithm-specific parameters. To examine the performance of BOA, it is applied to solve several benchmark tests functions of different complexities. Comparative assessment is carried out to establish its efficacy. The proposed algorithm is found to be performing better than many existing optimization algorithms in obtaining an optimal solutions for benchmark test functions. To identify its statistical significance, Wilcoxon's signed rank test is conducted. The test reveals that BOA produces more significant results in comparison to other state-of-art algorithms. Further, BOA is utilized to solve EDP while minimizing the total cost involved subjected to practical constraints. The results obtained from BOA are found to be minimum when compared to the results of state-of-art optimization algorithms reported in the literature.

6.1 Introduction

The security and reliability of modern power system is a prime concern of electric utilities presently. The optimal operation of the system aids in maintaining required security and reliability. To ensure optimal operation of the system, an efficient optimization tool is of utmost needed. Basically, these tools enable the power system to operate in an economical manner while considering several inherent limitations. Over the years, optimization methods are considered to be an effective tool to solve constrained optimization problems which are evidently present in our modern power system.

In general, an optimization algorithm either minimizes or maximizes an objective function taking into account all associated constraints. Broadly, optimization algorithms can be classified as classical methods, evolutionary, nature-inspired and other algorithms. In classical methods, several methods are available in literature like gradient-based methods [1], direct-search methods [2], linear programming [3], quadratic programming [4], etc.

Generally, classical methods start finding the optimum solutions with an initial guess. Consequently, the performance of classical methods is decided by initial guess and continuity of objective and constraints, and thus, fitness function may or may not converge to global optima. To overcome this

limitation, evolutionary optimization algorithms came into existence that do not require any initial guesses. Evolutionary algorithms are methods mainly inspired by the evolution process. Genetic Algorithm (GA) is considered as first developed evolutionary algorithm [5]. It replicates the behavior of genes. Particle Swarm Optimization (PSO) is developed as an evolutionary algorithm mimicking the behavior of a swarm of birds/fishes [6]. Differential Evolution (DE) is another developed evolutionary algorithm [7]. The introduction of Evolutionary Programming (EP) [8] is another addition. These algorithms are successfully applied to various engineering optimization problems. They overcame the limitations of classical methods to a great extent but are prone to get trapped in local minima.

With the success of evolutionary algorithms and to eliminate the problems of local minima trappings, several other algorithms which are mainly inspired by the phenomenon of nature are developed. These methods are categorized as nature-inspired algorithms. Some of the important algorithms in this category are Simulated Annealing (SA) [9], firefly algorithm (FA) [10], Bat Algorithm (BA) [11], Ant-Lion Optimization (ALO) [12], Grey-Wolf Optimizer (GWO) [13], Krill Herd Optimization (KHO) [14], Imperialist Colony Algorithm (ICA) [15], Wild Goats Optimization (WGO) [16], whale Optimization Algorithm (WOA) [17], Gravitational Search Algorithm (GSA) [18], etc. Most of the above evolutionary or nature-inspired algorithms possess algorithm-specific parameters (like social and cognitive parameters, c_1 and c_2, and inertia weight w_i in PSO) apart from common control parameters (like size of the population and a maximum number of iterations). It is worthy to note here that the performance of algorithms having algorithm-specific parameters depend heavily on these parameters since it is indispensable to tune algorithm-specific parameters before the application of the concerned algorithms in order to achieve global optima or near global optima. The aforementioned step sometimes proves to be cumbersome than the solution of the problem itself. Hybridization of existing optimization algorithms is another way suggested improving the performance of parent algorithms. However, the hybridization of two or more algorithms into one increases the computation time appreciably. And, if there are some algorithm-specific parameters in a hybrid algorithm, then it will become a cumbersome task to tune them. The aforementioned limitations motivated the author to develop a novel optimizer that is free from algorithm-specific parameters and is computationally efficient.

Consequently, a novel nature-inspired optimizer based on the pedal scent marking and sniffing behaviors of brown-bears is introduced to solve

real-world optimization problems. The developed optimizer is named as brown-bear Optimization Algorithm (BOA) which is computationally efficient and does not possess any algorithm-specific parameters. The balance between exploration of search space and exploitation of the best solution is maintained efficiently thus, converting it into a powerful optimization algorithm. The performance of the proposed algorithm is examined through a test on benchmark functions. Statistical significance of the algorithm is established by Wilcoxon's signed rank test. To validate the efficient performance of a proposed algorithm, a widely reported real-world optimization problem i.e. Economic Dispatch Problem (EDP) is solved in this work.

6.2 Brown-bear Optimization Algorithm

In this segment, the influencing factors acting as a source of inspiration for the proposed BOA are discussed at first. Followed by the inspirational background, the developed mathematical model is presented.

6.2.1 Inspirational Background

It is a well-known fact that the mode of communication based on chemical signals is adopted in the majority by both terrestrial and aquatic organisms [19]. In a recent study, the presence of pedal scent communication in brown-bears is investigated and found to be existing [20]. The study concluded the existence of such communication in brown-bears based on the observations confirming the presence of pedal glands, the biochemical compositions of secretions from the glands and their behavior linked to pedal scent marking. The detailed study and discussions can be referred to from [20].

The brown-bear (ursus arctos) is a bear of large size and is extensively distributed among any living ursid. They are dominantly distributed in North America and the northern part of Eurasia. They are regarded as one of the largest territorial carnivorans living in this present era and are often described as nocturnal. The study in [20] shows the pedal scent marking behavior of these bears which proves that these bears possess some intellectual abilities. This pedal scent marking behavior is an effective tool for their communication. Mostly this behavior is observed in male brown-bears. The pedal marks of these bears are spread over their territory with each group having distinctive pedal scent marks. Basically, the pedal scent marking behavior of a group can be characterized in the following manner.

- A characteristic gait while walking
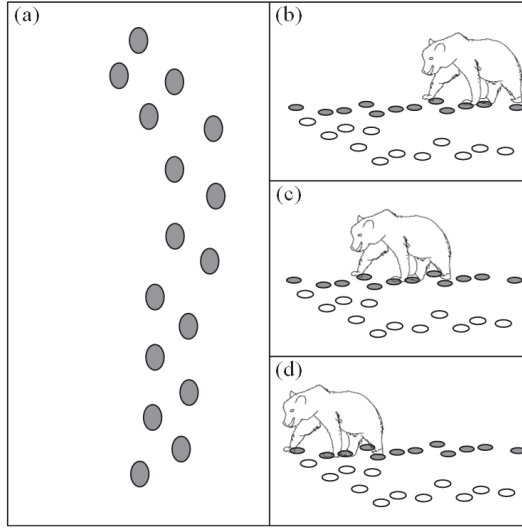
Figure 6.1 Pedal scent marking and sniffing behaviors of brown-bears. (a) Pedal marks in an area. (b-d) A brown-bear stretching to its pedal marks.

- Careful stepping characteristic.
- Twisting of the feet on the depressions made in the ground.

These bears repeatedly use the above characteristics for scent marking in their territory over a long time. Another behavior of sniffing pedal marks is observed in these bears apart from marking behavior. It is found that male, female, and other members of respective groups show this behavior. This behavior strengthens their communication further. Figure 6.1 shows the pedal scent marking and sniffing behaviors of brown-bears [20].

The pedal scent marking and sniffing behavior found in brown-bears are their unique features. As a result, these two behaviors of these bears are mathematically represented to design an optimization algorithm. The detailed model and discussions are carried out in the following subsection.

6.2.2 Proposed BOA with Mathematical Model

The proposed optimization algorithm is designed to incorporate two major phases based on pedal scent marking and sniffing behaviors of the brown-bears. Further, the pedal scent marking behavior is subdivided into three subcategories according to characteristics stated in the previous section with equal probability of their occurrences.

6.2.2.1 Group formation

In this algorithm, the different groups of brown-bears within a territory are assumed to be analogous to each solution set of a population while the pedal scent marks formed by each group are analogous to the number of decision variables present in each solution set. The territory of brown-bears is analogous to the search space of a problem. Like other population based optimization techniques, the initialization of the population in this algorithm is performed. The different groups of brown-bears within a territory are randomly generated with a fixed number of pedal scent marks. However, each mark of different groups are of distinctive features and remain within the territory. Their limits are defined by the boundaries of the decision variables of the respective problems. The mathematical expression for random initialization of the groups within a territory is represented below.

$$P_{i,j} = P_{i,j}^{\min} + \lambda \cdot (P_{i,j}^{\max} - P_{i,j}^{\min}) \tag{6.1}$$

where $P_{i,j}$ is the jth pedal mark of ith group of brown-bears. $P_{i,j}^{\min}$ and $P_{i,j}^{\max}$ are the minimum and maximum range of pedal marks, respectively. λ is any random number evenly distributed in the range $[0,1]$. If the total number of groups within a territory (i.e. population) are defined by N_{pop} and the total number of pedal marks (i.e. number of decision variables) in each group is defined by D then, the solution set P is represented as

$$P = \begin{bmatrix} P_{1,1} & P_{1,2} & \cdots & P_{1,D} \\ P_{2,1} & P_{2,2} & \cdots & P_{2,D} \\ \vdots & \vdots & \ddots & \vdots \\ P_{N_{pop},1} & P_{N_{pop},2} & \cdots & P_{N_{pop},D} \end{bmatrix} \tag{6.2}$$

6.2.2.2 Pedal scent marking behavior

As mentioned earlier that pedal scent marking behavior found in brown-bears are unique in nature. It is characterized by characteristic gait while walking, careful stepping, and twisting of feet onto the depressions made in the ground. These three characteristics are modeled mathematically to represent pedal scent marking behavior. The occurrences of these characteristics are divided with equal probability. Considering the total number of iterations in the algorithm to be N_{iter}, the occurrence of each characteristic stated above is equal to $\frac{N_{iter}}{3}$. The mathematical model of the characteristics is defined below.

- **Characteristic gait while walking**: In the majority, only male members show the pedal scent marking behavior. For simplification, the number of

the male members in each group is considered to be one. Male members of each group possess distinctive gait while walking. As a result, the pedal scent marks formed by a male bears of each group are very much distinctive in nature. It is assumed that pedal scent marks formed on the basis of characteristic gait while walking is continued till the first one third of the total number of iterations, N_{iter}. Mathematically this characteristic is expressed as

$$P_{i,j,k}^{new} = P_{i,j,k}^{old} - (\theta_k \cdot \alpha_{i,j,k} \cdot P_{i,j,k}^{old}) \tag{6.3}$$

where $P_{i,j,k}^{new}$ is jth updated pedal mark of ith group of brown-bears during kth iteration and $P_{i,j,k}^{old}$ is the previous jth pedal mark of ith group of brown-bears during the same iteration. $\alpha_{i,j,k}$ is any random number evenly distributed in the range $[0,1]$ associated with jth pedal mark of ith group of bears for kth iteration. θ_k is the occurrence factor for kth iteration which increases linearly with an increase in a number of iterations. It is defined as the ratio of the current iteration number to the total number of iterations and is represented as

$$\theta_k = \frac{C_{iter}}{N_{iter}} \tag{6.4}$$

where C_{iter} is the current iteration number.
- **Careful stepping characteristic**: From the first one-third to second-third of the total iterations, the pedal marks are updated according to this characteristic. The characteristic of careful stepping undertaken by brown-bears primarily exists to make the relevant pedal marks more recognizable. A brown-bear used to step on the previous pedal marks repeatedly in order to make them more visible to other members of the respective group. The mathematical model of this characteristic is expressed in the following manner.

$$P_{i,j,k}^{new} = P_{i,j,k}^{old} + F_k \cdot (P_{j,k}^{best} - L_k \cdot P_{j,k}^{worst}) \tag{6.5}$$

where $P_{j,k}^{best}$ and $P_{j,k}^{worst}$ are the jth best and jth worst pedal scent marks among the total groups of brown-bears during kth iteration, respectively. F_k is the step factor for kth iteration and its value depends upon occurrence factor θ_k in the following manner.

$$F_k = \beta_{1,k} \cdot \theta_k \tag{6.6}$$

where $\beta_{1,k}$ is any random number in the range $[0,1]$ during kth iteration. L_k is the step length during kth iteration. It is incorporated here to show how the pedal marks should be modified from the available information on the best and worst pedal marks of the whole population. The step length L_k takes a value of 1 or 2. Depending upon the step length L_k, a male brown-bear of the respective group takes its step carefully in either forward or backward direction in order to form newer pedal marks. Mathematically, the step length L_k is expressed as

$$L_k = \text{round}(1 + \beta_{2,k}) \tag{6.7}$$

where $\beta_{2,k}$ is any random number uniformly distributed in the range $[0,1]$.

- **Twisting feet characteristic**: From the second-third part of the iteration to the last iteration, the updating of pedal marks is defined by the twisting feet characteristic. The male brown-bear of each group twists his feet onto the depressions made in the ground formed in previous stages. This characteristic of the bears helps in the formation of more firm pedal scent marks which are used to create the scent maps by other members of group. The previous pedal marks are chosen on the basis of information available from the best and worst pedal marks out of the total pedal marks. The angular velocity with which each male brown-bear of a group twists its feet is expressed as

$$\omega_{i,k} = 2\pi \cdot \theta_k \cdot \gamma_{i,k} \tag{6.8}$$

where $\omega_{i,k}$ is the ith angular velocity of twist during kth iteration. $\gamma_{i,k}$ is an evenly distributed random number in the range $[0,1]$. A brown-bear will only twist its feet onto the previous pedal marks which are closer to the best pedal marks and far away from the worst pedal marks. This characteristic is defined through expression in the following manner.

$$P_{i,j,k}^{\text{new}} = P_{i,j,k}^{\text{old}} + \omega_{i,k} \cdot \left(P_{j,k}^{\text{best}} - \left|P_{i,j,k}^{\text{old}}\right|\right) - \omega_{i,k} \cdot \left(P_{j,k}^{\text{worst}} - \left|P_{i,j,k}^{\text{old}}\right|\right) \tag{6.9}$$

It is worth mentioning here that after this phase, the selected better group of bears take part in the next phase.

6.2.2.3 Sniffing behavior

Sniffing behavior is common in every group member of brown-bears. This behavior helps them to communicate with each other by sniffing the pedal sent marks and thus, this behavior controls their movement in the territory. In

order to move, bears start sniffing the pedal marks chosen randomly within the territory. They move towards the pedal marks which belong to their group and leave the other pedal marks. This behavior is mathematically modeled by choosing two random candidate solutions and updating the move of the bear according to the following model.

$$
P_{m,j,k}^{\text{new}} = \begin{cases} P_{m,j,k}^{\text{old}} + \lambda_{j,k} \cdot \left(P_{m,j,k}^{\text{old}} - P_{n,j,k}^{\text{old}}\right) \text{if } f\left(P_{m,k}^{\text{old}}\right) < f\left(P_{n,k}^{\text{old}}\right) \\ P_{m,j,k}^{\text{old}} + \lambda_{j,k} \cdot \left(P_{n,j,k}^{\text{old}} - P_{m,j,k}^{\text{old}}\right) \text{if } f\left(P_{n,k}^{\text{old}}\right) < f\left(P_{m,k}^{\text{old}}\right) \end{cases} \tag{6.10}
$$

where $P_{m,j,k}^{\text{new}}$ is the jth updated pedal marks of mth group of bears during kth iteration. $P_{m,j,k}^{\text{old}}$ and $P_{n,j,k}^{\text{old}}$ are the jth pedal marks of mth and nth group of bears during kth iteration, respectively and $m \neq n$. $f\left(P_{m,k}^{\text{old}}\right)$ and $f\left(P_{n,k}^{\text{old}}\right)$ are the fitness function value was evaluated for mth and nth groups of bears during kth iteration. $\lambda_{j,k}$ is an evenly distributed random number in the range of $[0,1]$ for jth pedal marks during kth iteration. The above stated phase is applied to all groups of bears in the population. The better group of bears from the updated population and the old population are retained and moved to the next iteration. The process of updating and selection described in the above two behaviors are repeated till any termination criteria are met.

The performance of any optimization depends upon its exploitation and exploration capabilities. The local search is the exploitation phase whereas the global search is the exploration phase. In the proposed algorithm, the local search is accomplished by the pedal scent marking phase. The algorithm exploits the surrounding knowledge to update its position until the first one-third part of the total iterations characterized by sub-phase of characteristic gait while walking. When the surroundings are exploited, the positions are updated with the knowledge of best and worst pedal marks in sub-phase of careful stepping until the second-third part of the iterations. While the last third part of the iterations describe the exploitation phase by updating the position vector of pedal marks towards best pedal marks and away from worst pedal marks. The local search capability of the proposed algorithm in this manner avoids the local minima trappings. The exploration phase is undertaken by the sniffing behavior phase in this algorithm. The algorithm updates the position vector of the pedal marks based on randomly chosen two vectors of pedal marks in the population. Thus, this phase helps in maintaining the exploration capability of the algorithm. The pseudo code of the proposed BOA is presented in Algorithm 1.

Algorithm 1 Pseudo code of proposed BOA.

Require: N_{iter}, N_{pop}, D and boundaries of variables.
Ensure: Fitness function $f(P)$ is defined.
1:    **Initialize** random group of bears using (6.1).
2:    **Form** population P of group of bears as shown in (6.2).
3:    **Initialize** best fitness $f^{best} = \inf$ and $k = 1$.
4:    **while** $(k \leq N_{iter})$ **do**
5:        **for** $(i = 1 : \text{size}(P, 1))$ **do**
6:            Check limit constraints of pedal marks.
7:            Evaluate fitness function $f(P_i)$.
8:            **if** $(f^{best} > f(P_i))$ **then**
9:                $f^{best} = f(P_i);$
10:                $P_k^{best} = P(i, :);$
11:            **end if**
12:        **end for**
13:        ***Pedal scent marking behavior** starts...* \\
14:        Select best and worst group of bears.
15:        $\theta_k = \frac{k}{N_{iter}};$
16:        **for** $(i = 1 : \text{size}(P, 1))$ **do**
17:            % *Characteristic gait while walking*
18:            **if** $\left(\theta_k > 0 \,\&\&\, \theta_k \leq \frac{N_{iter}}{3}\right)$ **then**
19:                Update $P_{i,k}$ using (6.3).
20:                % *Careful stepping characteristic*
21:            **else if** $\left(\theta_k > \frac{N_{iter}}{3} \,\&\&\, \theta_k \leq \frac{2N_{iter}}{3}\right)$ **then**
22:                Update $P_{i,k}$ using (6.5).
23:                % *Twisting feet characteristic*
24:            **else if** $\left(\theta_k > \frac{2N_{iter}}{3} \,\&\&\, \theta_k \leq 1\right)$ **then**
25:                Update $P_{i,k}$ using (6.9).
26:            **end if**
27:        **end for**
28:        Select better group of bears.
29:        ***Pedal scent marking behavior** ends...* \\
30:        ***Sniffing behavior** starts...* \\
31:        **for** $(m = 1 : \text{size}(P, 1))$ **do**
32:            Select one random group of bears $P_{n,k}$ where $m \neq n$.
33:            Update $P_{m,k}$ using (6.10).
34:        **end for**
35:        Select better group of bears.
36:        ***Sniffing behavior** ends...* \\
37:        $k = k + 1;$
38: **end while**
39: **print** f^{best} and P^{best}.

6.3 Performance Evaluation of BOA on Standard Test Functions

In this section, the performance of BOA is evaluated on widely used benchmark test functions and competition on "Evolutionary Computation" (CEC) test functions. The performance evaluation is concentrated on finding the mean and standard deviation values for the test functions, depicting convergence characteristics, and performing statistical tests. The results obtained from BOA are compared to state-of-art algorithms reported in the literature.

6.3.1 Evaluation on Benchmark Test Functions

The performance of the proposed BOA is evaluated on widely documented benchmark test functions. A total of 23 functions comprising variable dimensional unimodal and multimodal functions and fixed dimensional multimodal functions are used to test the effectiveness of proposed optimizer. The details of the functions are presented in Tables 6.1 and 6.2. The performance of algorithms like PSO, ICA, WGO, WOA, ALO, and GWO reported in literature along with proposed BOA is evaluated on benchmark functions tabulated

Table 6.1   Details of benchmark test functions

Function	Range	Dim	f_{min}
$f_1(p) = \sum_{j=1}^{D} p_i^2$	$[-100, 100]$	30	0
$f_2(p) = \sum_{j=1}^{D} |p_j| + \prod_{j=1}^{D} |p_j|$	$[-10, 10]$	30	0
$f_3(p) = \sum_{j=1}^{D} \left(\sum_{k=1}^{j} p_k \right)^2$	$[-100, 100]$	30	0
$f_4(p) = \max_j \{|p_j|, 1 \le j \le D\}$	$[-100, 100]$	30	0
$f_5(p) = \sum_{j=1}^{D-1} \left(100(p_{j+1} - p_j^2)^2 + (p_j - 1)^2 \right)$	$[-30, 300]$	30	0
$f_6(p) = \sum_{j=1}^{D} (p_j + 0.5)^2$	$[-100, 100]$	30	0
$f_7(p) = \sum_{j=1}^{D} j \cdot p_j^4 + \text{rand}()$	$[-1.28, 1.28]$	30	0
$f_8(p) = \sum_{j=1}^{D} -p_j \cdot \sin(\sqrt{|p_j|})$	$[-500, 500]$	30	0
$f_9(p) = \sum_{j=1}^{D} \left(p_j^2 - 10\cos(2\pi p_j) + 10 \right)$	$[-5.12, 5.12]$	30	0
$f_{10}(p) = \begin{aligned} &-20\exp\left(-0.2\sqrt{\frac{1}{D}\sum_{j=1}^{D} p_j^2}\right) \\ &- \exp\left(\frac{1}{D}\sum_{j=1}^{D}\cos(2\pi p_j)\right) + 20 + e \end{aligned}$	$[-32, 32]$	30	0
$f_{11}(p) = \frac{1}{4000}\sum_{j=1}^{D} p_j^2 - \prod_{j=1}^{D}\cos\left(\frac{p_j}{\sqrt{j}}\right) + 1$	$[-600, 600]$	30	0
$f_{12}(p) = \begin{aligned} &\frac{\pi}{D}\left(10\sin^2(\pi q_1) + \sum_{j=1}^{D-1}(q_j - 1)^2(1 + 10\sin^2(\pi q_{j+1})) \right. \\ &\left. + (q_D - 1)^2)\right) + \sum_{j=1}^{D} x(p_j, 10, 100, 4) \end{aligned}$	$[-50, 50]$	30	0
where, $q_j = 1 + \frac{p_j + 1}{4}$			
and $x(p_j, a, b, c) = \begin{cases} b(p_j - a)^c & p_j > a \\ 0 & -a < p_j < a \\ b(-p_j - a)^c & p_j < -a \end{cases}$			

Table 6.2   Details of benchmark test functions

Function	Range	Dim	$f_{\min}$
$f_{13}(p) = \begin{aligned}0.1\Big(&\sin^2(3\pi p_1) + \sum_{j=1}^{D}(p_j-1)^2\big(1+\sin^2(3\pi p_j+1)\big)\\ &+(p_D-1)^2\big(1+\sin^2(2\pi p_D)\big)\Big) + \sum_{j=1}^{D}x(p_j,5,100,4)\end{aligned}$	$[-50,50]$	30	0
$f_{14}(p) = \left[\frac{1}{500} + \sum_{k=1}^{25}\frac{1}{k+\sum_{j=1}^{2}(p_j-a_{jk})^6}\right]^{-1}$	$[-65.54,65.54]$	2	1
$f_{15}(p) = \sum_{j=1}^{11}\left(a_j - \frac{p_1(b_j^2+b_jp_j)}{b_j^2+b_1p_3+p_4}\right)^2$	$[-5,5]$	4	0
$f_{16}(p) = 4p_1^2 - 2.1p_1^4 + \frac{1}{3}p_1^6 + p_1p_2 - 4p_2^2 + 4p_2^4$	$[-5,5]$	2	-1.0316
$f_{17}(p) = \left(p_2 - \frac{5.1}{4\pi^2}p_1^2 + \frac{5}{\pi}p_1 - 6\right)^2 + 10\left(1-\frac{1}{8\pi}\right)\cos(p_1) + 10$	$\begin{aligned}&[-5,10]*\\&[0,15]\end{aligned}$	2	0.39789
$f_{18}(p) = \begin{aligned}&(1+(p_1+p_2+1)^2(19-14p_1+3p_1^2-14p_2\\ &\quad+6p_1p_2+3p_2^2)) \times \big(30+(2p_1-3p_2)^2\\ &(18-32p_1+12p_1^2+48p_2-36p_1p_2+27p_2^2)\big)\end{aligned}$	$[-2,2]$	2	3
$f_{19}(p) = -\sum_{j=1}^{4}c_j\exp\left(\sum k=1^3 a_{jk}(p_k-x_{jk})^2\right)$	$[0,1]$	3	-3.8628
$f_{20}(p) = -\sum_{j=1}^{4}c_j\exp\left(\sum k=1^6 a_{jk}(p_k-x_{jk})^2\right)$	$[0,1]$	6	-3.322
$f_{21}(p) = -\sum_{j=1}^{5}\left[(P-a_j)(P-a_j)^T+c_j\right]^{-1}$	$[0,10]$	4	-10.1532
$f_{22}(p) = -\sum_{j=1}^{7}\left[(P-a_j)(P-a_j)^T+c_j\right]^{-1}$	$[0,10]$	4	-10.4029
$f_{23}(p) = -\sum_{j=1}^{10}\left[(P-a_j)(P-a_j)^T+c_j\right]^{-1}$	$[0,10]$	4	-10.5364

in Tables 6.1 and 6.2 and the obtained evaluations are listed in Table 6.3. For all evaluations, 51 number of independent trials, a population size of 30 and a maximum number of iterations of 500 are considered. Table 6.3 lists the mean fitness function value and Standard Deviation (SD) for considered trials. From Table 6.3, it can be seen that the proposed BOA algorithm is able to obtain a minimum value i.e. global optima or near to global optima for 18 functions out of total of 23 functions. The algorithm is found to be capable of obtaining global optima for 14 functions. From the results, it is evident that proposed BOA is an effective optimization algorithm and robust in nature.

The function plot of functions f_1, f_5, f_{10}, f_{15}, and f_{20} along with the trajectory of first dimension, the fitness function history and convergence curve for 100 iterations are shown in Figure 6.2. A closer look at the trajectory of the first dimension in all sub-figures reveals that initially, the trajectory is varying but after some iterations, it settles down and stays at a constant value. This fact signifies that within a few iterations, the dimension reaches its final value which further suggests that the proposed BOA converges very fast to global or near to global optima. From the convergence curve, it can be observed that in all cases, the solution converges to global or near to global optima in less than 50 iterations.

Table 6.3 Performance evaluation on benchmark test functions

F	Measure	PSO [16]	ICA [16]	WGO [16]	WOA [17]	ALO [12]	GWO [13]	BOA (proposed)
f_1	Mean	3.69e-37	1.58e-58	**0**	1.41e-30	2.59e-10	6.59e-28	**0**
	SD	2.46e-36	4.63e-58	**0**	4.91e-30	1.65e-10	6.34e-05	**0**
f_2	Mean	2.92e-24	3.9e-30	**0**	1.06e-21	1.84241e-06	7.18e-17	**0**
	SD	1.14e-23	4.19e-30	**0**	2.39e-21	6.58e-07	0.029014	**0**
f_3	Mean	1.2e-03	1.07e+03	7.28e-10	5.39e-07	6.06847e-10	3.29e-06	**8.4971e-290**
	SD	2.11e-03	3.24e+02	1.03e-09	2.93e-06	6.34e-10	79.14958	**0**
f_4	Mean	0.41	1.36	9.12e-276	0.072581	1.36061e-08	5.61e-07	**0**
	SD	2.5e-01	4.01e-01	**0**	0.39747	1.81e-09	1.315088	**0**
f_5	Mean	3.74e+01	4.67e-04	**1.57e-10**	27.86558	0.346772393	26.81258	25.3792
	SD	3.21e+01	1.48e-03	**2.11e-10**	0.763626	0.109584	69.90499	1.1176
f_6	Mean	0.15	2.33e+03	**0**	3.116266	2.56183e-10	0.816579	1.1117
	SD	0.42	5.05e+03	**0**	0.532429	1.09e-10	0.000126	1.1262
f_7	Mean	9.9e-03	2.58e-04	5.68e-03	0.001425	4.292492e-03	0.002213	**5.3156e-07**
	SD	3.54e-02	7.43e-05	1.98e-03	0.001149	5.089e-03	0.100286	**5.1959e-05**
f_8	Mean	-9.67e+03	-1.11e+04	-6.98e+03	-5080.76	-1606.27643	-6123.1	-9934.6447
	SD	4.64e+02	7.49e+02	8.76e+02	695.7968	314.4302	-4087.44	1215.6828
f_9	Mean	2.08e+01	1.44e+02	9.99	**0**	7.71411e-06	0.310521	**0**
	SD	5.94	8.67	1.94	**0**	8.45e-06	47.35612	10.5391
f_{10}	Mean	1.34e-03	1.67e+01	9.41e-02	7.4043	3.73035e-15	1.06e-13	**8.8818e-16**
	SD	4.24e-02	4.97	2.88e-01	9.897572	1.5e-15	0.077835	**0**
f_{11}	Mean	2.32e-01	1.28e-02	4.83e-21	2.89e-04	0.018604494	0.004485	**0**
	SD	4.43e-01	1.19e-02	3.28e-20	1.586e-03	9.545e-03	0.006659	**0**
f_{12}	Mean	3.95e-02	**1.56e-32**	1.57e-32	0.339676	9.74645e-12	0.053438	0.075538
	SD	9.14e-02	5.7e-35	**0**	0214864	9.33e-12	0.020734	0.13115
f_{13}	Mean	5.05e-02	1.10e-26	**2.75e-32**	1.889015	2.00222e-11	0.654460	1.6851
	SD	0.57	0.77e-26	**3.42e-32**	0.266088	1.13e-11	0.004474	0.40322
f_{14}	Mean	1.02	**9.98e-01**	3.19	2.111973	**0.998***	4.042493	**0.998**
	SD	0.15	0	2.47	2.498594	2.4788*	4.252799	0.52792
f_{15}	Mean	3.81e-04	5.61e-04	3.075e-04	5.72e-04	6.9604e-04*	0.000337	**0.00030749**
	SD	2.51e-04	**1.43e-04**	0	3.24e-04	0.021693*	0.000625	0.0028463
f_{16}	Mean	-1.02	**-1.0316**	**-1.0316**	-1.03163	**-1.0316***	-1.03163	**-1.0316**
	SD	1.28e-02	**0**	**0**	4.2e-07	2.1089e-13*	-1.03163	7.6506e-09
f_{17}	Mean	0.40	0.3979	0.3979	0.397914	0.39789*	0.397889	**0.39789**
	SD	6.88e-02	0	0	2.7e-05	**5.2759e-13***	0.397887	1.1438e-06
f_{18}	Mean	3.01	**3**	**3**	**3**	**3***	3.000028	**3**
	SD	1.21e-02	**0**	**0**	4.22e-15	7.277e-12*	3	**0**
f_{19}	Mean	-3.86	-3.86	-3.86	-3.85616	**-3.8628***	-3.86263	**-3.8628**
	SD	3.21e-03	**3.48e-13**	0	2.706e-03	0.015159*	-3.86278	7.1838e-07
f_{20}	Mean	-3.18	-3.32	-3.32	-2.98105	**-3.322***	-3.28654	**-3.322**
	SD	6.11e-02	**1.23e-15**	0	0.376653	0.11375*	-3.25056	0.062564
f_{21}	Mean	-7.54	-9.95	**-10.1532**	-7.04918	**-10.1532***	-10.1514	**-10.1532**
	SD	3.03	1.00	**0**	3.629551	2.3553*	-9.14015	0.92528
f_{22}	Mean	-8.36	-1.01e+01	**-10.4029**	-8.18178	**-10.4029***	-10.4015	**-10.4029**
	SD	2.02	1.39	**0**	3.829302	3.4692*	-8.58441	1.6538
f_{23}	Mean	-8.94	-1.01e+01	**-10.5364**	-9.34238	**-10.5364***	-10.5343	**-10.5364**
	SD	1.63	1.47	**0**	2.414737	3.3619*	-8.55899	1.9207

* indicates that the results are obtained under same test conditions.
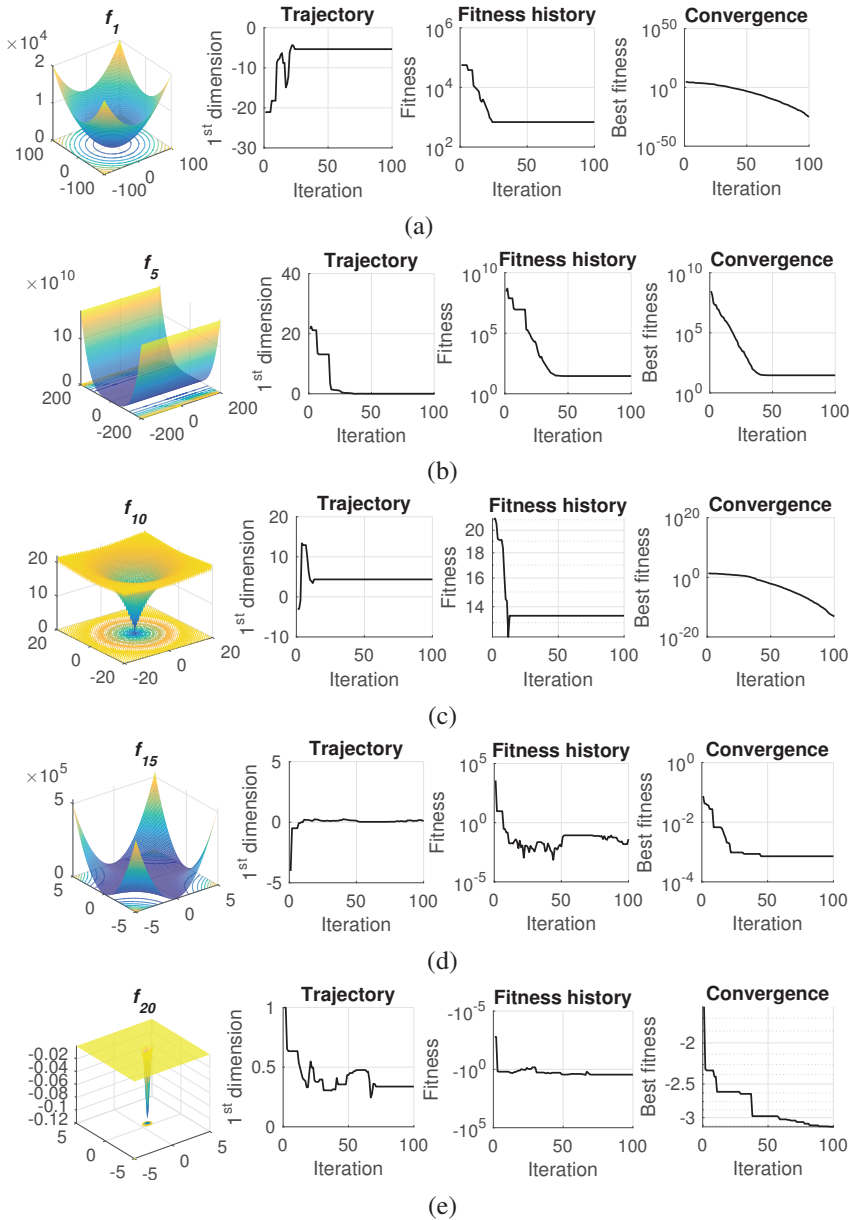
Figure 6.2 Function plot, trajectory of 1st dimension, fitness history and convergence curve for different functions. (a) Function f_1. (b) Function f_5. (c) Function f_{10}. (d) Function f_{15}. (e) Function f_{20}.

Further, to depict an illustrative aspect of the performance of BOA algorithm, the convergence characteristics of all 23 benchmark test functions obtained from BOA along with GWO, ALO, WOA, and PSO are presented in Figure 6.3. From the sub-figures, it can be clearly observed that the test functions converge to global optima or near to global optima at a faster
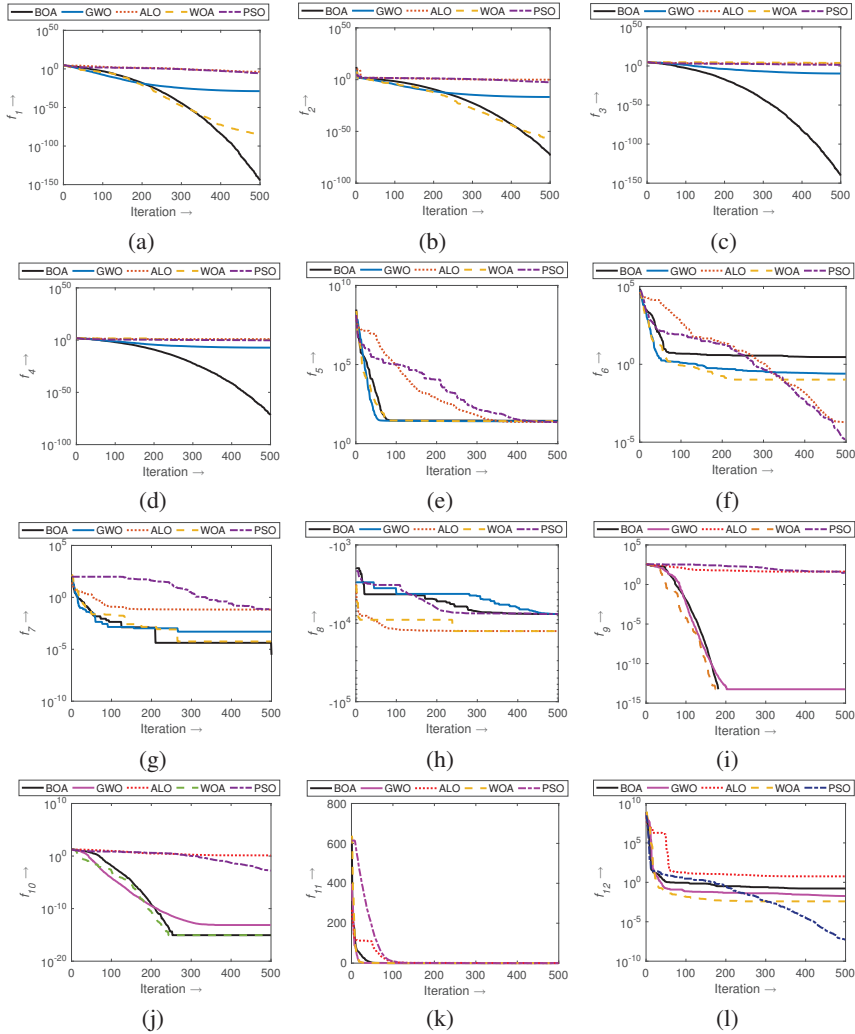
Figure 6.3   Convergence characteristics for benchmark test functions. (a) f_1. (b) f_2. (c) f_3. (d) f_4. (e) f_5. (f) f_5. (g) f_7. (h) f_8. (i) f_9. (j) f_{10}. (k) f_{11}. (l) f_{12}.
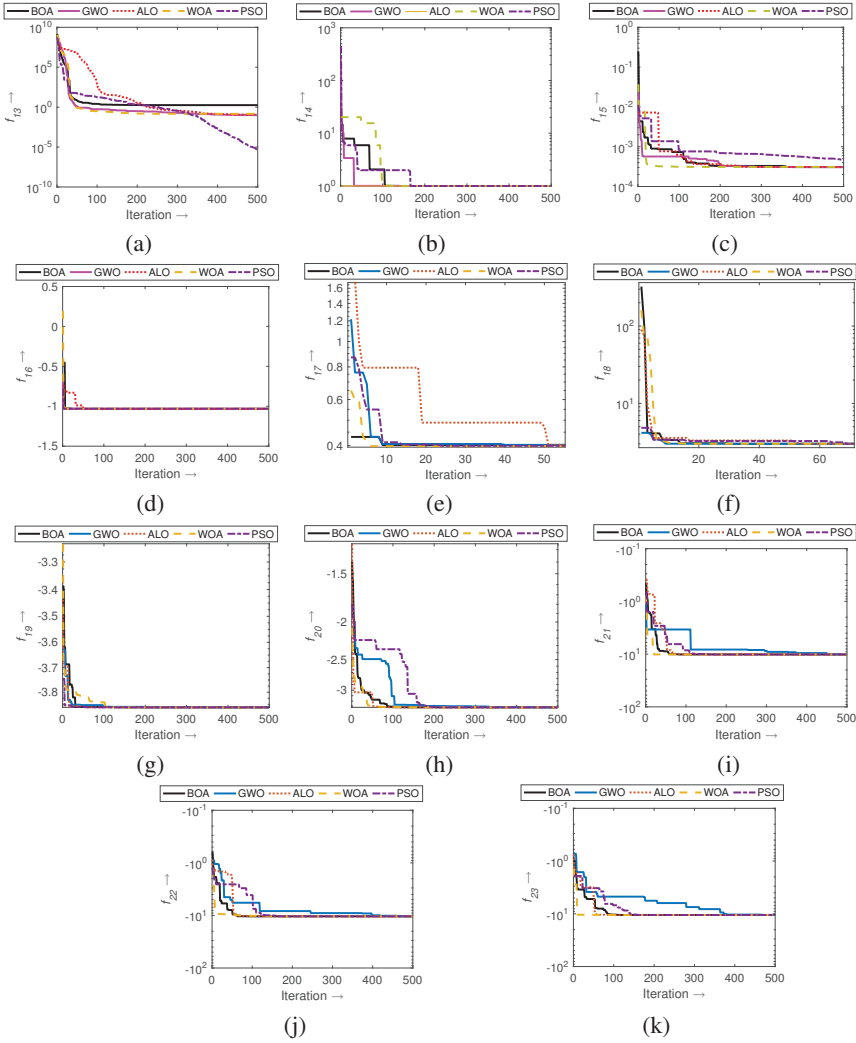
Figure 6.4 Convergence characteristics for benchmark test functions. (m) f_{13}. (n) f_{14}. (o) f_{15}. (p) f_{16}. (q) f_{17}. (r) f_{18}. (s) f_{19}. (t) f_{20}. (u) f_{21}. (v) f_{22}. (w) f_{23}.

rate with BOA for most of the functions compared to other algorithms. Aforementioned fact certifies the consistent performance of BOA.

Additionally, a statistical test to determine the significance of the results obtained from BOA is undertaken for all considered benchmark test

Table 6.4   Wilcoxon signed rank test on benchmark test functions

Function	BOA vs. GWO		BOA vs. ALO		BOA vs. WOA		BOA vs. PSO	
	p	h	p	h	p	h	p	h
f_1	7.5569e-10	1	7.5569e-10	1	7.5569e-10	1	7.55692e-10	1
f_2	7.5569e-10	1	7.5569e-10	1	1.7569e-09	1	7.5569e-10	1
f_3	7.5569e-10	1	7.5569e-10	1	7.5569e-10	1	7.5569e-10	1
f_4	7.5569e-10	1	7.5569e-10	1	7.5569e-10	1	7.5569e-10	1
f_5	7.5569e-10	1	5.3659e-09	1	9.6344e-10	1	1.4992e-08	1
f_6	7.5569e-10	1	7.5569e-10	1	7.5569e-10	1	7.5569e-10	1
f_7	7.5569e-10	1	7.5569e-10	1	1.0872e-09	1	7.5569e-10	1
f_8	0.00620580	1	0.16597741	0	7.5569e-10	1	0.00120086	1
f_9	6.9956e-10	1	7.5569e-10	1	1	0	7.5569e-10	1
f_{10}	6.9908e-10	1	7.5569e-10	1	1.3922e-08	1	7.5569e-10	1
f_{11}	0.00012207	1	7.5569e-10	1	1	0	7.5569e-10	1
f_{12}	7.5569e-10	1	7.5569e-10	1	8.0311e-10	1	7.5569e-10	1
f_{13}	7.5569e-10	1	7.1594e-09	1	7.5569e-10	1	7.5569e-10	1
f_{14}	2.0113e-07	1	0.00606446	1	0.00191227	1	0.00022162	1
f_{15}	0.00954460	1	1.1303e-08	1	4.1239e-07	1	1.4171e-08	1
f_{16}	0.00204084	1	6.0119e-07	1	0.49615238	0	1.6479e-08	1
f_{17}	3.3821e-05	1	1.0651e-06	1	6.6920e-06	1	3.5681e-08	1
f_{18}	9.6344e-10	1	2.2979e-06	1	3.5699e-09	1	7.5313e-10	1
f_{19}	2.4737e-07	1	3.9194e-07	1	7.5569e-10	1	5.1734e-09	1
f_{20}	0.23319070	0	0.98844710	0	5.1316e-05	1	0.10382687	0
f_{21}	0.79809609	0	4.5325e-05	1	0.12841263	0	0.00024887	1
f_{22}	0.20087613	0	0.00828640	1	3.5411e-07	1	0.83841637	0
f_{23}	0.07976175	0	0.00474899	1	0.00263842	1	0.36272893	0

functions. For a statistical test, Wilcoxon signed-rank test [21] is considered where p-value denotes the significance level of null-hypothesis and h-value denotes whether the hypothesis is true or false. A significance level of 5 % (i.e. 0.05) is set for all tests. A p-value less than 0.05 confirms that the results obtained from BOA are more significant. In above stated case, the h-value will be 1 (i.e. true). If h-value is 0 then p-value will be more than 0.05 which clearly indicates that the obtained results from BOA are not significant. The statistical results are tabulated in Table 6.4. From the results, it can be noted that the results obtained from BOA are more significant than the results obtained from GWO, ALO, WOA, and PSO for 19, 21, 19, and 20 functions, respectively. This fact signifies that BOA is more robust in nature than others considered algorithms.

Table 6.5   Details of CEC-C06 2019 test functions [22]

Function	Name	Range	Dim	C_{min}
C_1	Storn's Chebysheb polynomial fitting problem	[-8192,8192]	9	1
C_2	Inverse Hilbert matrix problem	[-16384,16384]	16	1
C_3	Lennard-Jones minimum energy cluster	[-4,4]	18	1
C_4	Rastrigin's function	[-100,100]	10	1
C_5	Griewangk's function	[-100,100]	10	1
C_6	Weierstrass function	[-100,100]	10	1
C_7	Modified Schwefel's function	[-100,100]	10	1
C_8	Expanded Schaffer's F6 function	[-100,100]	10	1
C_9	Happy cat function	[-100,100]	10	1
C_{10}	Ackley function	[-100,100]	10	1

6.3.2 Evaluation on CEC Test functions

The performance of BOA is validated on CEC-C06 test functions i.e. The 100-digit challenge [22]. There is a total of ten test functions developed as single optimization problems. The details of test functions are given in Table 6.5. Further details of presented functions are mentioned in [22]. BOA along with GWO, ALO, WOA, and PSO is applied to these test functions. A total of 51 independent trials with a population size of 30 and maximum iterations of 1000 are considered for all test cases. The obtained results are presented in Table 6.6. From the results, it can be noted that BOA is able to find the best mean value for seven test functions and performed better a few few algorithms for rest of the three functions. The convergence characteristics of the algorithms obtained for considered test functions are illustrated in Figure 6.5. The convergence characteristics of the algorithms agree with the listed results in Table 6.6. Further, it is ascertained that BOA converges at faster rate in most of the cases compared to others.

In addition to the above performance analysis, a statistical test (i.e. Wilcoxon signed-rank test) is conducted to evaluate the significance of results obtained from BOA. The results are listed in Table 6.7. From the tabulated results, it can be clearly seen that for most of the cases BOA produces more significant results in comparison to other considered algorithms. This fact establishes the robustness of BOA.

6.4 Application of Proposed Algorithm to Solve EDP

In this section, the proposed BOA is applied to solve EDP that is an important part of power system operation. EDP is an optimization problem which

Table 6.6 Performance evaluation on CEC-C06 2019 test functions [22]

Function	Measure	ALO	GWO	PSO	WOA	BOA
C_1	Mean	1.3132e+09	2.7545e+06	3.7138e+10	7.4146e+10	**3.8288e+04**
	SD	2.2348e+09	3.4286e+06	5.3267e+10	8.4353e+10	**1.0109e+04**
C_2	Mean	17.3431	**17.3430**	8.1363e+02	17.3431	**17.3430**
	SD	0.0017	**1.5722e-04**	3.1846e+03	0.0471	0.2506
C_3	Mean	**12.7024**	**12.7024**	**12.7024**	**12.7024**	**12.7024**
	SD	4.0124e-15	2.4523e-04	**3.5887e-15**	8.5498e-08	8.1452e-07
C_4	Mean	7.9596	13.9799	**4.9760**	80.3148	21.8977
	SD	12.1230	6.6948e+02	**3.8964**	97.0121	3.2956e+02
C_5	Mean	1.0393	1.0733	1.0319	1.1529	**1.0251**
	SD	0.1244	0.2488	**0.0527**	0.3754	0.3519
C_6	Mean	**1.8239**	5.8952	2.9047	5.0828	4.2203
	SD	1.5906	**0.9964**	2.1445	1.4023	1.3502
C_7	Mean	-18.7860	-97.6206	-77.3236	-1.8908e+02	**-0.0090**
	SD	2.5767e+02	2.7072e+02	**1.0220e+02**	3.0685e+02	1.7131e+02
C_8	Mean	3.5383	2.8627	3.7150	4.0926	**2.7545**
	SD	0.6962	0.9988	**0.5294**	0.6596	0.7238
C_9	Mean	2.3566	2.9491	**2.3407**	3.1757	2.5498
	SD	0.0408	0.8003	**0.0061**	0.7348	50.0283
C_{10}	Mean	1.1551	1.2810	4.4409e-15	20.0547	**1.0591**
	SD	3.6518	2.7074	3.9938	**0.1104**	4.5971

Table 6.7 Wilcoxon signed rank test on CEC 2019 test functions [22]

Function	BOA vs. GWO		BOA vs. ALO		BOA vs. WOA		BOA vs. PSO	
	p	*h*	*p*	*h*	*p*	*h*	*p*	*h*
C_1	1	0	1	0	1	0	1	0
C_2	8.0311e-10	1	8.0311e-10	1	1.1548e-09	1	7.5569e-10	1
C_3	0.00022216	1	1.1167e-08	1	0.00372199	1	1.1167e-08	1
C_4	8.6631e-08	1	7.5569e-10	1	3.8512e-08	1	7.5569e-10	1
C_5	3.1082e-05	1	2.5085e-09	1	0.74640381	0	9.0680e-10	1
C_6	1.1994e-05	1	9.6344e-10	1	0.13085518	0	0.00019072	1
C_7	0.65352005	0	0.80555945	0	0.52091017	0	5.3659e-09	1
C_8	0.43143278	0	0.75372493	0	0.00204084	1	0.38232429	0
C_9	3.5275e-05	1	7.5569e-10	1	0.00033554	1	7.5569e-10	1
C_{10}	1.7204e-07	1	0.00217731	1	0.51466162	0	0.29049606	0

primarily finds out optimal generation schedule of available generating units to meet specific power demands keeping the total cost of generation to be minimum. The minimization of cost is subjected to equality and inequality constraints.
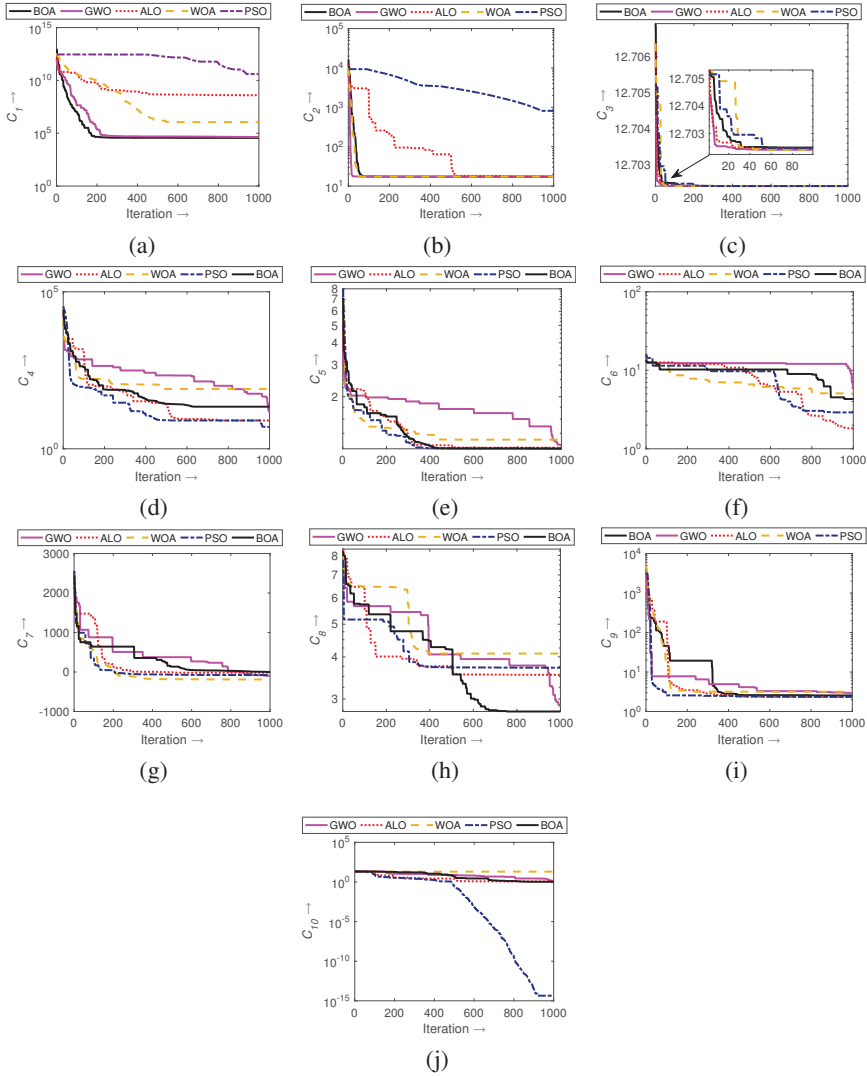
Figure 6.5 Convergence characteristics for CEC 2019 test functions [22]. (a) C_1. (b) C_2. (c) C_3. (d) C_4. (e) C_5. (f) C_5. (g) C_7. (h) C_8. (i) C_9. (j) C_{10}.

In literature, several optimization algorithms are successfully applied to solve EDP. Some of the important algorithms are GA [23], PSO [24], Cuckoo Search Algorithm (CSA) [25], DE [26], Artificial Bee Colony (ABC)

[27], Firefly Algorithm (FA) [28], Bacterial Foraging Optimization (BFO) [29], Teacher-Leaner Based Optimization (TLBO) [30] etc. However, the complexity of the existing power system is increasing day-by-day due to the incorporation of technological advancements and thus, a more efficient optimization tool is required to solve EDP. Consequently, the proposed algorithm i.e. BOA is applied to solve EDP in this work. The following subsections will present the EDP formulation and subsequent application of BOA on solving EDP of standard test systems.

6.4.1 EDP Formulation

In an EDP, the objective function is defined as the minimization of total fuel cost incurred in generation of power due to available units subjected to equality and inequality constraints.

6.4.1.1 Objective function

The objective function for EDP is expressed as

$$F_{total}^{cost} = \sum_{m=1}^{M} F_m(P_m) \tag{6.11}$$

where M is the total number of generating units, P_m, $m \in (1,2,\ldots,M)$, is the output power of mth unit in MW and F_m is the fuel cost of mth unit in \$/h. The cost characteristic of generating units can be either smooth or non-smooth.

- *Smooth cost function*: The cost characteristic function of a generating unit in its simplest form is represented as

$$F_m(P_m) = a_m P_m^2 + b_m P_m + c_m \tag{6.12}$$

where a_m, b_m and c_m are the cost coefficients of mth generating unit.
- *Non-smooth cost function*: The inclusion of valve-point loading points introduces multiple non-differential points into smooth cost characteristics, thus converting the function into a non-smooth function. It is expressed in the following manner.

$$F_m(P_m) = a_m P_m^2 + b_m P_m + c_m + e_m |\sin(f_m(P_m^{\min} - P_m))| \tag{6.13}$$

where e_m, and f_m are the cost coefficients with valve-point loading effects and $P_m^{\min}$ is the minimum power output of mth generating unit.

6.4.1.2 Constraints

EDP is solved by minimizing total fuel costs subjected to equality and inequality constraints. These constraints are described as follows.

- *Equality constraint*: The sum of power generated by each unit must be in total equal to total load demand P_d. This means that there should be a power balance in the system. The aforementioned constraints are represented as

$$\sum_{m=1}^{M} P_m = P_d \tag{6.14}$$

- *Inequality constraint*: The generation limits of each unit constitute inequality constraint. The power output of a unit must remain within its minimum and maximum output limit. This constraint is expressed as

$$P_m^{\min} \leq P_m \leq P_m^{\max} \tag{6.15}$$

where $P_m^{\min}$ and $P_m^{\min}$ are the minimum and maximum output power of mth generating unit.

6.4.1.3 Constraint handling technique

A penalty function technique is adopted in this work to efficiently handle the constraint violations [30]. A static penalty function is added to the objective function expressed in 6.11 and the final modified function which is minimized in his work is represented below.

$$F(P) = F_{total}^{cost} + \sum_{i=1}^{j} \alpha_i \times \max[0, q_i(P_m)]^2 + \sum_{k=1}^{l} \beta_k \times \max[0, r_k(P_m)]^2 \tag{6.16}$$

where j is the number of inequality constraints $(q_i(P_m) \geq 0)$ and l is the number of equality constraints $(r_k(P_m) = 0)$. α_i and β_k are static coefficients of penalty. For formulation, a high value of coefficients is considered. Thus, for obtaining the solution of EDP, (6.16) is required to be minimized while considering the cost functions defined in (6.12) or (6.13) subjected to constraints represented in (6.14) and (6.15).

6.4.2 Numerical Results and Discussion

For solution of EDP with or without valve-point loading effects, two standard IEEE test systems widely reported in the literature are considered. The data of generation limits and cost coefficients for all considered cases are taken

Table 6.8 Simulation results of EDP for six generator system

Description	PSO [24]	BBO [26]	ABC [27]	BFO [29]	BOA
P_1 (MW)	451.97	438.65	400.00	438.21	469.4007
P_2 (MW)	173.16	167.90	186.55	172.58	183.5863
P_3 (MW)	261.16	262.82	289.00	257.42	267.9583
P_4 (MW)	136.85	136.77	150.00	141.09	85.6397
P_5 (MW)	166.70	171.76	200.00	179.37	171.8935
P_6 (MW)	85.68	97.67	50.00	86.88	84.6259
P_{out} (MW)	1275.52	1275.57	1275.55	1275.73	1263.10
P_{loss} (MW)	12.52	12.52	12.55	12.55	0.10
F_{total}^{cost} \$/h (MW)	15458.00	15445.90	15452.00	15446.00	**15324.73**

from [31]. A total of 10 independent trials are undertaken with the population size of 30 and a maximum iteration of 1000. The aforementioned values of control parameters (i.e. total runs, population size, and maximum iteration) are maintained for all considered cases in this work. The description of three different test cases is presented below.

6.4.2.1 Case 1: Six generator system

For this case, EDP is solved for IEEE standard six bus test system with valve-point loading effects. A total load demand P_d of 1263 MW is considered. The optimal generation of available generating units with total fuel cost is presented in Table 6.8. Additionally, the results reported in the literature are shown in the mentioned table. From the table, it can be noted that the minimum fuel cost for the considered case is obtained from the proposed algorithm. This fact certifies the effective performance of BOA in solving EDP. Further, the convergence characteristic for the considered case is depicted in Figure 6.6. From the figure, it can be observed that the convergence rate of the proposed algorithm is fast which further ascertains the effectiveness of BOA in solving EDP.

6.4.2.2 Case 2: Fifteen generator system

For this case, EDP is solved for the IEEE standard fifteen bus test system without considering valve-point loading effects. A total load demand P_d of 2630 MW is considered. The power output of available generating units with
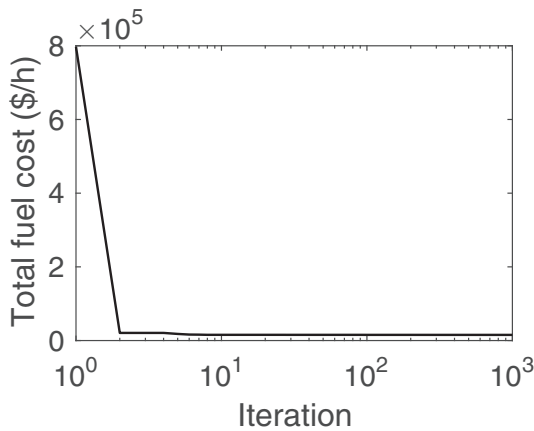
Figure 6.6   Convergence characteristics of BOA for six generator system.
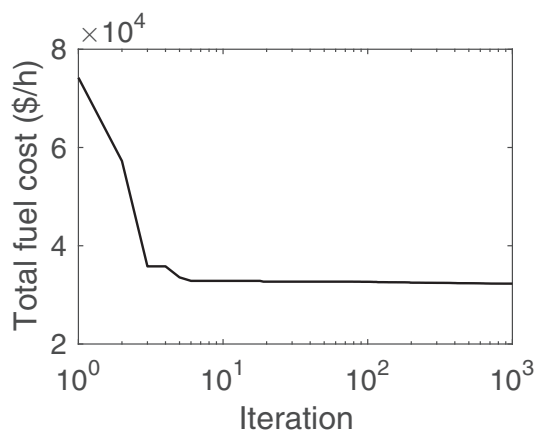

Figure 6.7   Convergence characteristics of BOA for fifteen generator system.

total fuel cost is tabulated in Table 6.9. The results from algorithms available in the literature for the considered test system are listed in the same table. From the table, it is seen that the minimum total fuel cost for the system is obtained from the proposed BOA. Thus, the effective performance of BOA in solving EDP is established. To further validate the effectiveness of BOA in solving EDP, the convergence characteristics for the considered case are shown in Figure 6.7. From the figure, the rate of convergence of BOA is found to be fast. This signifies that BOA is an effective tool for solving EDP.

Table 6.9 Simulation results of EDP for fifteen generator system

Description	PSO [24]	GA [23]	FA [28]	DE [30]	QOSLTLBO [30]	BOA
P_1 (MW)	439.12	415.31	455.00	434.47	369.66	340.2232
P_2 (MW)	407.97	359.72	380.00	268.02	330.67	454.7541
P_3 (MW)	119.63	104.42	130.00	114.63	126.45	130.0000
P_4 (MW)	129.99	74.98	130.00	125.77	129.74	129.9999
P_5 (MW)	151.07	380.28	170.00	226.39	333.79	371.1780
P_6 (MW)	459.99	426.79	460.00	441.33	423.40	445.8539
P_7 (MW)	425.56	341.32	430.00	441.64	348.16	464.9999
P_8 (MW)	98.56	124.79	71.745	128.37	126.93	60.1459
P_9 (MW)	113.49	133.14	58.9164	60.44	100.37	30.5618
P_{10} (MW)	101.11	89.26	160.00	158.84	131.89	25.4385
P_{11} (MW)	33.91	60.06	80.00	68.65	61.75	79.9410
P_{12} (MW)	79.96	50.00	80.00	63.06	43.40	41.5129
P_{13} (MW)	25.00	38.77	25.00	42.37	28.62	25.0114
P_{14} (MW)	41.41	41.94	15.00	26.96	51.62	15.0608
P_{15} (MW)	35.61	22.64	15.00	28.56	14.99	15.0022
P_{out} (MW)	2662.41	2668.44	2662.38	–	–	2629.68
P_{loss} (MW)	32.42	38.28	30.66	–	–	0.32
F_{total}^{cost} $/h (MW)	32858	33113	32704	32513.41	32340.45	32256.26

6.5 Conclusion

In this work, a novel nature-inspired optimization algorithm named BOA is proposed to solve EDP. The mathematical model of BOA is based on the pedal scent marking and sniffing behaviors of brown-bears. The major conclusions drawn from this chapter are as follows.

- BOA presents a proper balance between exploration of search space and exploitation of best results and is free from algorithm-specific parameters.
- BOA is found to be effective in obtaining global or near to global optima for benchmark and CEC test functions.
- The convergence rate of BOA is found to be faster (in most of cases) than others and statistical analysis proves that BOA produces more significant results.
- BOA is successful in finding optimum fuel cost while solving EDP for different standard test systems.

The future scope of current work lies in validation of the proposed algorithm for different complex engineering optimization problems. Additionally, the performance of binary and multi-objective versions of the proposed BOA will be validated on widely reported optimization problems.

References

[1] Lawrence Hasdorff. *Gradient optimization and nonlinear control*. Wiley New York, 1976.

[2] Tamara G Kolda, Robert Michael Lewis, and Virginia Torczon. Optimization by direct search: New perspectives on some classical and modern methods. *SIAM review*, 45(3):385–482, 2003.

[3] George Bernard Dantzig. *Linear programming and extensions*, volume 48. Princeton university press, 1998.

[4] Marguerite Frank and Philip Wolfe. An algorithm for quadratic programming. *Naval research logistics quarterly*, 3(1-2):95–110, 1956.

[5] JH Holland. An introductory analysis with applications to biology, control, and artificial intelligence. *Adaptation in Natural and Artificial Systems. First Edition, The University of Michigan, USA*, 1975.

[6] James Kennedy and Russell Eberhart. Particle swarm optimization. In *Proceedings of ICNN'95-International Conference on Neural Networks*, volume 4, pages 1942–1948. IEEE, 1995.

[7] Kenneth Price, Rainer M Storn, and Jouni A Lampinen. *Differential evolution: a practical approach to global optimization*. Springer Science & Business Media, 2006.

[8] Thomas Back. *Evolutionary algorithms in theory and practice: evolution strategies, evolutionary programming, genetic algorithms*. Oxford university press, 1996.

[9] Scott Kirkpatrick, C Daniel Gelatt, and Mario P Vecchi. Optimization by simulated annealing. *science*, 220(4598):671–680, 1983.

[10] Xin-She Yang. Firefly algorithms for multimodal optimization. In *International symposium on stochastic algorithms*, pages 169–178. Springer, 2009.

[11] Xin-She Yang and Amir Hossein Gandomi. Bat algorithm: a novel approach for global engineering optimization. *Engineering computations*, 2012.

[12] Seyedali Mirjalili. The ant lion optimizer. *Advances in engineering software*, 83:80–98, 2015.

[13] Seyedali Mirjalili, Seyed Mohammad Mirjalili, and Andrew Lewis. Grey wolf optimizer. *Advances in engineering software*, 69:46–61, 2014.

[14] Amir Hossein Gandomi and Amir Hossein Alavi. Krill herd: a new bio-inspired optimization algorithm. *Communications in nonlinear science and numerical simulation*, 17(12):4831–4845, 2012.

[15] Esmaeil Atashpaz-Gargari and Caro Lucas. Imperialist competitive algorithm: an algorithm for optimization inspired by imperialistic competition. In *2007 IEEE congress on evolutionary computation*, pages 4661–4667. Ieee, 2007.

[16] Alireza Shefaei and Behnam Mohammadi-Ivatloo. Wild goats algorithm: An evolutionary algorithm to solve the real-world optimization problems. *IEEE Transactions on Industrial Informatics*, 14(7):2951–2961, 2017.

[17] Seyedali Mirjalili and Andrew Lewis. The whale optimization algorithm. *Advances in engineering software*, 95:51–67, 2016.

[18] Esmat Rashedi, Hossein Nezamabadi-Pour, and Saeid Saryazdi. Gsa: a gravitational search algorithm. *Information sciences*, 179(13):2232–2248, 2009.

[19] Tristram D. Wyatt. *Pheromones and Animal Behaviour: Communication by Smell and Taste*. Cambridge University Press, 2003.

[20] Agnieszka Sergiel, Javier Naves, Piotr Kujawski, Robert Maślak, Ewa Serwa, Damián Ramos, Alberto Fernández-Gil, Eloy Revilla, Tomasz Zwijacz-Kozica, Filip Zieba, Johanna Painer, and Nuria Selva. Histological, chemical and behavioural evidence of pedal communication in brown bears. *Scientific reports*, 7(1):1–10, 2017.

[21] RF Woolson. Wilcoxon signed-rank test. *Wiley encyclopedia of clinical trials*, pages 1–3, 2007.

[22] KV Price, NH Awad, MZ Ali, and PN Suganthan. The 100-digit challenge: Problem definitions and evaluation criteria for the 100-digit challenge special session and competition on single objective numerical optimization. *Nanyang Technological University*, 2018.

[23] Gerald B Sheble and Kristin Brittig. Refined genetic algorithm-economic dispatch example. *IEEE Transactions on Power systems*, 10(1):117–124, 1995.

[24] Jong-Bae Park, Ki-Song Lee, Joong-Rin Shin, and Kwang Y Lee. A particle swarm optimization for economic dispatch with nonsmooth cost functions. *IEEE Transactions on Power systems*, 20(1):34–42, 2005.

[25] Subham Sahoo, K Mahesh Dash, RC Prusty, and AK Barisal. Comparative analysis of optimal load dispatch through evolutionary algorithms. *Ain Shams Engineering Journal*, 6(1):107–120, 2015.

[26] Aniruddha Bhattacharya and Pranab Kumar Chattopadhyay. Biogeography-based optimization for different economic load dispatch problems. *IEEE transactions on power systems*, 25(2):1064–1077, 2009.

[27] Dervis Karaboga and Bahriye Basturk. Artificial bee colony (abc) optimization algorithm for solving constrained optimization problems. In *International fuzzy systems association world congress*, pages 789–798. Springer, 2007.

[28] Xin-She Yang, Seyyed Soheil Sadat Hosseini, and Amir Hossein Gandomi. Firefly algorithm for solving non-convex economic dispatch problems with valve loading effect. *Applied soft computing*, 12(3):1180–1186, 2012.

[29] BK Panigrahi and V Ravikumar Pandi. Bacterial foraging optimisation: Nelder–mead hybrid algorithm for economic load dispatch. *IET generation, transmission & distribution*, 2(4):556–565, 2008.

[30] Tapan Prakash, VP Singh, Sugandh P Singh, and SR Mohanty. Economic load dispatch problem: quasi-oppositional self-learning tlbo algorithm. *Energy Systems*, 9(2):415–438, 2018.

[31] Victoria S Aragón, Susana C Esquivel, and CA Coello Coello. An immune algorithm with power redistribution for solving economic dispatch problems. *Information Sciences*, 295:609–632, 2015.

7

Analysis of Shunt Active Filter Performance under Different Supply and Loading Conditions

Kumar Reddy Cheepati

Dept. of Electrical & Electronics Eng., KSRM College of Engineering (Autonomous), Kadapa, India
E-mail: kumareeephd@gmail.com

Abstract

The main source of harmonic generation in any power system network is due to the tremendous growth of loads which exhibits nonlinear behavior. These types of loads are the major cause of degrading the power quality and will create the problems such as unnecessary circuit breaking, excess temperature rise in neutral line, and increased copper and iron losses in static and rotatory machinery. Extracting the references of currents in the active filtering is of utmost importance in mitigating the current harmonics. In this chapter, the average pq-SRF reference current extraction technique has been proposed which combines the merits and demerits of conventional p-q and SRF control by the matrix average correlation between two reference currents. The proposed technique has been implemented in a shunt active filter and tested with simulation and digital controller. Simulation and hardware results reveal that the proposed technique is efficient than existing techniques under various supply and load conditions.

Keywords: Average pq-SRF control, harmonics, power quality, reference current extraction

7.1 Introduction

The poor power quality is the most alarming for utilities and industries [1]. A good power quality refers to maintaining a pure noise-free sine wave supply voltage with power frequency. The harmonic producing loads are the major cause of poor power quality and create the problems such as unnecessary circuit breaking, excess temperature rise in neutral line, increased copper and iron loss in static and rotatory machinery [2–4].

The active and passive harmonic filtering enhances the quality of the power supply by mitigating the current and voltage harmonics. Passive filtering exhibits few demerits such as source impedance dependency, bulky size, frequent resonance, and fixed compensation but it offers a cost-effective solution and gives excellent performance in mitigating lower order current harmonics [5, 6]. The drawbacks of passive filtering will be overcome by active filtering with a small increment in cost; however, the design is complex [7–9]. The proposed system adopts the IEEE-519-2014 standard to control voltage and current harmonic distortion [10–14]. The faster response of time domain techniques over the frequency domain entails the converting of RYB phases into a transformation of Clarke and Park.

The p-q theory based shunt active filter provides harmonic and reactive power compensation [9]. It fails to work under unbalanced and/or distorted supply voltage conditions; however, it works well under unbalanced loading [15]. Further, a positive sequence voltage detector circuit design is required to enable the shunt active filter to perform with unbalanced and/or distorted supply conditions [16].

The SRF algorithm based shunt active filter requires only sensing the load currents whereas the p-q control requires sensing both source voltages and currents [17]. Unlike the p-q theory, the SRF control based shunt active filter does not work well under unbalanced loading and reactive power compensation is a mystery in it. SRF control uses a Phased-Locked Loop (PLL) circuit in its design and it involves very complex equations. The PLL circuit is replaced with a unit vector due to its simple design and enables it to be implemented in digital controllers [18, 19].

The merits of p-q and SRF techniques can be combined by means of the proposed averaging pq-SRF (Apq-SRF) reference current extraction technique. This technique gives the optimized operation under all kinds of balanced and unbalanced supply and load conditions. The diagram showing the operation of the proposed Apq-SRF compensation technique is shown in Figure 7.1. The salient features are as follows:

- No use of positive sequence voltage detector under unbalanced supply
- Use of simple unit vector in place of PLL.
- Limited sensors
- Multi-functional operation capability of shunt active filter
- Excellent tracking between compensating and reference currents.

The main contribution of this chapter is to prove the excellence of the proposed Apq-SRF control technique over existing techniques. The efficient operation of the VSI DC link voltage controller along with the proposed Apq-SRF control technique plays a major role in shunt active filter. It regulates VSI capacitor voltage along with energy balancing between source and load. The PI controller acts as a voltage regulator across the VSI capacitor and it is designed using Ziegler and Nicholas technique [19]. Pulse generation is extremely vital to produce necessary pulses to the inverter switches. Hysteresis Current Controller (HCC) is implemented for the purpose of pulse generation for the active filter [19].

7.2 The Apq-SRF Control Technique

Initially, reference currents derived from p-q and then from SRF techniques are obtained separately. These two currents will do the similar operations but the first current is obtained using Clark and the other is obtained from Park transformation. Achieving the correlation between these two references and getting merits from the correlation is the major contribution in this chapter. The correlation is achieved by a simple matrix averaging method as shown in Figure 7.1 [12].
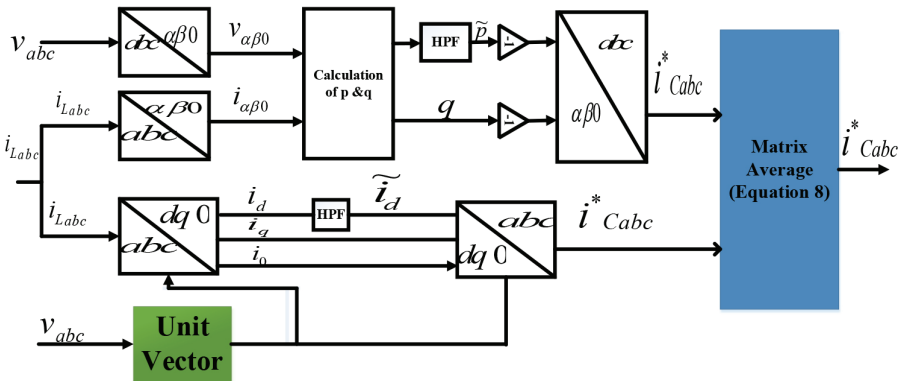
Figure 7.1   Block diagram of Apq-SRF technique

7.3 Modelling of the Apq-SRF Technique

The Clarke transformed $\alpha\beta 0$ grid voltages and currents are specified by (7.1) and (7.2).

$$
\begin{bmatrix} v_0 \\ v_\alpha \\ v_\beta \end{bmatrix} = \sqrt{\frac{2}{3}} \begin{bmatrix} \frac{1}{\sqrt{2}} & \frac{1}{\sqrt{2}} & \frac{1}{\sqrt{2}} \\ 1 & -\frac{1}{2} & -\frac{1}{2} \\ 0 & \frac{\sqrt{3}}{2} & -\frac{\sqrt{3}}{2} \end{bmatrix} \begin{bmatrix} v_a \\ v_b \\ v_C \end{bmatrix} \tag{7.1}
$$

$$
\begin{bmatrix} i_0 \\ i_\alpha \\ i_\beta \end{bmatrix} = \sqrt{\frac{2}{3}} \begin{bmatrix} \frac{1}{\sqrt{2}} & \frac{1}{\sqrt{2}} & \frac{1}{\sqrt{2}} \\ 1 & -\frac{1}{2} & -\frac{1}{2} \\ 0 & \frac{\sqrt{3}}{2} & -\frac{\sqrt{3}}{2} \end{bmatrix} \begin{bmatrix} i_{La} \\ i_{Lb} \\ i_{Lc} \end{bmatrix} \tag{7.2}
$$

From (7.1) and (7.2), the instantaneous real, reactive and zero sequence real power are calculated as represented by (7.3).

$$
\begin{bmatrix} p_0 \\ p \\ q \end{bmatrix} = \begin{bmatrix} v_0 & 0 & 0 \\ 0 & v_\alpha & v_\beta \\ 0 & v_\beta & -v_\alpha \end{bmatrix} \begin{bmatrix} i_0 \\ i_\alpha \\ i_\beta \end{bmatrix} \tag{7.3}
$$

The term (p) is the sum of $(\bar{p})$ and $(\tilde{p})$. The first one is fundamental and the other is oscillating in nature. The term $(\tilde{p})$ is not useful since it oscillates between source and load. Similarly, the term (q) is also the sum of fundamental and oscillating components; however, both these terms are oscillating in nature. Hence, the terms $(\tilde{p})$ and (q) compensation is the major task of the shunt active filter; hence negative polarity is assigned as in (7.4). The zero sequential components remain the same irrespective of transformations. That is the beauty behind these transformations.

The p-q theory based compensating currents in $\alpha\beta$ form is given by (7.4).

$$
\begin{bmatrix} i_{C\alpha} \\ i_{C\beta} \end{bmatrix} = \frac{1}{\sqrt{v_\alpha^2 + v_\beta^2}} \begin{bmatrix} v_\alpha & v_\beta \\ -v_\beta & v_\alpha \end{bmatrix} \begin{bmatrix} -\tilde{p} + \Delta\bar{p} \\ -q \end{bmatrix} \tag{7.4}
$$

The inverse Clarke transformed currents in abc frame are given by (7.5). These currents perform their intended function under balanced supply conditions but not under other conditions.

$$
\begin{bmatrix} i_{Ca}^* \\ i_{Cb}^* \\ i_{Cc}^* \end{bmatrix} = \sqrt{\frac{2}{3}} \begin{bmatrix} \frac{1}{\sqrt{2}} & 1 & 0 \\ \frac{1}{\sqrt{2}} & -\frac{1}{2} & \frac{\sqrt{3}}{2} \\ \frac{1}{\sqrt{2}} & -\frac{1}{2} & -\frac{\sqrt{3}}{2} \end{bmatrix} \begin{bmatrix} -i_0 \\ i_{C\alpha} \\ i_{C\beta} \end{bmatrix} \tag{7.5}
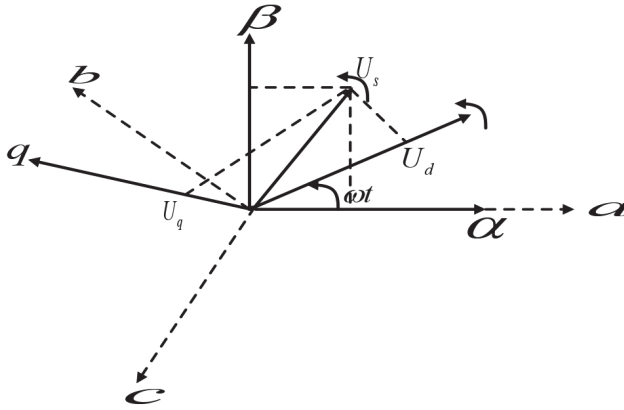$$

Figure 7.2   Phasor relationship between $abc - \alpha\beta0 - dq0$ frames

The SRF control will make use of $dq0$ transformation. Equation (7.6) gives load currents in $dq0$ frame. It requires only the load currents to sense for the system control. Figure 7.2 shows the correlation between $abc-\alpha\beta0-dq0$.

The sine based transformation is utilized in this chapter. With the sine based relationship, the load currents in $dq0$ frame are given by (7.6)

$$\begin{bmatrix} i_d \\ i_q \\ i_0 \end{bmatrix} = \begin{bmatrix} \cos\theta & \cos(\theta - 120) & \cos(\theta + 120) \\ -\sin\theta & -\sin(\theta - 120) & -\sin(\theta + 120) \\ \frac{1}{2} & \frac{1}{2} & \frac{1}{2} \end{bmatrix} \begin{bmatrix} i_{La} \\ i_{Lb} \\ i_{Lc} \end{bmatrix} \quad (7.6)$$

The term (i_d) refers to the direct component of the current having two terms $(\bar{i}_d)$ and $(\tilde{i}_d)$. First one is fundamental and the other is oscillatory in nature. The term $(\tilde{i}_d)$ must be extracted since it is oscillating. The term (i_q) also has fundamental and oscillating components but both these should be extracted because these two are reactive in nature. The SRF control reference currents are obtained by inverse Clarke transformation as given by (7.7).

$$\begin{bmatrix} i*_{Ca} \\ i*_{Cb} \\ i*_{Cc} \end{bmatrix} = \sqrt{\frac{2}{3}} \begin{bmatrix} \cos\theta & -\sin\theta & 1 \\ \cos(\theta - 120) & -\sin(\theta - 120) & 1 \\ \cos(\theta + 120) & -\sin(\theta + 120) & 1 \end{bmatrix} \begin{bmatrix} \tilde{i}_d - i_{loss} \\ i_q \\ i_0 \end{bmatrix} \quad (7.7)$$

Compared to the p-q technique, The SRF technique works well with biased and/or disturbed supply conditions even but the drawback of SRF control is that reactive power and load balance is a mystery as revealed in (7.7).
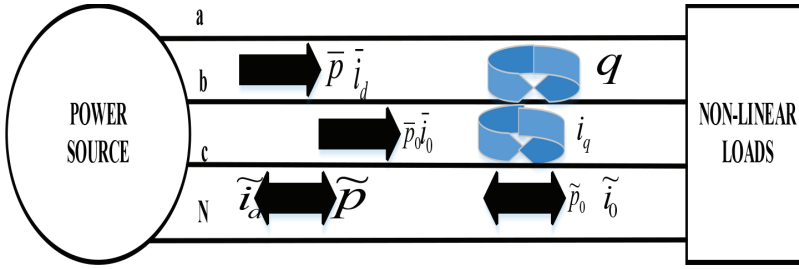
Figure 7.3   The Apq-SRF control power flow diagram.

Equations (7.5) and (7.7) are correlated by a simple matrix averaging method to get the new multi-functional Apq-SRF control technique equation as given by (7.8).

$$
\begin{bmatrix} i_{Ca}^* \\ i_{Cb}^* \\ i_{Cc}^* \end{bmatrix} = \sqrt{\frac{1}{6}} \begin{bmatrix} i_{c\alpha} + i_{c\beta} + (\tilde{i}_d - i_{loss})\cos\theta - i_q \sin\theta + 0.3i_0 \\ -0.5i_{c\alpha} + \frac{\sqrt{3}}{2}i_{c\beta} + (\tilde{i}_d - i_{loss})\cos(\theta - 120) - \\ i_q \sin(\theta - 120) + 0.3i_0 \\ -0.5i_{c\alpha} - \frac{\sqrt{3}}{2}i_{c\beta} + (\tilde{i}_d - i_{loss})\cos(\theta + 120) - \\ i_q \sin(\theta + 120) + 0.3i_0 \end{bmatrix}
$$

(7.8)

The power flow diagram for the Apq-SRF technique is shown in Figure 7.3. It indicates that the oscillating components from p-q and SRF control have been extracted together as can be seen in (7.8). This control technique performs well in all practical conditions with multi-functional capability.

7.4 The Shunt Active Filter Configuration with Apq-SRF Control

The block diagram of the Apq-SRF control based shunt active filter is shown in Figure 7.4. Shunt active filter operation requires three main controls, namely

- Reference current extraction control techniques
- Constant DC link voltage controller across VSI capacitor
- Pulse generation control.

All controls must cooperate with each other to get the desired shunt active filter operation. Since the main contribution in this chapter is to introduce the
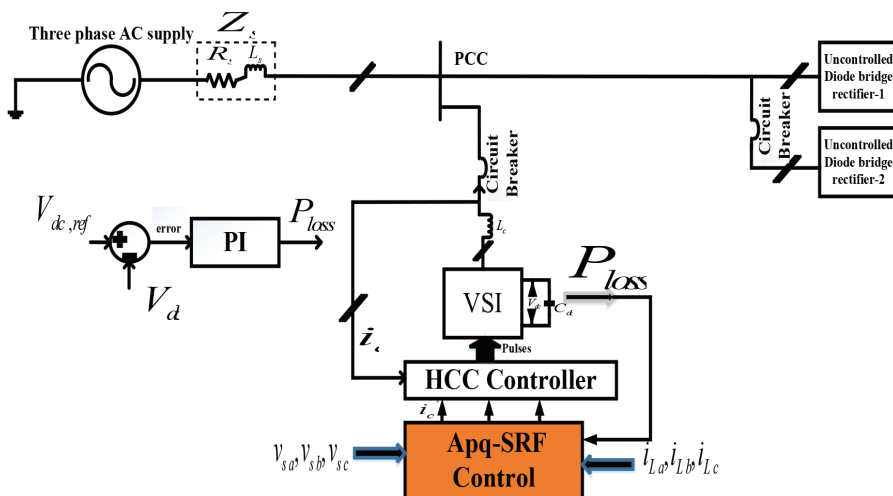
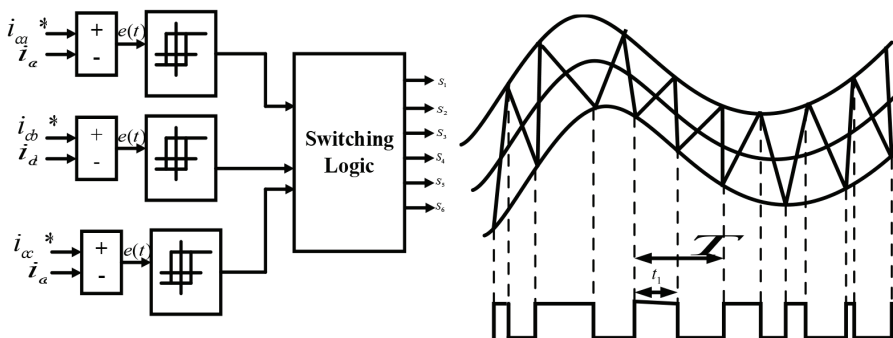**Figure 7.4**   Filter configuration with proposed Apq-SRF control

Figure 7.5   (a) Hysteresis controller (b) Pulse generating pattern

Apq-SRF technique, a simple PI DC link voltage regulator and hysteresis current controller have been considered in association with the Apq-SRF technique. Direct control method of the hysteresis current controller and its switching pattern is shown in Figure 7.5. It triggers the VSI switches so that the shunt active filter injects the compensating currents through the coupling inductor into the power distribution network [20–22].

The tuning of PI type VSI capacitor voltage controller utilizes a heuristic method of Ziegler-Nichols to estimate the proportional and integral gains. In this method, K_i and K_d gains are initially set to the lowest. Then, the gain K_p is enhanced gradually till it obtains the maximum gain K_u, at which the loop

Table 7.1 Ziegler-Nichols approximation method of gain calculations

Control Type	K_p	K_i	K_d
P	$0.50K_u$	-	-
PI	$0.45K_u$	$1.2K_p/P_u$	-
PID	$0.60K_u$	$2K_p/P_u$	$K_pP_u/8$

output begins to fluctuate [23–25]. The gain K_u and the fluctuation period P_u are utilized to estimate the gains as depicted in Table 7.1.

7.5 Simulation Results

The Apq-SRF technique is implemented in simulation and verified in a digital controller (TMS5700-XL). The following supply and load conditions are considered in the simulation.

(i) Pure supply conditions

    (a) Fixed loading conditions
    (b) Sudden load switching conditions

(ii) Impure supply conditions

    (a) Fixed loading conditions
    (b) Sudden load switching conditions

7.5.1 Pure Supply Conditions

The pure supply conditions are subcategorized into fixed loading and dynamic loading conditions.

7.5.1.1 Fixed loading conditions

In this case, the supply voltage is pure and clean. The load is constant in nature throughout the simulations. Figure 7.6 shows the currents of the grid, load, and filter. When a filter is turned on at 0.1 sec, it is injecting compensating reference currents as per the Apq-SRF control technique as shown in Figure 7.6(c). The source current is sinusoidal after connecting the filter at 0.1 sec at the PCC which is shown in Figure 7.6(b).

The real and reactive power demands are shown in Figure 7.7. It is observed that the real and reactive power demands are decreased after connecting the filter at 0.1 sec.
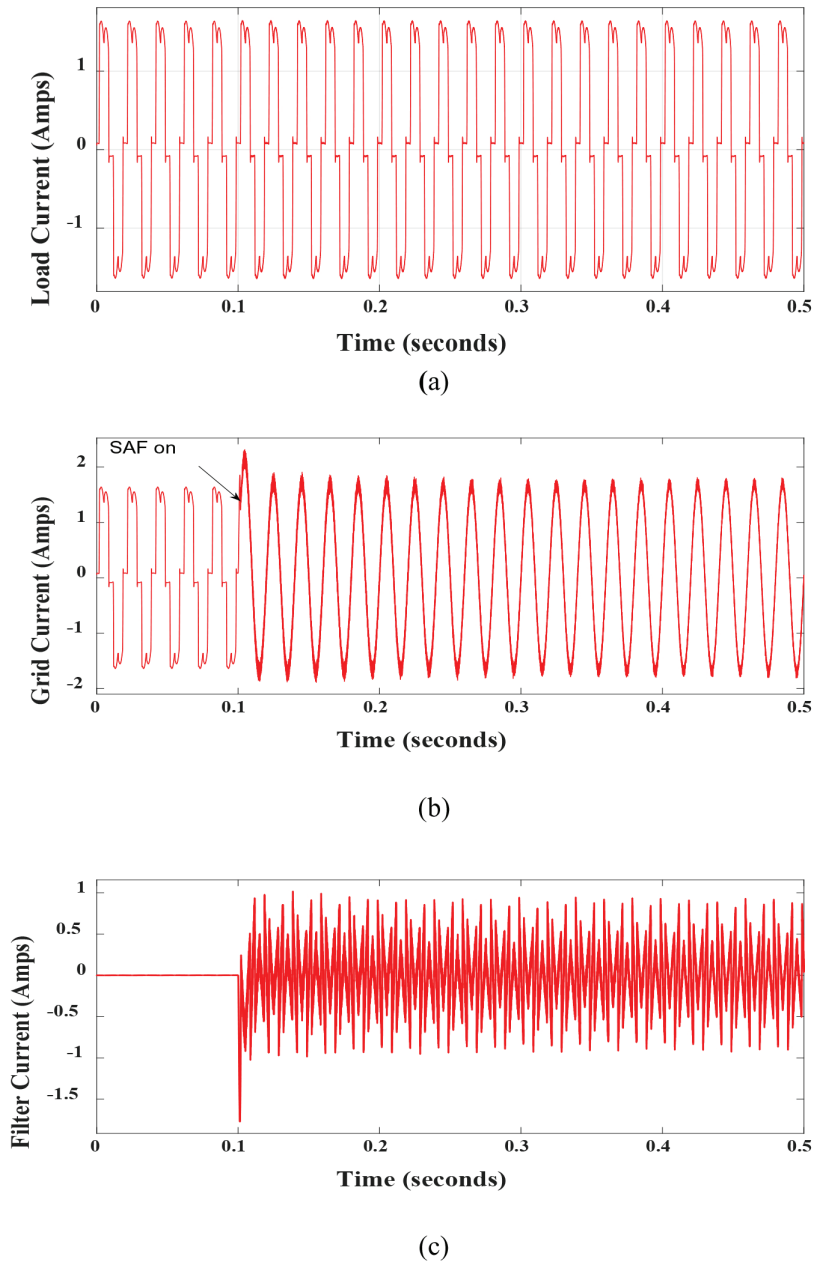
Figure 7.6 (a) Load current (b) grid current and (c) filter currents under balanced supply and fixed loading conditions
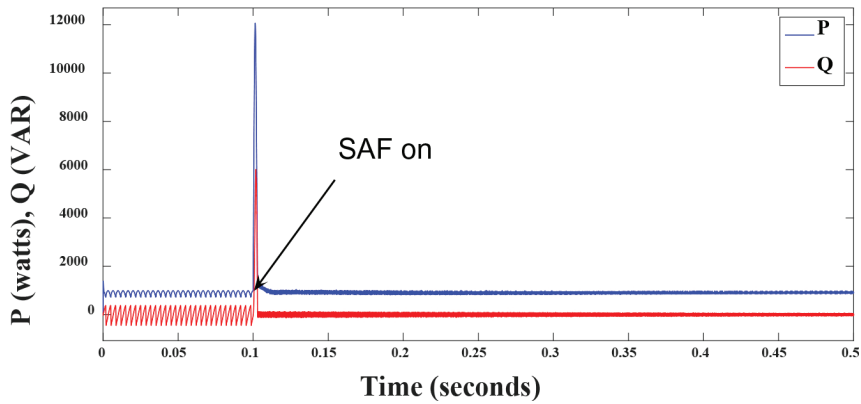
Figure 7.7   Real and reactive power demands under pure and clean supply
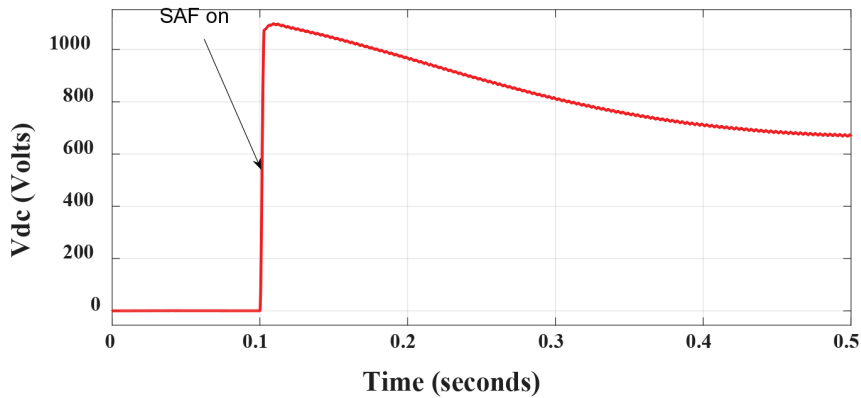

Figure 7.8   VSI capacitor voltage under pure and clean supply

The VSI capacitor voltage is perfectly maintained constant to its reference level when the filter is connected at 0.1 sec as shown in Figure 7.8. The source voltage and currents are in phase after connecting the filter at 0.1 sec as shown in Figure 7.9, thus the unity power factor operation is obtained.

The THD of the source current when the filter is connected at 0.1 sec. is shown in Figure 7.10. The THD is decreased well below the IEEE 519-2014 standards. The THD of the load current for uncompensated system is 48.9%.

7.5.1.2 Transient conditions
In this case, a sudden load is switched on at 0.5 sec. Figure 7.11 indicates the grid, load, and filter currents under sudden load switching conditions. The
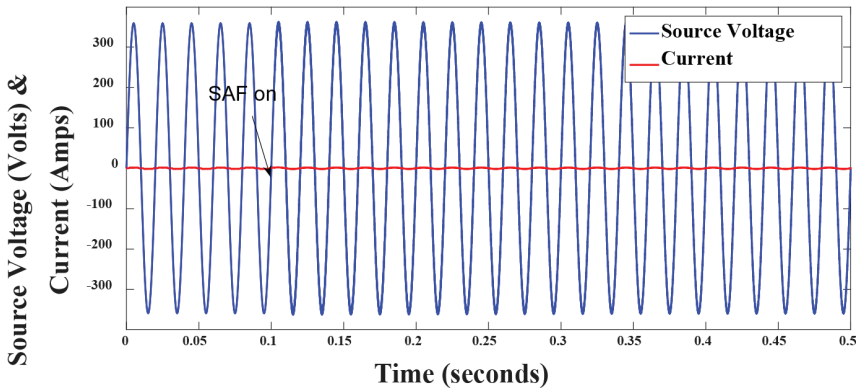
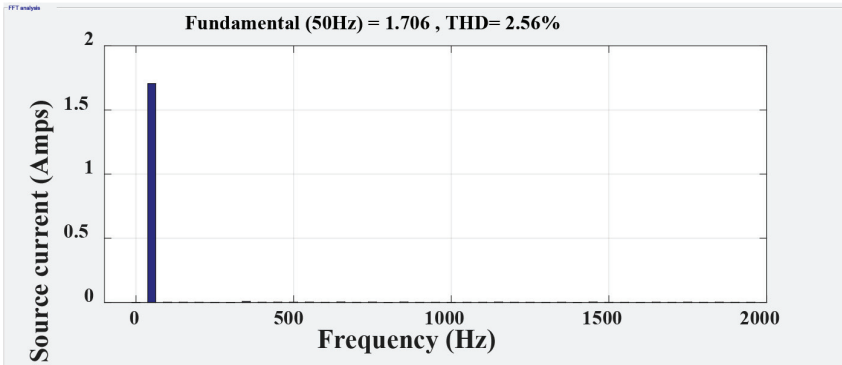**Figure 7.9**   Grid voltage and current under pure and clean supply

Figure 7.10   THD of the grid current under pure and clean supply

filter is turned on at 0.1 sec, it is injecting counter currents. It is indicated that the grid current is ideal after the filter is turned on at 0.1 sec.

From Figure 7.12, it is seen that the real and reactive power demands are decreased after connecting filter at 0.1 sec.

The grid voltage and load currents are crossing natural zero after connecting the filter at 0.1 sec as shown in Figure 7.13, thus the power factor correction is happening. The VSI capacitor voltage is perfectly maintained stiff to its reference level when the filter is connected at 0.1 sec as shown in Figure 7.14.

The THD of the source current for the proposed system with filter is shown in Figure 7.15. The THD is decreased well below the IEEE standards. The THD of the load current for an uncompensated system under dynamic loading conditions is 48.9%.
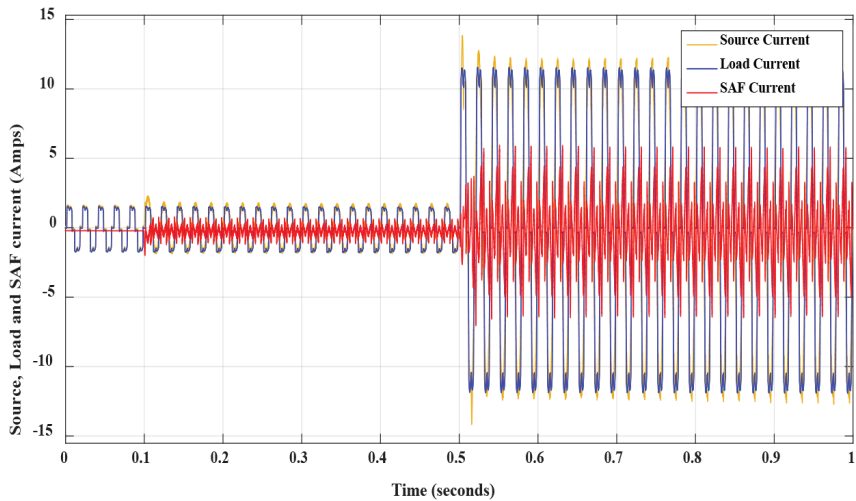
Figure 7.11   Grid, load and filter currents under balanced supply and dynamic loading conditions
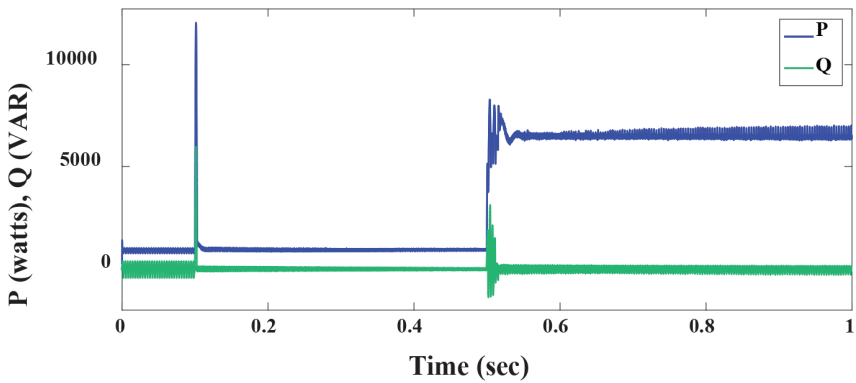

Figure 7.12   Real and reactive power and power factor correction under balanced supply and transient conditions

7.5.2 Unbalanced and Distorted Supply Conditions

In this case, a sudden load is switched on at 0.5 sec. Figure 7.16 indicates the grid, load, and filter currents under sudden load switching conditions. The filter is turned on at 0.1 sec, it is injecting counter currents. It is indicated that the grid current is ideal after the filter is turned on at 0.1 sec.

The supply voltage and currents are in phase after connecting the filter at 0.1 sec as shown in Figure 7.17, thus maintaining the unity power factor.
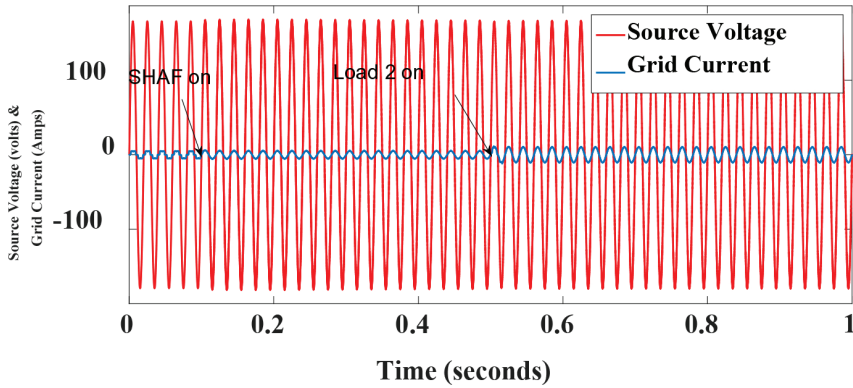
Figure 7.13 Grid voltage and current under balanced supply and dynamic loading conditions
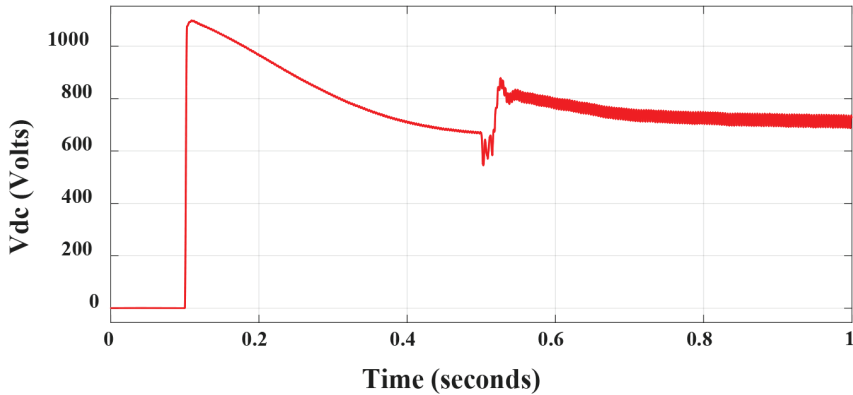

Figure 7.14 VSI capacitor voltage under balanced supply and transient conditions

The real and reactive power demands are shown in Figure 7.18. It is observed that the real and reactive power demands are decreased after connecting the filter at 0.1 sec.

The THD of the source current for the proposed system with filter is shown in Figure 7.19. The THD is decreased well below the IEEE standards. The THD of the load current for the uncompensated system under dynamic loading conditions is 59.8%. The VSI capacitor voltage is as shown in Figure 7.20, it is maintained constant even under distorted supply conditions.

The performance comparison of the Apq-SRF technique with various existing filter control techniques under balanced supply conditions is indicated in Figure 7.21. The Apq-SRF filter control technique is performing extremely well in steady-state and transient state conditions.
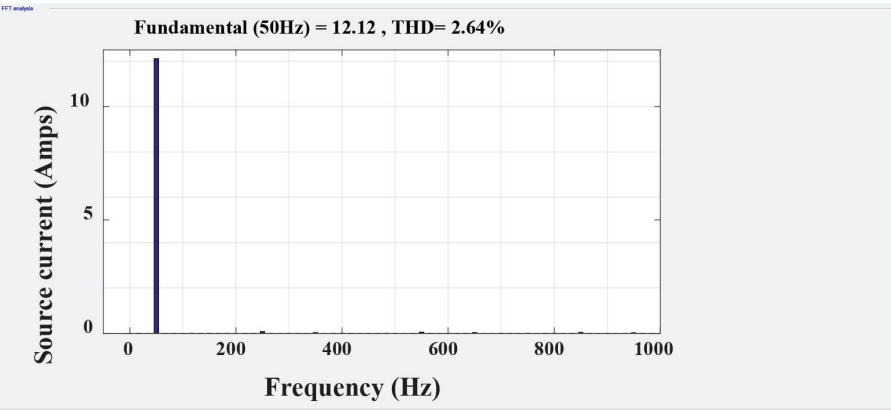
Figure 7.15   THD of the grid current with balanced supply and transient conditions
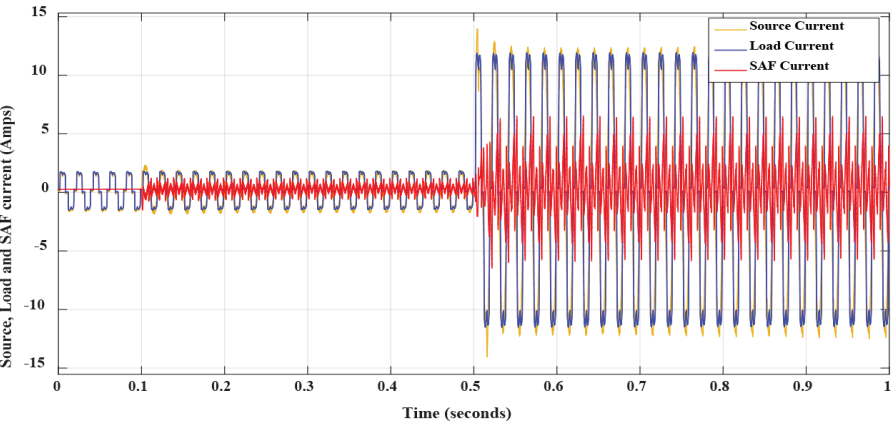

Figure 7.16   Grid, load and filter currents with impure supply conditions

The advantage of the proposed Apq-SRF technique is that it performs well in both balanced and unbalanced supply and load conditions whereas, other control techniques failed to give satisfactory operation as shown in Figure 7.22.

7.6 Hardware Results

The block diagram of the proposed shunt active filter hardware is shown in Figure 7.23. The hardware developed in the laboratory is shown in Figure 7.24. To realize the effectiveness of the Apq-SRF reference current
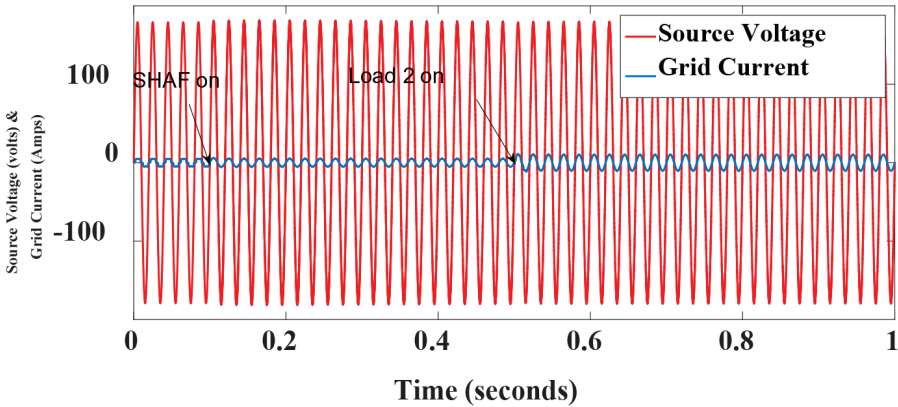
Figure 7.17 Source voltage and current under unbalanced distorted supply conditions
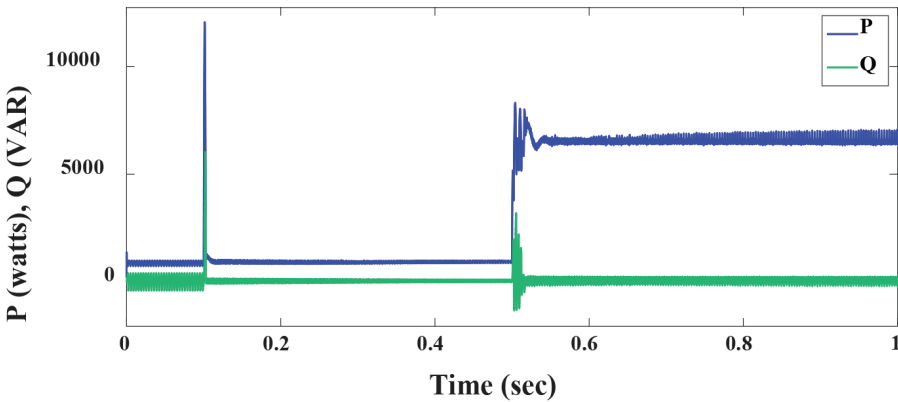

Figure 7.18 The real, reactive and power factor with impure supply conditions

technique in the shunt active filter hardware, the following conditions are assumed.

(i) Source is perfectly balanced
(ii) Load is balanced and fixed

7.6.1 Before Compensation

The source voltage and load current waveforms before compensation are shown in Figure 7.25. It is observed that both the voltage and current waveforms are distorted from their ideal waveform. The power factor is less than
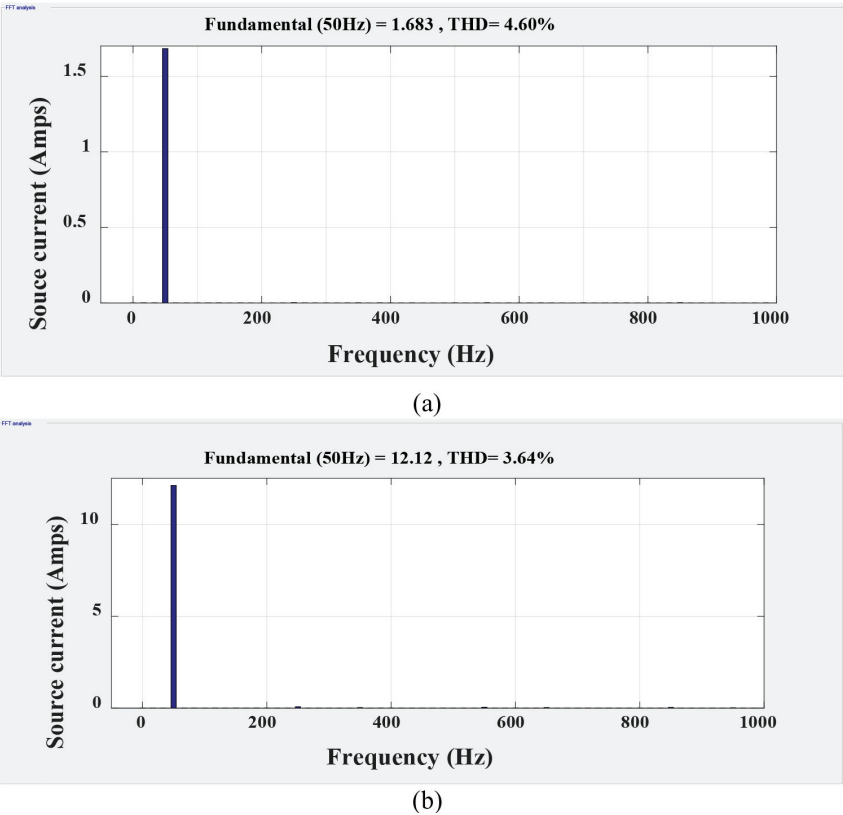
(a)

(b)

Figure 7.19   THD of source current with impure supply conditions (a) fixed loading (b) transient switching conditions

unity as both the current and voltage wave form are not in phase as shown in Figure 7.25. The THD of load current at the PCC is as shown in Figure 7.26; it can be observed that it is far beyond the IEEE harmonic standards.

7.6.2 After Compensation

The source voltage and load current waveforms after the filter compensation with the Apq-SRF technique are shown in Figure 7.27. It is worth noting that both the voltage and current waveforms are ideal in nature and free from harmonics. The power factor correction has been done since both current and voltage are crossing natural zero instantly as shown in Figure 7.27. The THD of load current at the PCC with the proposed shunt active filter is shown
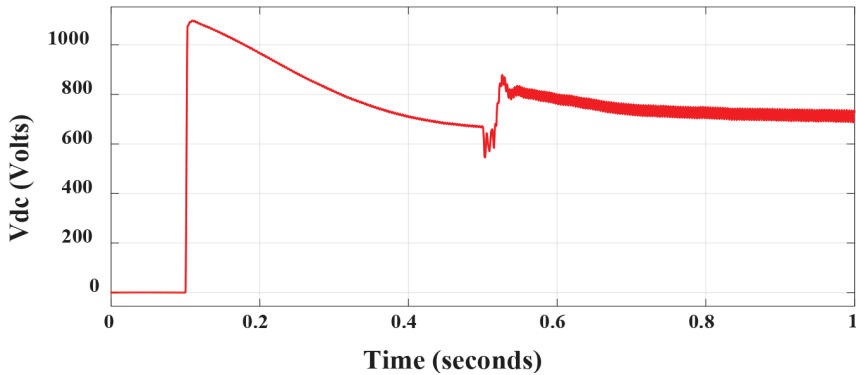
Figure 7.20   VSI capacitor voltage under unbalanced and distorted supply conditions

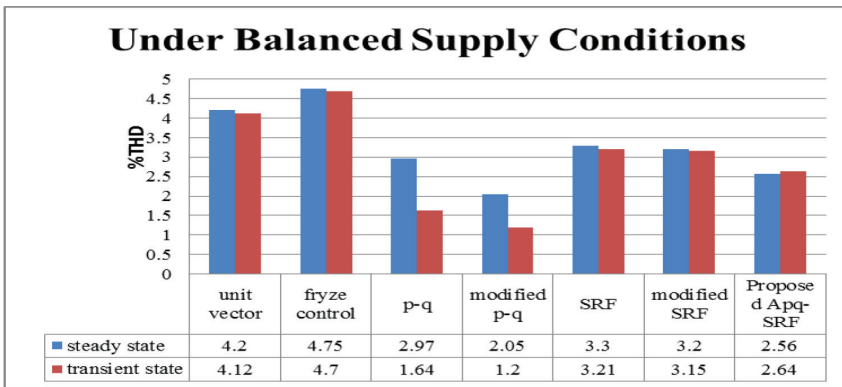|	unit vector	fryze control	p-q	modified p-q	SRF	modified SRF	Propose d Apq-SRF
■ steady state	4.2	4.75	2.97	2.05	3.3	3.2	2.56
■ transient state	4.12	4.7	1.64	1.2	3.21	3.15	2.64

Figure 7.21   Comparison of Apq-SRF control with existing techniques under balanced supply conditions

in Figure 7.28; it can be observed that it is well below the IEEE harmonic standards.

The filter current is shown in Figure 7.29. It is observed that the proposed filter is able to generate filter currents 180 degrees out of phase with load current harmonics.

The VSI capacitor voltage with the proposed shunt active filter is shown in Figure 7.30. It can be observed that the proposed filter is able to maintain the constant DC voltage across the VSI capacitor.

The comparison of the simulation and the hardware results with the proposed Apq-SRF control based shunt active filter is shown in Figure 7.31. The hardware performance in THD reduction is almost the same as the
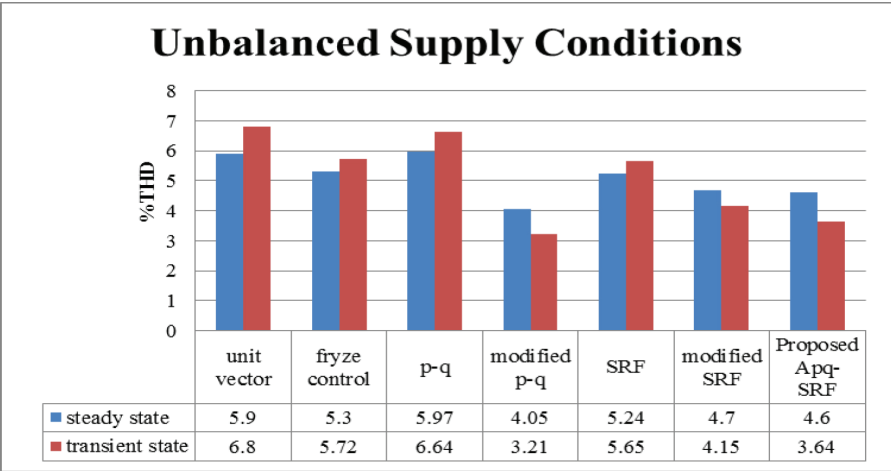
Unbalanced Supply Conditions

	unit vector	fryze control	p-q	modified p-q	SRF	modified SRF	Proposed Apq-SRF
■ steady state	5.9	5.3	5.97	4.05	5.24	4.7	4.6
■ transient state	6.8	5.72	6.64	3.21	5.65	4.15	3.64

Figure 7.22 Comparison of Apq-SRF control with existing techniques under unbalanced supply conditions
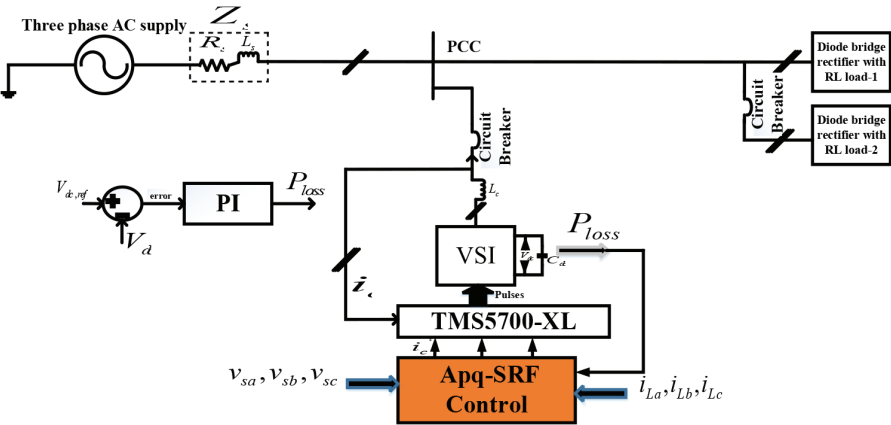
Figure 7.23   Block diagram of the proposed shunt active filter hardware

simulation, thus validating the proposed shunt active filter with the Apq-SRF control technique.

The parameters of the proposed Apq-SRF technique based filter remain the same for other existing techniques as shown in Table 7.2.
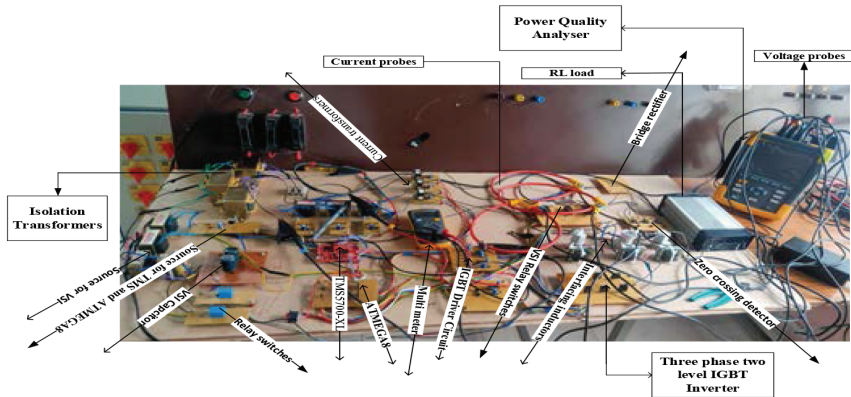
Figure 7.24 Hardware developed in the laboratory
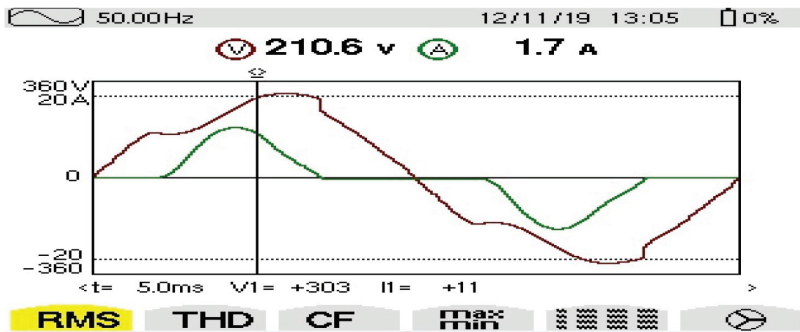
Figure 7.25 Source voltage and load current before compensation
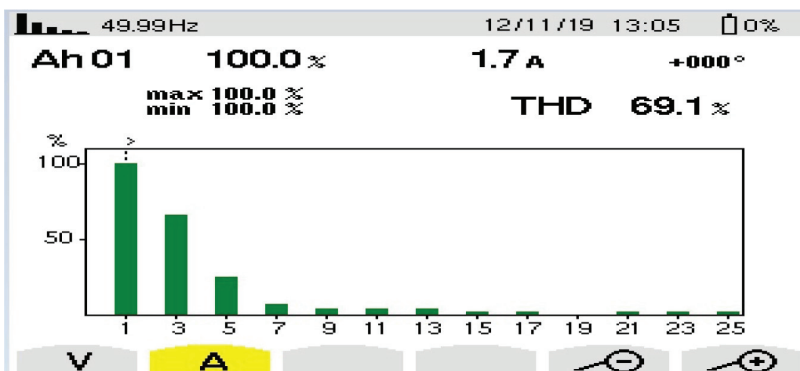
Figure 7.26 THD of load current before compensation
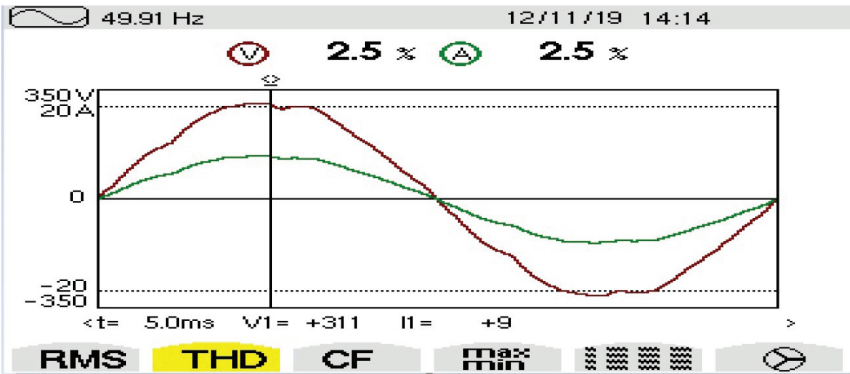
Figure 7.27 Load current after compensation
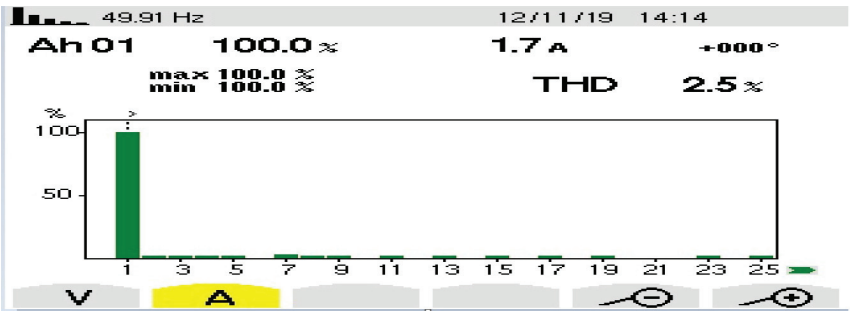
Figure 7.28 THD of load current after compensation
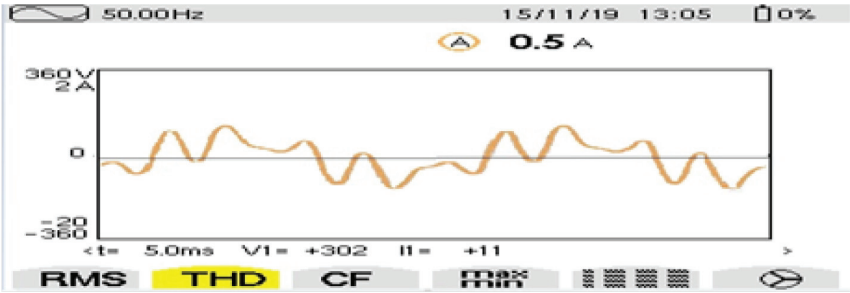
Figure 7.29 Filter current for phase A
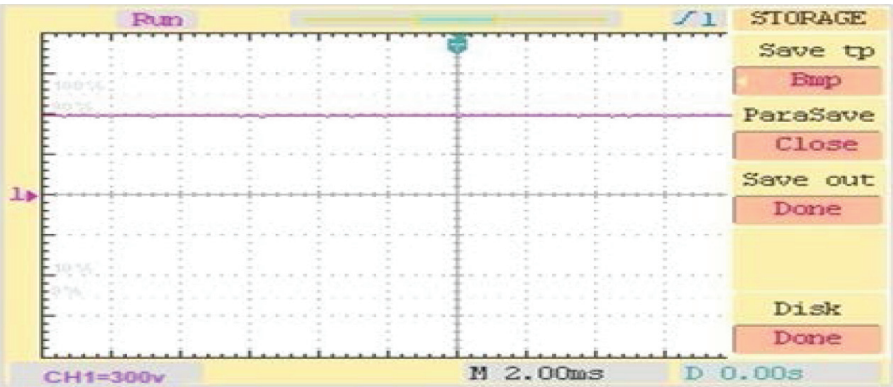
Figure 7.30 VSI capacitor voltage after compensation

	Simulation	Hardware
■ THD of grid current without compensation under steady state	48.9	69.1
■ THD of grid current with SAF compensation under steady state	2.56	2.5

Figure 7.31 Comparison of simulation and hardware results for the proposed shunt active filter with Apq-SRF control

Table 7.2 Filter parameters

Supply voltage/frequency	440 volts / 50 Hz
Source impedance (Rs, Ls) Line impedance (Rline, Lline)	0.1Ω, 0.15 mH 0.4Ω, 3.55mH
Diode rectifier Load resistor (RL) and inductor (LL)	6-diode, uncontrolled 390 Ω, 20 mH
Interface inductor (Lc)	15 mH
DC-side capacitance (Cdc)	35 μF
Reference voltage (Vdc, ref)	660 V
Voltage source inverter	6 IGBTS/Diodes
Kp and Ki values for PI controller	0.2, 1.5

7.7 Conclusions

From the results of both simulation and digital controller, the proposed Apq-SRF technique is found far better in comparison to the other existing techniques under all supply and load conditions.
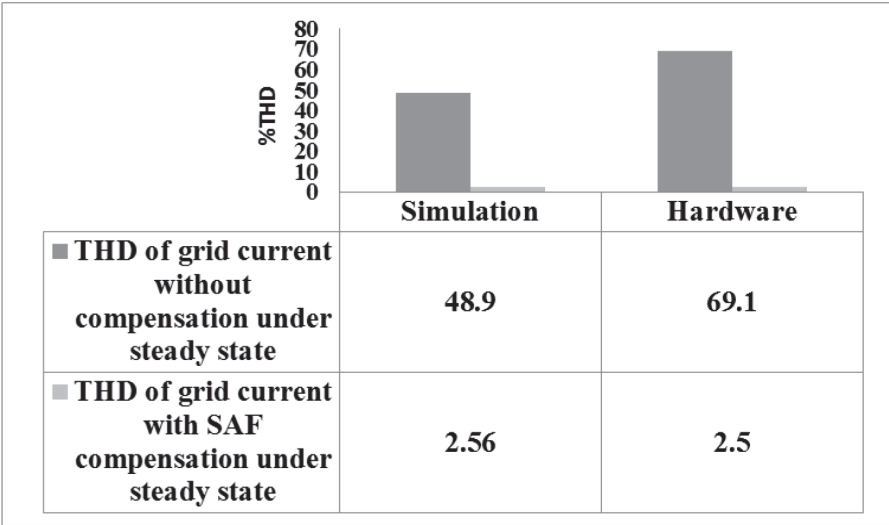
References

[1] A. Javadi, A. Hamadi, A. Ndtoungou, and K. Al-Haddad, "Power Quality Enhancement of Smart Households Using a Multilevel-THSeAF With a PR Controller," *IEEE Transactions on Smart Grid,* vol. 8, pp. 465-474, 2017. DOI: 10.1109/TSG.2016.2608352

[2] S. Makasheva and P. Pinchukov, "Power Quality: Harmonic Current Distortion, Standards, Field Testing and Evaluation," *2020 International Ural Conference on Electrical Power Engineering (UralCon)*, Chelyabinsk, Russia, 2020, pp. 44-49, doi: 10.1109/UralCon49858.2020.9216281. DOI: 10.1109/UralCon49858.2020.9216281

[3] J. Yaghoobi, A. Abdullah, D. Kumar, F. Zare and H. Soltani, "Power Quality Issues of Distorted and Weak Distribution Networks in Mining Industry: A Review," in *IEEE Access*, vol. 7, pp. 162500-162518, 2019, doi: 10.1109/ACCESS.2019.2950911. DOI: 10.1109/ACCESS.2019.2950911

[4] G. S. Chawda *et al.*, "Comprehensive Review on Detection and Classification of Power Quality Disturbances in Utility Grid With Renewable Energy Penetration," in *IEEE Access*, vol. 8, pp. 146807-146830, 2020, DOI: 10.1109/ACCESS.2020.3014732.

[5] Y. Tian, L. Luo, Q. Liu, Y. Li and Z. Huang, "A New Harmonic Mitigation System With Double Balanced Impedance Filtering Power Transformer for Multistage Distribution Network," in *IEEE Transactions on Industrial Electronics*, vol. 68, no. 6, pp. 4565-4575, June 2021, DOI: 10.1109/TIE.2020.2984989.

[6] A. G. Peter and K. A. Saha, "Comparative study of harmonics reduction and power factor enhancement of six and 12-pulses HVDC system using passive and shunt APFs harmonic filters," *2018 International Conference on the Domestic Use of Energy (DUE)*, Cape Town, South Africa, 2018, pp. 1-10, DOI: 10.23919/DUE.2018.8384395.

[7] F. Manzano-Agugliaro, M. Montoya, A. Garcìa-Cruz and F. Montoya, *Power quality techniques research worldwide: A review. Renewable and Sustainable Energy Reviews*, 2016. DOI: 10.1016/j.rser.2015.10.091

[8] X. Nie and J. Liu, "Current Reference Control for Shunt Active Power Filters Under Unbalanced and Distorted Supply Voltage Conditions," in *IEEE Access*, vol. 7, pp. 177048-177055, 2019, DOI: 10.1109/ACCESS.2019.2957946.

[9] A. Amerise, M. Mengoni, G. Rizzoli, L. Zarri, A. Tani and D. Casadei, "Comparison of Three Voltage Saturation Algorithms in Shunt Active Power Filters With Selective Harmonic Control," in *IEEE Transactions on Industry Applications*, vol. 56, no. 3, pp. 2762-2772, May-June 2020, DOI: 10.1109/TIA.2020.2972853

[10] "IEEE Approved Draft Recommended Practice for Conducting Harmonic Studies and Analysis of Industrial and Commercial Power Systems," in *IEEE P3002.8/D7, June 2018* , vol., no., pp.1-98, 27 Sept. 2018.

[11] "IEEE Recommended Practice for Conducting Harmonic Studies and Analysis of Industrial and Commercial Power Systems," in *IEEE Std 3002.8-2018* , vol., no., pp.1-79, 22 Oct. 2018, DOI: 10.1109/IEEESTD.2018.8479357

[12] "IEEE Draft Recommended Practice for Conducting Harmonic Analysis Studies of Industrial and Commercial Power Systems," in *IEEE P3002.8/D6, December 2017* , vol., no., pp.1-110, 1 Jan. 2018.

[13] S. Makasheva and P. Pinchukov, "Power Quality: Harmonic Current Distortion, Standards, Field Testing and Evaluation," *2020 International Ural Conference on Electrical Power Engineering (UralCon)*, Chelyabinsk, Russia, 2020, pp. 44-49, DOI: 10.1109/UralCon49858.2020.9216281.

[14] Y. Y. Chen, J. L. Liao, G. W. Chang, L. Y. Hsu, Y. Li and H. J. Lu, "Applying IEEE standard 1159.3 for Power Quality analysis platform implementation," *2016 IEEE Power and Energy Society General Meeting (PESGM)*, Boston, MA, USA, 2016, pp. 1-5, DOI: 10.1109/PESGM.2016.7741942.

[15] S. Jiao, K. R. Ramachandran Potti, K. Rajashekara and S. K. Pramanick, "A Novel DROGI-Based Detection Scheme for Power Quality Improvement Using Four-Leg Converter Under Unbalanced Loads," in *IEEE Transactions on Industry Applications*, vol. 56, no. 1, pp. 815-825, Jan.-Feb. 2020, DOI: 10.1109/TIA.2019.2942798.

[16] S. Devassy and B. Singh, "Modified pq-Theory-Based Control of Solar-PV-Integrated UPQC-S," in *IEEE Transactions on Industry Applications*, vol. 53, no. 5, pp. 5031-5040, Sept.-Oct. 2017, DOI: 10.1109/TIA.2017.2714138.

[17] Y. Han *et al.*, "Floquet-Theory-Based Small-Signal Stability Analysis of Single-Phase Asymmetric Multilevel Inverters With SRF Voltage Control," in *IEEE Transactions on Power Electronics*, vol. 35, no. 3, pp. 3221-3241, March 2020, DOI: 10.1109/TPEL.2019.2930326.

[18] A. Bouhouta, S. Moulahoum, N. Kabache and I. Colak, "Experimental Investigation of Fuzzy Logic Controller Based Indirect Current Control Algorithm for Shunt Active Power Filter," *2019 8th International Conference on Renewable Energy Research and Applications (ICRERA)*, Brasov, Romania, 2019, pp. 309-314, DOI: 10.1109/ICRERA47325.2019.8997115.

[19] K. R. Cheepati, N. R. Maddala, & S.K. Munagala, A Novel Reference Current Extraction Technique with Multi-Functional Capability for Shunt Active Filter. J. Electr. Eng. Technol. 15, 657–672 (2020). DOI: 10.1007/s42835-020-00371-3

[20] A. K. Mishra, S. R. Das, P. K. Ray, R. K. Mallick, A. Mohanty and D. K. Mishra, "PSO-GWO Optimized Fractional Order PID Based Hybrid Shunt Active Power Filter for Power Quality Improvements," in *IEEE Access*, vol. 8, pp. 74497-74512, 2020, DOI: 10.1109/ACCESS.2020.2988611.

[21] M. T. Shah, S. K. Chauhan and P. N. Tekwani, "Fractal Approach Based Simplified and Generalized Sector Detection in Current Error Space Phasor Based Hysteresis Controller Applied to Multilevel Front-End Converters," in *IEEE Transactions on Power Electronics*, vol. 35, no. 10, pp. 11082-11095, Oct. 2020, DOI: 10.1109/TPEL.2020.2977977.

[22] J. Peter, M. Shafi K.P., R. Lakshmi, and R. Ramchand, "Nearly Constant Switching Space Vector Based Hysteresis Controller for VSI Fed IM Drive," in *IEEE Transactions on Industry Applications*, vol. 54, no. 4, pp. 3360-3371, July-Aug. 2018, DOI: 10.1109/TIA.2018.2816561

[23] M. Nasir Uddin and R. S. Rebeiro, "Fuzzy logic based speed controller and adaptive hysteresis current controller based IPMSM drive for improved dynamic performance," *2011 IEEE International Electric Machines & Drives Conference (IEMDC)*, Niagara Falls, ON, Canada, 2011, pp. 1-6, DOI: 10.1109/IEMDC.2011.5994845.

[24] J. Doktian, W. Pongyart and P. Vanichchanunt, "Development of a Semi Auto-Tuning Algorithm for PI+CI Reset Controller," *2019 First International Symposium on Instrumentation, Control, Artificial Intelligence, and Robotics (ICA-SYMP)*, Bangkok, Thailand, 2019, pp. 155-158, DOI: 10.1109/ICA-SYMP.2019.8646092.

[25] R. Sinha, "Design of Shunt Active Power Filter with Optimal PI Controller - A Comparative Analysis," *2019 International Conference on Applied Machine Learning (ICAML)*, Bhubaneswar, India, 2019, pp. 205-212, DOI: 10.1109/ICAML48257.2019.00046.

8

Harris' Hawks Optimization Algorithm for Sizing and Allocation of Renewable Energy Based Distributed Generators

Sumit Verma[1], Suprava Chakraborty[2], and Aprajita Salgotra[3]

[1,3]Dept. of Industrial and Management Eng., Indian Institute of Technology, Kanpur, India
[2]TIFAC-CORE, Vellore Institute of Technology, Vellore, India
E-mail: drsumitverma007@gmail.com; suprava1008@gmail.com; aprajita.salgotra3@gmail.com

Abstract

The reconfiguration of power systems as well as the rising electricity demand has resulted in congestion in power system networks. The use of Decentralized Renewable Energy Resources (DRER) plays an important role in resolving such issues. DRERs can be connected to electric power system networks to control the power drift in transmission lines, increase the line capacity of power transfer, and enhance the overall network performance. In this chapter, an efficient approach founded on the Harris' Hawks Optimization Algorithm (HHOA) has been used to select the appropriate capacity and position of the DRERs to minimize the voltage variance and real power loss. The suggested HHOA was tested in two scenarios using a complicated benchmark function before being implemented in IEEE 33 bus radial distribution systems. It turns out that adding more DRERs improves the overall system performance. The simulation results have been compared with the most recent results, suggesting that the proposed HHOA is able to process complex high-dimensional benchmark functions and successfully solve power distribution difficulties.

191

Keywords: DRER, HHOA, efficient power flow, optimization, transmission loss.

8.1 Introduction

In recent years, the installation of Distributed Renewable Energy Resources (DRER) power supplies in distribution network systems have become a standard practice to minimize total energy loss and improve energy quality [1–2]. The optimal size and location of the DRER in the electrical system network are essential to maximize the advantages of these facilities. Incorrect configuration and improper selection of DRER in power system networks can lead to increased voltage flicker, voltage drop, fault current, harmonic distortion, and power loss. Electrical system losses can be reduced by up to 13% after the installation of DRER units [3, 4]. In electrical system operation, economic losses and voltage collapse can be avoided by improving voltage stability and reducing power loss [5]. Therefore, investigating the optimal location and size of DRER devices in a distribution network is a measure toward a profitable power supply [6–7]. The primary goal of most techniques to find out the optimal location and size of a DRER device is to reduce power loss and improve voltage distribution. To accomplish the above goals in the distribution network by means of proper allocation and size of DRER units, various techniques such as Particle Swarm Optimization (PSO), Genetic Algorithms (GA), ant bee colony (ABC), Taboo Search (TS), fuzzy systems, evolutionary programming, and dynamic programming, among others, have been used. GA is commonly used in the literature to estimate the position and size of the DRER unit in order to enhance voltage distribution and reduce power loss. Voltage stability and loss reduction will considerably increase if the DRER unit is properly installed in the distribution system network. To solve the DRER size and allocation problem, the GA has been utilized as the most convenient optimization technique [9]. In the radial distribution system, the multi objective genetic optimization method is employed to identify the appropriate position and size of the DRER unit depending on renewable energy [10]. GA-based multi objective optimization is used to reduce real power loss in the distribution networks with the constant power, current, and impedance models for site determination based on DRER planning and performance indicators [11]. Alambaout et al. [12] suggested an improved genetic algorithm for determining the optimal position and ability for simultaneous DRER/SC allocation in a radial system combining the advantages of GA and local search. The distribution of multiple dispersed power sources in

the distribution network is optimized using a mix of analytical and genetic algorithm approaches to reduce system losses [13]. The GA was proposed by Madhusudhan et al. [14] to find the appropriate position, as well as the size of the DRER units in the distribution network, to decrease real power loss and enhance the voltage profile. In Ref. [15] GA has been used to determine the best renewable energy technology meant for the optimal power system operation, as well as the best DRER placement and sizing to minimize power loss in the network. GA is used to improve system stability as well as reduce system expansion costs [16, 17]. However, a convergence of GA takes a long time, particularly when dealing with complex problems and can give incorrect results. After comparing TS and GA techniques, Simulated Annealing (SA) has been employed in [18, 19] to identify and designate the capacity of the DRERs while reducing the computation time. The SA technique, on the other hand, has downsides such as a local minimum termination, a long processing time, no information on the local minimum's divergence from the global minimum, and no upper time-constraint. Ref. [20, 21] used the TS technique to focus on DRER optimal planning with aim of reducing both loss and line loading. On the other hand, the TS method has the disadvantage of necessitating a high number of iterations and parameters to be determined. The ideal scale as well as distribution of DRER units in the power system, as well as their benefits, were determined using PSO [22].

The PSO [23–25] is one of the most successful and extensively utilized optimization algorithms. In Ref. [26] a multi objective PSO technique has been proposed for identifying the optimal placement and number of DRER units while accounting for economic and technological aspects. In the DRER allocation and sizing issues, sophisticated variants of PSO techniques, such as enhanced PSO, social learning PSO, binary PSO, PSO with constriction factor, and PSO with inertia weight are also used [27–30]. The PSO approach, on the other hand, has several drawbacks, such as difficulties in initializing design parameters and inapplicability to scattering issues. The Ant Colony Optimization (ACO) approach was designed to handle the problem of placement and size of renewable energy resource-based DRERs in radial distribution networks, with an aim to minimize overall system loss [31, 32]. According to their findings, ACO is a better option than GA and takes less time to calculate. Due to the complexity of the issue, ACO takes longer to converge, yet it is still faster than analytical approaches. The ACO approach has a significant disadvantage in terms of time to convergence. The Artificial Bee Colony technique was used in [33] and [34] to compare the outcomes of the PSO method and found that ABC gives a high quality solution with

a fast convergence rate. Yuvraj and Ravi [35] employed Cuckoo Search Algorithm to optimize voltage profiles and minimize power losses in the biomass and solar-thermal DRER units. A shuffled frog jump algorithm has been employed in [36] to minimize line losses and optimize the system voltage profile.

In [37] a plant growth modeling program has been employed with the goals of reducing losses and improving voltage profiles. The big bang–big crunch technique is used in [38] to discover the optimal DRER units for minimizing energy loss in a distribution network system. Sudabattula and Kausalya [39] proposed a bat algorithm for efficient allocation of solar-based DRER in distribution networks. Duong et al. [40] devised an effective biogeography-based optimization for optimal placement and size of solar photovoltaic distributed generating units to reduce power losses while maintaining voltage profile. The Teaching Learning Based Optimization (TLBO) technique has the drawback of providing a near-optimal solution rather than an optimum one in a limited number of iteration cycles [41]. Sultana et al. [41] presented a unique Quasi-Oppositional Teaching Learning Based Optimization (QOTLBO) approach for locating the best distributed generator placement while concurrently optimizing power loss, voltage stability index, and voltage deviation in a radial distribution network. To enhance network loss reduction, voltage profile, and yearly energy savings, the teaching learning-based optimization (CTLBO) approach for the optimal placement of DRERs in radial distribution systems is used [42]. By combining a strategy for order of preference by resemblance to an ideal solution and an enhanced elephant herding optimization approach, Meena et al. [43] proposed a novel methodology for solving a multi-objective Distributed Energy Resource (DER) accommodation problem of distribution systems. Ali et al. [44] presented an Improved Decomposition Based Evolutionary Algorithm (I-DBEA) for determining the best number, capacity, and location of DRERs in order to reduce real power losses and voltage variation while also increasing the voltage stability index. In IEEE 33-node radial distribution system and IEEE 14-node loop distribution system, the authors of [45] developed the clonal selection theory of the immune system which is integrated with particle swarm optimization to achieve optimal DG allocation. Harsh et al. [46] use loss sensitivity methods to determine the ideal position of the DG, and then apply the Particle Swarm Optimization (PSO) technique to determine the optimal size of the DG. Appropriate DRER unit deployment can provide a number of advantages, particularly cost savings through reduced power loss and increased buying power capacity.

8.2 Inspiration and Contributions

The main goal of this research is to develop a method for properly allocating and sizing solar photovoltaic DRERs to decrease power loss and improve voltage profiles. The generation of power from renewable energy resources is necessary for the world's long-term growth. The Government of India has taken certain steps to promote Renewable Energy (RE) that including setting state-specific RE targets in the form of Solar Purchase Obligations (SPOs) and Renewable Purchase Obligations (RPO). Under the requirements of RPO and SPO, each state aims to meet a major part of its overall energy demand with RE. The contributions of the work presented in this chapter are as follows:

- The proposed Harris' Hawks Optimization Algorithm (HHOA) has been tested with complex benchmark functions;
- Apply an innovative technique for proper DRER allocation and sizing in an IEEE 33-bus power system utilizing HHOA to reduce power loss and enhance the voltage profiles;
- Comparison of simulation results of a suggested method with already available techniques such as PSO, GA, BA, Teaching-Learning-Based Optimization (TLBO), Comprehensive Teaching Learning-Based Optimization (CTLBO), Quasi-opposition TLBO (QOTLBO), CTLBO ε-method, improved multi-objective elephant herding optimization (IMOEHO) and improved decomposition-based evolutionary algorithm (I-DBEA) to find out the effectiveness of the proposed algorithm on exciting ones.

8.3 Formulation of the Problem

The goal of this work is to decongest power lines by determining the optimum size and position of the DRERs while keeping losses to a minimum. Total system losses are used to frame the main Objective Function (OF). OF can be expressed using the equation given below:

$$OF = Minimize(P_{Loss}) \tag{8.1}$$

where

$$P_{Loss} = \sum_{k=1}^{n} g_k(V_i^2 + V_j^2 - 2V_i \times V_j \times cos(\delta_i - \delta_j)) \tag{8.2}$$

The suggested optimization problem's different restrictions are listed in (8.3)–(8.7).

$$V_i^{min} \leq V_i \leq V_i^{max} \tag{8.3}$$

$$P_{DRER}^{min} \leq P_{DRER} \leq P_{DRER}^{max} \tag{8.4}$$

$$Q_{DRER}^{min} \leq Q_{DRER} \leq Q_{DRER}^{max} \tag{8.5}$$

$$Q_{G_i}^{min} \leq Q_{G_i} \leq Q_{G_i}^{max} \tag{8.6}$$

$$P_{G_i}^{min} \leq P_{G_i} \leq P_{G_i}^{max} \tag{8.7}$$

where g_k is the branch conductance of k; V_i is the magnitude of the voltages at sending and V_j is the magnitude of voltages at receiving bus; δ_i is phase angle at i^{th} and j^{th} bus, respectively; P_{DRER} and Q_{DRER} represent active power and reactive power generation by DRER;. P_{G_i} and Q_{G_i} represent active power and reactive power generation at i^{th} bus.

In (8.3)–(8.7), superscripts (max / min) represents upper limit and lower limit of respective variables. The main goal is to minimize line congestion and reduce losses.

8.4 The Proposed HHOA

8.4.1 HHOA: Features

The hawks are assumed to belong to the intelligent bird category. Usually found in Arizona, USA, the Harris' hawks, is a famous bird of prey that lives in fairly steady groups. Unlike other raptors, they typically attack to search and catch a quarry, all alone, while the Harris' hawks attack together with the help of other family members belonging to a similar stable group. The main ploy of Harris' hawks attack is to capture a prey is "surprise pounce," which is also known as the "seven kills" strategy. In this intelligent foraging strategy, many hawks try to attack from different directions supportively and concurrently converge on a spotted escaping rabbit outside the shield. Based on escaping patterns and dynamic circumstances, Harris' hawks showcase the range of chasing styles in order to catch prey. The major benefit of these supportive tactics possessed by the Harris' hawks is that it may pursue the spotted rabbit to exhaustion which increases its vulnerability [47]. The Harris' hawks are a recent population-based gradient-free meta-heuristic that may be used to solve any optimization model or issue. The following subsections detail the various stages of Harris' hawk's formulation.

8.4.2 Exploration Phase

In this step, Harris' hawks look for prey at random sites and use a wait-and-watch technique to catch it, as described in (8.8) [47].

$$A\left(t+1\right) = \begin{cases} A_{rand}(t) - r_1|A_{rand}(t) - 2r_2 A(t)| & q \geq 0.5 \\ (A_r(t) - A_m(t)) - r_3(LB + r_4(UB - LB)) & q < 0.5. \end{cases}$$
(8.8)

where A_r is the current location of the rabbit and A(t+1) is the current position of the hawks for the following iteration, A(t) is the present position of the hawks. LB and UB represent the decision variables' maximum and minimum values. A_{rand} (t) is a set of hawks chosen at random from the present position. The $r_{(1-4)}$ displays a random number in the range [0,1].

$$A_m\left(t\right) = \frac{1}{N} \sum_{i=1}^{N} A_i\left(t\right)$$
(8.9)

where A_m represents the mean of current hawk population and N represents the overall hawk population.

Assuming the energy of rabbit as

$$E = 2\,E_o\left(1 - \frac{t}{T}\right)$$
(8.10)

where E, Eo, and T denote the prey's escape energy; primary energy; and the maximum number of repetitions, respectively.

8.4.3 Exploitation Phase

8.4.3.1 Soft besiegement
This behavior can be demonstrated by (8.11) [47].

$$A\left(t+1\right) = \triangle\,A\left(t\right) - E\,|JA_r\left(t\right) - A\left(t\right)|$$
(8.11)

$$\triangle\,A\left(t\right) = A_r\left(t\right) - A\left(t\right)$$
(8.12)

where A(t) and J denote the difference between the rabbit's position vector and the current place in iteration; and R is the rabbit's random leap strength, respectively.

8.4.3.2 Hard besiegement
This behavior can be showcased by (8.13).

$$A\left(t+1\right) = A_r\left(t\right) - E\,|\triangle\,A\left(t\right)|$$
(8.13)

8.4.3.3 Soft besiege along with rapid drives

In this behavior, one can assume that the hawks may choose their next step as given in the rule (8.14) [47].

$$B = A_r(t) - E|JA_r(t) - A(t)| \tag{8.14}$$

$$C = B + S \times LF(D) \tag{8.15}$$

where S, LF, and D, represent a random number of order $(1 \times D)$; the levy flight function; and the problem dimensions, respectively. Besides, u and v are random values (0 to 1); whereas β is a default constant (assuming as 1.5).

$$LF(A) = 0.01 \times \frac{\mathcal{U} \times \sigma}{|?|^{\frac{1}{\beta}}} \ , \ \sigma = \left(\frac{\Gamma(1+\beta) \times \sin\left(\frac{\pi\beta}{2}\right)}{\Gamma\left(\frac{1+\beta}{2}\right) \times \beta \times 2^{\left(\frac{\beta-1}{2}\right)}} \right)^{\frac{1}{\beta}} \tag{8.16}$$

Soft besiege is updating the position of hawks by

$$A(t+1) = \begin{cases} B, & if \ F(B) < F(A(t)) \\ C, & if \ F(C) < F(A(t)) \end{cases} \tag{8.17}$$

8.4.3.4 Rapid drives and a hard besiegement

Hard besiegement condition given by the following rule

$$A(t+1) = \begin{cases} B, & if \ F(B) < F(A(t)) \\ C, & if \ F(C) < F(A(t)) \end{cases} \tag{8.18}$$

$$B = A_r(t) - E|JA_r(t) - A_m(t)| \tag{8.19}$$

$$C = B + S \times LF(D) \tag{8.20}$$

The step wise procedure of HHOA is summarized to the pseudo-code, given in Algorithm 1 [47] and in flow chart shown in Figure 8.1.

8.5 Solution Approach

8.5.1 HHOA for DRER Placement and Location

The main objective is to find the ideal location and size for a large number of DRERs while minimizing the network's power losses and improving voltage profiles. Herein, the inequality constraints are translated into Penalty
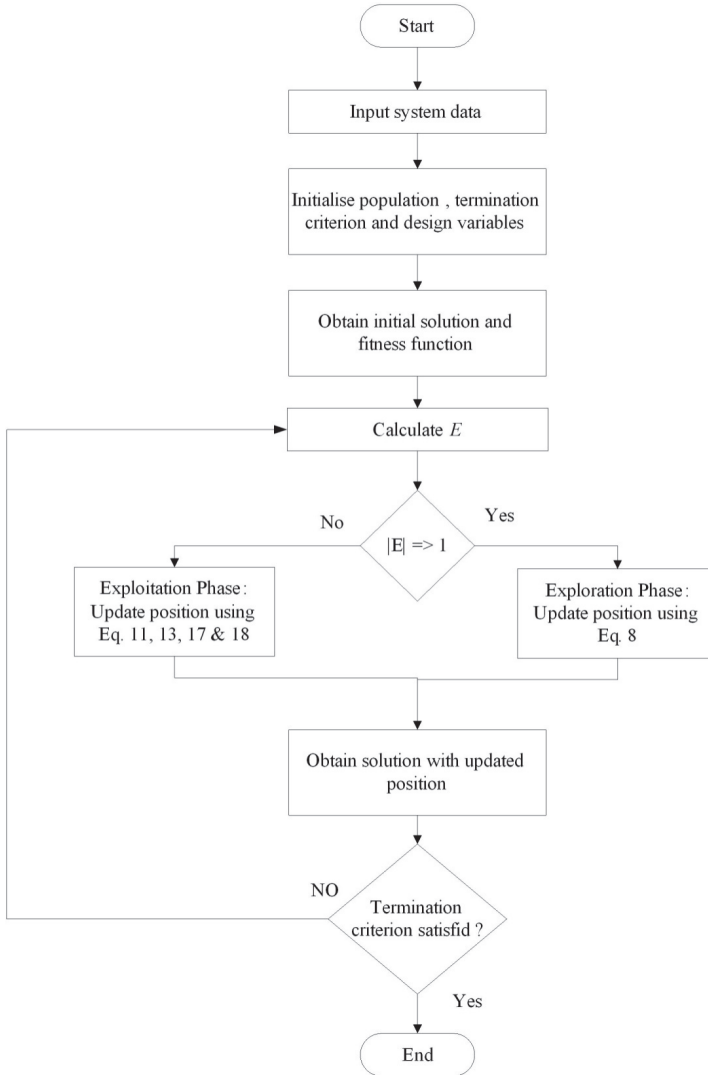
Figure 8.1   Flow chart of HHOA

Functions (PFs), and the PFs are combined with OF to form a fitness function (FF) as specified in (8.21).

$$Minimum\ FF = OF + PF \times \sum_{j=1}^{VB} (\Delta V_j)^2 \qquad (8.21)$$

Algorithm 1: Pidgin code of HHOA [47]

Define objective function $f(x)$; $x = (x_1, x_2, ..., x_{dim})$.

Initialize the population of harris hawks arbitrarily within confines.

while (*t<MaxGeneration*)

  Compute the appropriateness of hawks.

  Put X_r the best location of rabbit (optimum location).

  for *i =1: n*

    Update the initial energy E_0 and jump strength J

    Update E using (8.10).   % *Exploration*

    if ($|E| >= 1$) then update location using (8.8) % *Exploitation*

    if ($|E| < 1$) then

    if ($r >= 0.5$ and $|E| >= 0.5$) then % soft surround

    Update the location (8.11)

    elseif ($r >= 0.5$ and $|E| < 0.5$) then % hard surround

    Update the location (8.13)

      elseif ($r < 0.5$ and $|E| >= 0.5$) then % soft

    surround with advanced swift drives

    Update the location using (8.17).

      elseif ($r < 0.5$ and $|E| < 0.5$) then % hard

    surround with advanced swift drives

    Update the location using (8.18).

  end for

end while

In this case, FF must be minimized to obtain the minimum loss value, PF is the penalty factor and Vb denotes the set of overloaded lines and voltage violation load buses. The penalty function approach was used to deal with the violation of inequality restrictions in the form of load bus voltage and line power flow. The PF was set to 10,000.00 throughout the simulation. Newton-Raphson load flow method is used.

8.5.2 HHOA Computational Practice for DRER Values and Location

Step 1 Read the system's input data, such as the maximum iterations, the number of DRER units, and the population size.

Step 2 The same is represented in (8.22). Generate the size of DRER within the upper ($DRER^{max}$) and lower limits ($DRER^{min}$). This is shown in (8.22).

$$DRER_i = DRER_i^{min} + rand \times \left(DRER_i^{max} - DRER_i^{min}\right)$$
(8.22)

Here, $DRER_i$ indicates the size of ith DRER unit. Now, form a vector A_j, consisting of the possible locations (LC) and size of DRERs as shown in (8.23).

$$A_j = [DG_{j,1}, DG_{j,2}, \ldots\ldots\ldots, DG_{j,n},$$
$$LC_{j,1}, LC_{j,2}, \ldots\ldots\ldots, LC_{j,n}]$$
(8.23)

The LOC is generated randomly. Initial solution set Ais then formulated as shown in (8.24).

$$A = [A_1, A_2, \ldots\ldots\ldots\ldots, A_N]$$
(8.24)

Step 3 For individual Harris' hawks, the fitness function is evaluated using (8.21), and the optimal hawks site is recognized.

Step 4 E is Calculated using (8.10)

Step 5 Location updating of Harris' hawks using (8.8)

Step 6 Phase of exploitation: Use (8.11), (8.13), (8.17), and (8.20) to update the location (8.18).

Step 7 Terminate after the number of iterations has reached its maximum value. Otherwise, return to Step 3.

8.6 Results And Discussions

The computations were done on a MATLAB 9.9 loaded on a PC with a 2.4 GHz Intel i3 CPU and 4 GB of RAM. MATPOWER 7.2, a power modeling program, was used in this study.

8.6.1 Case I

The proposed HHOA has been examined with selected complex benchmark functions available in CEC-2014 in order to establish an algorithm

(Table 8.1). Table 8.2 contains a summary of the outcomes collected. In comparison to other contemporary meta-heuristic optimizers, the HHOA appears to produce extremely competitive results.

Table 8.1   Summary of the considered CEC-2014 benchmark functions

Type	ID	Functions	Fi*=Fi(x*)
Unimodal	F_1	Elliptic Rotated High Conditioned	$1*10^2$
	F_2	Bent Cigar:Rotated	$2*10^2$
Simple Multimodal	F_3	Shifted & Rotated Rastrigin's	$9*10^2$
	F_4	Shifted Schwefel's	$10*10^2$
Hybrid	F_5	Hybrid Function 3 (N=4)	$1.9*10^2$
	F_6	Hybrid Function 4 (N=4)	$20*10^2$
Composition	F_7	Composition Function 8 (N=3)	$30*10^2$

Table 8.2   Result comparison on the benchmark functions

ID		PSO	TLBO	CS	GSA	SFS	HHOA
F_1	max	$45.6*e^7$	$89.3*e^7$	$55.1*e^7$	$5.31*e^7$	$11.7*e^5$	$3.01*e^5$
	min	$24.7*e^7$	$4.39*e^7$	$11.8*e^7$	$4.56*e^6$	$1.54*e^5$	$1.43*e^4$
	median	$33.1*e^7$	$34.2*e^7$	$31.0*e^7$	$8.37*e^6$	$6.16*e^5$	$1.52*e^5$
	std	$7.92*e^7$	$34.2*e^7$	$10.5*e^7$	$1.32*e^7$	$2.35*e^5$	$1.23*e^5$
F_2	max	$36.3*e^9$	$40.6*e^3$	$24.2*e^3$	$16.1*e^3$	200	200
	min	$6.00*e^7$	$60.0*e^2$	$3.09*e^2$	$34.7*e^2$	200	**200**
	median	$15.5*e^9$	$15.2*e^3$	$80.8*e^2$	$83.8*e^2$	200	200
	std	$14.3*e^9$	$86.5*e^2$	$60.0*e^2$	$29.0*e^2$	$7.89*e^{-9}$	0. 00
F_3	max	$12.4*e^2$	$11.2*e^2$	$13.4*e^2$	$11.0*e^2$	984	920
	min	$11.3*e^2$	$10.6*e^2$	$11.5*e^2$	$10.2*e^2$	935	**903**
	median	$11.8*e^2$	$10.9*e^2$	$12.5*e^2$	$10.6*e^3$	961	919
	std	43.3	25	44.1	17.4	11.1	10.17
F_4	max	$79.0*e^2$	$59.2*e^2$	$32.1*e^2$	$52.5*e^2$	$27.1*e^2$	$10.5*e^2$
	min	$62.6*e^2$	$41.4*e^2$	$13.6*e^2$	$34.5*e^2$	$10.2*e^2$	**10.0*e²**
	median	$71.8*e^2$	$50.6*e^2$	$21.7*e^2$	$43.7*e^2$	$14.9*e^2$	$10.1*e^2$
	std	598	789	433	361	362	14.5
F_5	max	$21.0*e^2$	$19.1*e^2$	$20.4*e^2$	$20.0*e^2$	$19.1*e^2$	$19.2*e^2$
	min	$19.1*e^2$	$19.0*e^2$	$19.1*e^2$	$19.1*e^2$	$19.0*e^2$	**19.0*e²**
	median	$19.7*e^2$	$19.1*e^2$	$19.2*e^2$	$20.0*e^2$	$19.1*e^2$	$19.1*e^2$
	std	70.7	1.65	33.0	34.3	1.47	1.46
F_6	max	$43.7*e^2$	$53.4*e^2$	$60.2*e^3$	$68.2*e^3$	$21.0*e^2$	$27.5*e^2$
	min	$25.5*e^2$	$23.0*e^2$	$22.2*e^3$	$23.2*e^2$	$20.2*e^2$	**20.0*e²**
	median	$30.0*e^2$	$27.4*e^2$	$36.8*e^3$	$17.7*e^3$	$20.6*e^2$	$22.6*e^2$
	std	532	700	$84.2*e^3$	$13.9*e^3$	26	206
F_7	max	$97.0*e^4$	$15.6*e^5$	$50.8*e^4$	$11.4*e^4$	$76.6*e^2$	$56.2*e^2$
	min	$69*e^3$	$20.8*e^3$	$62.6*e^3$	$12.2*e^3$	$42.5*e^2$	**35.6*e²**
	median	$33.5*e^4$	$65.6*e^4$	$17.7*e^4$	$14.6*e^3$	$56.3*e^2$	$47.1*e^2$
	std	$36.3*e^4$	$56.4*e^4$	$91.1*e^3$	$18.4*e^3$	738	$13.0*e^2$

8.6.2 Case II

The suggested HHOA-based technique is used to determine the best position and capacity for the DRERs in the 33 bus IEEE radial distributed test system, using network and load data from [45]. Figure 8.2 shows a single-line diagram of the IEEE 33-bus RDS.

It is presumed that there is a DRER at that bus at any given time to find candidate buses for placing a DRER making use of this approach for each individual bus. At this stage, it is assumed that a DRER can generate electric power of any value within the possible ranges for optimal sizing (e.g., 0-1000 kW). The proposed HHOA is used to reduce overall loss as the problem's objective function, as well as to improve the voltage profile. To begin, only one DRER is used to relieve line congestion, with the results tabulated in Table 8.3. With the application of the proposed HHOA on the distribution problems, the losses get reduced to 129.2 kW from 202.67 kW with only one DRER in the installation of size 950 kW.
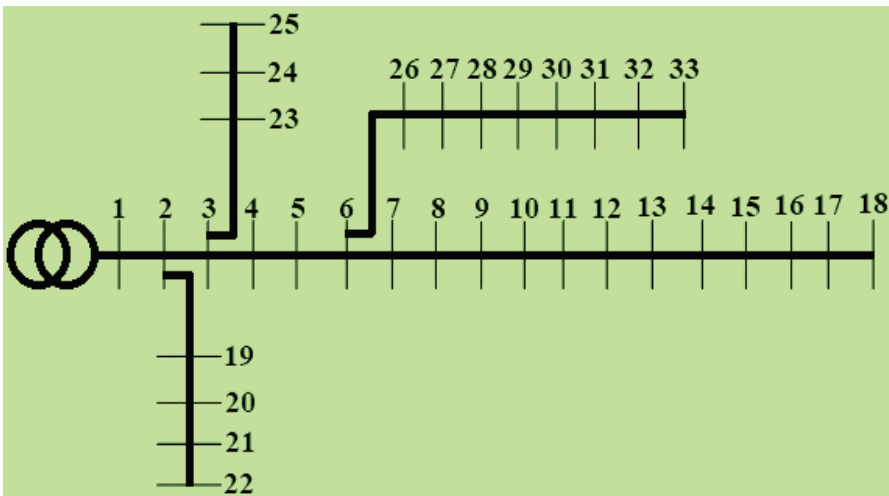

Figure 8.2 Single line diagram of 33-bus IEEE RDS

Table 8.3 Loss reduction in power with change in number of allocated DRERs

Test system	Buses count	Array location	P_{loss} (kW)	Loss reduction (%)
	1	30	129.20	38.76
33 bus system	2	12, 30	86.90	58.81
	3	13, 24, 30	72.10	64.42

The problem is further improved by putting 2 and 3 nos. of DRERs in the power network. Table 8.3 summarizes the outcomes collected. The overall active power losses have decreased to 86.9 kW and 72.10 kW with the application of two and three DRERs, respectively, using HHOA. Table 8.4

Table 8.4   Comparative results of optimal allocation and sizing of DRERs corresponding to Case II

Optimization approach	Location of array	DRER size (MW)	Total DRER size (MW)	P_{loss} (kW)	Loss reduction (%)
Base case	-	-	-	202.67	0.00
TLBO [40]	12	1.1826	3.560	124.70	38.47
	28	1.1913			
	30	1.1863			
GA [41]	11	1.5000	2.994	106.30	47.55
	29	0.4230			
	30	1.0710			
PSO [41]	8	1.1770	2.989	105.30	48.04
	13	0.9820			
	32	0.8300			
GA/PSO [41]	11	0.9250	2.998	103.40	48.98
	16	0.8630			
	32	1.2000			
QOTLBO [40]	13	1.0834	3.470	103.40	48.98
	26	1.1876			
	30	1.1992			
CTLBO ε-method [42]	13	1.1926	3.693	96.17	52.55
	25	0.8706			
	30	1.6296			
IMOEHO [43]	14	1.0570	3.852	95.00	53.13
	24	1.0540			
	30	1.7410			
I-DBEA [44]	13	1.0980	3.913	94.85	53.20
	24	1.0970			
	30	1.7150			
CTLBO [42]	13	1.0364	3.721	85.96	57.59
	24	1.1630			
	30	1.5217			
BA [39]	15	0.81630	2.721	75.05	62.97
	25	0.95235			
	30	0.95235			
HHOA [Proposed]	13	0.8311	2.731	72.10	**64.42**
	24	0.9500			
	30	0.9500			

shows the comparative results in terms of the optimal location and size of DRERs. Figure 8.3 shows the sites indicated by HHOA for installing DRERs in the IEEE 33 bus.

In comparison to TLBO [40], GA [41], PSO [41], GA/PSO [41], QOTLBO [40], CTLBO-method [42], IMOEHO [43], I-DBEA [44], CTLBO [42], and BA [39], the size and position indicated by HHOA (Table 8.4) gives the maximum decrease in losses. Figure 8.4 also shows the voltage graph of
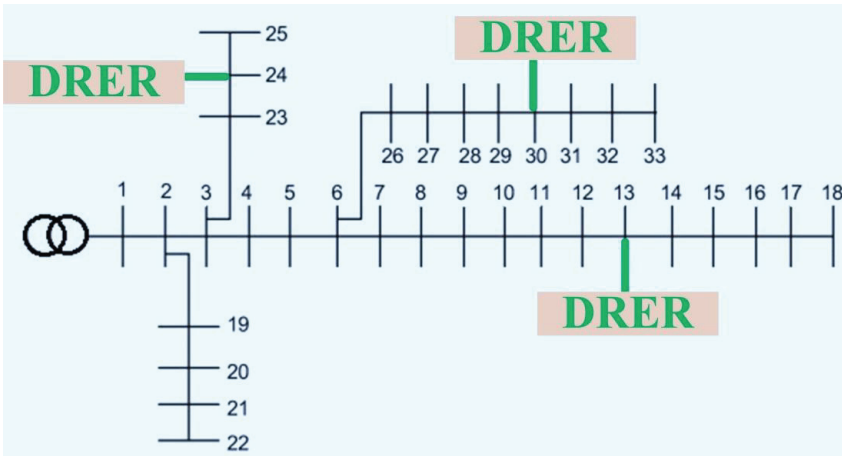

Figure 8.3   33-bus IEEE system line diagram with DRER at suggested locations by HHOA
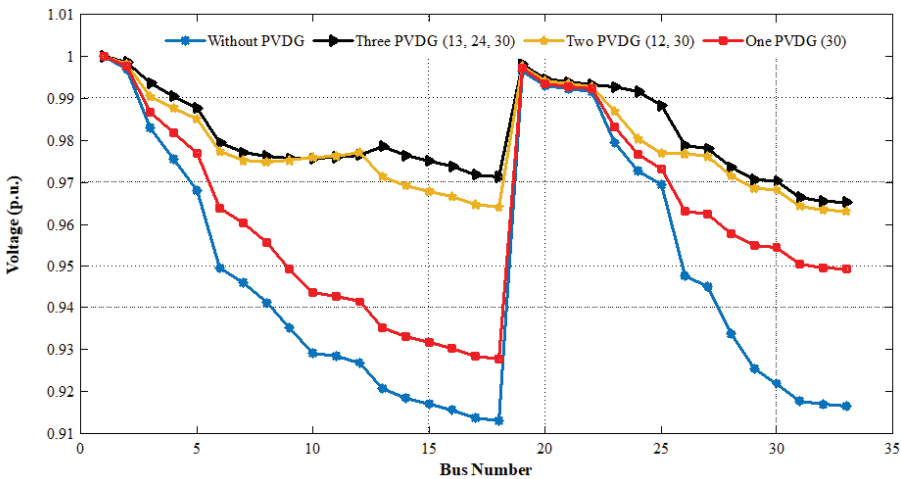
Figure 8.4   With and without DRER voltage graph in 33 bus IEEE system.
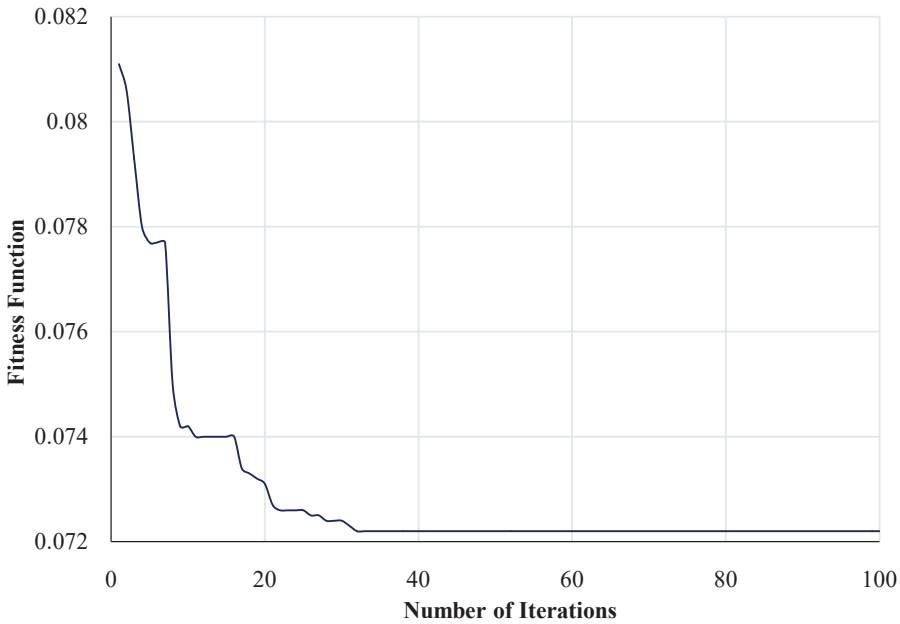
Figure 8.5   Fitness function's convergence characteristics associated with Case II

all the buses acquired following the usage of DRERs. The bus voltages were determined by analyzing the load flow. Under the use of three DRERs at their ideal locations, the bus voltage profile improves dramatically. Figure 8.5 shows the variance of the fitness function versus the number of iterations for the installation with 3 numbers of DRERs using HHOA. The iterative graph demonstrates that the HHOA converges to the best solution value in a relatively short number of iterations.

8.7 Conclusions

The suggested HHOA-based technique is efficient in determining the best locations and sizes for DRERs. The recommended technique's effectiveness is assessed using standard IEEE 33 bus test systems. It has been discovered that using optimally sized DRERs at their ideal placement improves the voltage profile of load buses and significantly reduces losses. The system's performance improves when additional DRERs are deployed. Comparing the suggested technique against the PSO, GA, BA, TLBO, QOTLBO, CTLBO, CTLBO-method, IMOEHO, and I-DBEA methods reveals that it outperforms

them all. The loss in active power is decreased by approx. 64 percent with the installation of three DRERs in IEEE 33 utilizing this method. The results show that the suggested approach decreases the loss of power by a higher percentage with a smaller DRER size and that it has superior convergence features to existing techniques.

With the use of DRERs, HHOA has been found as a reliable optimization approach to address the problem of congestion in power systems. The suggested technique provides a compelling alternative for both energy producers and system operators to address difficult issues such as large-scale system losses, voltage instability, and transmission congestion. The implementation of this optimization approach in desalination systems is a promising future application [48–50].

Acknowledgements

References

[1] K. Sandhya and K. Chatterjee, "A review on the state of the art of proliferating abilities of distributed generation deployment for achieving resilient distribution system," J. Clean. Prod., vol. 287, no. 125023, p. 125023, 2021.

[2] H. Wang et al., "The optimal allocation and operation of an energy storage system with high penetration grid-connected photovoltaic systems," Sustainability, vol. 12, no. 15, p. 6154, 2020.

[3] Sahib, J.T.; Ghani, A.R.M.; Jano, Z.; Mohamed, H.I. Optimum allocation of distributed generation using PSO: IEEE test case studies evaluation. Int. J. Appl. Eng. Res. 12, 2900–2906, 2017.

[4] N. M. Saad et al., "Impacts of photovoltaic distributed generation location and size on distribution power system network," Int. J. Power Electron. Drive Syst. (IJPEDS), vol. 9, no. 2, p. 905, 2018.

[5] R. A. Jabr, "Linear decision rules for control of reactive power by distributed photovoltaic generators," IEEE Trans. Power Syst., vol. 33, no. 2, pp. 2165–2174, 2018.

[6] E. A. Al-Ammar et al., "ABC algorithm based optimal sizing and placement of DGs in distribution networks considering multiple objectives," Ain Shams Eng. J., vol. 12, no. 1, pp. 697–708, 2021.

[7] Kumawat, A.; Singh, P. Optimal placement of capacitor and DG for minimization of power loss using genetic algorithm and artificial bee colony algorithm. Int. Res. J. Eng. Technol.3, 2482–2488, 2016

[8] Y. Y. Zakaria, R. A. Swief, N. H. El-Amary, and A. M. Ibrahim, "Optimal distributed generation allocation and sizing using genetic and ant colony algorithms," J. Phys. Conf. Ser., vol. 1447, p. 012023, 2020.

[9] K. S. Sambaiah and T. Jayabarathi, "Loss minimization techniques for optimal operation and planning of distribution systems: A review of different methodologies," Int. trans. electr. energy syst., vol. 30, no. 2, 2020..

[10] A. A. Hassan, F. H. Fahmy, A. E.-S. A. Nafeh, and M. A. Abu-elmagd, "Hybrid genetic multi objective/fuzzy algorithm for optimal sizing and allocation of renewable DG systems: Genetic/Fuzzy Optimization of Renewable DGS," Int. trans. electr. energy syst., vol. 26, no. 12, pp. 2588–2617, 2016

[11] D. K. Patel, D. Singh, and B. Singh, "Genetic algorithm-based multi-objective optimization for distributed generations planning in distribution systems with constant impedance, constant current, constant power load models," Int. trans. electr. energy syst., vol. 30, no. 11, 2020.

[12] E. A. Almabsout, R. A. El-Sehiemy, O. N. U. An, and O. Bayat, "A hybrid local search-genetic algorithm for simultaneous placement of DG units and shunt capacitors in radial distribution systems," IEEE Access, vol. 8, pp. 54465–54481, 2020

[13] M. Vatani, D. SolatiAlkaran, M. J. Sanjari, and G. B. Gharehpetian, "Multiple distributed generation units allocation in distribution network for loss reduction based on a combination of analytical and genetic algorithm methods," IET Gener. Transm. Distrib., vol. 10, no. 1, pp. 66–72, 2016

[14] M. Madhusudhan, N. Kumar, and H. Pradeepa, "Optimal location and capacity of DG systems in distribution network using genetic algorithm," Int. J. Inf. Technol., vol. 13, no. 1, pp. 155–162, 2021.

[15] T. R. Ayodele, A. S. O. Ogunjuyigbe, and O. O. Akinola, "Optimal location, sizing, and appropriate technology selection of distributed generators for minimizing power loss using genetic algorithm," J. Renew. Energy, vol. 2015, pp. 1–9, 2015.

[16] Ali, A.; U. Keerio, M.; A. Laghari, J. Optimal Site and Size of Distributed Generation Allocation in Radial Distribution Network Using Multiobjective Optimization. J. Mod. Power Syst. Clean Energy, 9 (2), 404–415, 2021.

[17] L. Liu, F. Xie, Z. Huang, and M. Wang, "Multi-objective coordinated optimal allocation of DG and EVCSs based on the V2G mode," Processes (Basel), vol. 9, no. 1, p. 18, 2020

[18] A. S. Hassan, Y. Sun, and Z. Wang, "Multi-objective for optimal placement and sizing DG units in reducing loss of power and enhancing voltage profile using BPSO-SLFA," Energy rep., vol. 6, pp. 1581–1589, 2020.

[19] Z. Fan et al., "Multi-objective planning of DGs considering ES and EV based on source-load spatiotemporal scenarios," IEEE Access, vol. 8, pp. 216835–216843, 2020.

[20] W. Liu, H. Xu, S. Niu, and J. Xie, "Optimal distributed generator allocation method considering voltage control cost," Sustainability, vol. 8, no. 2, p. 193, 2016.

[21] M. Azam Muhammad, H. Mokhlis, K. Naidu, A. Amin, J. Fredy Franco, and M. Othman, "Distribution network planning enhancement via network reconfiguration and DG integration using dataset approach and water cycle algorithm," J. Mod. Power Syst. Clean Energy, vol. 8, no. 1, pp. 86–93, 2020.

[22] W. Phuangpornpitak and K. Bhumkittipich, "Principle optimal placement and sizing of single distributed generation for power loss reduction using particle swarm optimization," Res. J. Appl. Sci. Eng. Technol., vol. 7, no. 6, pp. 1211–1216, 2014.

[23] Bhadoria, V. S., Pal, N. S., Shrivastava, V., & Jaiswal, S. P. (2017). Reliability improvement of distribution system by optimal sitting and sizing of disperse generation. International Journal of Reliability, Quality and Safety Engineering, 24(06), 1740006.

[24] Bhadoria V.S., Jaiswal S.P., Pal N.S., Shrivastava V. (2022) Application of Modified Clonal PSO in Distributed Generator Placement for Enhancement of Efficiency and Voltage Stability in Distribution System. In: Bansal R.C., Agarwal A., Jadoun V.K. (eds) Advances in Energy Technology. Lecture Notes in Electrical Engineering, vol 766. Springer, Singapore. https://doi.org/10.1007/978-981-16-1476-7_63

[25] Maurya H., Pal N.S., Bhadoria V.S. (2020) Performance Analysis of Optimal Placement of Multiple DGs Using PSO. In: Kapur P., Singh G., Klochkov Y., Kumar U. (eds) Decision Analytics Applications in Industry. Asset Analytics (Performance and Safety Management). Springer, Singapore. https://doi.org/10.1007/978-981-15-3643-4_18

[26] S. Barik, D. Das, and R. C. Bansal, "Zero bus load flow method for the integration of renewable DGs by mixed-discrete particle swarm

optimisation-based fuzzy max–min approach," IET Renew. Power Gener., vol. 14, no. 19, pp. 4029–4042, 2020.

[27] A. K. Bohre, G. Agnihotri, and M. Dubey, "Optimal sizing and sitting of DG with load models using soft computing techniques in practical distribution system," IET Gener. Transm. Distrib., vol. 10, no. 11, pp. 2606–2621, 2016.

[28] A. A. Yahaya, M. AlMuhaini, and G. T. Heydt, "Optimal design of hybrid DG systems for microgrid reliability enhancement," IET Gener. Transm. Distrib., vol. 14, no. 5, pp. 816–823, 2020.

[29] R. Cheng and Y. Jin, "A competitive swarm optimizer for large scale optimization," IEEE Trans. Cybern., vol. 45, no. 2, pp. 191–204, 2015.

[30] S. Ganguly, "Multi-objective planning for reactive power compensation of radial distribution networks with unified power quality conditioner allocation using particle swarm optimization," IEEE Trans. Power Syst., vol. 29, no. 4, pp. 1801–1810, 2014.

[31] Tolabi, H. B.; Ali, M. H.; Rizwan, M. Simultaneous Reconfiguration, Optimal Placement of DSTATCOM, and Photovoltaic Array in a Distribution System Based on Fuzzy-ACO Approach. IEEE Trans. on Sustainable Energy.6(1),210-218, 2015.

[32] A. Oloulade, A. ImanoMoukengue, R. Agbokpanzo, A. Vianou, H. Tamadaho, and R. Badarou, "New multi objective approach for optimal network reconfiguration in electrical distribution systems using modified ant colony algorithm," Am. j. electr. power energy syst., vol. 8, no. 5, p. 120, 2019.

[33] C. K. Das, O. Bass, G. Kothapalli, T. S. Mahmoud, and D. Habibi, "Optimal placement of distributed energy storage systems in distribution networks using artificial bee colony algorithm," Appl. Energy, vol. 232, pp. 212–228, 2018.

[34] A. A. Seker and M. H. Hocaoglu, "Artificial Bee Colony algorithm for optimal placement and sizing of distributed generation," in 2013 8th International Conference on Electrical and Electronics Engineering (ELECO), 2013.

[35] T. Yuvaraj and K. Ravi, "Multi-objective simultaneous DG and DSTAT-COM allocation in radial distribution networks using cuckoo searching algorithm," Alex. Eng. J., vol. 57, no. 4, pp. 2729–2742, 2018.

[36] L. D. Arya and A. Koshti, "Modified shuffled frog leaping optimization algorithm based distributed generation rescheduling for loss minimization," J. Inst. Eng. (India) Ser. B, vol. 99, no. 4, pp. 397–405, 2018.

[37] R. Rajaram, K. Sathish Kumar, and N. Rajasekar, "Power system reconfiguration in a radial distribution network for reducing losses and to improve voltage profile using modified plant growth simulation algorithm with Distributed Generation (DG)," Energy rep., vol. 1, pp. 116–122, 2015.

[38] M. M. Othman, W. El-Khattam, Y. G. Hegazy, and A. Y. Abdelaziz, "Optimal placement and sizing of distributed generators in unbalanced distribution systems using supervised big bang-big crunch method," IEEE Trans. Power Syst., vol. 30, no. 2, pp. 911–919, 2015.

[39] T. Yuvaraj, K. Ravi, and K. R. Devabalaji, "DSTATCOM allocation in distribution networks considering load variations using bat algorithm," Ain Shams Eng. J., vol. 8, no. 3, pp. 391–403, 2017.

[40] M. Duong, T. Pham, T. Nguyen, A. Doan, and H. Tran, "Determination of optimal location and sizing of solar photovoltaic distribution generation units in radial distribution systems," Energies, vol. 12, no. 1, p. 174, 2019.

[41] Sultana, S.; Roy, P. K. Multiobjective quasi-oppositional teaching learning based optimization for optimal location of distributed genera- tor in radial distribution systems. Int. J. of Electrical Power & Energy Systems 63, 534-545, 2014.

[42] I. A. Quadri, S. Bhowmick, and D. Joshi, "A comprehensive technique for optimal allocation of distributed energy resources in radial distribution systems," Appl. Energy, vol. 211, pp. 1245–1260, 2018.

[43] Meena, N. K.; Parashar, S. A.; Swarnkar et al. Improved elephant herding optimization for multiobjective DER accommodation in distribution systems. IEEE Transactions on Industrial Informatics 14(3), 1029-1039, 2018.

[44] Ali, A. U.; Keerio, M.; A. Laghari, J. Optimal site and size of distributed generation allocation in radial distribution network using multiobjective optimization. J. Mod. Power Syst. Clean Energy 9(2), 404–415, 2021.

[45] Bhadoria, V.S., Pal, N.S. &Shrivastava, V. Artificial immune system based approach for size and location optimization of distributed generation in distribution system. Int J Syst Assur EngManag 10, 339–349 (2019). https://doi.org/10.1007/s13198-019-00779-9

[46] Maurya, Harsh, Kumar Bohra, Vivek, Singh Pal, Nidhi & Singh Bhadoria, Vikas. Effect of Inertia Weight of PSO on Optimal Placement of DG, IOP Conference Series: Materials Science and Engineering, http://dx.doi.org/10.1088/1757-899X/594/1/012011

[47] A. A. Heidari, S. Mirjalili, H. Faris, I. Aljarah, M. Mafarja, and H. Chen, "Harris' hawks optimization: Algorithm and applications," Future Gener. Comput. Syst., vol. 97, pp. 849–872, 2019.

[48] B. D. H. Phuc, et.al. "A modified controller design based on symbiotic organisms search optimization for desalination system", Journal of Water Supply: Research and Technology – AQUA, Vol. 68, No. 5, pp. 337-345, 2019.

[49] V.P. Singh, "Design of optimal PID controller for the reverse osmosis using teacher-learner-based-optimization", Membrane Water Treatment, Vol. 9, No. 2, pp. 129-136, 2018.

[50] Rathore, N.S. and Singh, V.P. (2019) 'Whale optimisation algorithm-based controller design for reverse osmosis desalination plants', Int. J. Intelligent Engineering Informatics, Vol. 7, No. 1, pp. 77–88.

Index

About the Editors

Kirti Pal is presently working as an Associate Professor of Electrical Engineering at the School of Engineering, Gautam Buddha University, Greater Noida, India. She has over 15 years of academic experience and has published many research papers in various reputed national / international journals and conference proceedings as well. Dr. Pal has also been invited to deliver keynote and expert talks at several national / international conferences and workshops. She has been a Guest Editor of the special issue on: Advance Innovation and Technology with Sustainability Engineering, International Journal of Social Ecology and Sustainable Development (IGI Global, USA). She is a Life Member of the Indian Society for Technical Education. Her areas of current interest include Restructuring of power systems, Power system analysis and optimization, Soft computing techniques, Renewable energy systems, and Electric vehicles.

Saurabh Mani Tripathi is presently working as Associate Professor of Electrical Engineering at Kamla Nehru Institute of Technology, Sultanpur, India. He is a recipient of the prestigious "IEI Young Engineers Award 2018-19" presented by The Institution of Engineers (India). He is also a recipient of the "Best Teachers Award 2020" presented by Dr. A.P.J. Abdul Kalam Technical University, Lucknow, India. He got 'HIL Specialist Certification' from Typhoon HIL, Inc. Switzerland. At the age of 23 years, he authored his first book entitled 'A Course in Modern Control Systems'. Subsequently, he authored 02 other books in the domain of Electrical Engineering namely 'Analysis of Basic Systems' and 'Modern Control Systems: An Introduction'. He served as an Editor of the book entitled 'Energy Conversion Systems: An Overview'. He has published several papers in reputed international journals and various national/international conferences. He is a Member of several professional societies such as The Institution of Engineers (India); International Association of Engineers; World Academy of Science, Engineering and Technology. He is a Life Member of the Indian Society for Technical Education. His areas of current interest include 'Renewable energy

systems', 'Electrical drives', 'Real-time simulation' and 'Hardware-in-the-loop testing'.

Shruti Pandey is currently working as Assistant Professor of Electrical and Electronics Engineering at Krishna Institute of Engineering and Technology, Ghaziabad, India. She has published several research papers in various International Journals and conference proceedings. She has received the 'Best Research Paper Award' at several International Conferences. She is also the recipient of the 'Young Dronacharya Award 2021' presented by KIET Ghaziabad. She has worked with the National Institute of Technology, Delhi for a DST sponsored project in the specialized area of Power Electronics. She has actively contributed to delivering lectures on the subject "Power Electronics", broadcasted on the National television channel DD Swayam Prabha (an initiative of MHRD for imparting technical education to a student with no or limited internet connectivity). She is a Member of IEEE SIGHT and IEEE Power Electronics Society Technical committee. Her areas of current interest include Power electronics, Non-linear controllers, Micro-grid, and Battery management.

Advanced Control and Optimization Paradigms for Energy System Operation and Management

Editors:

Kirti Pal, Saurabh Mani Tripathi, and Shruti Pandey

Distributed energy technologies are gaining popularity nowadays; however, due to the highly intermittent characteristics of distributed energy resources, a larger penetration of these resources into the distribution grid network becomes of major concern. The main issue is to cope with the intermittent nature of the renewable sources alongside the requirements for power quality and system stability. Unlike traditional power systems, the control and optimization of complex energy systems becomes difficult in many aspects, such as modelling, integration, operation, coordination and planning etc.

This edited book serves as a resource for the engineers, scientists, academicians, experienced professionals, and researchers working on the energy systems. With eight original chapters, this edited volume is an extensive collection of the state-of-the-art studies intended to integrate current research and innovations for the control, optimization and management of electric energy systems. Readers will find this book inspiring and very useful when conducting their own research in the domain area of energy systems.

Key features

- An extensive collection of state-of-the-art studies intended to integrate current research and innovations for the control, optimization and management of electric energy systems.
- Emphasis on the optimization techniques to address problems in electrical energy systems.
- Serves as a valuable resource for engineers, scientists, academicians, experienced professionals, and research scholars who are working in the area of energy systems.